MITF-Dependent Phenotypic Plasticity Regulates Proton-Coupled Transport and Controls Lineage Resistance to Acidotic Stress

Oscar C.Y. Yang

Wolfson College
University of Oxford

ACADEMIC SUPERVISORS

Professor Shih-Hurng Loh, Professor Robert J.C. Gilbert

A thesis submitted for the degree of
Doctor of Philosophy

13th October 2020

GRAPHICAL ABSTRACT

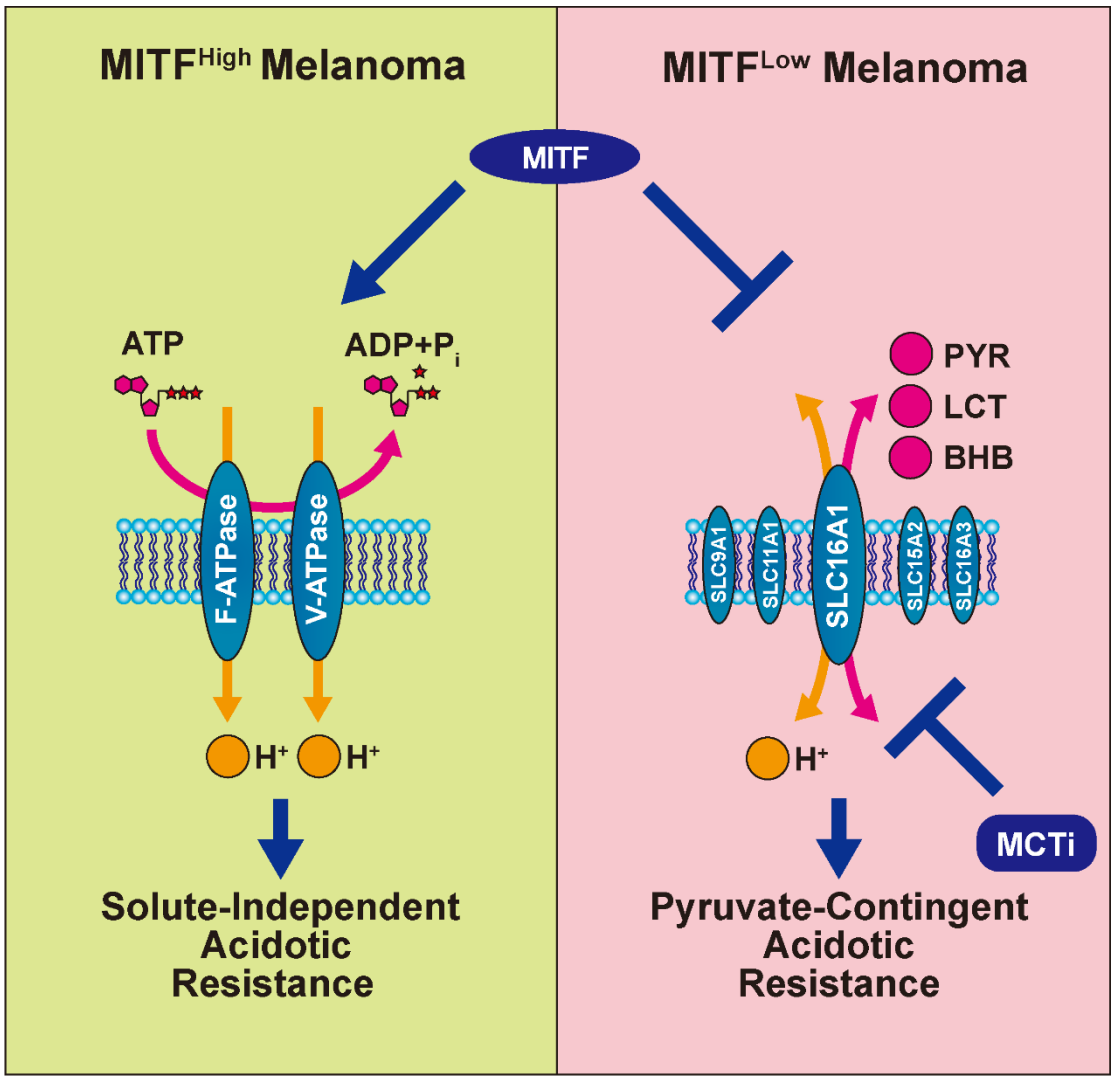

In Brief: MITF-High melanoma resists acidosis without requirement for specific solute conditions, whereas acidotic survival in MITF-Low melanoma relies on the presence of pyruvate, and may be curtailed upon the application of small molecule MCT1 inhibition.

ABSTRACT

The lineage addiction oncogene, Microphthalmia-Associated Transcription Factor (MITF), mediates melanoma phenotypic plasticity – a pathophysiological process that underlies intratumoural heterogeneity, where melanoma cells interchangeably alter their phenotypes and transcriptomic gene signatures depending on the expression levels of MITF. This thesis characterised the presence and nature of MITF-dependent phenotypic plasticity in relation to melanoma resistance to acidotic stress. We show that the acid-resistant phenotypes in MITF-High and MITF-Low cells consisted of distinctly different mechanisms. Analysis of the melanoma proton transporter transcriptome, with experimental verification, showed that while MITF-High melanomas asymmetrically expressed ATP hydrolysis-coupled proton pumps, MITF-Low melanomas favoured the expression of solute carrier proton transporters. This molecular dichotomy was epitomised by the increased expression of Monocarboxylate Transporter 1 (MCT1) in cells following experimental MITF knockdown, which was associated with increased proton-coupled transport activities for monocarboxylic pyruvate, L-lactate, and β-hydroxybutyrate. Interestingly, acidotic resistance following stable MITF-knockdown could be selectively abrogated by reducing ambient pyruvate concentration, or by treatment with the small molecule MCT1 inhibitor, AR-C155858, leading to apoptosis in the acidotic cells with MITF-knockdown. Furthermore, combining AR-C155858 treatment with the $BRAF^{V600E}$ inhibitor, vemurafenib, showed additive effects on the induction of apoptosis in acidotic MITF-knockdown cells. This study thus identified a novel approach to achieve cytotoxicity in the subset of MITF-Low melanoma cells by exploiting their dependency on monocarboxylate transport for acidotic survival.

AUTHORSHIP STATEMENT

Except where indicated otherwise, I declare that the findings described in this thesis are entirely my own.

Oscar Yang

CONTENTS

Glossary of Terms

pH_i	Intracellular pH
pH_e	Extracellular pH
MITF	Microphthalmia-Associated Transcription Factor
BRAF	Rapidly Accelerated Fibrosarcoma Viral Oncogene, Homologue B.
SLC	Solute Carrier.
NCBT	Sodium-Coupled Bicarbonate Transporter
NBCn1	Electroneutral Sodium-Bicarbonate Cotransporter 1
NBCe1	Electrogenic Sodium-Bicarbonate Cotransporter 1
NBCe2	Electrogenic Sodium-Bicarbonate Cotransporter 2
NDCBE	Sodium-Dependent Chloride-Bicarbonate Exchanger
NHE	Sodium-Hydrogen Exchanger
MCT	Monocarboxylate Transporter
ATP	Adenosine Triphosphate
CHC	(2-Cyano-3-(4-hydroxyphenyl)-2-propenoic acid
DIDS	4,4′-Diisothiocyanatostilbene-2,2′-disulfonic acid
MTT	3-(4,5-dimethylthiazol-2-yl)-2,5-diphenyltetrazolium
NH_4Cl	Ammonium Chloride
HEPES	4-(2-Hydroxyethyl)piperazine-1-ethanesulfonic acid
BCECF	2',7'-bis-(2-carboxyethyl)-5-(and-6)-carboxyfluorescein
PYR	Pyruvate
BHB	B-Hydroxybutyrate
LCT	Lactate
VEM	Vemurafenib
ARC	AR-C155858
TCGA	The Cancer Genome Atlas
CCLE	Cancer Cell Line Encyclopaedia
shLacZ	Short Hairpin RNA to β-Galactosidase
shMITF	Short Hairpin RNA to MITF
EV	Empty Vector
GAPDH	Glyceraldehyde 3-Phosphate Dehydrogenase
DAPI	4’-6-Diamidino-2-phenylindole
DMSO	Dimethyl Sulfoxide

CHAPTER 1

INTRODUCTION

The Scope of the Research Question: MITF-Dependent Phenotypic Plasticity in Melanoma Acidotic Resistance

Melanoma is a malignant skin cancer that can arise either from mature pigmented melanocytes in the basal stratum, or alternatively from melanocytic stem cells residing in the hair follicles (Köhler et al., 2017, Moon et al., 2017, Soengas and Patton, 2017). The world-wide estimated age-standardised incidence rates of melanoma is 2.8–3.1 cases per 100,000, and melanoma accounts for the most frequent cause of skin cancer-related deaths (Rastrelli et al., 2014). The incidence of melanoma varies between countries, where Australia reported the highest frequency (37 per 100,000) and the South-Central Asia reports the lowest (0.2 per 100,000) (Ali et al., 2013). Racial skin phenotypes and differences in sun exposure contributed to this trend – in the United States (US), for example, 98.2% of cases are reported amongst light-skinned individuals (Ali et al., 2013).

Similar to the treatment of other cancers, many patients with advanced melanoma achieve clinical responses with the myriad therapeutics currently available, yet retain

minimal residual disease (MRD), ultimately resulting in acquired treatment resistance and disease progression (Rambow et al., 2018). Therefore, understanding the biology of the melanoma MRD is critical for improving the treatment outcome and prognosis in advanced melanoma (Rambow et al., 2018). Several inroads have been made into understanding the biology of melanoma MRD (Kozar et al., 2019). Malignant melanomas that harbour a somatic missense mutation at the Valine 600 position in the *Rapidly Accelerated Fibrosarcoma, Homologue B* (*BRAF*) gene constitute 45-50% of total cases (Davies et al., 2002). Small molecule inhibitors have been developed to target $BRAF^{V600E}$ and its downstream phosphorylation target, Mitogen-Activated Protein Kinase Kinase (MEK), and currently these agents constitute first-line therapeutic treatments in advanced melanoma (Eroglu and Ribas, 2016). Currently, the five-year overall survival in advanced melanoma under combined $BRAF^{V600E}$ and MEK inhibition stands at 36% (Robert et al., 2019), which implies that after a finite period of responsive treatment, melanoma MRD frequently acquires resistance to small molecule $BRAF^{V600E}$ inhibition. Acquired drug resistance in melanoma occurs via the acquisition of gene mutations within the mitogen-activated protein kinase (MAPK) cascade – thereby reducing the sensitivity to BRAF inhibitors (BRAFi) – or alternatively via the activation of parallel molecular signal transduction pathways to bypass the blockade on MAPK signalling (Kozar et al., 2019). Among the mutations in the genes encoding the

different MAPK proteins are missense mutations in NRAS and MEK (Nazarian et al., 2010), and a truncation of the *BRAF*^{V600E} gene leading to autonomous activation (Poulikakos et al., 2011). Alternative signalling pathways activated to compensate for the blockade of the MAPK cascade include the PI3K second messenger system (Marsh Durban et al., 2013), and the AXL receptor tyrosine kinase (Müller et al., 2014).

More recently, functional genomics had enabled another approach to understanding melanoma MRD, via the mapping of transcriptomic gene signatures in therapeutically resistant melanoma cells (Bittner et al., 2000). Single-cell RNA sequencing of malignant cells isolated from patient-derived BRAFi-resistant melanoma tissues identified significant intratumoural heterogeneity, with disease progression and drug resistance emerging from cells expressing a variety of gene signatures (Tirosh et al., 2016). Some studies have shown that melanoma cells with increased expression of the melanoma lineage survival oncogene, Microphthalmia-Associated Transcription Factor (MITF), represent a sizeable subset of the total number of tumour cells that acquire phenotypic drug resistance in melanoma MRD. Others have shown that nelfinavir-induced SMAD2 activity, which resulted in reduced PAX3 and MITF expression, re-sensitised these melanoma cells to MAPK pathway inhibition (Smith et al., 2016). The MITF-High gene signature has thus been well-documented to promote therapeutic resistance to BRAF^{V600E} inhibition in melanoma (Hertzman Johansson et

al., 2013, Johannessen et al., 2013, Kozar et al., 2019).

On the other hand, tumour gene signatures with low levels of MITF expression have also been implicated in melanoma therapeutic resistance (Kozar et al., 2019). One of the best characterised BRAFi-resistant gene signatures in advanced melanoma is characterised by the expression of low levels of MITF, and high expression of AXL (Konieczkowski et al., 2014). Intratumoural regions of melanoma tissue that possess the MITF-Low signature tend to exhibit a slow-cycling phenotype (Ahn et al., 2017). Others have documented the existence of MITF-Low melanoma subpopulations that express high levels of Nerve Growth Factor Receptor (NGFR) (Shaffer et al., 2017), or high levels of the nuclear receptor, Retinoid X Receptor (RXR) (Rambow et al., 2018). It thus appears that flexibility and redundancy in the expression of drug resistance genes may be built into the system such that tumour cells with contrasting gene signatures may survive $BRAF^{V600E}$ inhibition, giving rise to the transcriptomic heterogeneity on display in BRAFi-resistant melanoma (Konieczkowski et al., 2014).

Although the resistant melanoma cells express different genes and fall into different phenotypic classes, they are still drug-resistant (Arozarena and Wellbrock, 2019). For example, the metabolism of $MITF^{high}$ melanomas was shown to be driven by mitochondrial oxidative phosphorylation and the formation of monounsaturated fatty acids (Haq et al., 2013, Vivas-García et al., 2020), whilst $MITF^{low}$ melanomas

favour aerobic glycolysis and the formation of saturated fatty acids (Vivas-García et al., 2020, Kumar et al., 2007). $MITF^{high}$ melanomas tend to proliferate due to direct effects of MITF on CDK2 regulation (Du et al., 2004), and via T-Box Transcription Factor 2 (TBX2)-mediated transrepression of cell cycle checkpoint inhibitors, $p21^{Cip1}$ and $p14^{ARF}$ (Pan et al., 2015), whereas $MITF^{low}$ melanomas demonstrate invasive phenotypes via downregulation of the diaphanous-related formin, Dia1, the reorganisation of the actin cytoskeleton, and subsequently increased ROCK-dependent cell migration (Carreira et al., 2006). It was therefore apparent that the intratumoural heterogeneity in drug resistant melanoma entailed tumour subpopulations that were phenotypically distinct, such that drug resistance itself may be mediated via different mechanisms in these tumour subpopulations, as reviewed in Arozarena and Wellbrock, 2019 (Arozarena and Wellbrock, 2019).

In addition to tumour heterogeneity, melanomas also show phenotypic plasticity (Arozarena and Wellbrock, 2019). Plasticity implies that the phenotypes on display in melanoma cells are not permanently fixed, but may be dynamic and changeable depending on circumstances such as the molecular pathway being targeted by drug treatment, or dosage of drug therapy (Bai et al., 2019). That is, mechanistically, melanoma drug resistance and intratumoural heterogeneity do not necessitate the acquisition of driver gene mutations, or the inheritance of such drug resistant gene

mutations from mother to daughter cancer cells (Shaffer et al., 2017). Instead, drug resistance and intratumoural heterogeneity in melanoma may be regulated epigenetically, through the reversible transcriptional regulation of gene expression, such that drug resistance may be a product of transient upregulation of drug resistant genes during periods of therapeutic stress (Shaffer et al., 2017). The transient and dynamic nature of drug resistance emphasises the plasticity of intratumoural phenotypic heterogeneity, and places transcription factors and their responsive transcriptomes at the forefront of research into melanoma drug resistance (Boumahdi and de Sauvage, 2020). As such, intratumoural heterogeneity in melanoma involves the plastic expression of contrasting gene signatures, which makes therapeutic responses highly unpredictable, and often short-lived (Zeng et al., 2020).

The basic hypothesis of this thesis was premised on the existence of intratumoural heterogeneity and phenotypic plasticity in advanced melanoma, as outlined above. It was hypothesised that phenotypic plasticity was a pathophysiologic feature not only affected therapeutic resistance, but may in suitable instances be applicable to resistance to microenvironmental stressors as well. Well-recognised pathophysiological stressors imposed by the dysplastic stroma include hypoxia, acidosis, oxidative stress, and nutrient deprivation (Pavlova and Thompson, 2016). Of the myriad microenvironmental resistance mechanisms, we reasoned that acidotic resistance may

be the trait most likely to exhibit phenotypic plasticity in melanoma. Intracellular pH homeostasis is mediated by a complex system of membrane proton transporters, encoded by more than 100 gene loci within the human genome, as reviewed in Bohme and Bosserhoff, 2016 (Bohme and Bosserhoff, 2016). Proton transport mechanisms utilised by these transporters are also highly diverse, broadly classifiable as proton pumps, carriers, and channels (Alexander et al., 2019). Given the mechanistic complexity involved in intracellular pH regulation, it was plausible that these proton transporters may be heterogeneously regulated within the melanoma tissue, in a manner consistent with intratumoural heterogeneity and phenotypic plasticity. We therefore set out in this thesis to investigate the presence and nature of phenotypic plasticity in melanoma acidotic resistance. We also tested therapeutic strategies deduced from the working experimental knowledge.

Clinical Aspects of Malignant Melanoma

Cell of Origin Currently there are different views of the cellular origin of malignant melanoma, with pigmented melanocytes of the basal epidermis and melanocytic stem cells within the hair follicles both shown to be capable of facilitating melanomagenesis (Köhler et al., 2017, Moon et al., 2017). Melanocytes themselves are neural crest derivates found predominantly in skin and eyes (Cichorek et al., 2013). In

the skin, melanocytes are present in the basal epidermis, attached to the basement membrane (Cichorek et al., 2013). In the eyes, melanocytes are located in the uveal tract and the retinal pigmented epithelium (Cichorek et al., 2013). The main physiological function of melanocytes is to produce melanin, a brown and non-refractile granular pigment that protects the skin from ultraviolet (UV) radiation, and determines skin and hair colour (MacKie, 2000). Melanoma arises when normal melanocytes undergo dysplasia and malignant transformation, as reviewed in Shain and Bastian, 2016 (Shain and Bastian, 2016). Clinically, melanoma hallmarks upon inspection include an irregularly shaped and coloured papule or plaque (Tsao et al., 2015). Four types of melanoma are clinically recognised: (1) Superficial spreading melanoma; (2) Lentigo maligna melanoma; (3) Nodular melanoma; and (4) Acral lentiginous melanoma (Table 1.1), as reviewed in Rabbie et al, 2019 (Rabbie et al., 2019).

Incidence and Epidemiology of Malignant Melanoma The annual European incidence of malignant melanoma varies between 3–5 cases per 100,000 population in Mediterranean countries and 12–35/100,000 in Nordic countries, whereas cases can exceed 50 per 100,000 population in Australia or New Zealand (Hollestein et al., 2012). Melanoma incidence peaks at 65 years-old of age, and any age can be affected (Forsea

et al., 2014). More than 55,000 new cases of melanoma are diagnosed yearly in the USA, with the majority occurring in the 15-50 years old group (Glazer et al., 2017). The current estimated lifetime risk of developing malignant melanoma in the US approaches 1 in 50 (Glazer et al., 2017).

Ultraviolet (UV) irradiation was identified as a major carcinogen involved in melanomagenesis, as reviewed in Lo and Fisher, 2014 (Lo and Fisher, 2014). UV irradiation is associated with a distinct DNA damage signature in melanocytes and a high rate of mutations per megabase (Mb) (Alexandrov et al., 2013). The best primary prevention for melanoma is thus physical protection using at least 1 sun protection behaviour, defined as specifically using sunscreen, wearing a hat, or staying mostly in the shade when outdoors during peak UV radiation hours (Tabbakh et al., 2019). In a randomised trial, prevention of UV exposure with measures including the regular use of sunscreen has been shown to diminish the incidence of primary cutaneous melanomas in an Australian population (Green et al., 2011).

Pathogenesis of Malignant Melanoma The pathogenesis of malignant melanoma remains largely undefined, as reviewed in Shain and Bastian, 2016 (Shain and Bastian, 2016). Energy from solar UVB radiation (280-320nm wavelength) is absorbed through the skin by cellular proteins and DNA, and UVB can cause extensive

mutagenic DNA lesions within melanocytes (von Thaler et al., 2010). Genetically, approximately 50% of melanomas exhibit an activating mutation in the gene encoding the BRAF protein (Flaherty et al., 2010, Davies et al., 2002). BRAF is a proto-oncogene that encodes a serine/threonine protein kinase as part of Mitogen-Activated Protein kinase (MAPK) signalling cascade, which in turn promotes cell growth and proliferation (Kumar et al., 2003). In the physiological setting, BRAF homo- or heterodimerises with another RAF kinase in response to growth signals (Matallanas et al., 2011). However, an activating missense mutation such as valine to glutamic acid at position 600 in the BRAF protein causes BRAF to act as a self-sufficient and continuously activated monomer (Solit and Sawyers, 2010). The result is uncontrolled cell proliferation, which drives tumourigenesis in melanocytes (Shain and Bastian, 2016). This $BRAF^{V600E}$ mutation is the most common *BRAF* alteration, and constitutes about 90% of the *BRAF* activating mutations, occurring in approximately 50% of all metastatic melanomas in the European population (Chapman et al., 2011). The V600K mutation is the second most common *BRAF* mutation (McCubrey et al., 2006).

Another critical genetic driver of melanomagenesis is the expression of the master lineage-specific transcription factor, Microphthalmia-Associated Transcription Factor (MITF) in melanoma (Hartman and Czyz, 2015b). MITF is a lineage-specific master transcription factor present in melanocytes, osteoclasts, and mast cells, whose

Table 1.1: The Clinical Features of Melanoma Subtypes. The clinical features of melanoma subtypes are described, including typical location, median age of onset, duration of pre-metastatic phase, frequency of occurrence, and ethnicity.

Table 1: Clinical Features of Melanoma Subtypes

Type	Location	Median Age (Years)	Pre-Metastatic	Frequency (%)[a]	Ethnicity
Lentigo Maligna	Sun-Exposed Surfaces (Head, Neck)	70	5-15 years	10	Caucasian
Superficial Spreading	All Surfaces (Back, Legs)	47	1-7 years	27	Caucasian
Nodular	All Surfaces	50	Months-2 years	9	Caucasian
Acral Lentiginous	Palms, Soles, Nail Beds	61	Months-8 years	1	Asian, Black

[a] 53% of melanomas are unclassified.

Wolff K et al. (2011). Fitzpatricks Dermatology in General Medicine 8th Edition. New York: McGraw-Hill.

transcriptional activity governs vital cellular functions such as differentiation, pigmentation, proliferation, survival, mitochondrial metabolism, and apoptosis (Kawakami and Fisher, 2017). High-density single nucleotide polymorphism arrays revealed *MITF* to be amplified in up to 20% of melanomas, and ectopic expression of MITF in conjunction with the $BRAF^{V600E}$ mutation transformed primary human melanocytes, demonstrating that MITF could function as a melanoma oncogene (Garraway et al., 2005). Transcriptionally, MITF can bind to the *Bcl2* promoter, and transactivation of anti-apoptotic effectors by MITF enables lineage survival and treatment resistance (McGill et al., 2002). A germline $MITF^{E318K}$ mutation has also been identified in melanoma as a causal factor in familial melanoma syndromes (Yokoyama et al., 2011, Bertolotto et al., 2011). These data suggest that MITF represents a key molecular driver of melanomagenesis (Hartman and Czyz, 2015a). Other selected somatic genetic alterations in melanomagenesis are listed in Table 1.2.

Germline mutations in melanoma can give rise to familial melanoma, which accounts for 5-10% of total cases, as reviewed in Rossi et al, 2019 (Rossi et al., 2019). *CDKN2A*, located in the 9p21 chromosomal region, is the major high-penetrance susceptibility gene in familial melnaoma, with germline mutations identified in up to 40% of melanoma families (Monzon et al., 1998). Mutations in the other melanoma predisposition genes are relatively rare – *MITF, CDK4, VAP1, TERT, POT1, ACD*, and

TERF2IP – contributing together to explain a further 10% of familial clustering of melanoma (Goldstein et al., 2006). The underlying germline genetic susceptibility remains unexplained in approximately half of melanoma families, as reviewed in Palmieri et al, 2015 (Palmieri et al., 2015).

In terms of molecular pathology, melanomas can also be classified genomically depending on the identified genomic alterations, through DNA, RNA, and protein-based analyses (Akbani et al., 2015). In this system, malignant melanomas were classified into one of four subtypes based on the pattern of the most prevalent significantly mutated genes: Mutant *BRAF*, mutant *RAS*, mutant *NF1*, and triple-wild type (which was enriched in *KIT* mutations and focal amplifications) (Akbani et al., 2015). *MITF* amplification in this context was observed at significant frequencies in the *BRAF* mutant subtype (Akbani et al., 2015). In addition, consensus hierarchical clustering analysis of the melanoma transcriptome in 329 samples identified three robust stable clusters, namely the "Immune", "Keratin", and the "MITF-Low" clusters (Akbani et al., 2015). The MITF-Low transcriptomic cluster was characterised by low expression of genes associated with pigmentation and epithelial expression, including several MITF target genes (Akbani et al., 2015). This MITF-Low cluster was significantly enriched with genes preferentially expressed within the nervous system and/or associated with neuronal development or other organ-specific embryologic

development (Akbani et al., 2015). Taken together, MITF features prominently in the pathogenesis of malignant melanaoma, displaying both somatic and germline mutations and gene amplifications that contribute to melanomagenesis, as well as being one of the main drivers of melanoma transcriptomic clustering, as reviewed in Goding and Arnheiter, 2019 (Goding and Arnheiter, 2019).

Clinical Features of Malignant Melanoma Clinically, there are four major subtypes of invasive cutaneous melanoma: Superficial spreading melanoma, nodular melanoma, lentigo maligna, and acral lentiginous melanoma (Table 1.1) (Hawryluk and Tsao, 2014). Most melanomas arise as superficial lesions that are limited to the confines of the epidermis, where they may remain comparatively nascent for several to many years (Knackstedt et al., 2018). During this stage, known as the horizontal or radial growth phase, the melanoma is in principle curable by surgical excision (Knackstedt et al., 2018). Melanomas that infiltrate into the dermis are considered to be in the vertical growth phase, and acquire invasive or metastatic potential (McDermott et al., 1998). Lentigo maligna melanoma, superficial spreading melanoma, and acral lentiginous melanoma are characterised by the presence of a horizontal growth phase that does not involve a breach in the dermal barrier (Clark et al., 1969). This radial growth allows for clinical detection before deeper invasion and metastasis develop (Tannous et al., 2000).

In contrast, nodular melanomas do not possess an identifiable radial growth or *in situ* phase, and appear to directly enter the vertical growth phase at neoplastic transformation, resulting in thicker tumour bulk at diagnosis (Erkurt et al., 2009).

The probability of metastases with an invasive, vertical growth-phase melanoma is predicted histologically by measuring tumour thickness, in millimetres, from the granular cell layer of the epidermis (or overlying area of ulceration) to the deepest malignant cell in the dermis or subcutaneous fat (Breslow, 1970). This thickness value is termed the Breslow depth (Breslow, 1970). Other histologic factors, including ulceration of the tumour, mitotic rate, presence of lymphovascular invasion, microsatellites, perineural invasion, and the presence of lymphocytes infiltrating the tumour, can also affect the risk of local recurrence and/or metastatic potential of the tumour (Levene, 1980).

Superficial spreading melanoma is the most prevalent histological melanoma subtype, accounting for approximately 70% of all melanomas (Lasithiotakis et al., 2006). Most superficial spreading melanomas are diagnosed as thin, highly curable tumours that are less than or equal to 1mm in thickness (Lasithiotakis et al., 2006). Approximately two-thirds of all melanomas arise *de novo* without a preceding naevus, though superficial spreading melanoma represents the clinical subtype most likely to be preceded by a pre-existing naevus (Pampena et al., 2017). Superficial spreading

Table 1.2: Selected Genetic Alterations in Malignant Melanomas, Adapted from Gray-Schopher and Colleagues (Gray-Schopfer et al., 2007). Common driver gene mutations found in malignant melanoma, and their frequency of occurrence.

Gene type	Gene	Alteration frequency/type(s) in melanoma (%)
Oncogenes	*BRAF*	50–70% mutated
	NRAS	15–30% mutated
	AKT3	Overexpressed
Tumour suppressors	*CDKN2A*	30–70% deleted, mutated or silenced
	PTEN	5–20% deleted or mutated
	APAF-1	40% silenced
	p53	10% lost or mutated
Others	Cyclin D1	6–44% amplified
	MITF	10–16% amplified

melanoma can occur in any anatomic region of the body, but there is a tendency to grow on the back in men and women, and on the lower appendages in women (Pampena et al., 2017). Superficial spreading melanoma classically presents as a heterogeneously pigmented macule or thin plaque with an irregular border, ranging from a few millimetres to several centimetres in diameter (Clark et al., 1969). Lesions may be coloured with multiple shades of brown, blue, black, grey, and white (Clark et al., 1969).

Nodular melanomas are the second most prevalent type of malignant melanoma, accounting for 15 to 30 percent of all cases (Clark et al., 1986). Nodular melanomas may appear as distinct darkly pigmented, polypoid, or pedunculated papules or nodules, but they may also present insidiously as lesions with uniform colour or be amelanotic, with symmetric borders, and relatively small diameter in size, making early detection more challenging (Geller et al., 2009). Most nodular melanomas are greater than 2mm in thickness at the time of the diagnosis, and they are typically larger than the superficial spreading melanoma counterparts (Warycha et al., 2008). Consistent with this observation, over 50 percent of melanomas greater than 2 mm in thickness will go on to be histologically shown as the nodular subtype (Demierre et al., 2005).

Lentigo maligna melanoma accounts for 10 to 15 percent of all melanomas, although the incidence is rising in the United States, particularly in older individuals (Swetter et al., 2005). Lentigo maligna melanoma frequently arises in chronically sun-

damaged skin areas in older individuals, and the lesions begin as tan or brown macules (Clark and Mihm, 1969). The lesion gradually increase in size over a period of years, and appearance-wise may develop darker, asymmetric foci of pigmentation, colour variegation, and raised areas that signify vertical growth within the precursor *in situ* melanoma (Kasprzak and Xu, 2015).

The acral lentiginous subtype accounts for <5% of all melanomas (Lee et al., 2015b). However, ethnically it is the most common type of melanoma among individuals with darker skin phototypes, who are inherently at lower risk for more UV-related melanoma subtypes (Kato et al., 1999). Acral lentiginous melanomas arise frequently on non-exposed areas of skin, including palmar, plantar, and subungual surfaces (beneath the nail plate) (Kato et al., 1999). Acral lentiginous melanomas first appear as dark brown to black, irregularly pigmented macules or patches, with raised areas, ulceration, bleeding, and/or larger diameter generally signifying deeper invasion in the dermis (Coleman et al., 1980). Occasionally, acral melanoma can present as amelanotic or hypomelanotic lesions mimicking benign diseases, such as warts, calluses, tinea pedis, nonhealing ulcers, or ingrown toenails (Buka et al., 2001).

Clinical Diagnosis of Melanoma. Diagnosis of melanoma relies first on clinical recognition, followed by subsequent histopathological confirmation (Davis et al., 2019).

Clinical diagnosis of melanoma may be challenging, even for the most experienced dermatologist, especially in the case of early melanoma (Davis et al., 2019). The estimated sensitivity of clinical diagnosis for experienced dermatologists is measured at approximately 70% (Gachon et al., 2005). Clinical diagnosis of melanoma may be greatly improved with the use of diagnostic aids such as dermoscopy (Jones et al., 2019).

In order to improve the clinical recognition of melanoma, the acronym ABCD (asymmetry, border irregularity, colour variegation, diameter >6mm) was devised by New York University in 1981 to educate primary care physicians on the identification of early melanoma (Abbasi et al., 2004). In terms of identifying the different clinical subtypes of melanoma, the ABCD criteria apply mostly to diagnosing superficial spreading melanoma, such that the criteria are less generalisable to the nodular and desmoplastic melanoma subtypes (Friedman et al., 1985). In 2004, the criteria were enhanced with the addition of "E" (evolution) to incorporate the fundamental concept of change, in terms of size, shape, or colour, or a new lesion (Abbasi et al., 2004). Thus, taken together, the ABCDE criteria for clinical diagnosis of melanoma currently stands as (Abbasi et al., 2004):

A: Asymmetry (if a lesion is bisected, one half is not identical to the other).

B: Border irregularities.

C: Colour variegation (presence of multiple shades of red/blue/black/grey).

D: Diameters >6mm.

E: Evolution (a lesion that is changing in size, shape, or colour).

Histopathologic Diagnosis of Melanoma. A complete full thickness excisional biopsy of suspicious lesions, with a defined margin of normal skin and part of the subcutaneous fat of 1-3mm, should be performed to achieve histopathologic diagnosis with curative intent (Marsden et al., 2010). No single pathologic feature of melanoma is histologically diagnostic, so tissue diagnosis of melanoma relies on a combination of architectural, cytologic, and host response features (Elmore et al., 2017). The presence of atypical melanocytes (i.e., melanocytes that are larger than normal and have large hyperchromatic nuclei, irregular nuclear shape and nuclear polymorphism, abnormal chromatin pattern, and prominent nucleoli), plus architectural disorder (i.e., asymmetry, poor circumscription, nests of melanocytes of various sizes and shapes in the lower epidermis and dermis) are required for the diagnosis (Price et al., 1976). Immunohistochemistry can be helpful in the evaluation of difficult melanocytic lesions (Ohsie et al., 2008). The most widely used markers are S-100, MART-1, and HMB-45 (Viray et al., 2013). Newer molecular techniques may also aid in melanoma diagnosis, including comparative genomic hybridisation, fluorescence *in situ* hybridisation (FISH), gene expression profiling, and adhesive patch genomic analysis (Ji et al., 2016).

Differential Diagnosis of Melanoma. Multiple melanocytic or non-melanocytic lesions resemble melanoma clinically, and sometimes histologically (Urso et al., 2005). They include: Common melanocytic naevus; atypical melanocytic naevus; traumatised naevus; blue naevus; lentigo (ink spot); Spitz naevus; pigmented actinic keratosis; seborrheic keratosis; pyogenic granuloma; cherry haemangioma; and dermatofibroma (Perez et al., 1993).

Systemic Treatment of Unresectable Advanced Melanoma The therapeutic options for unresectable advanced melanomas have been revolutionised by the advent of immunotherapies and targeted therapies (Michielin et al., 2019). Both strategies have shown markedly improved survival rates compared to the use of conventional chemotherapy regimens, such as dacarbazine (Chapman et al., 2011). However, despite the progress made in the treatment of advanced melanoma, a major barrier to therapy in advanced disease remains the onset of acquired therapeutic resistance following a period of clinical response (Winder and Virós, 2018). Treatment resistance is a key factor that negatively impacts on disease prognosis in the majority of melanoma patients (Winder and Virós, 2018).

Immunotherapy for advanced melanoma. Currently utilised immunotherapeutic agents for advanced melanoma include monoclonal antibodies against Cytotoxic T-Lymphocyte-Associated Antigen 4 (CTLA-4), and programmed cell death protein-1 (PD-1), collectively known as the immune checkpoint inhibitors (June et al., 2017). Some of the evidence for the use of these immunotherapy agents in advanced melanoma was derived from clinical trials using anti-CTLA-4 and anti-PD-1 antibodies for the management of locoregional melanoma disease in the adjuvant setting (Michielin et al., 2019).

Mechanistically, the complete activation of T-cells following antigen-T-cell receptor (TCR) activation requires further co-stimulation via the T-cell surface protein CD28 (Esensten et al., 2016). T-cell CD28 can be activated by binding to its ligands on the surface of antigen presenting cells – namely CD80 (B7-1) and CD86 (B7-2) (Esensten et al., 2016). Without the co-stimulation from CD28, isolated TCR activation leads to T cell anergy and the development of immune tolerance (Esensten et al., 2016). Cytotoxic T-Lymphocyte-Associated Protein 4 (CTLA-4) is a T cell surface protein homologue of CD28, and both CTLA-4 and CD28 compete antagonistically for CD80 and CD86 binding (Wei et al., 2018). Therefore, the presence of CTLA-4-ligand binding competes for the co-stimulatory signal transduced by CD28-ligand binding, and represents an endogenous mechanism to limit aberrant autoimmune activation

following inadvertent self-antigen-TCR binding (Wei et al., 2018). In contrast, the clinical use of a monoclonal antibody that binds to and disables T-Cell CTLA-4 permits sustained CD28 and T-cell activation and proliferation in response to tumour antigens in cancer (Boutros et al., 2016). In the EORTC 18071 trial that tested the use of the anti-CTLA-4 antibody ipilimumab in the treatment of advanced stage III melanoma following surgical resection, the rate of overall survival was 65.4% in the ipilimumab group, compared with 54.4% in the placebo group (HR for death, 0.72; 95% CI 0.58-0.88; P=0.001) (Eggermont et al., 2016). However, the treatment regimen involving ipilimumab, consisting of 10mg/kg every 3 weeks for four cycles, followed by treatment every three months for up to 3 years, was associated with a number of immune related adverse events (irAEs), including autoimmune colitis and endocrinopathies (Eggermont et al., 2016).

Due to the toxicity profile of anti-CTLA-4, anti-PD-1 immunotherapy represents the preferred treatment option in advanced melanoma (Michielin et al., 2019). Anti-PD1 therapy (nivolumab, pembrolizumab), or anti-PD-1 blockade combined with anti-CTLA-4 blockade (ipilimumab) are currently recommended as the first-line standard-of-care immunotherapy treatments for unresectable stage III/IV melanoma (Michielin et al., 2019). PD-1's role in mediating T cell activation occurs at a later mechanistic stage than CTLA-4 (Sharpe and Pauken, 2018). In the presence of the PD-1 ligand

(PDL-1) – PDL-1 being a member of the B7 family of CD28 ligands – PD-1-PDL-1 binding induces a form of terminal T cell differentiation termed T-cell exhaustion, and diminishes the immune response in order to limit collateral tissue damage (Salmaninejad et al., 2019). PD-1 knockout mice have been shown to develop lupus-like glomerulonephritis and dilated cardiomyopathy (Nishimura et al., 1999). In contrast, the expression of PD-L1 on the surface of tumour cells suppresses the anti-tumour activity of CD4 T- cells, by binding to T-cell PD-1 and inducing T-cell exhaustion (Iwai et al., 2002). Therefore, treatment of melanoma patients with anti-PD-1 enables sustained activation of the immune response against tumour antigens (Mahoney et al., 2015). The superiority of nivolumab compared with dacarbazine (DTIC) chemotherapy was demonstrated for BRAF-WT melanoma patients in the CheckMate066 trial, a prospective randomised, first-line trial, with an HR for death of 0.42; 99.79% CI 0.25-0.73; P<0.001, and a HR for death or progression of disease of 0.43; 95% CI 0.34-0.56; P<0.001 (Robert et al., 2015a). Superiority of anti-PD-1 antibodies (Nivolumab, Pembrolizumab) compared with ipilimumab has been further shown in two prospective randomised trials, CheckMate 067 and KEYNOTE-006 (Wolchok et al., 2017, Robert et al., 2015b). Based on these results, anti-PD-1 blockade has been propelled to the status of standard of care for all patients, regardless of their *BRAF* mutation status, in the first line setting for advanced melanoma (Michielin et al.,

2019).

Targeted Therapy in Advanced Melanoma. In the case of *BRAF*-Mutated Melanoma, additional first-line therapeutic options include small molecule BRAF and MEK inhibition. The BRIM-3 trial for use of single-agent $BRAF^{V600E}$ inhibitor, vemurafenib, in metastatic melanoma showed an improvement in overall survival at 6 months, with 84% overall survival in the vemurafenib arm, compared with 64% in the dacarbazine arm (Chapman et al., 2011). BRAF&MEK combinational therapy has subsequently been shown to achieve superior outcomes than single-agent BRAF inhibition, in terms of clinical response rates, progression-free survival, and overall survival (Robert et al., 2014). In addition to improved efficacy, dermatological side effects were reduced with combinational therapy, though the addition of MEK inhibition added specific toxicities (e.g. Muscle, heart, eye) (Long et al., 2015). Currently, single agent BRAFi is recommended for use in only cases where there is absolute contraindication to MEK inhibitors (Michielin et al., 2019).

Vemurafenib, the targeted therapeutic agent against $BRAF^{V600E}$, causes apoptosis in melanoma cell lines via disruption of the mitogen-activated kinase signalling pathway, which transduces second messenger signals through sequential BRAF-MEK-ERK phosphorylation events (Biechele et al., 2012). Vemurafenib only acts in

melanomas in which there is a $BRAF^{V600E}$ mutation (Fisher and Larkin, 2012). It also possesses efficacy against the rarer $BRAF^{V600K}$ mutation (McArthur et al., 2014). Against BRAF-wild type melanoma, vemurafenib paradoxically stimulates BRAF-wt activity and promotes tumour proliferation, and therefore is not indicated for therapeutic use (Halaban et al., 2010).

Treatment Resistance to Targeted Therapies in Advanced Melanoma. Although BRAFi and MEKi efficiently inhibit the MAPK pathway by reducing ERK activation and stalling cell proliferation in cells harbouring the $BRAF^{V600E}$ mutation, MAPK reactivation subsequently occurs in up to 80% of melanomas that acquire BRAFi resistance (Kozar et al., 2019). The consistent reactivation of MAPK cascade signalling in advanced melanoma indicates that melanoma cells are highly dependent on the MAPK pathway and rapidly adapt to its inhibition (Arozarena and Wellbrock, 2019). The main mechanisms leading to MAPK reactivation and sustained ERK signalling involve genetic alterations to the components within the cascade, such as mutations to *BRAF*, *NRAS*, *MEK*, and *NF1* (Nazarian et al., 2010). Additionally, the expression of the RAF isoform, CRAF (RAF1), can reduce the effectiveness of BRAF inhibitors and promote drug resistance via substitutive MEK activation (Kozar et al., 2019). Furthermore, the kinase COT, also known as MAP3K8, which directly activates

MEK/ERK signalling in a RAF-independent manner, can often be elevated in BRAFi-resistant melanomas to replace the function of RAF kinase (Kozar et al., 2019). Alternatively, *BRAF* gene amplification or splice variants, which can be identified in up to 30% of patients with BRAFi-resistant melanomas (Corcoran et al., 2010), have also been shown to lead to enhanced BRAF S729 phosphorylation, BRAF homo/heterodimerisation, and downstream MEK activation (Vido et al., 2018).

In addition to mechanistic reactivation of MAPK signalling, the PI3K-mTOR pathway is also frequently activated in drug-resistant melanomas to bypass the therapeutic $BRAF^{V600E}$ blockade (Atefi et al., 2011). Accentuated PI3K signalling can be induced via deletion or loss-of-function mutation to the tumour suppressor gene – *PTEN* – which occurs in approximately 10% of treatment-resistant melanomas (Yajima et al., 2012), or via activation of upstream receptor tyrosine kinases (RTKs) that phosphorylate PI3K (Haluska et al., 2007). The resultant increase in the flux through the PKB/AKT survival signalling cascade negates the effect of small-molecule inhibition of $BRAF^{V600E}$ and MAPK signalling in advanced melanoma (Davies, 2012).

As previously mentioned, an increasingly recognised aspect of therapeutic tolerance in melanoma is the concept of phenotypic plasticity in treatment resistance (Arozarena and Wellbrock, 2019). To elaborate on this mechanistic model, any given melanoma cell can exist in different and interchangeable phenotypic states, most of

which share the convergent trait of therapeutic resistance to BRAFi (Bai et al., 2019). A melanoma cell can enter and exit a given drug resistant cell state by altering its transcriptional program (Kozar et al., 2019). In effect, treatment resistance in melanoma need not be permanently acquired through defined gene mutations, but may alternatively constitute transient phenotypes reversibly expressed through differential regulation of key transcription factors (Shaffer et al., 2017). Shaffer and colleagues demonstrated the transient and non-heritable nature of melanoma cellular drug resistance by applying Luria and Delbruck's fluctuation analysis to model drug resistance (Luria and Delbruck, 1943). In this experiment, a fractional killing dose of 1μM vemurafenib selected out single resistant melanoma cells from a cell culture dish (Shaffer et al., 2017). These single cells were then expanded out for 7-8 divisions, before the cells were re-challenged with vemurafenib (Shaffer et al., 2017). The lack of large numbers of resistant colonies following re-challenge suggested that drug resistance was sporadic and transient, rather than an inheritable trait permanently acquired through defined genetic mutations in the parental cell (Shaffer et al., 2017). In this study, targeted DNA sequencing of 119 cancer related genes revealed no new mutations in the treatment resistant subclones (Shaffer et al., 2017). On the other hand, pre-selecting single cells with high transcriptional expression of resistance genes via single-cell RNA-Seq – for example, that of EGFR, NGFR, and AXL – followed by drug

treatment with vemurafenib in the selected cell population, resulted in increased number of drug resistant subclones, suggesting that drug resistance may be an epigenetic phenomenon governed by the reversible upregulation of resistance genes – an event that may also be partially dependent on the pre-existent gene expression signatures (Shaffer et al., 2017). Taken together, melanoma cells are not only capable of adapting to cytotoxic therapies via acquiring fixed genetic mutations, but also tend to transiently and reversibly alter their transcriptional phenotypes in order to survive therapeutic challenges (Shaffer et al., 2017).

The current paradigm for modelling phenotypic plasticity in melanoma's resistance to $BRAF^{V600E}$ inhibition involves the heterogeneous expression and regulation of the master transcription factor, MITF (Arozarena and Wellbrock, 2019). MITF is the melanocyte lineage-specific transcription factor that governs melanocytic survival, and MITF regulates the reversible transitioning between different cellular phenotypes including proliferation, cell migration, differentiation, pigmentation, and mitochondrial metabolism, as reviewed in Goding and Arnheiter, 2019 (Goding and Arnheiter, 2019). High MITF expression in melanoma promotes a proliferative and pigmented phenotype in melanoma, whereas low melanoma MITF expression permits the onset of epithelial-mesenchymal transition and metastatic invasion, as reviewed in Bai et al, 2019 (Bai et al., 2019). Low MITF expression in melanoma occurs in

conjunction with the upregulation of alternative transcription factors such as TEA Domain (TEAD) transcription factors (Verfaillie et al., 2015), Activator Protein 1 (AP-1) (Verfaillie et al., 2015), NF-κB (Konieczkowski et al., 2014), as well as the upregulation of receptor tyrosine kinases including Anexelekto (AXL) (Müller et al., 2014), Epidermal Growth Factor Receptor (EGFR) (Ji et al., 2015), Platelet-Derived Growth Factor Receptor (PDGFR) (Müller et al., 2014), Nerve Growth Factor Receptor (NGFR) (Shaffer et al., 2017), and the nuclear receptor, Retinoid X Receptor (RXR) (Rambow et al., 2018). BRAFi resistance is a phenotype observed in both MITF-high and low cells (Kozar et al., 2019). High MITF expression increases the direct transcription of the anti-apoptotic effector, B-cell lymphoma 2 (Bcl2) protein to prevent mitochondrial permeabilization (McGill et al., 2002), and high MITF expression augments Peroxisome Proliferator-Activated Receptor Gamma Coactivator 1α (PGC1α)-mediated mitochondrial biogenesis and oxidative phosphorylation to offset the inhibitory effects of blocking $BRAF^{V600E}$-mediated aerobic glycolysis (Vazquez et al., 2013). In contrast, low MITF expression permits the expression of RTKs such as EGFR and AXL to redirect growth factor signals through the PI3K/AKT survival pathway (Konieczkowski et al., 2014), and disinhibits ROCK-dependent cell migration to evade cytotoxic concentrations of BRAFi (Carreira et al., 2006). Accordingly, MITF-High drug-resistant cells have been coined the “Proliferative” melanoma cell state,

whilst the MITF-Low and AP-1-High drug resistant melanoma cells have been coined the “Invasive” cell state (Rambow et al., 2018).

Recently discovered treatment-resistant melanoma cell states with low expression of MITF are still being actively characterised, examples of which include the MITF-Low and RXR-High, “Neural Crest Stem Cell” (NCSC) cell state (Rambow et al., 2018), and the MITF-Low and NGFR-High, “Slow-Cycling Neural Crest” cell state (Su et al., 2017). It can therefore be seen that, depending at least in part on the expression or activity level of MITF, melanoma cells switch between phenotypically different and drug-resistant transcriptional cell states, most of which are proposed to be capable of resisting $BRAF^{V600E}$ inhibition (Arozarena and Wellbrock, 2019). Future research that enhances the understanding of these drug resistant melanoma cells may be key to re-sensitising advanced melanoma to existing melanoma therapies (Arozarena and Wellbrock, 2019). Below is an in-depth description of the molecular mechanics of MITF regulation in melanoma.

Microphthalmia-Associated Transcription Factor (MITF) in Melanoma

MITF in Melanocytes and Malignant Melanoma Melanocytes are cutaneous melanin pigment-producing cells that reside in the basal epidermis (Hartman and Czyz, 2015a). Melanocytic differentiation, proliferation and survival are primarily

regulated by MITF (microphthalmia-associated transcription factor), a melanocyte lineage-specific transcription factor, as reviewed in Goding and Arnheiter, 2019 (Goding and Arnheiter, 2019). The Microphthalmia (*mi*) gene locus was first named in 1942 by Hertwig, after she discovered an offspring with abnormally small eyes, among the progeny of an X-ray irradiated mouse (Hertwig, 1942). In 1993, Arnheiter's group discovered that the gene product of *mi* locus was a novel member of the basic-helix-loop-helix leucine zipper (bHLH-ZIP) family of transcription factors (Hodgkinson et al., 1993). MITF was found to be expressed in the developing eye, ear, and skin, the anatomical sites affected by *mi* (Arnheiter, 2010). Since its first description, more than 10,000 genes have seen been shown to harbour ChIP-seq peaks that indicate MITF binding (Strub et al, 2010), including target genes such as pigmentation enzymes *Tyrosinase*, *Tyrp1* and *DCT*, and lineage proliferation and survival factors including *BCL2, CDK2, CDKN1A* and *CDKN2A* (Hoek et al., 2008b). It is now clear that MITF, by controlling the transcription of numerous genes, is the source of multiple and complex molecular cascades that control melanocytic growth, survival, differentiation, and it also plays a crucial role in melanomagenesis (Goding and Arnheiter, 2019).

Melanoma is a melanocytic tumour in which, for at least a subset of the tumour cells, MITF dependence is retained (Kim et al., 2019). Thus, MITF represents a lineage-restricted oncogenic regulator whose activity is utilised by malignant

melanoma cells (Levy and Fisher, 2011). Through transactivating its target genes, MITF can regulate multiple important biological processes in melanoma cells, the most clinically relevant of which is treatment resistance to targeted BRAFi therapy (Johannessen et al., 2013). Recent studies implicate MITF in fatty acid metabolism in melanoma, where MITF is a lineage-restricted activator of the key lipogenic enzyme Stearol-CoA Desaturase (SCD), and that SCD is required for proliferation in the MITF-dependent melanoma cells (Vivas-García et al., 2020). Therefore, MITF plays key roles in both melanoma biology and pharmacotherapy.

Gene Structure and Transcriptional Function of MITF In humans, the *MITF* locus spans 229kbp, and is mapped to chromosome 3 (Sun et al., 2017). *MITF* encodes a transcription factor that belongs to the b-HLH-Zip (basic helix-loop-helix leucine zipper) family of transcription factors, which can also be classified under the MYC superfamily (Hallsson et al., 2007). MITF, together with Transcription Factor EB (TFEB), Transcription Factor EC (TFEC), and Transcription Factor E3 (TFE3), constitute the MiT (Microphthalmia) family of transcription factors (Hemesath et al., 1994). The MIT transcription factors share a common b-HLH-leucine zipper dimerisation motif used for DNA binding, and two N-terminal transactivation domains (TAD) required for transactivation of target promoters (Hemesath et al., 1994). A single

MITF gene produces several isoforms of MITF, including MITF-A, MITF-B, MITF-C, MITF-D, MITF-E, MITF-H, MITF-J, MITF-Mc, and MITF-M, due to differential usage of alternative promoters resulting in splice variants (Goding and Arnheiter, 2019). These isoforms differ in their N-termini encoded by exon 1, and different MITF isoforms show unique tissue-specific patterns of expression (Kawakami and Fisher, 2017). The expression of the shortest isoform MITF-M, consisting of a 419-residue protein, is limited to melanocyte lineage and melanoma cells (Selzer et al., 2002). Subcellularly, MITF-M expression is restricted to the nucleus due to a lack of the nuclear localisation sequence within exon 1 (Settembre et al., 2012). MITF-Mdel, a splice variant of MITF-M harbouring two skipped exons within exons 2 and 6, had also been identified as restrictedly expressed in melanoma cells (Wang et al., 2010).

MITF homoedimerises or heterodimerises with another member of the MIT transcription factors in order to bind to DNA (Hemesath et al., 1994). MITF binds to promoters of target genes by recognizing genetic sequences termed the E-Box (CAYRTG, where Y stands for purines and R stands for pyrimidines), or the M-Box (TCAYRTG and CAYRTGA) (Pogenberg et al., 2012). However, despite sharing the common ability to bind to the palindromic E-box motifs, MITF does not form heterodimers with other b-HLH-Zip transcription factors, such as MYC, MAX, or USF (Hemesath et al., 1994). Structurally, the heptad repeat register of MITF's leucine

zipper domain is broken by a three-residue insertion that generates a kink in one of the two zipper helices, and this kink limits the ability of MITF to form dimers with only bHLHZip transcription factors within the MIT family that share the same type of leucine zipper insertion (Pogenberg et al., 2012).

Genetic Alterations of MITF in Melanoma. Somatic mutations in the human MITF gene have been found in patients with malignant melanoma (Cronin et al., 2009), as well as the rare Type 2A Waardenburg (WS2A) and Tietz (TS) syndromes characterised by hypopigmentation and deafness (Amiel et al., 1998, Tassabehji et al., 1994). George and colleagues also described the coloboma, osteopetrosis, microphthalmia, microcephaly, albinism, and deafness (COMMAD) syndrome, associated with biallelic *MITF* mutations (George et al., 2016). A recent study listed and analysed the MITF mutants known to date, which included the well-known MITF mutants such as $MITF^{E318K}$ (Germline MITF mutation in familial melanoma syndrome), $MITF^{E87R}$ (MITF mutation in $BRAF^{V600E}$ melanoma), and $MITF^{L135V}$ (MITF mutation in metastatic melanoma) (Grill et al., 2013). Interestingly, *MITF* mutations associated with melanoma were determined to be spatially and functionally distinct from that of mutations leading to WS2A and TS syndromes. Whilst MITF mutations associated with malignant melanoma were frequently located at the amino- and carboxyl ends, the

mutations found in WS2A and TS patients are located in the basic region, the helix-loop-helix and the leucine zipper domains (Grill et al., 2013). Functional analysis showed that the WS2A and TS MITF mutants failed to bind DNA, and transcriptional activation potential was reduced in these mutants; whereas the DNA binding ability of MITF mutants associated with malignant melanoma was similar to wild-type MITF (Grill et al., 2013). Additionally, MITF mutants associated with melanoma tend to exert more subtle promoter-specific effects on transcription. For example, the E87R mutation in MITF showed statistically significant reduction in *TYR*, *TYRP1*, and *DCT* transactivation, whilst activating *MET* at normal levels (Grill et al., 2013). $MITF^{E318K}$, the germline MITF mutant found in familial melanoma syndromes as previously mentioned (Yokoyama et al., 2011, Bertolotto et al., 2011), showed significantly increased activation potential from *TYR*, 4M-box, and *MET* promoters, whilst activation of *TYRP1* was reduced (Grill et al., 2013). Therefore, the subset of MITF mutations occurring in melanoma appeared to modify the transcriptional activity of the transcription factor, without inducing a significant loss of function as occurred with the WS2A and TS mutants (Grill et al., 2013).

In addition to *MITF* mutation, gene amplification and alternative splicing are additional means by which the *mi* allele may be modified in melanoma (Wang et al., 2010, Ugurel et al., 2007). As previously discussed, *MITF* is amplified in up to 20% of

malignant melanoma (Garraway et al., 2005). Analysing SNP array-based genetic maps with mRNA expression signatures derived from melanoma cell lines, *MITF* was found to be the target of gene amplification (Garraway et al., 2005). *MITF* amplification was shown to be more prevalent in metastatic melanoma, and correlated with decreased overall patient survival (Garraway et al., 2005). Alternative splicing of *MITF-M* is another means of altering the *MITF* gene product in melanoma (Wang et al., 2010). Two spliced variants of *MITF-M* – MITF(+) and MITF(-) – have been described, where the MITF(+) splice variant contains an internal six-amino acid fragment encoded by exon 6a, and possesses anti-proliferative transcriptional properties (Steingrímsson et al., 1994). The MITF(-) splice variant lacks this fragment, and the expression of which has been shown to be increased in metastatic melanoma (Bismuth et al., 2005). The expression of these two different splice variants of *MITF-M* in melanoma appeared to affect activation of the MAPK pathway, independently of the mutational status of *BRAF* and *NRAS* (Anello et al., 2019).

Transcriptional Activators of MITF A number of transcription factors control the expression of MITF, which associates MITF expression with signalling pathways involved in diverse cellular processes (Wellbrock and Arozarena, 2015). For example, a SOX10 (sex-determining region Y-box-10)-responsive element was identified in the

MITF promoter between -264 and -266 (Bondurand et al., 2000). Activating frameshift or non-sense mutations in SOX10 are present in melanoma, and MITF and SOX10 mutations occur in a mutually exclusive manner (Verfaillie et al., 2015). SOX10 also cooperates with CREB (cAMP response element binding protein) to modulate MITF's responsiveness to α-MSH (α-Melanocyte stimulating hormone)-cAMP signalling (Huber et al., 2003). Via diverse mechanisms such as UV-induced p38 and KIT signal transduction, CREB can be activated by phosphorylation at Ser ^{133}, thus promoting its binding to the MITF promoter (Saha et al., 2006). $P21^{Cip1}$, an important cell cycle inhibitor, has also been shown to function as a CREB co-factor involved in cAMP-depending MITF expression in melanoma (Sestakova et al., 2010).

Two key effectors in the Wnt (wingless-type) signalling pathway, LEF1 (lymphoid enhancing binding factor 1) and β-catenin, also transcriptionally regulate MITF expression (Yasumoto et al., 2002). The *MITF* promoter contains a functional LEF-1 binding site, which enables LEF-1-dependent transactivation of *MITF* .(Saito et al., 2002) Exogenously added Wnt3a protein induces MITF expression, but MITF expression was abrogated by the co-expression of a dominant negative mutant of LEF-1 (Takeda et al., 2000b). Wnt3a has thus been proposed to recruit β-catenin and LEF-1 to the MITF promoter site for transcriptional regulation (Takeda et al., 2000b). In addition, MITF can cooperate with LEF1 as a non-DNA-binding coactivator to enhance

its own expression (Yasumoto et al., 2002). In terms of β-catenin, it has been shown that the mediators of the α-MSH/cAMP/PKA (protein kinase A) signalling pathway can redirect β-catenin to the CREB-specific promoters, in order to promote transcription of CREB target genes including *MITF* (Widlund et al., 2002).

Recently, a transcription factor involved in the epithelial-mesenchymal transition mechanism, ZEB2 (zinc finger E-box binding protein 2), has been shown to activate *MITF* expression (Denecker et al., 2014). ZEB2 is a zinc finger transcription factor that contributes to TGFβ signalling, and ZEB2 transcripts are expressed in tissues differentiated from the neural crest, such as melanocytes and the sympathetic ganglions (Caramel et al., 2013). ZEB2 loss results in a decreased MITF expression level and that of several MITF target genes, and ZEB2 loss was associated with melanoma progression (Caramel et al., 2013). In contrast, rather than activating the *MITF* promoter, ZEB1, the mammalian paralog to ZEB2, has been found to directly repress *MITF* expression in retinal pigment epithelium, leading to epithelial-mesenchymal transition in cancers such as melanoma and breast cancer (Liu et al., 2009b). Last, at the level of chromatin remodelling, it has been demonstrated that a SWI/SNF complex containing BRM (Brahma) or BRG1 (Brahma-related gene 1) promoted *MITF* expression (Liu et al., 2009b).

Transcriptional Repressors of MITF Several transcription factors directly repress the expression of *MITF*. In melanoma cells, inverse expression patterns of GLI2 (glioma-associated oncogene family member 2) and MITF-M have been observed, relating to the mutually exclusive transcriptional programs (Javelaud et al., 2011). GLI2, a Kruppel-like transcription factor activated by TGFβ (Transforming Growth Factor β), is able to bind directly to the -334/-296 region of the *MITF* promoter, confirming the direct inhibitory activity of GLI2 on *MITF* (Pierrat et al., 2012).

The PAX3 (Paired box 3) transcription factor's transrepression of *MITF* represents another lineage-specific mechanism for negative MITF regulation in melanoma (Yang et al., 2008). Although positive regulation of MITF by PAX3 in melanocytes is well-described (Yang et al., 2008), PAX3 has been shown to play a repressive role on MITF expression in melanoma, through its cooperation with the neural-lineage transcription factor BRN2 (Yang et al., 2008). siRNA knockdown of PAX3 leads to reduction in BRN2 expression levels, and increased MITF expression in melanoma cell lines (Eccles et al., 2013). In addition, BRN2 itself directly represses MITF expression and enhances invasion in melanoma cells (Goodall et al., 2008). Since BRN2 expression is significantly curtailed in primary melanocytes, the BRN2-mediated repression of MITF transcription additionally represents a distinguishing feature between melanoma cells and melanocytes (Goodall et al., 2008). A role for melanoma-specific $BRAF^{V600E}$-

mediated induction of BRN2 has been proposed (Goodall et al., 2004), as has a model for non-overlapping expression of BRN2 and MITF in melanoma driven by the microRNA, miR-211 (Boyle et al., 2011). In the miR-211 model, miR-211 activated the MITF transcription program whilst suppressing the cellular program driven by PAX3 and BRN2 (Simmons et al., 2017). Thus, both BRN2 and PAX3 have been shown to negatively regulate *MITF* in melanoma (Simmons et al., 2017).

HIF1 (hypoxia-inducible factor 1) has also been shown to mediate MITF repression through the transcriptional repressor DEC1 (differentially expressed in chondrocytes protein 1). DEC1 binds to the promoter of *MITF-M* under hypoxic conditions, as well as during treatment with the small-molecule prolyl-hydroxylase inhibitor, reducing *MITF-M* transactivation (Feige et al., 2011). This leads to a state of melanoma growth arrest that could be rescued by ectopic MITF expression *in vitro* (Feige et al., 2011).

Regulation of MITF Transcript Stability Melanoma cells express high amounts of Coding Region Determinant-Binding Protein (CRD-BP), an mRNA-chaperone protein that has been found to stabilise MITF transcripts in transit (Craig and Spiegelman, 2012). MITF transcript stability is also under the control of several small non-coding RNAs, microRNAs (miRs), whose roles are to either promote mRNA

degradation or conversely, to suppress protein synthesis via binding to the 3'-untranslated region of the target transcript (Bell and Levy, 2011). For example, miR-182 is frequently amplified in melanomas, and *MITF* transcript has been shown to be targeted for miR-182-mediated degradation in metastatic melanoma (Segura et al., 2009). P53-dependent miR-182 expression has been also found to downregulate *MITF* expression in uveal melanoma (Yan et al., 2012). In addition, the 3'-UTR of MITF transcript is targeted for degradation by miR-148 (Haflidadottir et al., 2010), miR-101 (Luo et al., 2013), and miR-218, and as such, inverse correlation between MITF expression and miR-218 has been observed in melanocytes and melanoma cell lines (Luo et al., 2013). Some studies have shown that exosome-dependent miR exchange between melanoma cells may also exert influence on MITF transcript stability (Gajos-Michniewicz et al., 2014).

Regulation of MITF Protein Expression and Activity The transcriptional activity of MITF depends at least in part on its post-translational modifications and availability of co-operating partners, so an understanding of its post-translational modifications is important for describing MITF function (Motzik et al., 2017). In terms of phosphorylation, MITF can be regulated by phosphorylation by various serine/threonine kinases such as ERK1/2 (at Ser^{73}) (Hemesath et al., 1998), $p90^{RSK}$ (at

Ser^{409}) (Wu et al., 2000), GSK3β (at Ser^{298}) (Takeda et al., 2000a), and p38 (at Ser^{73}) (Mansky et al., 2002). In general, phosphorylation of MITF contributes to its transcriptional enhancement (Terragni et al., 2011). For example, the phosphorylation at Ser^{73} promotes the interaction between MITF and its co-factor, the histone acetyl transferase, p300/CBP, within its transactivation domain (TAD) (Wu et al., 2000). However, the Ser^{73} phosphorylative modification also promotes the binding of MITF with PIAS3 (protein inhibitor of activated STAT3), via the interaction between the N-terminal fragment of PIAS3, and MITF's leucine zipper (Levy et al., 2003). MITF's Interaction with PIAS3 leads to paradoxical transcriptional attenuation of MITF (Levy et al., 2003), an inhibitory effect that is disrupted when MITF is further phosphorylated at Ser^{409} in a p90^{RSK}-dependent manner (Sonnenblick et al., 2004). Therefore, MITF's post-translational modifications encompass a complex set of interdependent reactions (Levy et al., 2006). The phosphorylation of MITF at Ser^{73}, a residue located within a degradation-promoting PEST sequence, is also a prerequisite for MITF's proteasome-dependent turnover (Xu et al., 2000).

MITF expression can be regulated by ubiquitination. Lys201 has bene identified as a site of UBC9-mediated ubiquitylation of MITF, leading to proteasomal degradation of the MITF protein (Xu et al., 2000). In contrast, the deubiquitinase, USP13 (ubiquitin-specific protease 13) has been shown to protect MITF from proteasomal degradation in

melanoma cells (Zhao et al., 2011). Proteasome-mediated MITF degradation can be induced by double phosphorylation of MITF at Ser^{73} and Ser^{409} via ERK kinase (Wu et al., 2000). An MITF mutant that cannot be phosphorylated at Ser^{73}/Ser^{409} has been shown to be expressively stable, but transcriptionally incompetent, which indicates the signals that promote transcriptional activity and degradation of the MITF protein are tightly linked in melanoma cells (Wu et al., 2000). Both the Ser^{73} and Ser^{409} phosphorylation events that promote MITF proteasomal degradation depend on melanoma-specific $BRAF^{V600E}$ activity, which phosphorylates ERK1/2 through the activity of MEK within the MAPK cascade (Haq et al., 2013). $BRAF^{V600E}$ has therefore been shown to be a negative regulator of MITF expression in melanoma (Haq et al., 2013). Effector caspases can also cleave MITF for post-translational modification (Larribere et al., 2005). It has been demonstrated in melanoma cells that caspase-dependent cleavage of MITF derives a C-terminal peptide that has a pro-apoptotic function (Larribere et al., 2005) .

MITF activity can be endogenously modulated by SUMOylation at two lysine residues, Lys^{182} and Lys^{316} (Murakami and Arnheiter, 2005). SUMOylation of MITF depends on the activity of an E1 SUMO-activating heterodimeric enzyme, SAEI/SAEII, and the E2 SUMO-conjugating enzyme, UBC9 (Murakami and Arnheiter, 2005). SUMOylation plays an essential role in the regulation of MITF activity, as non-

SUMOylatable MITF mutants displayed increased transcriptional activity on distinct sets of target genes (Murakami and Arnheiter, 2005). A study on melanoma patients bear the $MITF^{E318K}$ mutant, in which a point mutation occurs at the consensus binding site for SUMOylation, showed that this missense mutation near Lys^{316} affected the transcriptional activity of MITF – on target genes such as *TYR*, *MET*, and *TYRP1* – but did not alter dimerization, DNA-binding, stability, or nuclear localization of MITF (Grill et al., 2013). The study suggested a synergy control model in which the functional consequences of MITF SUMOylation depended on the context of the target gene promoters affected, and thereby providing a mechanism by which MITF activity can be modified though differential activation of its target genes (Miller et al., 2005).

Another means by which MITF function can be modified is through protein-protein interactions with the SWItch/Sucrose Non-Fermentable (SWI/SNF) nucleosome remodelling complexes composed with either Brahma (BRM) or Brahma-Related Gene 1 (BRG1) proteins (Keenen et al., 2010). SWI/SNF complexes are transcriptional regulators that possess ATPase and DNA Helicase activities, and they regulate gene transcription via altering the chromatin structure around the transcribed genes (Roberts and Orkin, 2004). Studies have shown that depending on the type of SWI/SNF complex interacting with MITF, different sets of MITF-dependent genes may be activated (Mehta et al., 2015). Modification of chromatin by HINT1 (histidine triad

nucleotide-binding protein 1) provides an additional route to inhibit the transcriptional activity of MITF. HINT1 adherence to histidine residues at the MITF binding sites can disrupt MITF function (Genovese et al., 2012). Interestingly, the loss of HINT1 expression at the onset of primary melanoma indirectly supports a role for MITF activity in melanomagenesis (Genovese et al., 2012).

MITF Target Genes Following the independent efforts of Hodgkinson and Hughes to clone MITF from the *Mi* locus (Hodgkinson et al., 1993, Hughes et al., 1993), MITF was shown to play a key role in melanocytic pigmentation through direct transcriptional control of the genes including Tyrosinase, Tyrosinase-Related Protein 1 (Tyrp1), and Dopachrome Tautomerase (DCT), the key enzymes involved in melanin synthesis (Yasumoto et al., 1994). Later, as MITF-deficient mice were also shown to be devoid of melanocytes, the role for MITF was revised to include the regulation of melanocytic developmental processes, such as growth and survival (Nakayama et al., 1998). Target genes that regulate growth and survival, and contain M-boxes in their respective promoters for MITF regulation have since been identified to include *BCL2*, *CDK2*, *CDKN1A*, and *CDKN2A*, providing the molecular links between MITF and melanocytic regulation (Hartman and Czyz, 2015b). It is now clear that MITF controls the transcription of numerous genes, and represents the source of complex molecular

cascades that control lineage-specific melanocytic function (Cheli et al., 2010).

MITF Target Genes involved in Melanocytic Pigmentation. Melanin synthesis occurs as an enzymatic reaction that converts the amino acid tyrosine to melanin pigment (D'Mello et al., 2016). The first two steps in melanin synthesis – the hydroxylation of tyrosine to dihydroxyphenylalanine (DOPA), and the oxidation of DOPA to DOPA quinine – are catalysed by tyrosinase (TYR), the rate-limiting enzyme in this reaction (Rios et al., 1999). Two other enzymes, dopachrome tautomerase (DCT) and tyrosinase-related protein 1 (TYRP1), are also involved in eumelanin synthesis, as demonstrated by the dramatic consequences of their mutations on melanin pigment production (Rios et al., 1999). These enzymes, and specifically tyrosinase, play additional key roles in melanocytic differentiation (Yaar and Gilchrest, 1991). MITF has been shown to transactivate the promoters of *TYR*, *TYRP1*, and *DCT*, and CATGTG E-Box motives have been identified in promoters of these genes (Bentley et al., 1994, Bertolotto et al., 1998). Importantly, MITF requires the SWI/SNF complexes to control the transcription of *TYR* and *TYRP1* (de la Serna et al., 2006).

Melanin synthesis takes place in melanosomes, which are lysosome-related organelles in melanocytes, where biogenesis and intracellular transport are key determinants of melanin synthesis and skin pigmentation (Wasmeier et al., 2008).

Among the genes responsible for melanin synthesis, Silver homologue and Melan-a (MART1), encoded in human by *SILV* and *MLANA*, respectively, are involved in the formation of melanosomal matrix and control melanosome maturation (Raposo and Marks, 2007). *SILV* and *MLANA* are direct transcriptional targets of MITF, which links MITF not only to melanin synthesis, but also to melanosomal biogenesis (Du et al., 2003). Two E-box sequences, CACATG and CACGTG, were shown to mediate the effects of MITF on *MLANA* promoter transcription (Du et al., 2003).

Other proteins important in melanosomal biology have also been identified as downstream direct MITF targets (Hertzman Johansson et al., 2013). This is the case for ocular albinism type 1 (formally known as OA1, or GPR143). *OA1* encodes a G protein-coupled receptor that is expressed on the melanosomal membrane, responsible for regulating melanosome maturation and size (Chen et al., 2016). An E-box, CACATG, has been identified in the proximal promoter region of *OA1* that binds to and mediates MITF transcriptional activity (Vetrini et al., 2004). RAB27A is a small GTP-binding protein that facilitates actin-mediated melanosome transport via its interaction with melanophilin and myosin Va (Bahadoran et al., 2001). MITF has been shown to transcribe *RAB27A* via binding two proximal E-boxes, CATATG (-52) and CAGCTG (-40), thereby implicating MITF in the regulation of melanosome trafficking (Chiaverini et al., 2008).

Other effectors implicated in MITF-regulated pigmentation function in melanocytes include SLC45A2 (also known as membrane-associated transport protein or MATP) (Du and Fisher, 2002), MC1R (a plasma membrane G-protein-coupled receptor that binds to αMSH) (Aoki and Moro, 2002), and PKCβ (Park et al., 2006).

MITF Target Genes Involved in Melanocytic Proliferation. The role that MITF plays in regulating cellular proliferation is complex, as it has been implicated to both promote and restrict melanocytic proliferation in different contexts (Goding and Arnheiter, 2019). Mechanistically, a role for MITF in the control of melanoblastic proliferation can be ascribed to its transcriptional activation of TBX2 (Béjar et al., 2003), a T-box family transcription factor that blocks melanocytic senescence through transrepression of the cyclin-dependent kinase inhibitor $p21^{Cip1}$ (Manu et al., 2019), and the tumour suppressor $p14^{ARF}$ (Brown et al., 2004). The effect of MITF on the *TBX2* promoter was demonstrated through a promoter mutational analysis that identified an E-box CATGTG motif (-204) on the *TBX2* promoter (Béjar et al., 2003). Cyclin-Dependent Kinase 2 (CDK2) is another G1-S cell cycle checkpoint regulator transcribed by MITF (Tadesse et al., 2019). *CDK2* is located on chromosome 12, in close proximity to *SILVER*, and the *CDK2* promoter overlaps with the regulatory regions of *SILVER*, which contain a CATGTG motif for MITF binding (Du et al., 2004).

MITF binding to this CATGTG motif regulates the transcriptional activity of the *CDK2* promoter, and through this mechanism MITF controls *CDK2* expression and melanoma growth (Du et al., 2004).

MITF silencing has also been shown to induce growth arrest in melanoma through the upregulation of $p27^{Kip1}$ – a cyclin-dependent kinase inhibitor that inhibits CDK2 and CDK4, restricting cell cycle progression at the G1 phase (Lloyd et al., 1999)– by reducing the levels of diaphanous-related formin (DIAPH) (Carreira et al., 2006). Three potential MITF-binding sites (CATGTG) were identified in the *DIAPH* promoter (E-box1: -509; E-box2: -677; E-box3: -794), with E-box2 and E-box3 elements being the most critical for *DIAPH1* promoter activity (Carreira et al., 2006). MITF silencing-dependent DIAPH reduction inhibited SKP2, a cell-cycle protein that complexes with Cyclin-A-CDK2 to degrade $p27^{Kip1}$ through ubiquitination and degradation (Carreira et al., 2006). Therefore, several mechanisms had been proposed to describe MITF's role in regulating the melanocytic proliferation (Cheli et al., 2010).

MITF Target Genes Involved in Melanocytic Survival. MITF has been shown to regulate cell survival through the transactivation of *BCL2* gene expression (McGill et al., 2002). ChIP, promoter, and gel supershift assays showed that *BCL2* is a direct MITF target gene, and enforced *BCL2* expression rescued apoptosis induced by a

dominant negative MITF in melanocytes (McGill et al., 2002). MITF mediates its effect on the *BCL2* promoter via an E-box motif CATGTG (-220) (McGill et al., 2002). In turn, Bcl2 knockout mice are born pigmented but then turn grey due to loss of melanocyte stem cells (Veis et al., 1993). Consistent with a role for MITF in melanocyte survival, MITF-silencing by siRNA caused decreased melanocytic viability, associated with an elevated caspase activity and nuclear condensation, indicating induced apoptosis (McGill et al., 2002).

Another mechanism for MITF-dependent cell survival has been proposed via the alleviation of cellular oxidative stress (Liu and Meyskens, 2007). Oxidative stress is relevant to pigment cell biology, since their cutaneous locality exposes them to environmental stressors that promote free radical damage, such as UV radiation (Venza et al., 2015). Reactive oxygen species (ROS) damages are repaired by DNA base-excision repair mechanisms that prevent cell cycle arrest and apoptosis (Whitaker et al., 2017). In this context, the apyrimidinic endonuclease 1 (APEX1) has been shown to be MITF target (Liu et al., 2009a). MITF transactivates the *APEX1* promoter through three identified E-boxes (E-box1: −10; E-box2: +52; E-box3: +73) (Liu et al., 2009a). Phenotypically, MITF silencing in melanocytes leads to poor survival following ROS induction, which can be rescued by forced APEX1 expression (Liu et al., 2009a).

Further studies also showed that MITF regulated the expression of the receptor

tyrosine kinase MET, via identification of E-box CACGTG motifs in the human *MET* promoter (McGill et al., 2006). MITF transactivation is therefore linked to MET activation by Hepatocyte Growth Factor (HGF), which facilitates melanoma migration and apoptotic protection (Beuret et al., 2007). Other receptor tyrosine kinases shown to be direct target genes of MITF include KIT and NGFR (Phung et al., 2011, Jippo et al., 1997), and these targets also promote melanocytic cell survival through the activation of downstream signal transduction effectors such as ERK and PI3K/AKT (Lemmon and Schlessinger, 2010).

MITF Target Genes Involved in Melanocytic Differentiation. . Whilst the above observations indicated that MITF plays important roles in melanocytic proliferation, MITF overexpression has also been shown to independently trigger melanocytic differentiation through arresting the cell cycle (Tachibana et al., 1996). That MITF-heterozygous mice produced fewer melanoblasts from the neural crest than MITF-homozygous mice, and proliferated faster during the migratory phase, suggested MITF expression could also inhibit proliferation in the context of cellular differentiation (Hornyak et al., 2001). It was thus proposed that MITF coordinated cell cycle regulation with the differentiation programme in melanocytes (Loercher et al., 2005). Mechanistically, MITF was shown to control the transcription and expression of

CDKN1A and *CDKN2A*, genes that encoded the cyclin-dependent kinase inhibitors (CKIs) $p21^{Cip1}$ and $p16^{INK4A}$, respectively (Carreira et al., 2005, Loercher et al., 2005). $P21^{Cip1}$ is a potent CKI that inhibits the activity of all CDKs, with the majority of effect observed on the Cyclin E-CDK2 complex, leading to a S-G2 cell cycle block (Manu et al., 2019); $p16^{INK4A}$ is a tumour suppressor that inhibits CDK4/6, thereby activating the retinoblastoma protein to inhibit E2F and block the cell cycle between G1-S phases (Ohtani et al., 2004). An E-box (−635) for MITF binding in the *CDKN1A* gene was located by EMSA and mutagenesis, and MITF binding to the *CDKN2A* promoter was demonstrated via Chromatin Immunoprecipitation (Loercher et al., 2005). The regulation of *CDKN1A* and *CDKN2A* by MITF suggested that MITF may promote G1-S arrest in melanocytes (Bennett, 2008). Indeed, forced expression of MITF increased $p21^{Cip1}$ and $p16^{INK4A}$ expressions and blocked growth in fibroblasts, whilst MITF silencing decreased $p16^{INK4A}$ expression and induced uveal melanocyte proliferation (Bennett, 2008). In melanoma cells, where $p16^{INK4A}$ is frequently mutated or inactivated, growth arrest evoked by ectopic MITF overexpression was mediated by $p21^{Cip1}$ (Bennett, 2008). Therefore, MITF expression arrested the cell cycle to promote terminal differentiation in melanocyte lineage cells (Goding, 2011).

MITF and Metastatic Invasion in Melanoma The control of genes

associated with cell cycle and differentiation enables a role for MITF to facilitate metastatic invasion in melanocytes (Goding, 2000). Differentiation in melanocytes is associated with E-Cadherin-mediated adherence to the basal stratum of the epidermis (Haass and Herlyn, 2005). In the case of melanoma, a loss of MITF has been shown to promote a dedifferentiated phenotype in melanoma cells, concurrent with melanoma invasion into the dermal blood supply (Fane et al., 2019). Indeed, Transgenic overexpression of the frequently mutated oncogene $BRAF^{V600E}$ in normal human melanocytes caused decreased expression of MITF via phosphor-ERK mediated degradation (Haq et al., 2013), and upregulated the expression of Epithelial-Mesenchymal Transition Transcription Factors (EMT-TFs), ZEB1 and TWIST1 via ERK-mediated Activator Protein-1 (AP-1) transcriptional activity (Caramel et al 2013). This $BRAF^{V600E}$-mediated switch from a MITF-dominant transcriptional program to one driven by AP-1/ZEB1/TWIST1 was found to be associated with a gain in invasive properties, loss of E-Cadherin, and onset of drug resistance to MAPK pathway inhibitors (Verfaillie et al., 2015). Conversely, enforced expression of SNAIL2 and ZEB2, EMT-TFs that reverts melanoma cells to a more differentiated phenotype, is capable of restoring MITF expression, as well as its target genes *Tyr*, *Tyrp1*, and M*LANA* (Caramel et al, 2013). This evidence suggests that melanoma cells can undergo phenotypic switching in differentiation status via altering the expression level of MITF,

and the differentiation status of the melanoma cells in turn influences their invasive potential (Ahn et al., 2017).

MITF Target Genes Involved in Metabolism Recent studies have begun to investigate the transcriptional capacity of MITF to regulate melanocytic metabolism (Ratnikov et al., 2016). In 2013, it came to light that MITF drove the overexpression of Peroxisome Proliferator-Activated Receptor Gamma Coactivator 1-Alpha (PGC1α) in a subset of human melanomas and derived cell lines (Vazquez et al., 2013). PGC1α is the master regulator of mitochondrial biogenesis, whereby through its interaction with the nuclear receptor, Peroxisome Proliferator-Activated Gamma (PPARγ), the PGC1α-PPARγ complex interacts with multiple transcription factors in the nucleus, such as the Nuclear Respiratory Factor 1 (NRF1), to facilitate mitochondrial DNA transcription (Tan et al., 2016). MITF- and PGC1α-positive melanoma cells were shown to upregulate mitochondrial energy metabolism and reactive oxygen species (ROS) detoxification, metabolic activities that enabled survival under oxidative stress (Vazquez et al., 2013). Conversely, MITF- and PGC1α-negative melanoma cells were shown to be more glycolytic and susceptible to pharmacological ROS induction (Vazquez et al., 2013).

Interestingly, $BRAF^{V600E}$ mutant melanomas with constitutively activated MAPK

signalling demonstrated suppressed levels of MITF and PGC1α – an effect attributed to ERK1/2-dependent phosphorylation of MITF at residue Ser^{73} (Haq et al., 2013) – and increased rates of glycolysis via the upregulation of glycolytic effector components including Glucose Transporter 1 (GLUT1), GLUT3, and Hexokinase 2 (Parmenter et al., 2014). Treatment of $BRAF^{V600E}$ mutant melanomas with BRAF inhibitors disinhibited MITF and PGC1α expression, and shifted the predominant cellular metabolic flux from aerobic glycolysis to oxidative phosphorylation (Haq et al., 2013). Metabolomically, ^{1}H NMR metabolic flux analysis of vemurafenib-treated WM266.4 melanoma cells harbouring a $BRAF^{V600E}$ mutation, revealed that *de novo* lactate synthesis and glycolysis were reduced by $BRAF^{V600E}$ inhibition, whilst oxidative and anaploretic pyruvate carboxylase mitochondrial activities were enhanced (Delgado-Goni et al., 2016). The activation of MITF was thus proposed to represent an adaptive metabolic program in melanoma cells to resist therapeutic $BRAF^{V600E}$ inhibition (Haq et al., 2013). Indeed, a subset of BRAF- and NRAS-mutant human melanomas resistant to the MEK inhibitor Selumetinib, was shown to display increased propensity for oxidative phosphorylation, mediated by MITF and the transcriptional coactivator PGC1α (Gopal et al., 2014). Pharmacological mTORC1/2 inhibition by AZD8055 triggered cytoplasmic localisation of MITF, which decreased PGC1a expression and inhibited oxidative phosphorylation, an effect that enabled resensitisation of the BRAF-

/NRAS-mutant melanoma cells to selumetinib (Gopal et al., 2014).

Consistent with the role of MITF in inducing mitochondrial oxidative phosphorylation, the expression of both MITF and its transcriptional target, PGC1α, can be further suppressed via a Hypoxia Inducible Factor (HIF)-dependent mechanism (Feige et al., 2011, LaGory et al., 2015). HIF1 transactivates the transcriptional repressor, Differentially Expressed in Chondrocytes Protein 1 (DEC1), which subsequently binds to and suppresses the promoters of both *MITF* and *PGC1α* (Feige et al., 2011, LaGory et al., 2015). At the transcriptional level, inhibition of MITF and PGC1α by HIF1 thus provides mechanistic insight as to how melanoma and melanocyte-lineage cells are able to switch from oxidative phosphorylation to glycolysis during periods of hypoxia (Widmer et al., 2013).

Recently, a role for MITF in the regulation of lipid metabolism has been further proposed (Vivas-García et al., 2020). MITF was shown to be a lineage-restricted activator of the key long chain fatty acid desaturase enzyme, Stearoyl-CoA Desaturase (SCD) (Vivas-García et al., 2020). SCD is the canonical lipogenic enzyme that catalyses the rate-limiting step in the formation of monounsaturated fatty acids – specifically, they convert stearoyl-CoA and palmitoyl-CoA to oleate and palmitoleate, respectively (Igal, 2016). Oleate and palmitoleate form the major components of membrane phospholipids, cholesterol esters, and alkyl-diaceylglycerol (Igal, 2016). MITF

expression was shown to upregulate SCD, and alter the cellular fatty acid composition in melanoma cells in favour of monounsaturated fatty acids (Vivas-García et al., 2020). In contrast, MITF-Low cells with curtailed SCD activity retained higher concentrations of saturated fatty acids (Vivas-García et al., 2020). The melanoma MITF-SCD axis was shown to suppress metastasis, inflammatory signalling, and inhibit an ATF4-mediated feedback loop that maintained melanoma differentiation (Vivas-García et al., 2020). On the other hand, MITF-Low cells were insensitive to pharmacological SCD inhibition (Vivas-Garcia 2020). Taken together, MITF exerts transcriptional control over multiple metabolic checkpoints and regulates flux through key metabolic pathways within melanoma cells (Ratnikov et al., 2016).

MITF Target Genes Involved in Solute and Proton Transport Solute transport is an understudied, but pathophysiologically important component of melanoma biology (Mongera and Dooley, 2013). An example of the importance of solute carriers in melanoma was shown in a recent research article describing the global transcriptomic profile of the SK-MEL-3 melanoma cell line – a BRAF mutant derived from a lymph node melanoma metastasis (Mazzio and Soliman, 2018). The whole-transcriptome profile showed a basic phenotype dominance in the SK-MEL-3 cell line for phagosome acidification, ATP hydrolysis-coupled proton pumps, and iron transport,

with the number of genes related to these biological processes enriched 13.91, 18.03, and 14.27-fold, respectively (Mazzio and Soliman, 2018). Another study showed that in the invasive melanomas, the expression of the long non-coding RNA, ZEB1-AS1 negatively correlated with gene signatures involved in ion transport, pH reduction, ATP-hydrolysis-coupled proton transport, and iron transport (Siena et al., 2019). These studies suggested that solute and proton transport are highly associated with metastatic invasion, and that transporter gene signatures may be transcriptionally regulated as part of the phenotypic plasticity phenomenon found in melanomas (Bohme and Bosserhoff, 2016).

Mechanistically, Steingrimsson and colleagues had previously used a Two-Step DNA Microarray Strategy to uncover novel MITF target genes, and certain solute and proton transporters were determined to be regulated by MITF transcription (Hoek et al., 2008b). These genes included the vacuolar ATPases (*ATP1A1*, *ATP6V1B2*, *ATP6V1C1*) and members of the Solute Carrier family (*SLC1A4*, *SLC7A8*, *SLC11A1*, *SLC19A2*, *SLC24A5*) (Hoek et al., 2008b). MITF was later shown to function as the master regulator of V-Type ATPase in melanoma, demonstrating transcriptional activity for multiple genes whose gene products assemble to form the V-Type ATPase proton pump (Zhang et al., 2015). Vacuolar ATPase functions to regulate melanosomal pH and melanin synthesis in melanocyte-lineage cells (Dooley et al., 2013); and more recently,

plasma membrane V-Type ATPase has also been shown to mediate oncogenic RAS-induced micropinocytosis in tumour cells (Ramirez et al., 2019).

In terms of SLC transporters, as discussed in the above paragraph, MITF has been shown to transcribe SLC loci in melanoma (Hoek et al., 2008b), although the number of studies delineating the regulation of SLC by MITF remains relatively sparse (Bohme and Bosserhoff, 2016). Nevertheless, many of the SLC proteins play important roles in the control of the ionic equilibrium in melanoma cells, a physiological prerequisite to the more complex traits regulated by MITF, such as proliferation and differentiation as outlined above. For example, SLC11A1 (Gelineau-van Waes et al., 2008), SLC7A11 (Shin et al., 2018), SLC24A5 (Gerstenblith et al., 2010),and SLC24A4 (Duffy et al., 2010) have all been reported to be involved in melanocytic ionic equilibrium. SLC45A2 is an MITF target gene that not only regulates ionic fluxes but also is directly involved in regulating melanocytic pigmentation (Wu et al., 2019). Therefore, proton and solute transport represents an important aspect of melanoma biology, and more studies are needed to delineate the relationship between MITF and SLC expression (Chen et al., 2019). Below is an in-depth description of the proton transporters and the intracellular pH environment they maintain.

Tumour Acidosis in Melanoma

The Physiological Relevance of pH for Melanocytes pH is an important physiological cue that regulates melanocytic biology, and pH plays a critical role in the skin barrier and the skin micromilieu in which melanocytes reside (Yajima et al., 2011). Surface acidity of the stratum corneum, often referred to as “acid mantle”, contributes to the cutaneous permeability barrier, which prevents excessive water loss from the skin, and acts as an antimicrobial defence mechanism (Koch and Schwab, 2019). Physiological skin surface pH ranges around pH 5.0, and rises towards deeper parts of the skin (Ohman and Vahlquist, 1994). Microenvironmental pH begins to neutralise as deeper layers of the skin are approached (Ohman and Vahlquist, 1994). For example, the superficial layers of the stratum granulosum have been shown to exhibit a measurable pH of 6.9, and deeper layers of stratum granulosum exhibit pH values of 7.0-8.0 (Ohman and Vahlquist, 1994). However, the available evidence indicates that melanocytes are affected by acidic pH values in their physiological environment, an important observation taking into consideration that melanocytic dendrites extend from the basal stratum towards the surface of the skin for melanin transport (Koch and Schwab, 2019). A recent study reported intracellular pH differences of up to 0.3 pH units between the cell body and dendrites of melanocytes (Koch and Schwab, 2019).

The pathophysiological relevance of the (epi)dermal pH landscape for melanoma biology becomes further evident when considering large melanoma lesions, for

example superficial spreading melanomas that progress from horizontal to vertical growth phase, or nodular melanomas that grow towards the surface of the skin (Schmid-Wendtner and Korting, 2006). Such vertical growth breaks through the epidermal basement membrane, and exposes the melanoma tumour body to the entire range of pH gradient that the skin entails (Matsui and Amagai, 2015) . Hence, it is pathologically plausible to consider that pH acidity would mechanistically contribute to melanomagenesis and intratumoural heterogeneity (Bohme and Bosserhoff, 2016).

Intracellular and Extracellular pH in Melanoma Biology For melanoma, both intracellular and extracellular pH are tightly controlled parameters that influence tumour behaviour (Bohme and Bosserhoff, 2016). Intracellular acidification from cancer metabolic activity leads to the extracellular extrusion of lactate and protons via cell membrane proton transporters, and in consequence hydrogen ions accumulate in the extracellular matrix (ECM) (Webb et al., 2011). On the other hand, studies have shown that extracellular acidosis leads to the development of a more aggressive phenotype in melanoma cells (Corbet and Feron, 2017). Mice injected with melanoma cell cultured in acidic media developed more xenograft metastases *in vivo* (Rofstad et al., 2006a). Mechanistically, acidified melanoma cells released more matrix metalloproteinases (MMPs) and cathepsins into the microenvironment, which

promoted the enzymatic degradation of the extracellular matrix, and facilitated enhanced tumour invasion ((Martinez-Zaguilan et al., 1996, Rothberg et al., 2013).

Intracellular pH (pH_i) is an important determinant of melanoma metabolism and signal transduction (Corbet and Feron, 2017). As pH_i acidifies, nuclear histones are globally deacetylated by histone deacetylases (HDACs) and Sirtuins, and the released nuclear acetate anions are co-exported with protons out of the cell by monocarboxylate transporters (MCTs) to maintain intracellular pH balance (McBrian et al., 2013). Intracellular acidification thus directly impacts on the access of transcription factors to euchromatin via its effect on nuclear histone deacetylation (Raja et al., 2020). Nuclear-translocated Acetyl-CoA Synthetase Short Chain Family Member 2 (ACSS2) has been shown to bind to the MiT family transcription factor EB (TFEB) during periods of acidification and glucose starvation, which enabled localised production of acetyl-CoA and acetate to support TFEB-related histone acetylation, TFEB transcriptional activity, lysosomal biogenesis and autophagic activity (Li et al., 2017). Abnormal intracellular acidity is also mutagenic and impairs DNA repair mechanisms, thereby promoting genomic instability and sensitises cells to other mutagens such as UV irradiation and hypoxia (Yuan et al., 2000). Thus, both intracellular and extracellular pH play important roles in melanomagenesis (Corbet and Feron, 2017).

Aetiologies of melanoma cell and melanoma microenvironmental acidification The pH_e of the melanoma microenvironment ranges between pH 5.5 and 7.4, whilst normal differentiated cells reside in an extracellular pH (pH_e) of approximately 7.4 (Tannock and Rotin, 1989). The relative acidification of the melanoma microenvironment occurs due to several reasons: Vertical growth of the melanoma towards the skin surface exposes melanoma to low pH; angiogenic melanoma neovessels are structurally deficient and promote idiosyncratic tumour hypoxia and acidosis; localised or systemic inflammation associated with tumour growth lowers the ambient pH of the tumour tissue; and the increased metabolic rate within the melanoma tissue drives increased proton export into the microenvironment (Bohme and Bosserhoff, 2016). Of particular interest to this thesis is the main cellular metabolic pathways that contribute to cellular and microenvironmental acidification by generating intracellular metabolic acids (Chiche et al., 2010). These acid-generating metabolic pathways will be discussed below.

Upregulated Glycolysis in Melanoma In most physiological mammalian cells, glycolytic conversion of pyruvate to lactate by lactate dehydrogenase is inhibited in the presence of molecular oxygen, allowing the transport of pyruvate into the mitochondria for oxidative phosphorylation to take place (Gatenby and Gillies, 2004). This inhibition

is termed the Pasteur Effect, named after Louis Pasteur, the French biologist who first demonstrated that glucose flux was reduced in the presence of oxygen in 1857 (Racker, 1974). Physiological mammalian cells preserve this oxygen-dependent glycolytic flexibility to maintain adequate energy production throughout the entire range of oxygen concentrations (Gatenby and Gillies, 2004). In contrast, increased conversion of pyruvate to lactate even in the presence of abundant amounts of oxygen is known as aerobic glycolysis, or the Warburg Effect, named after Otto Warburg, the German physiologist who first observed this abnormal form of cancer cell energy metabolism (Warburg, 1956a, Warburg, 1956b). Many cancer cells show increased glycolytic rate even in the presence of oxygen, where the end product pyruvate is then converted to lactate, and exported from the cells to facilitate ATP production (Liberti and Locasale, 2016). Measurably, the glycolytic flux of rapidly growing cancer cells may be increased by up to 200 times compared with normal differentiated cells (Warburg, 1956a).

Stoichiometrically, glycolysis itself generates 2 net ATPs per cycle in the cytosol. Thereafter, aerobic decarboxylation of pyruvate, tricarboxylic acid cycle, and aerobic respiration catabolise pyruvate to CO_2 and H_2O, yielding 36 additional ATPs per glucose molecule (Yetkin-Arik et al., 2019). Hence, Warburg metabolism in melanoma cells, which drives glycolysis and reduce mitochondrial flux in the presence of Oxygen, is biochemically inefficient in nature (Vander Heiden et al., 2009). On the contrary, the

pathological advantage that aerobic glycolysis provides for melanoma cells over cellular respiration is that glycolytic metabolism is faster, and shunting through the pentose phosphate pathway for nucleotide synthesis is more robust (Bohme and Bosserhoff, 2016). Microarray studies showed that a significant portion of the upregulated genes in cancer is involved in glycolysis (Altenberg and Greulich, 2004). Consequently, melanoma cells reprogram their metabolism to maintain constitutively upregulated glycolytic flux, which results in increased glucose uptake as well as increased lactic acid export, at the expense of interstitial and cellular acidification (Jiang, 2017).

Highly Active Pentose Phosphate Pathway in Melanoma The anabolic Pentose Phosphate Pathway (PPP) is diverted from glycolysis and shunts glucose-6-phosphate to generate NADPH, pentoses, and ribose-5-phosphate, the latter of which represents precursor for nucleotide synthesis (Kowalik et al., 2017). PPP is highly active within melanoma cells, and constitutes a major metabolic pathway for nucleotide synthesis, as well as providing the reductive potential for anabolic metabolism and melanoma growth (Jin and Zhou, 2019). PPP is a significant producer of CO_2 and contributes one CO_2 molecule per glucose molecule shunted (Horecker, 2002). CO_2 freely diffuses across the plasma membrane, and can be reversibly hydrated to carbonic

acid, protons and bicarbonate by the catalytic activity of carbonic anhydrase II intracellularly and carbonic anhydrase IX and XII extracellularly (Supuran, 2018). PPP thus provides an alternative source of melanoma intracellular acidification, via the generation of carbonic acid as metabolic byproduct (Jin and Zhou, 2019).

Glutaminolysis in Melanoma Glutaminolysis also contributes to acidification of the melanoma cell and its microenvironment (Kallinowski et al., 1987). Glutaminolysis occurs through a series of biochemical reactions, which converts the amino acid glutamine to glutamate and α-ketoglutarate, intermediary metabolites that can then be metabolised to cellular nutrients such as aspartate, alanine, pyruvate, lactate, and citrate (Yang et al., 2017). Glutaminase catalyses the first step of glutaminolysis, hydrolysing the amino group of glutamine to yield glutamate and ammonium (Peyton et al., 2018). Glutamate can then be further metabolised to α-ketoglutarate (αKG) by glutamate dehydrogenase (Plaitakis et al., 2017). Glutaminolysis is primarily used in ammonium transport, and provides substrate for nucleotide and protein biosynthesis (Wang et al., 2014b). Biochemically, the production of αKG by glutaminolysis refuels the TCA cycle, and αKG can also be used as an intermediate in the malate-aspartate shuttle to generate NADH, a metabolite used to sustain the electron transport chain (Wang et al., 2014b). Keeping the malate-aspartate shuttle active via a steady supply of

αKG enables the cytosolic NAD(P)-dependent malate decarboxylase (malic enzyme) to convert Malate to pyruvate (Feron, 2009). The generation of pyruvate via glutaminolysis thus provides an additional source of lactic acid production, and promotes intracellular acidification in melanoma cells (Wang et al., 2014b).

Hypoxia-Regulated HIF Pathway Activity in Melanoma One of the best-characterised microenvironmental factors that shapes melanoma behaviour is tumour hypoxia (Wykoff et al., 2000). Low oxygen tension ensues within rapidly expanding tumours that possess disorganised neovascularisation and angiogenesis (Harris, 2002). Hence, the further the melanoma mass growths away from its primary blood supply – and the poorer the quality of the microvasculature – the more hypoxic the melanoma parenchyma becomes (Peers et al., 2007). Hypoxia activates the potent and well-known signal transduction pathway involving the transcription factor hypoxia inducible factor (HIF), where HIF becomes stabilised under hypoxic conditions for transcriptional activity (Seagroves et al., 2001). Under normal oxygen tension, HIF is prolyl-hydroxylated in an oxygen-sensitive manner, and degraded via the tumour suppressor VHL-E3 Ubiquitin ligase pathway (Semenza, 2003). During hypoxia, prolyl hydroxylation of HIF is absent, leading to HIF stabilisation and homodimerization (Semenza, 2003). The stabilised and homodimerised HIF undergoes nuclear-

translocation, and initiates gene transcription by recognising hypoxia response elements on target gene promoters, thereby transactivating HIF-dependent pathways (Semenza, 2003).

HIF transcription augments anaerobic glycolysis and upregulates lactate dehydrogenase, both biochemical reactions that lead to lactic acid production and intracellular acidification (Semenza, 2003). HIF also upregulates pyruvate dehydrogenase kinase 1 (PDK1), which through phosphorylation inhibits pyruvate dehydrogenase, and prevents the decarboxylation of pyruvate into Acetyl-CoA, inhibiting the entry point of mitochondrial Kreb's cycle and cellular respiration (Kim et al., 2006). To facilitate glucose transport into the melanoma cell, HIF directly upregulates the expression of glucose transporters GLUT1 and GLUT3 (Kilic et al., 2007). To promote export of waste lactic acid out of the tumour cell, HIF also transcribes the monocarboxylate transporter MCT4 (Ullah et al., 2006). HIF thus regulates not only the cellular entry of glycolytic substrates, but also the exit of metabolic acids generated as byproducts of glycolytic metabolism, including that of lactic acid (Shimoda et al., 2006). In addition, HIF transactivates Carbonic anhydrase II and XII, which directly acidifies the cellular cytosol and extracellular interstitium, respectively, via catalysing the enzymatic interconversion of carbon dioxide and water, to the dissociated ions of carbonic acid (Potter and Harris, 2004). Therefore, not only

does HIF play the role of the molecular oxygen sensor in melanoma, but by nature of its transcriptional activity, HIF also promotes metabolic acidosis within the melanoma microenvironment, exerting a profound influence on melanoma pH (Balamurugan, 2016).

In malignant melanoma cells, HIF activity may be constitutively upregulated in the absence of hypoxia, through activating mutations in the mediators of the MAPK cascade, prominent examples of which include the $BRAF^{V600E}$ mutation (Kumar et al., 2007), and the $NRAS^{Q61K}$ mutation (Papale et al., 2018). HIF can also be pathologically upregulated by the loss of PTEN (Phosphatase and Tensin Homolog) tumour suppressor, leading to unopposed PKB/AKT signal transduction (Zundel et al., 2000). Furthermore, acidosis has been shown to induce HIF2α expression in glioma (Hjelmeland et al, 2011), thus creating a feedback loop regulation where HIF signalling is increased in the presence of acidic pH (Corbet and Feron, 2017). As such, HIF activity can be pathologically upregulated by melanoma driver gene mutations, which subsequently induces tumour acidosis in the setting of melanomagenesis (Corbet and Feron, 2017).

Proton Transporters in Melanoma

Presented with various metabolic sources of intracellular lactate, acetate, and proton production, melanoma cells require molecular mechanisms to dispose of these

acidic byproducts, in order to maintain cellular viability (Bohme and Bosserhoff, 2016). A set of proton transporters embedded within the plasma membrane of the melanoma cell are tasked with exporting metabolic acids from the cell in order to maintain intracellular pH homeostasis (Hiremath et al., 2018). Acting via primary or secondary active transport, these ionophores facilitate the movement of protons and monocarboxylates in and out of the various subcellular compartments to maintain pH and solute concentrations within the physiological range (Ives and Rector, 1984). Several well-described classes of proton transporters exist – (1) Sodium Hydrogen Exchangers (NHE); (2) Bicarbonate transporters, including the Sodium Bicarbonate Cotransporters (NBC) and Anion exchangers (AE); (3) Monocarboxylate Transporters (MCT); and (4) V-Type ATPase, as reviewed in Pugnini et al, 2015 (Spugnini et al., 2015).

In total, more than 100 types of proton transporter genes are present in the melanoma cell, and the proton transporter gene products can be functionally sub-classified as proton pumps, carriers, and channels, depending on the mechanism of proton transport (Alexander et al., 2019). Proton transporters that have been functionally and molecularly characterised in melanoma cells to date are discussed below.

Functional and Molecular Characterisation of Proton Transporters in Melanoma Sarangaranjan and Colleagues were the first to functionally and molecularly characterize the sodium-hydrogen exchanger in cultured melanocytes and melanoma cells (Sarangarajan et al., 2001). The presence of NHE isoforms 1-5 in melanoma cell lines were detected using RT-PCR, western blotting, Immunofluorescence, and Immunohistochemistry techniques (Sarangarajan et al., 2001). Functional activity of NHE was measured in melanoma cells using BCECF microspectrofluorometry (Sarangarajan et al., 2001). Similar to other cell types, NHE1 was shown to be the predominant NHE isoform functionally existent in melanoma cells (Sarangarajan et al., 2001). Migratory functions including lamellipodia formation, adhesion to and migration on collage matrix in human melanoma cells are also dependent on NHE function (Stock et al., 2005).

Wahl and Colleagues showed that MCT1, MCT4, and NHE1 were all present and functionally active in melanoma cell lines (Wahl et al., 2002). Proton extrusion functions of these melanoma cells were tested in the presence of specific inhibitors, including HOE642 (Cariporide, an NHE1 inhibitor), 2-Cyano-3-(4-hydroxyphenyl)-2-propenoic acid (CHC, a non-selective inhibitor of MCT1 and 4), and 4,4-di-isothiocyanato-stilbene-2,2-disulfonate (DIDS, a non-selective inhibitor of AE and NBC) (Wahl et al., 2002). The activity of MCT1 was potentiated by incubation in low

pH_e, but that of NHE1 was not (Wahl et al., 2002). Furthermore, MCT1, rather than NHE1, was shown to be the major determinant of pH_i equilibrium in the xenograft-derived melanoma cell line DB-1, suggesting that proton-coupled monocarboxylate transport played an important role in melanoma biology (Wahl et al., 2002).

Smith and Colleagues identified the presence of V-Type ATPase, as well as NHE isoforms in human melanocytes, and that the NHE inhibitor EIPA regulated melanosomal pH and tyrosinase activity in melanocytes (Smith et al., 2004). Cleistanthin A, a diphyllin glycoside that acts as a novel V-Type ATPase inhibitor, directly inhibited V-Type ATPase activity, lysosomal pH, cell viability, wound-healing and Transwell migration in A375 melanoma cells (Pan et al., 2017). Nishisho and colleagues also demonstrated that the V-Type ATPase isoform a3 was highly expressed in high-metastatic B16-F10 melanoma cells (Nishisho et al., 2011). They showed that in B16-F10 murine melanoma cells, knocking down a3 V-ATPase reduced B16-F10 invasiveness, migration and MMP-2 and MMP-9 expression (Nishisho et al., 2011). Thus, studies have documented the functional presence and importance of proton transporters in melanoma cells (Bohme and Bosserhoff, 2016).

Some controversies exist currently in terms of showing the presence of bicarbonate handling in melanoma cells (Koch and Schwab, 2019). In some studies, Carbonic anhydrase II and XII were shown to be histochemically present in normal skin and a

series of skin cancers, but absent in melanomas (Feichtinger et al., 2018, Syrjanen et al., 2014). In other studies, the use of CA IX inhibitors FC9-399A and S4 were shown to inhibit cell proliferation and induce apoptosis in melanoma cells ((Federici et al., 2016, Andreucci et al., 2017). It remains unknown if other classes of bicarbonate transporters including the Cl^-/HCO^- exchangers (CBEs), Na^+/HCO_3^- cotransporters (NBC), the Na^+-dependent $Cl^-/HCO3^-$ exchanger (NDCBE), and anion exchangers (AEs) play a role in human melanoma cells (Koch and Schwab, 2019).

Sodium Hydrogen Exchanger The sodium hydrogen exchanger is an integral membrane proton transporter that mediates electroneutral exchange of proton with sodium (Loo et al., 2012). Nine mammalian NHE isoforms (NHE1-9) have been identified thus far, and they display considerable variation in tissue expression, subcellular localisation, ion transport characteristics, pharmacological properties, and regulatory mechanisms (Ohgaki et al., 2011). In terms of subcellular localisation, NHEs can be categorised into two types: plasma membrane NHEs (NHE 1-5), and organellar NHEs (NHE 6-9) (Ohgaki et al., 2011). Plasma membrane NHEs largely localises to the plasma membrane of cells, and mediate the classical functions attributed to NHE transporters, including pH regulation, osmolarity and cell volume regulation, and cell migration (Slepkov et al., 2007). On the other hand, organellar NHEs localise to various

intracellular compartments along the secretory and endocytic pathways, and contribute to the establishment and/or fine-tuning of organellar luminal pH (Schwede et al., 2014). In terms of tissue expression, NHE1 is ubiquitously expressed, whilst NHE2 and 3 are present abundantly in the stomach, intestinal tract, skeletal muscle and kidney, but also in the brain, testes, and uterus (Orlowski and Grinstein, 2004). NHE4 is mainly found in the stomach, and NHE5 is expressed significantly in the brain. NHE6-9 are expressed broadly across most cell types – NHE6 and 9 found in sorting and recycling endosomes, NHE7 in the transgolgi network (TGN) and endosomes, and NHE8 in the mid/trans-Golgi stacks (Ohgaki et al., 2011). Nevertheless, organellar NHEs are particularly expressed in skeletal muscle (NHE6-8), brain (NHE6 and 7), and kidney (NHE8) (Ohgaki et al., 2011).

NHE1 is the best characterised isoform of the sodium hydrogen exchanger family to date (Amith and Fliegel, 2013). The human sodium hydrogen exchanger 1 (NHE1) is a membrane transporter that is 815 amino acids in length, with residues 1-500 comprising the membrane domain that contains 12 transmembrane helices, and residues 501-815 comprising the cytoplasmic tail (Amith and Fliegel, 2013). The transmembrane domain functions as a secondary active transporter that extrudes one intracellular proton in exchange for one extracellular sodium ion, thus regulating intracellular pH (Ding et al., 2007). Ion flux is powered by the transmembrane sodium

electrochemical gradient and requires no direct metabolic input from the cell (Ding et al., 2007). The transmembrane domain also pockets a proton-binding allosteric regulatory domain, which potentiates sodium-hydrogen exchange as pHi decreases, resulting in auto-regulation of NHE activity in response to a decrease in pHi (Valles et al., 2015).

NHE1 is also allosterically regulated by post-translational modifications, including phosphorylation of key residues in its C-terminal cytoplasmic tail, as well as interactions of its C terminal with intracellular binding proteins and lipids (Amith and Fliegel, 2013). The C-terminal regulators of NHE1 activity may be activated by autocrine, paracrine, and endocrine signalling via growth factors, hormones, and other agonists such as serum, thrombin, EGF, insulin, angiotensin II (Stock and Pedersen, 2017). The effect of these allosteric regulators of NHE1 cytoplasmic tail is to alter the affinity of the transmembrane domain for intracellular protons, thus setting its transport activity to be potentiated at a more alkaline pH, and maintaining a more alkaline intracellular pH overall (Putney et al., 2002).

Allosteric binding proteins of NHE1's C-terminal tail include various signal transduction intermediary proteins, such as Phosphatidylinositol 4,5-bisphosphate (PIP2), which binds to residues 513-520, and 556-564 of NHE1, and subjects NHE1 to G Protein-Coupled Receptor signalling via Gq (Abu Jawdeh et al., 2011). Closely

related calcium-based regulation of NHE1 also includes binding sites for calmodulin (CaM) at residues 636-700 (Wakabayashi et al., 1994). Calmodulin also blocks an autoinhibitory site, thereby activating NHE1 (Wakabayashi et al., 1997). In addition, Calcineurin Homologous Proteins 1 and 2 (CHP1 and CHP2) bind to NHE1 at residues 518-537, thus enabling calcium signalling to exert multiple control mechanisms to influence NHE1 activity (Ammar et al., 2006). PI3K signalling also controls NHE1, with PKB/Akt binding to NHE1 at residue 648, linking the Akt-mediated survival pathways with NHE1-mediated intracellular alkalinisation (Meima et al., 2009). Furthermore, Receptor tyrosine kinase signalling induces NHE1 C-terminal activity, with HER2-phosphorylating NHE1 at Ser^{703}, which induces 14-3-3 proteins to interact with NHE1 (Lehoux et al., 2001). Downstream MAP kinases influence NHE1 activity, with p38 MAPK phosphorylating NHE1 at residues 718, 723, 726, and 729 (Díaz et al., 2019), whilst ERK1/2 phosphorylate NHE1 at residues 770 and 771 (Luo et al., 2007). Carbonic Anhydrase II (CAII) can bind to NHE1 at residues 790-802 (Li et al., 2002), and Actin-binding ERM proteins also interact with NHE1 at residues 552 and 560 (Denker et al., 2000) , localising NHE1 to the microfilament-abundant regions of the plasma membrane, and implicating NHE1 activity in cell migration at the leading edge (Clement et al., 2013). Taken together, NHE1 is a highly important functional regulator of intracellular pH, not only driven by the sodium electrochemical gradient, and

equipped with autoregulatory activity for pH maintenance, but also is allosterically regulated by various key signal transduction pathways that govern cell proliferation, survival, and cell shape (Orlowski and Grinstein, 2004).

Monocarboxylate Transporter The Monocarboxylate Transporter (MCT) is a membrane-bound transporter, which mediates the bidirectional co-transport of protons with monocarboxylates, a metabolically important class of molecules that includes pyruvate, lactate, acetate, and ketone bodies – Acetoacetate and beta-hydroxybutyrate (Halestrap and Meredith, 2004). The monocarboxylates are produced and utilized by many important metabolic pathways, including, and not limited to, intracellular pH regulation, glycolysis, tricarboxylic cycle, electron transport chain, fatty acid and protein metabolism, and ketolysis (Poole and Halestrap, 1993). The co-transportation of lactate with protons balances stoichiometrically because metabolic pathways such as glycolysis tend to produce lactic acid, rather than the lactate anion in isolation (Meredith and Christian, 2008). As such, cytosolic concentrations of both monocarboxylates and protons need to be regulated to maintain cellular viability, and MCTs functions to rapidly transport excesses of both substrates across the plasma membrane and out of the cells to achieve pH_i homeostasis (Halestrap and Price, 1999).

MCTs are part of a family of transporter proteins, known as the SLC16 solute carrier

family, and they share common sequence motifs (Halestrap and Price, 1999). The MCT family members possess 12 transmembrane helices (TMs), with cytoplasmic N- and C-terminal ends (Poole et al., 1996), and a large cytosolic loop also exists between TM 6 and 7 (Halestrap and Meredith, 2004). The MCT family has a total of 14 members, but only MCTs 1-4 have been confirmed to function as monocarboxylate-proton co-transporters (Halestrap, 1975). MCT10 was identified as an aromatic amino acid transporter named T-Type amino acid transporter 1 (TAT1) (Kim et al., 2001), whilst MCT8 had been shown to be an important thyroid hormone transporter (Friesema et al., 2003). Neither MCT8 nor MCT10 is proton-linked (Friesema et al., 2003, Kim et al., 2001). The function of the other 8 MCTs is currently undetermined (Halestrap, 2012). A discrepancy in the MCT and SLC16 nomenclature systems for these monocarboxylate transporters also exist, and the numbering of MCT and SLC16 family members do not perfectly coincide (Halestrap, 2012). MCT1 is also termed SLC16A1, but MCT2 is termed SLC16A7, MCT3 named SLC16A8, and MCT4 SLC16A2 (Jones and Morris, 2016). This difference arose because MCTs were named in order of their characterisation at the functional level, while the SLC16 nomenclature were decided after their cDNA sequences became available (Jones and Morris, 2016).

Major differences between the 4 isoforms of the proton-monocarboxylate co-transporting MCTs exist in terms of their relative substrate and inhibitor affinities, the

regulation of their expression, their tissue distribution, and subcellular localization (Halestrap, 1975). MCT1 is expressed in almost all tissues, and has been shown to transport a broad range of short-chain monocarboxylates across the plasma membrane, adhering to Michaelis Menten kinetics (Jackson and Halestrap, 1996). Monocarboxylates transported by MCT1 include monocarboxylates with side chain substitutions at the 2- and 3- positions – for example, with halides, hydroxyl, and carboxyl groups (Jackson and Halestrap, 1996). These monocarboxylates include L-lactate, D-lactate, pyruvate, glyoxylate, oxamate, and formate (Jackson and Halestrap, 1996). In addition, the transport of unsubstituted short-chain fatty acids, such as acetate, propionate, and butyrate, is also strongly facilitated by MCT1, though these substrates also freely diffuse across the plasma membrane without the need for any transporter activity (Vijay and Morris, 2014). By far, the predominant role of MCT1 is to facilitate the unidirectional proton-linked transport of L-Lactate across the plasma membrane (Ideno et al., 2018). This may represent either influx or efflux of lactic acid depending on the prevailing intracellular and extracellular substrate concentrations and the pH gradient across the plasma membrane (Ideno et al., 2018). In myocytes and neurons, MCT1 transports both lactate and ketone bodies into the cell to be used as respiratory fuel (Kobayashi et al., 2005). In contrast, under conditions of hypoxia, anaerobic glycolysis necessitates the export of lactic acid, which is also mediated by MCT1 as the

predominant isoform expressed in most tissues (Doherty et al., 2014).

The ordered mechanism for MCT transport predicts that when transporting lactate into cells, MCT1 has a substrate binding site open to the extracellular matrix that binds a proton first, followed by the lactate anion (Deuticke, 1982). Lysine (K38) in MCT1's hydrophobic catalytic pocket is normally uncharged, but when accepting a proton, the resultant positive charge provides the binding site for the subsequent monocarboxylate anion (Manoharan et al., 2006). Following proton and monocarboxylate binding, the protein undergoes conformational change to a new "Closed" conformation that exposes both the proton and lactate to the opposite surface of the membrane where they are released, lactate first and then the proton (Manoharan et al., 2006). Aspartate and arginine (D302/R306) residues are likely to be critical for MCT1 conformational change, allowing K38 to pass the proton to D302/R306, and returning MCT1 to its basal relaxed state (Manoharan et al., 2006).

MCT2 is the second isoform of MCT and has a higher affinity for substrates than MCT1 (Poole et al., 1989). MCT2 expression is thus predominantly confined to tissues that take up lactic acid in significant quantities for metabolic fuel (eg. Neurons) or for gluconeogenesis (eg. Liver parenchymal cells and kidney proximal convoluted tubules) (Edlund and Halestrap, 1988). In Xenopus oocytes, K_m for pyruvate and L-Lactate were 0.1 and 0.74mM for MCT2, respectively, compared to values of 1 and 3.5mM for

MCT1 (Bröer et al., 1999). In the brain, MCT2 expression is largely confined to the post-synaptic density of neurons, and this may reflect a unique functional role related to its high substrate affinity, facilitating the uptake of lactate for oxidation as a respiratory fuel (Bergersen et al., 2001). MCT3 on the other hand was identified as a developmentally expressed protein in chick retinal pigment epithelium, with a Km for L-Lactate of approximately 6mM (Grollman et al., 2000). Expression of MCT3 is confined to the RPE and choroid plexus epithelia, and is thought to play an important role in facilitating the transport of glycolytically derived lactic acid out of the retina (Philp et al., 1995).

MCT4 is widely expressed in terms of tissue distribution and especially so in glycolytic tissues such as white skeletal muscle fibres, astrocytes, white blood cells, and chondrocytes (Price et al., 1998). Whilst MCT4 exhibits a lower affinity for most substrates and inhibitors than MCT1 (Halestrap and Meredith, 2004), with Km and Ki values some 5-10 times higher at 28 and 150mM, respectively (MCT4 also shows little inhibition by DIDS or CHC at the concentrations above the IC50 of MCT1) (Halestrap and Meredith, 2004), functionally MCT4 is well-suited for exporting lactic acid derived from glycolysis, since its Km for pyruvate is significantly higher than that for lactate, allowing cells to preserve pyruvate for maintaining cytosolic NADH/NAD+ ratio by further reducing pyruvate to lactate (Fox et al., 2000). Tumour cells in particular are

highly dependent on aerobic glycolysis for ATP synthesis (Fadaka et al., 2017). Though some tumour cells use MCT1 to export the lactic acid produced from aerobic glycolysis, more invasive tumours in particular are known to possess upregulated MCT4 activity, which may be the result of induction by HIF1a activation during tumourigenesis (Kim et al., 2018). MCT4 in this pathophysiological capacity may mediate the specialised role of glycolytic lactic acid export in tumour pseudohypoxia (Kim et al., 2018).

Ancillary Proteins of the Monocarboxylate Transporter MCTs are physically associated with their ancillary proteins, embigen (also known as gp-70) (Poole and Halestrap, 1997) and basigin (also known as CD147, OX-47, EMMPRIN, or HT7) (Iacono et al., 2007). Basigin in particular is widely expressed in many tissue types (Iacono et al., 2007). Both basigin and embigin have a single transmembrane domain, a short intracellular C-terminus, and a large glycosylated extracellular domain with two or three immunoglobulin domains depending on the splice variant (Iacono et al., 2007). Basigin enables MCT1 and MCT4 to be correctly targeted to the plasma membrane, as such it is an essential chaperone for both MCTs (Kirk et al., 2000). Immunoprecipitation and FRET studies suggest MCT1 and basigin may exist as a heterodimer (Wilson et al., 2002). In contrast, embigin is the preferred binding partner for MCT2 (Ovens et al., 2010b).

The importance of these ancillary proteins for MCT can be demonstrated when organomercurial agents are used to inhibit MCTs, where the resultant conformational change and loss of association with basigin appears to inhibit MCT's transporter activity (Wilson et al., 2005). In addition, inhibition of MCT2 by AR-C155858 was greatly reduced when MCT2 was co-expressed with embigin in Xenopus (Ovens et al., 2010b). Therefore, basigin and embigin may be important components that enable MCT function (Poole and Halestrap, 1997).

Regulatory Mechanisms of Monocarboxylate Transporter There are a limited number of studies that address the allosteric regulation of MCT activity (Halestrap, 2012). The second messenger cAMP has been reported to stimulate MCT1 activity in rat brain endothelial cells, though the results have been inconsistent (Smith et al., 2012). Both MCT1 and MCT4 have been shown to interact with the cytosolic carbonic anhydrase II (CA-II), and this interaction induces MCT transporter activity (Halestrap, 2012). MCT2 on the other hand interacts with and is enhanced by the extracellular CAIV (Klier et al., 2011). The binding of MCT and CAII is mediated by the His^{64} residue on CAII (Noor et al., 2018), whilst residues Glu^{69} and Asp^{72} on CAII are important for proton shuttling between the two proteins (Noor et al., 2018). Such experiments show that MCTs cooperate with the carbonic anhydrases to ensure rapid

shuttling of metabolites across the cell membrane (Halestrap, 1975).

Transcriptionally, in human and rat skeletal muscle, numerous studies have demonstrated the upregulation of MCT1 in response to chronic stimulation or exercise (Coles et al., 2004). In contrast, downregulation of MCT1 expression occurred in denervation or spinal cord injuries (Kitaoka et al., 2014). In the context of exercise, upregulation of MCT1 was thought to be consequent to activation of gene expression, mediated by the calcium and AMP signal transduction pathways, involving calcineurin and AMP kinase, respectively (Takimoto et al., 2013). Similarly, addition of 5-aminoimidazole-4-carboxamide-1-b-D-ribonucleotide (AICAR), the analog of AMP that is capable of stimulating AMPK activity, induced MCT1 promoter activity, as shown by luciferase assays in L6 myoblasts and HepG2 hepatoma cells (Pierre and Pellerin, 2005).

In T-lymphocytes, proliferation involves the concurrent upregulation of glycolysis and lactic acid efflux, and thus T-lymphocytic activation is accompanied by a significant increase in MCT1 expression (Wang and Green, 2012). The *MCT1* promoter contains several consensus binding sequences for Nuclear Factor of Activated T-Cells (NFAT), and as such, Cyclosporine and FK506, the inhibitors of NFAT, have both shown to be capable of inhibitor *MCT1* expression in skeletal muscle (Pérez-Escuredo et al., 2016). The association between Cyclosporin-mediated immunosuppression and

concurrent inhibition of MCT expression also points to a role for MCT in immunomodulation (Murray et al., 2005).

The major regulatory mechanism governing MCT4 expression is hypoxia, and this is consistent with the proposed role for MCT4 in exporting lactic acid derived from glycolysis (Ullah et al., 2006). Hypoxia increases the expression of MCT4 mRNA and protein in a variety of cells, and *MCT4* transactivation can also be reproduced by cobalt treatment (Pérez de Heredia et al., 2010). These experiments implicate HIF1α in transcriptional regulation of *MCT4* (Ullah et al., 2006). Luciferase promoter construct experiments showed that the *MCT4* promoter is indeed transactivated in the hypoxic environment, an effect that was not observed for *MCT1* and *MCT2* promoters (Ullah et al., 2006). Hypoxic *MCT4* promoter luciferase luminescence was abolished in cells with HIF1α silencing, consistent with the identification of hypoxic response elements in the *MCT4* promoter (Doran et al., 2011).

Monocarboxylate Transporter Inhibitors Numerous pharmacological competitive inhibitors of MCT1 have been described (Payen et al., 2019). The classical inhibitors of MCT were developed in the 1970s, including the α-Cyanocinnamate derivatives such as α-Cyano-4hydroxycinnamate (CHC), and stilbene disulfonates such as 4,4-di-isothiocyanato-stilbene-2,2-disulfonate (DIDS) and 4,4'-

dibenzamidostilbene-2,2'-disulfonate (DBDS) (Curtis et al., 2017). CHC and DBDS were shown to be relatively non-specific inhibitors of MCT (Halestrap, 1976). For example, CHC inhibited the mitochondrial pyruvate transporter at 2 orders of magnitude more potently than MCT1 itself, whilst DBDS inhibits the chloride/bicarbonate exchanger AE1 more potently than MCT1 (Halestrap, 1975). Second generation MCT inhibitors have since been developed to specifically target the MCT class of transporters with greatly reduced IC50 (Murray et al., 2005).

In 1995, a novel structural class of immunomodulatory compounds, known as the Pteridine Di/Triones, was discovered by AstraZeneca (Michne et al., 1995). These pharmacological immunomodulators produced specific inhibition of human and rat T lymphocyte proliferation in vitro with nanomolar potency (Michne et al., 1995). These compounds were shown to bind specifically to MCT1 and MCT2, but not to MCT4 (Murray et al., 2005). As T-lymphocyte activation and proliferation were accompanied by a significant (up to 14- fold) upregulation of glycolysis, it was reasoned that inhibiting MCT1 induced the immunosuppression of T-Cells by curtailing the efflux of the glycolytic waste, lactic acid from T cells, thus hampering proliferative metabolism (Murray et al., 2005).

One of the best characterised compounds from the series of Pteridine Di/Trione MCT1 inhibitors was AR-C155858 (Ovens et al., 2010a). AR-C155858's

pharmacological activity was attributed to its binding to an intracellular site within MCT1 and MCT2, located in the Transmembrane Helices 7-10 (Ovens et al., 2010a). Key residues responsible for MCT1 binding to AR-C155858 included Phe^{360} (TM10) and Asp^{302} plus Arg^{306} (TM8) (Ovens et al., 2010a). Other potent MCT1 inhibitors derived from the Pteridine Di/Trione series of MCT1 inhibitors included AR-C122982 (also known as SR13800) (Wang et al., 2014a), AR-C141990 (Pahlman et al., 2013), and AZD3965 (Ekberg et al., 2007).

Whilst some preclinical studies continued to focus on the immunosuppressive properties of the Pteridine Di/Trione MCT1 inhibitors (Ekberg et al., 2007), others began to test the anti-cancer effects of specific pharmacological MCT inhibition (Doherty et al., 2014). Disrupting MCT1 function using AR-C155858 led to an accumulation of intracellular lactate that rapidly disables tumour cell growth and inhibited glycolysis in tumour cells (Doherty et al., 2014). MCT1 inhibition also provoked marked alterations in intracellular concentrations of glycolytic intermediates, as well as reducing GLUT-mediated glucose transport (Guan et al., 2019). AR-C155858 treatment lowered the concentrations of glycolytic end-products ATP, NADPH, and ultimately, glutathione (GSH) (Guan et al., 2019). In one report, reductions in GSH from pharmacological MCT1 inhibition led to increases in hydrogen peroxide, mitochondrial damage, and apoptosis in tested cancer cell lines, such as Raji

Burkitt's lymphoma cells and the breast cancer cell line MCF7 (Doherty et al., 2014). These studies were supported by evidence that RNAi targeting MCT1 induced cell death in glioma cell lines (Mathupala et al., 2004).

AZD3965 is the orally bioavailable MCT1-specific inhibitor, derived from ARC155858 (Ekberg et al., 2007). AZD3965 is undergoing phase I clinical trial evaluation in the United Kingdom for targeted therapy in advanced solid tumours (Halford et al., 2017) . In SCLC murine xenografts, AZD3965 reduced tumour growth *in vivo* and increased intratumoural lactate (Polanski et al., 2014). A recent study using AZD3965 in melanoma showed that inhibition of MCT1 reduced lactate uptake, and resulted in depletion of circulating melanoma cells, an outcome that lowered the metastatic disease burden in patient-derived xenografts and murine melanomas (Tasdogan et al., 2020). In addition, inhibition of MCT1 suppressed the oxidative pentose phosphate pathway and increased levels of reactive oxygen species in murine melanoma xenografts (Tasdogan et al., 2020). Therefore, Pteridine Di/Trione MCT1 inhibitors represent an emerging class of compounds with the potential for future use as targeted therapy in malignant melanoma (Corbet and Feron, 2017).

Recently, a dedicated cell-based screen identified a novel MCT1 inhibitor – the potent and orally available MCT1 inhibitor BAY-8002. (Quanz et al., 2018). Diffuse large B-cell lymphoma cell lines, and a subset of solid tumours were sensitive to MCT1

inhibition by BAY-8002 (Quanz et al., 2018). The study also showed that resistance to single-target MCT1 inhibition can develop via upregulation of MCT4 even in the presence of sufficient oxygen, as well as by shifting energy production towards oxidative phosphorylation (Quanz et al., 2018). Therefore, future pan-MCT inhibitors that also target the MCT4 isoform may prove to be superior to current generation MCT1-specific inhibitors, such as AZD9365 and BAY-8002 (Benjamin et al., 2018).

Solute Carrier 4 Family of Sodium Bicarbonate Transporters and Anion Exchangers The sodium bicarbonate transporters and anion exchangers belonging to the Solute Carrier 4 (SLC4) family include the gene products of ten genes (*SLC4A1-5*, *SLC4A7-11*) (Romero et al., 2013). The names of the SLC4 transporters reflect their transport functions: (1) SLC4A1, SLC4A2, and SLC4A3 are chloride-bicarbonate (or anion) exchangers (the AEs); (2) SLC4A4, SLC4A5, SLC4A7, and SLC4A10 are Na-HCO_3 cotransporters (the NBCs); and (3) SLC4A8 functions as a sodium-dependent chloride-bicarbonate exchanger (NDCBE) (Alper, 2009). Because SLC4A9's role as an anion exchanger has not been conclusively established (ie. AE4), its name should be considered provisional until it has been assigned permanently (Ko et al., 2002). *SLC4A6* has been shown to be a pseudogene (Romero et al., 2013). Of the NBCs, SLC4A4 and SLC4A5 are known as electrogenic NBCs (NBCe1 and NBCe2, respectively), based

on their ability to transport bicarbonate anions in an electrogenic manner (Romero, 2001) SLC4A7 and SLC4A10 are electroneutral NBCs (NBCn1 and NBCn2, respectively), as their transport activities do not alter the net membrane potential (Choi et al., 2000).

As discussed above, eight SLC4 family members have well-established functions, and represent key membrane proteins that transport bicarbonate, with at least one monoatomic ion (typically sodium or chloride) across the plasma membrane (Romero et al., 2013). The general structures of the SLC4 family members were modeled on SLC4A1 (AE1) and SLC4A4 (NBCe1) (Zhu et al., 2003). NBCe1 is composed of a long N-terminal hydrophilic domain, and a much shorter C-terminal hydrophilic domain, both of which are situated intracellularly (Zhang et al., 2000). The N-terminus of AE1 is a dimer according to X-ray crystallographic analysis, and 10-14 alpha-helical transmembrane segments separate the hydrophilic N and C termini (Zhang et al., 2000). A pharmacological similarity shared amongst some SLC4 members is their collective sensitivity to drug inhibition by the disulfonic stilbene derivative, 4,4-diisothiocyanatostilbene-2,2'-disulphonate (DIDS) (Romero et al., 2013). NBCn1 is the exception, as NBCn1 transport activity is largely DIDS-insensitive (Park et al., 2002). Another similarity the SLC4 family members share is their pattern of post-translational glycosylation (Romero et al., 2013). AE1 is N-glycosylated on only its 4th extracellular

loop, whereas AE2, AE3, and NBCe1 are all N-glycosylated on their third extracellular loops (Cheung et al., 2005).

Though SLC4 transporters share many common features as outlined above, the most striking difference between the SLC4 group members is their divergent modes of transport function (Parker and Boron, 2013). AE1, 2, and 3 transport bicarbonate anions via an exchange mechanism using monovalent anions from the opposite side of the membrane (Sekler et al., 1995). In contrast, the NBCs unidirectionally move bicarbonate anion together with a sodium cation from one side of the membrane to the other (Soleimani and Burnham, 2001). On the other hand, NDCBE functions as a hybrid co-transporter/exchanger, which co-transports a sodium cation with two bicarbonate anions into the cell, in exchange for the antiport of a single chloride anion (Virkki et al., 2003). Understanding how such closely related proteins can mediate such fundamentally different modes of bicarbonate transport represents one of the major challenges in the field of SLC4 study (Romero et al., 2013).

The second distinguishing feature between the different NBCs is the respective electrogenicity of their transport activities (Parker et al., 2008). NBCe1 and NBCe2 are electrogenic transporters: that is, one complete cycle of transporter activity results in the movement of one or two net negative charges across the membrane (Romero, 2001). Thus the bicarbonate transport activity of the electrogenic NBCs carries an

accompanying electrical current, and induces a shift in the net membrane potential (Romero, 2001). In contrast, electroneutral NBCs, as well as the other SLC4 family members move bicarbonate without shifting the net membrane potential – that is, a complete cycle of electroneutral transporter activity results in no net movement of electrical charge across the membrane (Choi et al., 2000). As such, electrogenicity represents a unique feature amongst a subset of the SLC4 proteins (Romero et al., 2013).

Anion Exchanger Isoforms The three anion exchangers within the SLC4 family mediate the electroneutral exchange of one monovalent anion for another across the plasma membrane (Jennings, 1976). The preferred substrates of the anion exchangers are bicarbonate and chloride, although the AEs can also transport hydroxide; and AE1 can co-transport SO_4^{2-} and proton, in exchange for Cl^- – albeit at a very low rate compared to monovalent anion exchange (Jennings, 1976). The physiologically relevant transport activity for the AEs is Cl^-/HCO_3^- exchange, and the transmembrane chemical gradients for these two ions determine the net direction of solute transport (Alper, 2009). In most cell types, it is the inward chloride gradient that dominates, which drives the outward movement of intracellular bicarbonate (Alper, 2010). This dominant reaction causes acidification of intracellular pH (Alper, 2010). For RBCs, in which anion exchanger function is critical, erythrocytic circulation in the systemic or

pulmonary bloodstream determines the net direction of anion transport (Boron et al., 2009). All three members of the anion exchangers are sensitive to DIDS inhibition (Barzilay et al., 1979).

AE1 is the anion exchanger of the erythrocytes, and one of the first transporters of any kind to be cloned and identified (Kopito and Lodish, 1985). AE1 is also known as "Band 3", named after its relative position among RBC membrane proteins, as stratified by SDS-PAGE electrophoresis (Kopito and Lodish, 1985). It is the most abundant membrane protein in RBCs, where it accounts for approximately 1/4 of all membrane protein (Zhu et al., 2003). The cytoplasmic N-terminal domain of human AE1 is 404 amino acids-long, and provides anchorage sites for several proteins, including components of the cytoskeleton, some glycolytic enzymes, and haemoglobin (Zhu et al., 2003). The membrane spanning domain of AE1 consists of 467 amino acids and is responsible for the anion-exchange function of the protein. The final 40AAs of human AE1, which is the cytoplasmic C-terminal of the protein, contains an anchorage site for GAPDH, and is a proposed binding site for cytoplasmic CAII (Vince and Reithmeier, 1998). In RBCs, AE1 plays a key role in CO_2 carriage, facilitating the pulmonary transfer of CO_2 from the erythrocytes to the alveolar epithelium, in a process called the Jacobs-Stewart Cycle (Jennings, 2013).

AE2 was cloned from the human kidney and lymphoma cells, and it is coined the

non-erythroid band 3 protein (Demuth et al., 1986). AE2 is widely distributed across the basolateral membranes of most epithelia (Alper et al., 1994, Stuart-Tilley et al., 1994). In gastric parietal cells, AE2 presumably plays a key role in facilitating gastric proton secretion, by exporting into the blood the excess bicarbonate that is generated via carbonic anhydrase-mediated deprotonation of carbonic acid (Stuart-Tilley et al., 1994). It can be reasonably deduced that in most cells in which AE2 is expressed, the anion exchanger actively contributes to the regulation of intracellular pH, by exporting bicarbonate in response to an intracellular alkali load. AE2 may also regulate cell volume by its uptake of chloride anions (Stewart et al., 2002).

AE3 was first identified in 1989 (Kopito et al., 1989). Human AE3 has two alternative promoters that yield two splice variants transcriptionally – the cardiac AE3 isoform (cAE3), and the brain AE3 isoform (bAE3) (Linn et al., 1992). The nomenclature of the AE3 isoforms is of historical significance only, as both splice variants have subsequently been found in the heart, brain, and elsewhere (Romero et al., 2013). Recent evidence showed that AE3 is distributed mostly to excitable tissues: the brain, retina, heart, and smooth muscles (Kobayashi et al., 1994). However, AE3 variants can also be expressed in epithelial cells, including those of the kidney and GI tract (Romero et al., 2013). AE3 activity is induced by intracellular alkalinisation (Salameh et al., 2017). Thus, it is hypothesised that AE3 contributes to the regulation

of pH_i by exporting HCO_3, in response to intracellular alkali loads (Salameh et al., 2017).

The electrogenic Na-Coupled Bicarbonate Transporters The two identified electrogenic sodium bicarbonate cotransporters, NBCe1 and NBCe2, mediate the co-transport of one sodium cation with either two or three bicarbonate anions (Romero and Boron, 1999). As a result, two negative charges cross the plasma membrane with each sodium, resulting in a net change in membrane potential (Romero and Boron, 1999). In most cases, the electrogenic NBC moves the equivalent of one sodium cation with two bicarbonate ions in one complete cycle of transport activity (Kurtz et al., 2004). The disulfonic stilbenes SITS and DIDS block the transport activity of both NBCe1 and NBCe2 (Liu et al., 2007). However, these compounds also inhibit the activity of the anion exchangers (Dix et al., 1979). Therefore, care in the interpretation of experimental data must be taken when using these stilbenes except for when cellular overexpression of a specific transporter is carried out (Romero et al., 2013).

NBCe1 was first described to be present in the renal proximal tubule, and it was first cloned in 1997 (Romero et al., 1997). Protein localisation studies have shown that NBCe1 is present in the basolateral membranes of renal proximal tubule, pancreatic ducts, and epididymis, as well as in astrocytes and neurons in several regions of the

brain, several tissues within the eye, as well as blood vessels and intercalated disks within the heart (Bok et al., 2001, Jensen et al., 1999, Schmitt et al., 1999).

In the kidney, NBCe1 mediates the movement of bicarbonate equivalents from the proximal tubule cells into the blood, thereby completing the resorption of bicarbonate from the renal tubular lumen to blood (Romero et al., 1997). In the pancreas, NBCe1 plays a major role in the accumulation and secretion of bicarbonate, from the exocrine pancreatic gland into the lumen of the pancreatic duct (Ishiguro et al., 1996). In non-epithelial cells, NBCe1 contributes to pHi regulation by moving alkali into cells in response to intracellular acid loads (Sciortino and Romero, 1999).

NBCe2 is expressed most abundantly in the liver, testes, and spleen (Pushkin et al., 2000). Lower levels are present in the heart, kidney, stomach, lung, and brain (Pushkin et al., 2000). NBCe2 has been identified as a positional candidate for hypertension, and polymorphisms of the *NBCe2* gene are associated with changes in baseline blood pressure in a 10yr follow-up study (Barkley et al., 2004). In mice, disruption of NBCe2 has been shown to cause both arterial hypertension and metabolic acidosis (Gröger et al., 2012).

Electroneutral Na coupled Bicarbonate transporters. The NBCn1 gene was discovered in the year 2000 (Pushkin et al., 2000), and in contrast to the two original

electrogenic NBCs discovered, NBCn1 transport activity was demonstrated to be electroneutral (Choi et al., 2000). This new family member was shown to be poorly sensitive to DIDS, and completely insensitive to EIPA (Park et al., 2002). The molecular basis for the poor sensitivity of NBCn1 to DIDS is apparently the lack of an intact DIDS motif at the extracellular end of the putative TM5 (Park et al., 2002).

High levels of NBCn1 mRNA is expressed in the spleen and testis, and low levels in the heart, brain, lungs, liver, and kidneys (Choi et al., 2000). In the kidneys, NBCn1 is expressed in the basolateral membrane of the thick ascending loop of Henle (Kwon et al., 2002), and in the inner medullary collecting ducts (Praetorius et al., 2004). The protein expression of NBCn1 can be induced by acidotic exposure, a cellular response to increase net epithelial ammonium transport (Lee et al., 2010). An NBCn1 knockout mouse model was recently created, and the mice developed blindness and auditory impairment as the result of sensory receptors degeneration (Bok et al., 2003) In breast cancer, multiple studies have also suggested a link between breast cancer susceptibility and presence of an SNP in *NBCn1* (Ahmed et al., 2009) The breast cancer cell line MCT-7, when overexpressing a truncated HER2 receptor, exhibited an enhanced acid-extruding capability, at least in part by upregulating the plasma membrane expression of the NBCn1 transporter (Gorbatenko et al., 2014).

The Na-dependent Cl-HCO3 exchanger was the first acid-base transporter shown

to play a role in pH_i regulation (Boron and De Weer, 1976). This transporter normally mediates the intracellular uptake of one sodium cation and two bicarbonate anion equivalents, in exchange for the export of one chloride anion (Boron et al., 1988). Northern blot analysis showed robust expression of the NDCBE transporter in the human brain and testis, as well as weaker expression in the kidneys and ovaries (Grichtchenko et al., 2001).

Vacuolar-Type Adenosine Triphosphatase V-Type ATPase is a primary active proton pump coupled to ATP-hydrolysis (Breton and Brown, 2013). V-Type ATPase transports protons out of the cytosol, either into the lumina of intracellular compartments, or in the case of plasmalemmal V-Type ATPase, into the extracellular space (Cotter et al., 2015b). V-Type ATPases are present in both the organellar membranes of lysosomes, endosomes, and secretory vesicles, as well as in the plasma membrane (Forgac, 2007). The role of endolysosomal V-Type ATPase is to acidify lysosomal pH, a necessary event for the subsequent breakdown of biomolecules, including peptides, nucleic acids, carbohydrates, and lipids (Kane, 2012). Mechanistically, low pH within the lysosome – measured at approximately pH 5.0 – is a prerequisite for the activation of approximately 50 different classes of lysosomal acid hydrolases, including proteases such as cathepsins; acid phosphatases, lysosomal acid

lipases, nucleases, glycosidases, sulfatases, and phospholipases (Marshansky et al., 2014). These acid-potentiated lysosomal effectors are responsible for carrying out the degradative functions that characterise lysosomal activity (Sun-Wada and Wada, 2013). The pH gradient across the lysosomal membrane is also used to facilitate the proton-coupled secondary active transport of many solutes in and out of the lysosome, including that of the amino acids and calcium (Breton and Brown, 2013). Solutes can thus be transported from the lysosome into the cytosol for re-use, with the aid of the V-Type ATPase proton pump (Cotter et al., 2015b). As such, the proton pumping function of V-Type ATPase is tightly linked to cellular processes that include autophagy, endocytosis, phagocytosis, and micropinocytosis (Forgac, 2007). In the case of plasma membrane V-Type ATPase, ATP hydrolysis-coupled proton pumping also contributes to the proton export, and the resultant acidification of the extracellular matrix (Marshansky et al., 2014).

Structurally, V-Type ATPases are large multisubunit protein complexes that are organised into a peripheral V_1 domain, which mediates ATP hydrolysis, and a transmembrane V_0 domain responsible for ATP hydrolysis-coupled proton transport (Zhao et al., 2015). V_1 is composed of 8 different subunits (ATP6V1A to ATP6V1H), arranged into a complex of $A_3B_3CDE_3FG_3H$ (Powell et al., 2000). The V_0 subunit is comprised of five subunits (ATP6V0a, ATP6V0c, ATP6V0c', ATP6V0d, and

ATP6V0e), arranged into a complex of $ac_9c'de$ (Supek et al., 1994). Ancillary proteins that may be bound to V-Type ATPases include Ac45 (Supek et al., 1994), and the prorenin receptor (PRR) (Cruciat et al., 2010).

Mechanistically, ATP hydrolysis takes place at each of the three structural interfaces between subunits ATP6V1A and ATP6V1B (MacLeod et al., 1998). V-Type ATPase operates by a rotary mechanism whereby ATP hydrolysis in the A3B3 catalytic head causes rotation of a central stalk composed of subunits ATP6V1D, ATP6V1F, and ATP6V0d (Hirata et al., 2003). ATP6Vod on the V0 complex is positioned at the centre, connected to a 10-membered ring of V0 subunits, c9c' (Zhao et al., 2015). Each $ATP6V_0c/c'$ subunit contains an essential glutamic acid residue that undergoes reversible protonation during proton pumping (Hirata et al., 1997). ATP-driven rotation of the central stalk causes rotation of the $ATP6V_0c/c'$ ring relative to the $ATP6V_0a$ domain (Wang et al., 2008). $ATP6V_0a$ is a 100kDa transmembrane protein that harbours an N-terminal cytoplasmic domain and a C-terminal transmembrane domain (Wang et al., 2008). The C-terminal domain contains two proton-conducting hemi-channels, which lead from the cytoplasmic side of the membrane, through the plasmalemmal interior, to the extracellular or luminal side of the membrane (Toei et al., 2011). Protons enter the V_0 complex from the cytosol through the first hemi-channel within the ATP6V0a subunit (Kawasaki-Nishi et al., 2001). Protons then proceed to protonate the

essential glutamate residue present on each of the ATP6V0c/c' subunits (Kawasaki-Nishi et al., 2001). ATP-driven rotation of the c9c' ring then brings the c9c' subunits into contact with ATP6V_0a's luminal hemi-channel (Kawasaki-Nishi et al., 2001). The transported proton is then released into the luminal hemichannel via interaction with a positive charged arginine residue within ATP6V_0a, thus enabling the proton to translocate to the luminal or extracellular compartment (Kawasaki-Nishi et al., 2001). Hence, via ATP-hydrolysis and rotation of the V-ATPase motor, catalytic energy potential is transduced to drive the unidirectional primary active transport of protons across biological membranes (Zhang et al., 2008).

Regulatory Mechanisms of V-Type ATPase Two of the most important means of regulating V-Type ATPase activity are the reversible dissociation and reassembly of V-Type-ATPase, as well as its regulated trafficking to various membrane compartments (Stransky et al., 2016). Increased assembly of V-Type ATPase V_1 and V_0 subunits can be observed in response to a number of physiological stimuli, including elevated glucose concentration, amino acid starvation, exposure to growth factors, dendritic cell maturation, and during viral infection (Stransky et al., 2016). High levels of glucose and cytosolic glycolysis require efficient V-Type ATPase assembly, in order to match the production of metabolic acids with removal of intracellular protons (Sautin et al.,

2005). In contrast, disassembly of V-Type ATPase may conserve the intracellular ATP pool during periods of low ambient glucose (Sautin et al., 2005). V-Type ATPase assembly and function may also be necessary for exporting adequate amounts of lysosomal amino acids generated from acid-dependent proteolysis, a mechanistic step towards stimulating the mechanistic target of rapamycin complex 1 (mTORC1) (Stransky and Forgac, 2015). Envelope viruses such as influenza may promote V-Type ATPase assembly in the early endosomes to enable acid-dependent fusion of their viral coats with the endosomal membrane – a necessary step for transferring viral RNA into the host cytoplasm (Marjuki et al., 2011). In addition, several proteins of the Rabonnectin family have been shown to promote V-Type ATPase assembly and luminal acidification (Einhorn et al., 2012). These proteins are homologous to the RAVE complexes in yeast, which are required for V-Type ATPase assembly (Schwab et al., 2012).

A second means of controlling V-Type ATPase activity is through regulated trafficking (Stransky and Forgac, 2015). Renal intercalated cells respond to decreased plasma pH by increasing the fusion of V-Type ATPase vesicles with the apical membrane (Breton and Brown, 2013). Similarly, epididymal clear cells control the pH of the epididymal lumen by controlling the density of V-Type ATPase in the apical membrane, through vesicle-mediated insertion and retrieval of pump-laden vesicles

(Alzamora et al., 2010). In both of these systems, vesicle fusion and endocytosis of V-Type ATPase-containing vesicles are controlled through PKA-dependent phosphorylation, a reaction modulated by a bicarbonate-sensitive adenylate cyclase (Pastor-Soler et al., 2003).

mTORC1 Activation and the Role of V-Type ATPase in Nutrient Sensing V-Type ATPase function is necessary for the activation of mechanistic target of rapamycin complex I (mTORC1) (Zoncu et al., 2011). The mTOR pathway is frequently dysregulated in cancer (Laplante and Sabatini, 2012). mTOR is a protein kinase that is involved in assembling two protein complexes – mTORC1 and mTORC2 (Bar-Peled et al., 2012). mTORC1 is a central node of cellular signalling, receiving inputs from growth factor receptors, nutrient availability, and energy status (Dechant et al., 2014). mTORC2 is involved in survival signalling, and its activity is independent of V-Type ATPase function, unlike mTORC1 (Stuttfeld et al., 2018).

It was first reported that inhibition of V-Type ATPase via esomeprazole induced autophagic flux and accumulated autophagosomes – processes that are physiologically controlled by mTORC1 (Marino et al., 2010). Esomeprazole was shown to decrease mTOR signalling, as demonstrated by reduced phosphorylation of p70-S6K and 4-EBP1 (Marino et al., 2010). This suggested that V-Type ATPase inhibition resulted in

inactivation of mTORC1 (Bar-Peled et al., 2012). Further mechanistic studies revealed that during amino acid starvation, the V1 subunit of V-Type ATPase tightly associates with the pentameric Ragulator complex and Rag GTPases on the surface of lysosomes, forming a complex that excludes mTORC1 from binding onto the lysosomal surface, thus disabling mTORC1 activity (Efeyan et al., 2013). Upon repletion of cellular amino acids, V-Type ATPase is able to sense lysosomal luminal amino acid concentrations, and transduce this signal to the Ragulator, which alters its interaction with the Rag GTPases to recruit mTORC1 to the lysosomal surface, an event that activates mTORC1 (Kim et al., 2008).

Interestingly however, recent studies showed that changes in V-Type ATPase activity in response to starvation of individual amino acids is variable and does not necessarily correlate with changes in mTORC1 activity (Stransky and Forgac, 2015). In addition, treatment with chloroquine does not suggest a causal relationship for V-Type ATPase assembly regulating mTORC1 activity (Stransky and Forgac, 2015). Therefore, though inhibition of V-Type ATPase is sufficient to inhibit mTORC1 activity, V-Type ATPase assembly may not an absolute requirement for amino acid-induced mTORC1 activity (Stransky and Forgac, 2015). It is possible that V-Type ATPase may play an indirectly permissive role in activating mTORC1 activity by acidifying the lysosomal lumen, enhancing acidic proteolysis, and enabling the concentration of free

amino acids to rise and stimulate mTORC1 activity (Stransky et al., 2016). For example, EGF and GPCR signalling have been proposed to induce acidification of lysosomes and lysosomal proteolysis via enhancing V-Type ATPase assembly and activity, raising the pool of essential amino acids in the cell to activate mTORC1 (Fan et al., 2015). Taken together, though the exact mechanism by which V-Type ATPase is able to regulate mTORC1 activity remains to be elucidated, it is clear from these studies that the two protein complexes are functionally related (Wang et al., 2014c).

V-Type ATPase and Autophagy Autophagy is induced during periods of starvation and metabolic stress (Tschan and Simon, 2010). Autophagy involves the formation of double membrane vesicles (autophagosomes) that sequester cytoplasmic contents and deliver them to lysosomes, allowing degradation by lysosomal hydrolases and recycling of autophagosomal contents (Yang et al., 2011). The autophagic process reduces cellular stress by removing damaged cellular components, including dysfunctional proteins and organelles (Tschan and Simon, 2010). The recycled substances can also provide cellular energy and anabolic substrates during periods of nutrient deprivation and hypoxia (Yu et al., 2018). However, prolonged or overactive autophagy is ultimately unsustainable and detrimental, leading to induced cell death (von Schwarzenberg et al., 2013).

The role of autophagy in cancer is complex (Yang et al., 2011). A reduction in autophagic activity is correlated with the accumulation of cellular stressors such as misfolded and aggregated proteins, and defective mitochondria (Mathew et al., 2009). This can result in the generation of reactive oxygen species, which may damage DNA and promote tumourigenesis (Mathew et al., 2009). On the other hand, extensive autophagy can also lead to irreversible organellar degradation and cell death (Tschan and Simon, 2010). Cancer cells thus navigate a tight course in the regulation of autophagy, to derive a viable survival mechanism in the face of nutrient deprivation, hypoxia, acidosis, and therapeutic treatment (Yang et al., 2011). Autophagy provides a means to recycle damaged cellular components, and to break them down into cellular nutrients and building blocks for biosynthesis (Tschan and Simon, 2010). The right amount of autophagy can thus curtail the onset of apoptosis in cancer cells under stress (Yu et al., 2018).

In this context, V-Type ATPase enables tumour cell survival through its active participation in autophagy (Namkoong et al., 2015). Autophagy requires V-Type ATPase activity to support the activities of pH-dependent lysosomal hydrolases (Kallifatidis et al., 2013). In turn, the pharmacological inhibition of V-Type ATPase blocks autophagic flux (Mauvezin et al., 2015). Induction of autophagy involves the transactivation of V-Type ATPase expression by MiT/TFE transcription factors,

including that of MITF and TFEB (Sardiello et al., 2009). 14-3-3 protein-bound MITF is physically released by mTORC1 inactivation during periods of nutrient deprivation, permitting MITF to translocate to the nucleus to mediate V-Type ATPase transactivation (Bouché et al., 2016). MITF and mTORC1 thus cooperate with V-Type ATPase to enhance lysosomal biogenesis and support cancer autophagy (Bouché et al., 2016).

Expression and Localisation of V-Type ATPase in Cancer Cells Using fluorescent pH indicators that localise to specific cellular components to study V-Type ATPase function, it has been shown that V-Type ATPase participates in the control of both cytoplasmic and lysosomal pH in a variety of human cancer cell lines (Martinez-Zaguilan et al., 1993). V-Type ATPase has been shown to be expressed in the plasma membrane of invasive cancer cell types, including melanoma, breast cancer, Ewing sarcoma, liver, lung, ovarian, oesophageal, prostate, and pancreatic cancers (Stransky et al., 2016). Furthermore, certain subunits of V-Type ATPase may be overexpressed in cancer cell lines and human tumour samples (Otero-Rey et al., 2008). For example, ATP6V_1C is overexpressed in oral SCC (García-García et al., 2012), and V_0c overexpressed in liver HCC samples (Xu et al., 2012). ATP6V_1A and V_1E are overexpressed in pancreatic and gastric cancer, respectively, and expression levels can correlate with tumour grading (Alonso-Curbelo et al., 2014).

V-Type ATPase in Tumour Cell Migration and Invasion The presence of V-Type ATPase on the plasma membrane of invasive cancers suggests a possible role for V-Type ATPase in cancer cell migration and invasion (Capecci and Forgac, 2013). Several studies have demonstrated that *in vitro* migration and invasion is dependent on V-Type ATPase activity (Hinton et al., 2009). Treatment of MB231 and MCF10CA1a human breast cancer cells with the specific V-Type ATPase inhibitor Concanamycin A and Bafilomycin results in a significant decrease in *in vitro* invasion as measured by transwell assay (Cotter et al., 2015a). Similar results have been obtained in other cancer cell types (Wiedmann et al., 2012). Drug treatment studies are supported by the results of siRNA knockdown experiments, where knockdown of $ATP6V_0c$ and $ATP6V_1A$ reduced the invasiveness of liver and gastric cancer cell lines, respectively (Lu et al., 2005, Liu et al., 2015). In contrast, overexpression of $ATP6V_1C$ in Drosophila wing epithelia resulted in a tumour-like transformation of the wing disk, marked by epithelial cell overgrowth and enhanced invasiveness, further supporting the role for V-Type ATPase in tumour cell invasion (Petzoldt et al., 2013).

Mechanistically, several hypotheses have been proposed to explain V-Type ATPase's contribution to tumour cell migration and invasion (Forgac, 2007). One possibility is that plasma membrane V-Type ATPase-dependent proton pumping and

extracellular acidification permit the activation of extracellular acid-dependent proteases, which may either directly cleave the extracellular matrix to enable tumour cell invasion, or alternatively may act on other proenzymes to mediate metastatic invasion (Cotter et al., 2015a). In this regard, two important classes of proteases have been implicated in V-Type ATPase-mediated tumour invasion – the cathepsins and the matrix metalloproteases (MMPs) (Marshansky et al., 2014). Cathepsins are a class of lysosomal hydrolases that require low pH for activation and subsequent proteolytic activity (Forgac, 2007). MMPs are not directly pH-dependent, though low pH can potentiate their catalytic activities (Jabłońska-Trypuć et al., 2016). Both cathepsins and MMPs are secreted by tumour cells and have been shown to participate in tumour invasion (Olson and Joyce, 2015). Altering of the extracellular pH microenvironment by V-Type ATPase-mediated proton pumping plays a facilitative role in the activation of these proteolytic enzymes, and in turn mediates vertical melanoma invasion into the dermal tissue. (Stransky et al., 2016)

Intracellular V-Type ATPase can also contribute to the promotion of tumour invasion via lysosomal and secretory vesicular activation of cathepsins and MMPs prior to the release into the extracellular microenvironment (Chung et al., 2011). It has been shown that neutralisation of the acidic extracellular microenvironment reduces both metastasis of breast cancer cells in mice and extracellular MMP activities in breast

tumours (Ohta et al., 1998). Similarly, inhibition of V-Type ATPase activity reduces extracellular MMP2 and MMP9 activity in a variety of invasive cancer cell lines (Liberman et al., 2014).

Aim of the Thesis: Characterising MITF-Dependent Phenotypic Plasticity in Melanoma Acidotic Resistance

The above introduction suggests that MITF-dependent phenotypic plasticity represents a key attribute that defines intratumoural heterogeneity in melanoma. This thesis aims to address the presence and nature of MITF-dependent phenotypic plasticity in relation to proton transporter expression and acidotic resistance in melanoma. Novel insights into melanoma biology may be gained to inform innovative therapeutic approaches for treating advanced melanoma and cancer in general.

CHAPTER 2

MATERIALS AND METHODS

Cell Culture and Plasmids

Cell lines A375, HS696T, MeWo (Bioresource Collection and Research Centre, Taipei, Taiwan), IGR37, and IGR39 (German Collection of Microorganisms and Cell Cultures, Braunschweig, Germany), were grown in Dulbecco's modified Eagle's medium (DMEM) (+ 4mM L-glutamine), 10% fetal bovine serum (FBS), 100μg/mL penicillin and 100U/mL streptomycin supplement (all from Invitrogen Life Technologies, Carlsbad, CA). Cell line authentication via Short Tandem Repeat-Polymerase Chain Reaction (STR-PCR) profiling was performed at the BCRC and DSMZ. The pCMV-TAG4A-MITF-M (wt) (Noguchi et al., 2017) plasmid was a kind gift from Professor Yardena Samuels (Addgene plasmid #31151). The *MITF-M* coding DNA sequence was subcloned into the lentiviral expression vector pLAS2w.Ppuro (Kuo et al., 2016) from RNAi Core, Academia Sinica, Taiwan. pLKO-*MITF* shRNAs (a pool of four shRNAs with clone IDs TRC0000019119–TRC0000019123, and TRCN0000329863) (Choi et al., 2017) were purchased from RNAi Core, Academia Sinica, Taiwan, in lentiviral-based vectors. For serum-free adjustment of the culturing

media, FBS was eliminated from culture. For pH adjustments of the culturing media, DMEM media without sodium bicarbonate ($NaHCO_3$) was manually titrated with standardised amounts of $NaHCO_3$ to derive the buffered extracellular pH (pH_e). For concurrent pyruvate and pH adjustment of the culturing media, sodium pyruvate (Thermo Fisher, Waltham, MA) and $NaHCO_3$ were added to basic DMEM (D5030, Sigma-Aldrich, St Louis, MO), Osmolarity of the culturing media was balanced using NaCl throughout. For drug treatments assays, the experiments were controlled with cells treated with Dimethyl Sulfoxide (DMSO) diluted 1:1000, a concentration that exceeded the maximal drug concentration under experimentation.

Lentiviral Production

Lentivirus was generated by seeding 293T in 60mm dishes, and transfecting with plasmids pLAS2w.Ppuro, pCMV-dR8.91, and pMDG (Academia Sinica, Taipei, Taiwan) using TransIT-LT1 (Mirus Bio, Madison, WI) or X-tremeGENE HP (Roche, Mannheim, Germany). 48-72 hours post-transfection the media was harvested. Viral supernatant was cleared by centrifugation and sterile-filtered, prior to storage at -80˚C until use.

Lentiviral Transduction

MITF was ectopically expressed in human melanoma cell lines A375 and IGR39 using previously reported lentiviral protocols (Mann et al., 2015, Licciulli et al., 2011). For lentiviral transduction of larger dishes, volumes were scaled up proportionally. Melanoma cells were plated the night before lentiviral transduction. The next day, cells were infected in serum-free medium mixed with lentiviral particles (Mann et al., 2015), and polybrene (Sigma-Aldrich). Cells were assayed for downstream experiments at 72 hours post-infection. MITF was also knocked down in the human melanoma cell line IGR37 using published protocols (Licciulli et al., 2011). Cells were seeded and incubated until reaching a confluence of approximately 50%. Lentiviral transduction was then performed using serum-free medium mixed with lentiviral particles and polybrene. Cells were assayed for downstream experiments at 72 hours post-infection. Stably transduced cell lines were generated by selecting the transiently transduced cell lines in 1.5μg/mL puromycin, starting 48hr post-lentiviral transduction. Dishes of untransduced cells were concurrently treated with the same concentration of puromycin. Complete cytotoxicity in the untransduced cells was typically observed within 1 week of commencing puromycin selection, at which point the stably transduced cells under selection were switched to maintenance culture with 1.0μg/mL puromycin.

Quantitative Reverse Transcriptase-Polymerase Chain Reaction

RNA was extracted from cells using the QIAGEN RNeasy Mini Kit (Qiagen, Germantown, MD) as described by the manufacturer. Reverse transcription was performed using the GoScript Reverse Transcriptase Kit (Promega, Madison, WI), followed by Quantitative PCR using the SyBr Green-based GoTaq qPCR Kit (Promega). All reactions were run and analysed using a QuantStudio 5 Real-Time PCR System Thermocycler (Applied Biosystems, Waltham, MA). The sequences of primers used for PCR are listed below in Table 2.1. Relative mRNA expression was normalized to the *ACTB*/*β-actin* gene. The fold changes in gene expression changes were calculated using the $2^{-\Delta\Delta Ct}$ method (Schmittgen and Livak, 2008).

Antibodies

The following antibodies were used in our experiments: Anti-MITF (Clone C5; GeneTex, Irvine, CA), Anti-ATP6V1C (Clone H-5; Santa Cruz Biotochnology, CA), Anti-ATP6V1D (Atlas Antibodies, Bromma, Sweden), Anti-SLC16A7 (Bioss, Woburn, MA), Anti-SLC16A3 (Proteintech, Rosemont, IL), Anti-SLC16A1 (Proteintech), SLC4A2 (Bethyl Laboratories), SLC4A3 (Novus Biologicals, Littleton, CO), SLC9A1 (Atlas Antibodies), SLC9A2 and SLC9A5 (Origene, Rockville, MD), Anti-GAPDH (GeneTex). Anti-NBCe1 and Anti-NBCe2 (Origene, Rockville, MD), Anti-NBCn1 (Abgent, San Diego, CA), Anti-NDCBE (Aviva Systems Biology, San Diego, CA).

Anti-NHE3 (Thermo Fisher), Anti-NHE7 (GeneTex, Irvine, CA), and Anti-NHE9 (Abcam, Cambridge, UK).

Western Blotting

For SDS-PAGE electrophoresis, denatured proteins were homogenized in sample buffer (Bio-Rad, Hercules, CA), fractionated on Fastcast gels of either 7.5%, 10%, or 12%, depending on the molecular weight of the proteins of interest (Bio-Rad). Fractionated proteins were wet-transferred to PVDF membranes (GE Healthcare, Pittsburgh, PA), blocked in 5% BSA (Bioshop, Burlington, Canada), and probed with primary antibodies (as listed above at the stated dilutions) overnight at 4˚C. Membranes were washed three times in TBST (Sodium Chloride, Trizma Base, 0.1% Tween-20, all from Sigma), and incubated with HRP-conjugated secondary goat anti-rabbit (1:2000, Cell Signaling Technology), or HRP-conjugated secondary horse anti-mouse (1:2000, Cell Signaling Technology) antibodies. Following secondary antibody incubation, the membranes were further washed three times in TBST, and incubated with enhanced chemiluminescence substrate (Bio-Rad). Western blot images were obtained on a UVP BioSpectrum 500 imager (UVP, Upland, CA). Equal loadings were confirmed by probing with rabbit anti-GAPDH antibody (1:10000, GeneTex). Blot densitometry was analysed using ImageJ software.

Immunofluorescence

Cells were grown on 0.1% gelatin (Invitrogen)-coated glass coverslips and fixed with 4% paraformaldehyde diluted in phosphate-buffered saline (PBS) for 10 minutes. Permeabilisation was performed with 0.1% Tween-20 for 10 minutes. All cells were washed and then blocked with a mixture of 5% bovine serum albumin, 5% normal goat serum, and 0.1% Tween 20 in PBS, at room temperature for 1 hour. Cells were then incubated with primary antibodies in parallel, overnight at 4˚C (Mouse monoclonal to MITF, GeneTex; Rabbit polyclonal to SLC9A1, Atlas Antibodies; Rabbit polyclonal to SLC16A1, Proteintech; Rabbit polyclonal to SLC16A3, Proteintech; and Rabbit polyclonal to ATP6V1D, Atlas Antibodies). Following overnight incubation, cells were washed three times with PBST (PBS with 0.1% Tween-20), and probed with secondary antibodies in parallel for 1 hour at room temperature (Goat anti-Rabbit IgG, Alexa-488 Conjugated, Invitrogen; Goat anti-Mouse IgG, Alexa-594 Conjugated, Invitrogen). Nuclear counterstaining was performed using DAPI (Invitrogen). Images of the specimens were captured using a Leica DM IRB microscope (Leica, Wetzlar, Germany). Fluorescent intensity of the images was analysed using the ImageJ software. (McCloy et al., 2014).

Electric Cell-Substrate Impedance Sensing.

Electrical impedance, resistance, and capacitance of A375 cells were measured using the Electric Cell-Substrate Impedance Sensing (ECIS) system (Applied Biophysics, Troy, NY). Cells were seeded on electrode-fitted wells at a subconfluent density of 30,000 cells per 0.8cm^2, and electrode parameters were monitored at 32000Hz over time. Medium change with different pH_e values occurred at 24hrs after cell seeding.

4.3. 3-(4,5-dimethylthiazol-2-yl)-2,5-diphenyltetrazolium bromide (MTT) Assay.

Cells were seeded in 96-well plates and allowed to attach overnight. Culturing media with different pH_e values were administrated to a final volume of 200µl. After treatment for 24 or 48 hours, the cells were incubated at 37°C with 20µl of 3-(4,5-dimethylthiazol-2-yl)-2,5-diphenyltetrazolium bromide (MTT) solution (5 mg/ml, Abcam, Cambridge, UK) for 4 hours. The MTT formazan crystals were dissolved in 150µl Dimethyl Sulfoxide (Sigma), and a microplate reader (Tecan, Mannedorf, Switzerland) was used to measure colourimetric absorbance at 562nm.

Resazurin Reduction Assay

Cells were seeded in different 24-well-plate wells and incubated overnight to permit cell attachment. Culturing media with the specified experimental conditions

were then administered to the wells to a final volume of 900µl. At the different timing end-points of 0, 24, 48, and 72hrs, the Prestoblue stock solution (Invitrogen) was added to different 24-well-plate wells at 1:10 dilution (with respect to total volume) (Xu et al., 2015). Following an incubation period of 1hr at 37˚C, a microplate reader (Tecan, Zurich, Switzerland) was used to measure Resorufin fluorescence, using an excitation wavelength of 560 nm and an emission wavelength of 590 nm. For each cell line tested, Resorufin production in individual wells was normalised to Resorufin production in the specified positive or negative control well for each cell line.

Caspase 3/7 Activity Assay.

Cells were seeded in different 24 well-plate wells and incubated overnight to achieve cell attachment. Culturing media with the specified experimental conditions were then administered to a final volume of 1000µl. At the different timing end-points of 0, 24, 48, and 72hrs, the CellEvent Caspase 3/7 Green Reagent (Invitrogen) was added to different 24-well-plate wells, achieving a working concentration of 5µM (Zhu et al., 2012). Following an incubation period of 30min at 37˚C, live-cell green fluorescent images of individual wells were captured with a Leica DM IRB microscope (Leica) using an excitation wavelength of 488nm, and caspase 3/7 activation in individual wells was recorded as green count/mm^2. For each cell line tested, caspase

3/7 activation in individual wells were normalised to caspase 3/7 activation in the specified positive or negative control well for each cell line.

Hoechst 33342 Cell Counting

Cells were seeded in different 24 well plates and incubated overnight to achieve cell attachment. Culturing media with the specified experimental conditions were then administered to a final volume of 1000µl. At the different timing end-points of 0, 24, 48, and 72hrs, culturing media were withdrawn from the culture wells, and Heoscht33342 (Sigma-Aldrich) diluted to 2µg/mL with PBS was added to different 24-well-plate wells (Richards et al., 1985). Following an incubation period of 5min at 37˚C, live-cell blue fluorescent images of the individual wells were captured with a Leica DM IRB microscope (Leica) using an excitation wavelength of 405nm, and Hoechst 33342 nuclear counts in individual wells were recorded as blue count/mm^2. For each cell line tested, Hoechst33342 nuclear counts in individual wells were normalised to the Hoechst33342 nuclear count in the specified positive or negative control well for each cell line.

Solutions and Chemicals

HEPES-Buffered Tyrode's Solution contained (mM): NaCl 140, KCl 4.5, $MgCl_2$

1, $CaCl_2$ 2.5, HEPES 20 and glucose 11. This was adjusted to pH 7.4 at 37˚C with 1M NaOH.

MCT Buffer Solution contained (mM): NaCl 140, KCl 5, $MgCl_2$ 1.2, $CaCl_2$ 2, Na_2HPO_4 1, and HEPES 10. This was adjusted to pH 7.4 at 25˚C with 1M NaOH.

5% CO_2/HCO_3^- Buffer Solution contained (mM): NaCl 117, KCl 4.5, $MgCl_2$ 1, $CaCl_2$ 2.5, $NaHCO_3$ 23, and glucose 11. This was adjusted to pH 7.4 at 37˚C with 1M NaOH, and equilibrated with 5% CO_2.

Nigericin Calibration Solution contained (mM): KCl 140, $MgCl_2$ 1, and nigericin 0.01, buffered with one of the following organic buffers: 20mM MES (pH 5.5 and 6.5), 20mM HEPES (pH 7.0, 7.5, and 8.5) or 20mM CAPSO (pH 9.5), and were adjusted to the correct pH with 1M NaOH at 37˚C.

HOE694 (3-methylsulphonyl-4-piperidinobenzoyl, guanidine hydrochloride, Sanofi-Aventis, Paris, France), Bafilomycin A1 (LC Laboratories, Woburn, MA), CHC (2-Cyano-3-(4-hydroxyphenyl)-2-propenoic acid, Tocris Bioscience, Minneapolis, MN), DIDS (4,4′-Diisothiocyanatostilbene-2,2′-disulfonic acid, Sigma-Aldrich, St. Louis, MO)L-Lactate, FCCP, Iodoacetic acid, and Ionomycin (all from Sigma) were added to solutions at the indicated concentrations shortly prior to use.

BCECF Microspectrofluorometry

For cytosolic pH (pH_i) measurement, cells were loaded with 3μM BCECF-AM (Loh et al., 1996) (Thermo Fisher). BCECF epifluorescence was collected at 530nm with a converted inverted microscope, with alternative and repetitive excitation of the BCECF fluorophore at 490 and 440nm under monochromator control (Cairn Research, Kent, UK). Signals were digitised using a CED digitizer, and the fluorescence emission ratios were calculated and converted to pH_i values by dividing the F490 by the F440 emission. BCECF fluorescence ratios were calibrated using the high-[K^+] nigericin technique (Loh et al., 1996). Few poorly loaded cells showing low signal-to-noise ratio were excluded from analysis. Intracellular acidification was induced by transiently superfusing melanoma cells with 20mM ammonium chloride (NH_4Cl, a procedure known as NH_4Cl prepulse (Ch'en et al., 2008). During Chloride-free treatment, intracellular acidification was alternatively induced by transiently superfusing melanoma cells with 20 mM ammonium sulfate, $(NH_4)_2SO_4$ (Yamamoto et al., 2005). For monocarboxylate treatments, including that of pyruvate, L-lactate, and β-hydroxybutyrate, intracellular acidification was induced by transiently superfusing melanoma cells with either 10mM or 3mM of the respective monocarboxylates (Jackson and Halestrap, 1996). Measurements of pH_i recovery rates typically commenced 1min after NH_4Cl, $(NH_4)_2SO_4$, and monocarboxylate removal (Yang and Loh, 2019). Rates of pH change were calculated from change in pH_i over a 1min time

period (dpH_i/dt).

Mechanisms of Weak Acid/Base Pre-pulse Techniques

Ammonium Chloride Prepulse technique was used in the present work to induce acute acid-loading. Ammonium chloride prepulses were achieved with 3-5 minutes of extracellular superfusion of 20mM NH_4Cl. Ammonium chloride was added to the solution without osmotic compensation. Briefly, the mechanism of weak acid/base prepulse technique relies on the characteristic of incomplete dissociation. Although both the charged and uncharged species of a weak acid exists simultaneously in solution, the uncharged species is lipid-soluble and therefore able to penetrate the lipid bi-layer of the cell membrane. In contrast, the charged species permeates relatively slowly, through various membrane protein routes. The details of prepulsing procedure are given below.

Ammonium Chloride Prepulse Technique

A typical example used in the present study is ammonium chloride prepulse technique, which induces an intracellular acid load. The mechanism of acid loading by ammonium chloride superfusion can be explained in four phases: (1) Rapid entry of dissociated ammonia leading to transient alkalinisation; (2) slow entry of dissociated

H+ and Cl- and gradual acidification. (3) Rapid withdrawal of ammonia leading to transient acidification; and (4) Active proton extrusion by enzymatic acid extruders leading to pH_i recovery.

(1) The rapid entry of NH_3 into the cell causes consumption of intracellular protons to form NH_4^+. The consumption of intracellular protons leads to acute alkalinisation of the cell.

(2) The delayed entry of HCl leads to gradual decrease of intracellular pH.

(3) Once the external NH4Cl is removed, intracellular NH3 freely diffuses out of the cell, causing intracellular acidification.

(4) In order the alleviate the intracellular acidification induced by NH4Cl withdrawal, the cell activates pHi regulatory mechanisms to recover from low pH_i.

Calibration of fluorescent pH indicators

The BCECF fluorescence emission ratios were calibrated using the K^+-Nigericin method. Briefly, this consisted of sequentially exposing a fluorophore-loaded cell to the three-nigericin calibration solutions, 20mM 2-(N-morpholino) ethanesulphonic acid (MES, pH 5.5 and 6.5), 20mM HEPES (pH 7.0, 7.5, and 8.5), and 20mM 3-(cyclohexylamino)-2-hydroxyl-1-propane-sulphonic acid (CAPSO, pH 9.5) (listed above in solution section). This clamps pH_i to the value of pH_e in the calibration

solution. The intracellular F490/440 fluorescence ratios were then measured at the above standard pH values (pH 5.5/R_{min}, 6.5, 7.0, 7.5, 8.5, and 9.5/R_{max}). These fluorescence ratios then converted to pH_i, using the following equation: pH = pKa-log(R-R_{min})/(R_{max}-R)-log ($F490/440_{max/min}$), where pKa is the pK of intracellular BCECF (approximately 7.2; pKa can be computationally modeled using the above F490/440 ratios at standard pH_i values). Finally, the calibrated pH_i signal was averaged over 0.5s intervals.

Bioinformatics

The raw count matrix composed of 471 samples was downloaded from the human Skin Cutaneous Melanoma (SKCM) dataset available at The Cancer Genome Atlas(The Cancer Genome Atlas Research, 2008) (TCGA, http://cancergenome.nih.gov). The mRNA expression levels of MITF, and 102 proton transporter loci (Supplementary Table S1) in 471 melanoma tumors of the SKCM dataset were analysed. Spearman correlations were performed between the 102 protein transporters reads per kilobase per million mapped reads (RPKM) expression, and invasive or proliferative gene expression signatures from Verfaillie et al (Verfaillie et al., 2015), as well as the expression levels of AXL and MITF. Relative expressions of MITF and the proton transporters were also analysed in the 62 human melanoma cell lines available from the

Cancer Cell Line Encyclopaedia (Barretina et al., 2012) (CCLE, https://broadinstitute.org/ccle).

Statistical Analysis.

Data were analysed using Prism (GraphPad Software, La Jolia, CA), with the tests specified in the figure legends. All error bars represent SEM.

Table 2.1: List of Primers Used in Quantitative Reverse Transcriptase Polymerase Chain Reaction.

Gene	**Forward Primer**	**Reverse Primer**
MITF	CATAAAAAGGGAGCTCACAGCG	AGATGGTTCCCTTGTTCCAGC
ATP5A1	CGCCCTGCAATTAACGTTGG	GCAACTCAGTTAGACGCACG
ATP5B	GTGTCTGCATTATTGGGCCG	AGCATCCAAATGGGCAAACG
ATP5C1	TACCGTTGCAAGTGCTGACA	TTTGTGATGACAGCTTGGCG
ATP5S	TCGAGGATGACTGTTTGCTGAG	GTGCTGTCTTAAAGGCTTGGAC
ATP6V0a1	GTGTGTACCTTGGATGCTGC	CCAAAGTCAAACTCGTCTGCG
ATP6V1A	AGTACTTCCGTGACATGGGC	ATAAAACGAGGCCAGACGGG
ATP6V1C	ATGGGAGAAATTGCATGCGG	CCAAGTCCACTCCATTAGCC
ATP6V1D	CGCAAGTGAAGATTCGAGCG	GGCATTTACACGCCTGTTGG
SLC9A1	ATCTTCCCTTCCTTACTCGTGG	CGGAATGATTAACAGGGCGGC
SLC9A7	CCAGAAGCACGTTTTCAGCC	CAAATGCCATTGCTCCCCTG
SLC9A9	TCAAGCCTATGGGGAACAGC	AATGTTTTCCTTGCCTGGCG
SLC11A1	CTATGGTTCCATCTCCAGCCC	CCAGCCTGAAGATCTGACTCG
SLC15A2	CAAAATGTCCATTGCGTGGC	TGAACTGTGCCACAACAAGC
SLC16A1	TACAAGAGGCGACCATTGGC	TCTTTCCCTGCCTTGGTTGG
SLC16A3	TCTTTGGCATCTCCTACGGC	ATGTAGACGTGGGTCGCATC

CHAPTER 3

MOLECULAR AND FUNCTIONAL CHARACTERISATION OF PROTON TRANSPORTERS IN A375 MELANOMA CELLS

Abstract

Melanoma cells preserve intracellular pH (pH_i) within a viable range despite an acidic ambient pH that typically falls below pH 7.0. The molecular mechanisms underlying this form of acidic preservation in melanoma remain poorly understood. Previous studies had demonstrated that proton transporters including the monocarboxylate transporter (MCT), the sodium hydrogen exchanger (NHE), and V-Type ATPase mediate acid extrusion to counter intracellular acidification in melanoma cells. In this report, the expression and function of the Sodium-Coupled Bicarbonate Transporter (NCBT) family of base loaders were further characterized in melanoma cell lines. NCBT family members found to be expressed in three different melanoma cell lines – A375, MeWo, and HS695T – included the electrogenic sodium-bicarbonate cotransporter isoforms 1 and 2 (NBCe1 and NBCe2), the electroneutral sodium-bicarbonate cotransporter (NBCn1), and the sodium-dependent chloride-bicarbonate exchanger (NDCBE). These transporters facilitated 4,4′-diisothiocyanatostilbene-2,2′-disulfonic acid (DIDS)-dependent pH_i recovery in melanoma cells, in response to intracellular acidification induced by ammonium chloride prepulse. Furthermore, the expression of NCBTs was increased upon chronic exposure to extracellular acidification. Given the current research interest in the NCBTs as a molecular driver of

tumourigenesis, characterising NCBT in melanoma provides impetus for developing novel therapeutic targets for melanoma treatment.

Attributions

This chapter is a slightly modified version of a manuscript published in *Scientific Reports* and has been reproduced here with the permission of the copyright holder.

All experiments and analyses were performed by Oscar Yang except as follows:

Experiments in **Figures 6a** and **10a** were performed by Chun-Fong Yang.

Sectioning and staining for **Figures 9** and **11** were performed by Chun-Fong Yang.

INTRODUCTION

Intracellular acidification represents one of the defining parenchymal features that influence melanoma metabolism, as reviewed in Pavlova and Thompson, 2016 (Pavlova and Thompson, 2016). As a consequence of Warburg aerobic glycolysis and upregulated hypoxic transcriptional reprogramming – reviewed in Bohme and Bosserhoff, 2016 (Bohme and Bosserhoff, 2016) – endogenous metabolic acids accumulate within the melanoma cytosolic space, subjecting melanoma cells to the physiological stress of cytoplasmic acidification (Kato et al., 2013). The cutaneous locality of melanoma growth also increases the vulnerability of melanoma to the effects of intracellular acidification from its pH micromilieu (Koch and Schwab, 2019).

Vertical growth and invasion into the acidic skin surface, often referred to as the "Acid Mantle" (Ohman and Vahlquist, 1994), requires melanoma cells encounter a hostile pH environment in the superficial layers of the stratum granulosum, where pH had been recorded to be as low as pH 5.0 (Schmid-Wendtner and Korting, 2006). Active maintenance of intracellular pH (pH_i) at above pH 7.2 during periods of acidic stress permits melanoma cells to continue to proliferate and evade apoptosis (Webb et al., 2011). In doing so, melanoma cells require a functional set of molecular acid extruders to neutralise and balance its internal pH in response to intracellular acidification (Huber

et al., 2017).

Major acid extruder protein families that are known to operate in melanomas include the monocarboxylate transporter (MCT), the sodium-hydrogen exchanger (NHE) (Sarangarajan et al., 2001), and the V-Type ATPase (Nishisho et al., 2011). MCT consists of an enzymatic solute carrier that mediates the equimolar cotransport of monocarboxylates and protons across the plasma membrane(Iwanaga and Kishimoto, 2015). The MCT isoform 1 has been shown to be the predominant isoform expressed in melanoma cells (Wahl et al., 2002). Since lactate and protons represent the majority of accumulated intracellular acidic metabolites in the glycolytically favoured melanoma cells (Koch and Schwab, 2019), MCT1 also constitutes the dominant modality of pH_i regulation in melanoma cells (Wahl et al., 2002). Intracellularly located protons are additionally removed from the cytosol by NHEs in melanomas (Sarangarajan et al., 2001). NHE enzymatically catalyzes the movement of protons across the plasma membrane via the active coupling to sodium antiport (Stock and Pedersen, 2017). NHE isoform 1 is predominantly expressed in human melanomas, and amiloride-dependent NHE1 proton transport activity has been detected in cultured melanoma cells (Sarangarajan et al., 2001). In addition, V-Type ATPase and NHE isoform 3 had been shown to co-localize with melanosomal proteins, and these proton transport effectors regulate melanosomal pH *in vitro* (Smith et al., 2004). V-Type

ATPase functions as a rotary proton pump that extrudes protons via energy derived from catalytic ATP hydrolysis using its V_1 subunit (Cotter et al., 2015b). Melanoma pH_i is thus tightly controlled by a set of functionally overlapping proton transporters, which regulate intracellular acidity to sustain cellular viability and metabolism in melanoma (Corbet and Feron, 2017).

In order to identify a suitable melanoma cell line model for investigating the effects of MITF expression on proton transport regulation, a melanoma cell line that has demonstrable baseline proton transport activity and a viable MITF transactivation mechanism in place needs to be first identified. This study thus first screened various melanoma cell lines for a range of proton transport activities. The A375 cell line was characterized as a suitable melanoma cell line for further experiments, since NHE, MCT, V-Type ATPase, and NCBT transport activities were present. This chapter showed that above the extracellular pH (pH_e) of 6.8, A375 cells remained viable and slowly proliferated. Additionally, at this acidic pH_e, A375 cells kept pH_i within the viable range via an endergonic reaction that was significantly curtailed upon serum deprivation. This observation prompted a further search for active acid extrusion mechanisms that were responsible for preserving pH_i in melanoma cells, and yielded definitive evidence of NCBT's expression and function in melanoma cells. NCBT transport function has in melanoma cells had remained poorly characterized to date. This study further showed

that the expression of NCBTs in A375 melanoma cells could be upregulated by the exposure to chronic acidity, a relevant feature of NCBT's regulation in melanoma cells.

RESULTS

A375 Melanoma Cells Survive and Proliferate at Mildly Acidic pH.

A375 cells were cultured in different pH conditions and cell coverage of electrode, viability, and intracellular pH were evaluated over 48 hours. Documented doubling time for A375 cells ranges from 6-12 hours on day 1 (Benga, 2001), to 18-24 hours when seeded at subconfluent densities of 1000 cells per well in 6-well plates (Yamazaki et al., 2012). Electrode coverage was a continuous recording, and represented the combinational effect of both changes in cell proliferation and cell shape, and as such the nature of curve progression may not be identical to what is expected of conventional growth curves derived from cell counting (Robilliard et al., 2018). MTT viability assay was thus performed in conjunction with ECIS to aid interpretation (Kling et al., 2014). As indicated in figure 3.1, acidic pH reduced the cell coverage rate of detecting microelectrodes in a dose-dependent manner, as measured and quantified by electrode impedance (Figure 3.1a-c), resistance (Figure 3.1d-f), and capacitance (Figure 3.1g-i) at the 24- and 48-hr time points. Values for electrode impedance and resistance were proportional to the rate of cell coverage of electrodes over time, whereas capacitance was inversely related to electrode coverage (Figure 3.1). Cellular electrode coverage occurred at the fastest rate in the neutral pH 7.4 condition, and slowest in the acidic pH 6.5 condition. At 48hr, absolute cell coverage also plateaued at the highest impedance value in A375 cells cultured in pH 7.4 (Figure 3.1a). Absolute cell coverage at 48-hr increased incrementally with the rise in culturing pH in a dose-titrated fashion (Figure 3.1a). Interestingly, aside from pH 6.5, where net coverage was negative (Figure 3.1a-c), A375 cells were still able to increase electrode coverage slowly at the mildly acidotic threshold of pH 6.8 (Figure 3.1a-c).

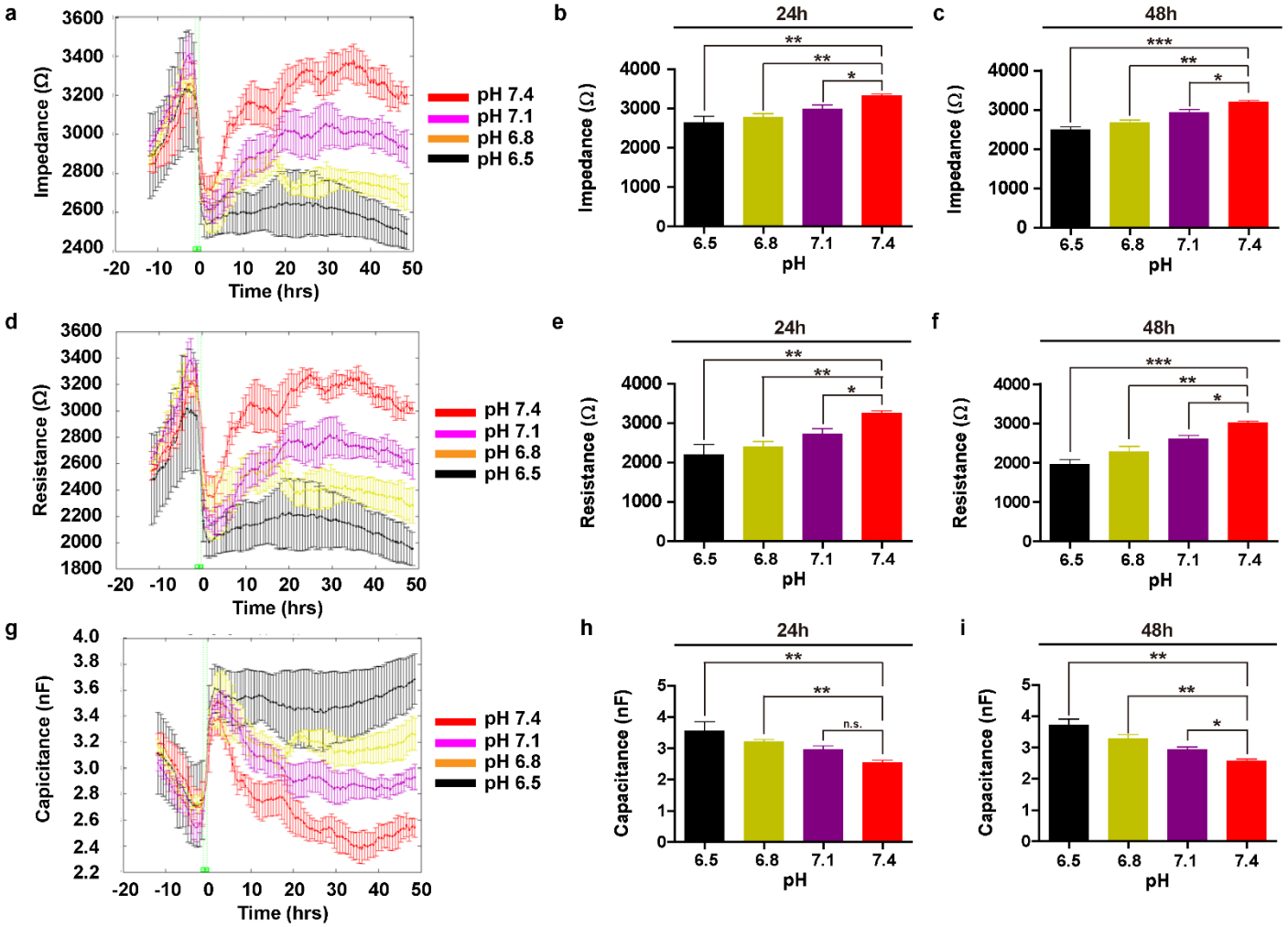

Figure 3.1: Proliferation Rate of Melanoma Cell Line A375 is Dependent on Ambient pH. (a) Impedance measurement of ECIS electrodes continuously recorded for 48 hours (n=4). A375 cells were seeded into the electrode-fitted wells, and at 0-hour, pH of the culturing media was adjusted to 7.4, 7.1, 6.8, and 6.5, respectively. Quantification of electrode impedance values at (b) 24-hours and (c) 48-hours is shown (n=4). (d) Resistance and (g) Capacitance measurements of ECIS electrodes continuously recorded for 48 hours (n=4). Quantification of electrode resistance was performed at (e) 24-hours and (f) 48-hours (n=4). That of electrode capacitance is shown in (h) and (g), respectively (n=4). Error bars: mean ± SEM. *P<0.05; **P<0.01; ***P<0.001; n.s.: Non-significant. Statistical significance was calculated using unpaired t-test.

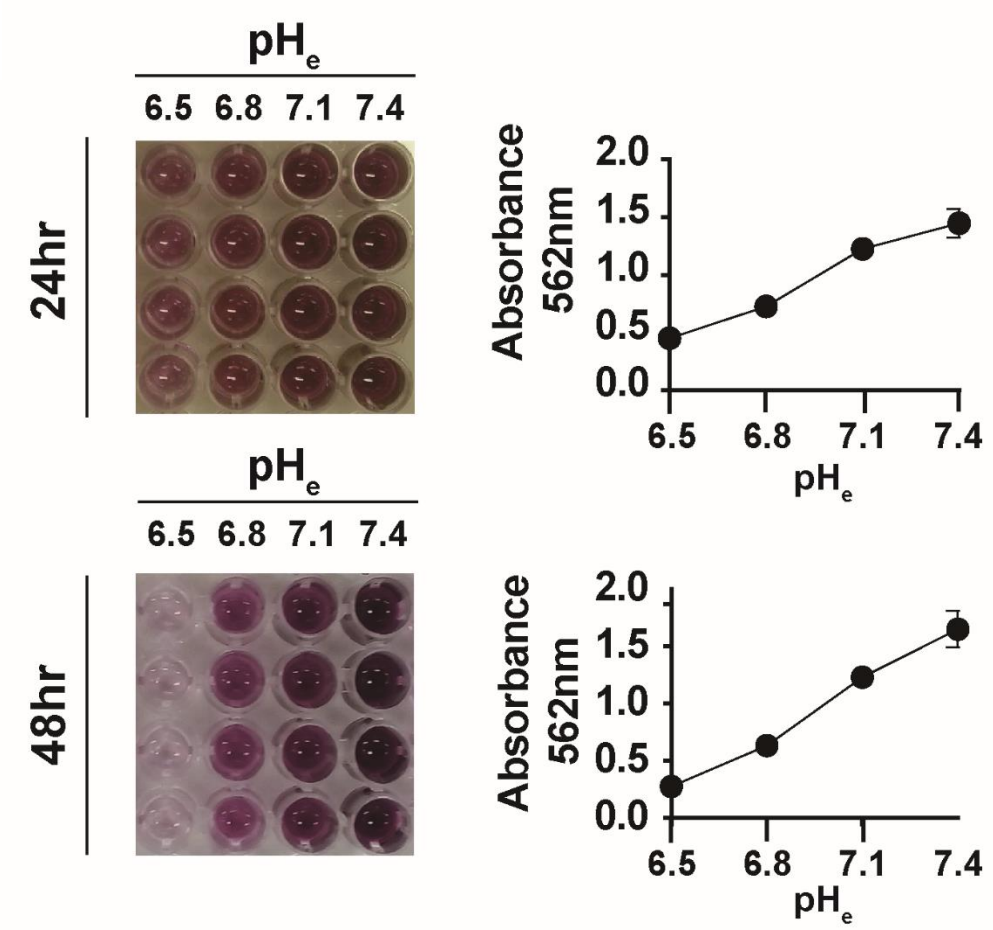

Figure 3.2: Viability and Intracellular pH of Melanoma Cell Line A375 are Dependent on Ambient pH. (a) A375 melanoma cells were plated at low density and incubated in culturing media that had pH adjusted to 7.4, 7.1, 6.8, and 6.5, respectively. At 24- and 48-hour time points, the cells were treated with MTT (n=4). Quantification of the colourimetric absorbance at 562nm was recorded for the wells at the prescribed time points as shown (n=4). Error bars: mean ± SEM.

To confirm the above findings, 3-(4,5-dimethylthiazol-2-yl)-2,5-diphenyltetrazolium bromide (MTT) viability assay was performed in A375 cells cultured in same pH acidities over the same 48hr period (Figure 3.2). As shown in figure 2a, dose dependent reduction in formazan production was already detectable due to decreasing ambient pH conditions at 24-hours, and this effect became more apparent at 48-hours. A375 cells were the most viable at pH 7.4, and least viable at the acidic pH of 6.5 (Figure 3.2). Again, pH 6.8 appeared to be the pH at which cell viability in A375 was still maintained, as formazan formation was virtually undetectable at pH 6.5 at the 48hr time point (Figure 3.2). pH 6.8 thus represented an appropriate pH to investigate how A375 cells were able to adapt to survive and slowly proliferate in acidic conditions.

A375 melanoma cells survive acidic pH by preserving intracellular pH neutrality

To determine how A375 cells were able to survive and proliferate at mildly acidic conditions of pH 6.8, BCECF spectrophotometry used to measure the intracellular pH (pH_i) in A375 cells cultured for 24hr at different acidity values (Figure 3.3). Surprisingly, despite lowering the extracellular pH (pH_e) of the culturing medium to pH_e 6.8, A375's intracellular pH (pH_i) remained 7.45 ± 0.05 (n=4) in the presence of FBS, and 7.24 ± 0.03 (n=4) in serum free conditions (Figure 3.3) – such pH_i values were still compatible with survival and cell proliferation in A375 cells, which may at least in part explain their slow proliferation despite acidification of the external environment. In contrast, at the pH_e of 6.5, pH_i in A375 significantly decreased to 7.27

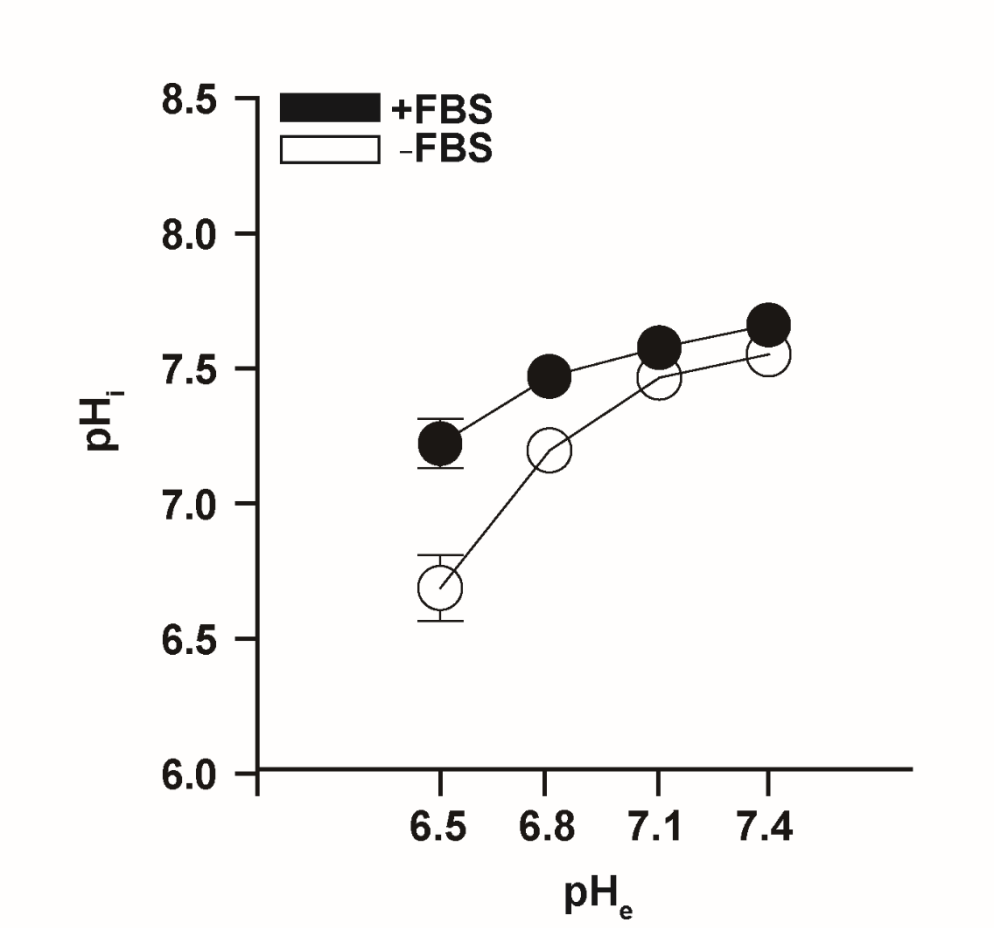

Figure 3.3: FBS-Dependent Maintenance of pHi in response to Extracellular Acidification in A375 Cells. Quantification of the changes in intracellular pH (pH_i) after 24-hours of exposure to decreasing extracellular pH (pH_e). A375 Cells were incubated with or without FBS (n=4). Error bars: mean ± SEM.

± 0.12 (n=4) in the presence of FBS, and 6.73 ± 0.23 (n=4) in serum free conditions (Figure 3.3). These findings suggested that at mildly acidic conditions of pH_e 6.8, some form of FBS-dependent, endergonic acid-extrusion mechanism was in place in A375 cells, and this mechanism preserved intracellular pH despite the imposed extracellular acidity. However, this acid extrusion faculty was likely overwhelmed at the extremes of low pH, especially without FBS nourishment.

Multiple Proton Extruders Act Synergistically to Neutralise Intracellular pH in A375 Cells in Response to Acute Intracellular Acidification

A review of current literature (Bohme and Bosserhoff, 2016, Koch and Schwab, 2019) suggested that the proton extruders known to actively regulate intracellular pH in melanoma cells included the sodium hydrogen exchanger (NHE) (Sarangarajan et al., 2001), the monocarboxylate transporter (MCT) (Wahl et al., 2002), and the V-type ATPase (Pan et al., 2017, Smith et al., 2004). BCECF microspectrofluorometry was thus used to investigate whether these documented transporters were functional in maintaining pH_i balance during periods of acute acidification in A375 cells (Figure 3.4-3.6). Figure 3.4 demonstrates the fluorescence of intracellular de-esterified BCECF in A375, under the 488nm emission filter. Figure 3.5 show the calibration and quantification of BCECF fluorescent intensity to pH_i values in A375. The pKa of BCECF was determined according to the modified Henderson-Hasselbalch equation

(Geisow, 1984) in the form of: $pH_i = pKa + \log_{10} (R-R_{min})/(R_{max}-R)$, where R represents the F490/440 fluorescence ratio of BCECF at various pH_i levels; R_{max} represents the F490/440 fluorescence ratio of the deprotonated form of BCECF (at pH_i 9.5); and R_{min} represents the F490/440 fluorescence ratio of the protonated form of BCECF (at pH_i 5.5)(Geisow, 1984). pKa of BCECF was determined to be 7.234 in this experiment.

Under fluorescent inverted microscopy with continuous HEPES superfusion of the cells, the NH_4Cl prepulse technique was used to induce serial acute intracellular acidification events, in order to record and measure the isolated pH_i recovery activities of different types of proton transporters (Figure 3.6). Compared to control recovery in the presence of HEPES superfusion (Figure 3.6), restricting sodium from the superfusate during the pH_i recovery phase significantly reduced the ability of A375 cells to recover from intracellular acidification, as did the application of HOE694, a specific inhibitor of NHE1 (Figure 3.6a-b). This experiment showed that upon acute acidic exposure, NHE1 was functionally active in neutralising intracellular pH in A375 cells.

Interestingly, neither sodium-free condition nor HOE694 treatment could completely inhibit pH_i recovery in A375 cells, suggesting some form of sodium- and NHE-1 independent mechanism was also active in these melanoma cells (Figure 3.7a-b). Concurrent application of bafilomycin A1, the specific V-Type ATPase inhibitor during the sodium-free pH_i recovery phase achieved near-complete inhibition of pH_i

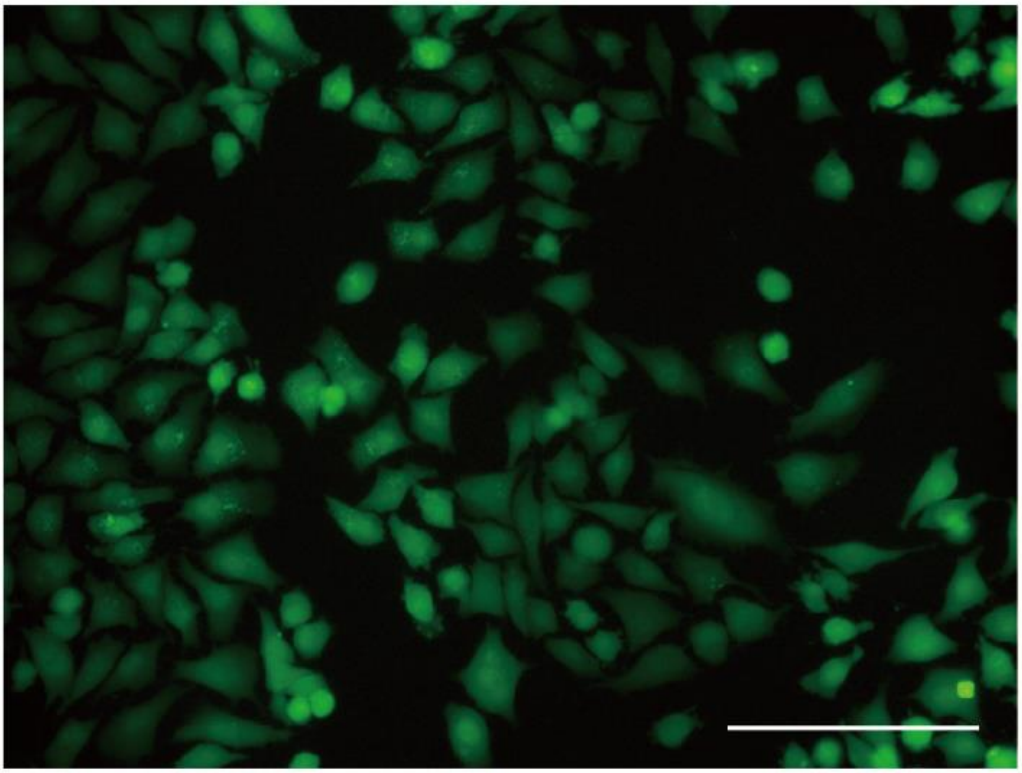

Figure 3.4 Fluorescence of intracellular BCECF in A375 cells. Scale bar: 100μm.

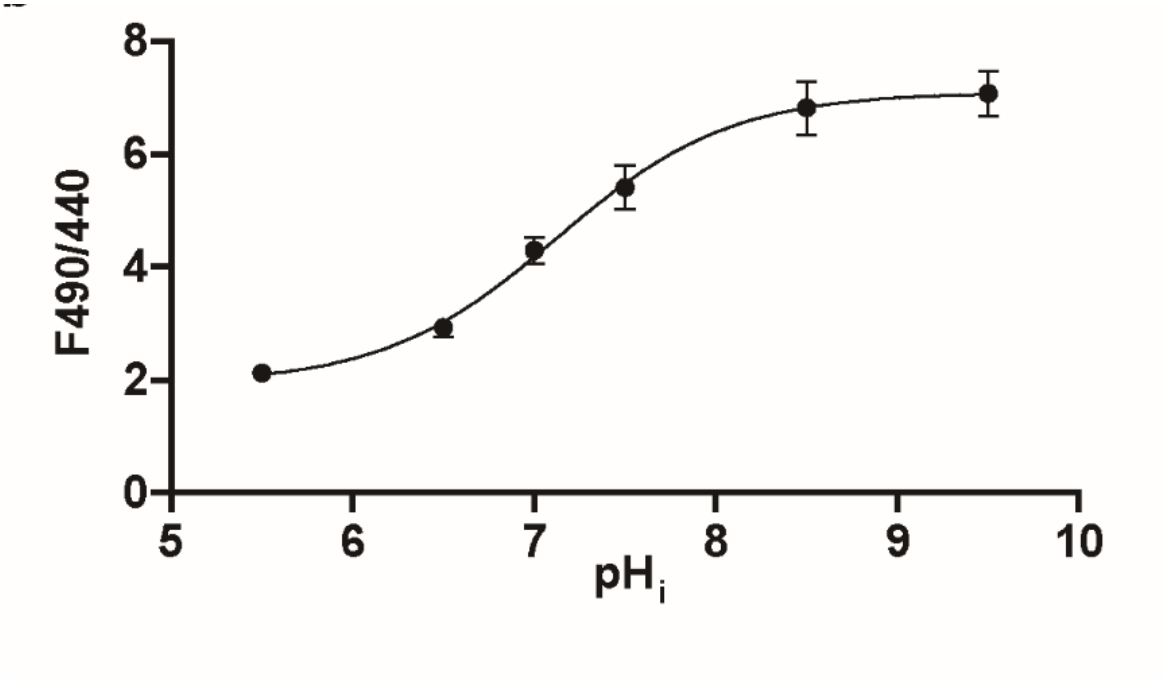

Figure 3.5 Calibration of A375 BCECF fluorescence to pHi values. Quantification of the relationship between F490/440 fluorescence ratio and pH_i in A375 cells (n=9). Error bars: mean ± SEM.

recovery in A375 cells (Figure 3.7a-b), suggesting that V-Type ATPase and NHE1 were synergistic in mediating recovery from intracellular acidity in the A375 melanoma cells.

Next, A375 cells were superfused with sodium lactate, which induced transient acidification of the cytosol (Figure 3.8a). Compared to control recovery in the presence of MCT buffer superfusion, CHC treatment – a specific inhibitor of MCT – during the pH_i recovery phase also significantly reduced the neutralization of intracellular pH (Figure 3.8a-b), suggesting that the MCT transporters were also functionally active in maintaining pH_i in A375 cells. These experiments supported the current literature in showing that A375 cells employed a set of functionally overlapping proton extruders to mobilise H^+ out of the cytosol during periods of acute intracellular acidification (Corbet and Feron, 2017).

Western blotting of the whole-cell lysates from melanoma cell lines A375, MeWo, and HS695T showed that different protein isoforms of NHE, MCT, and the V-Type ATPase were indeed expressed in these melanoma cells (Figure 9). NHE1 and 2, as well as MCT1 and V-Type ATPase were the dominant isoforms of molecular acid extruders present in the melanoma cell lines surveyed (Figure 3.9).

Sodium-Coupled Bicarbonate Transporters Are Expressed and Mediate Acute pH_i Recovery in A375 Melanoma Cells in the Presence of Ambient CO_2/Bicarbonate.

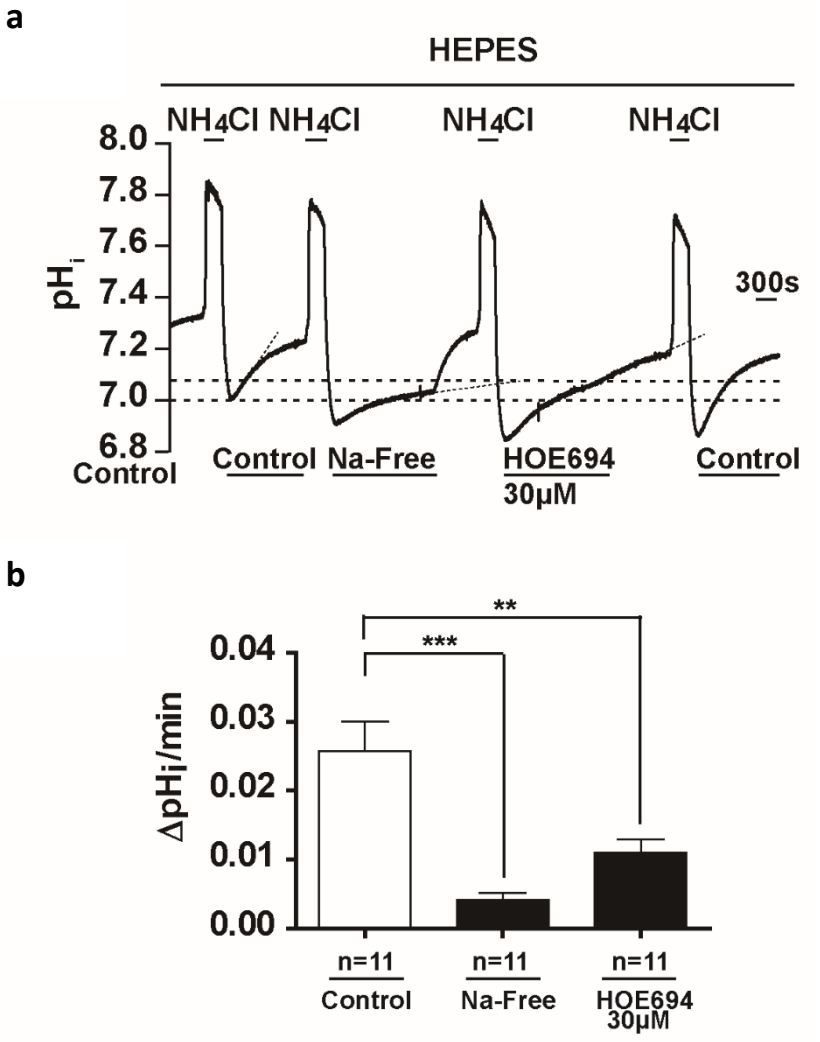

Figure 3.6 NHE proton transport activity is present in A375 cells. Representative pH_i signal of A375 cells serially treated with 20mM NH_4Cl prepulses, Sodium-free condition and HOE694 treatment were applied during the pH_i recovery periods, as indicated. (d) Quantification of pH_i recovery rates under control, sodium-free condition, and HOE694 treatment (n=11). Error bars: mean ± SEM. **P<0.01; ***P<0.001. Statistical significance was calculated using unpaired *t*-test.

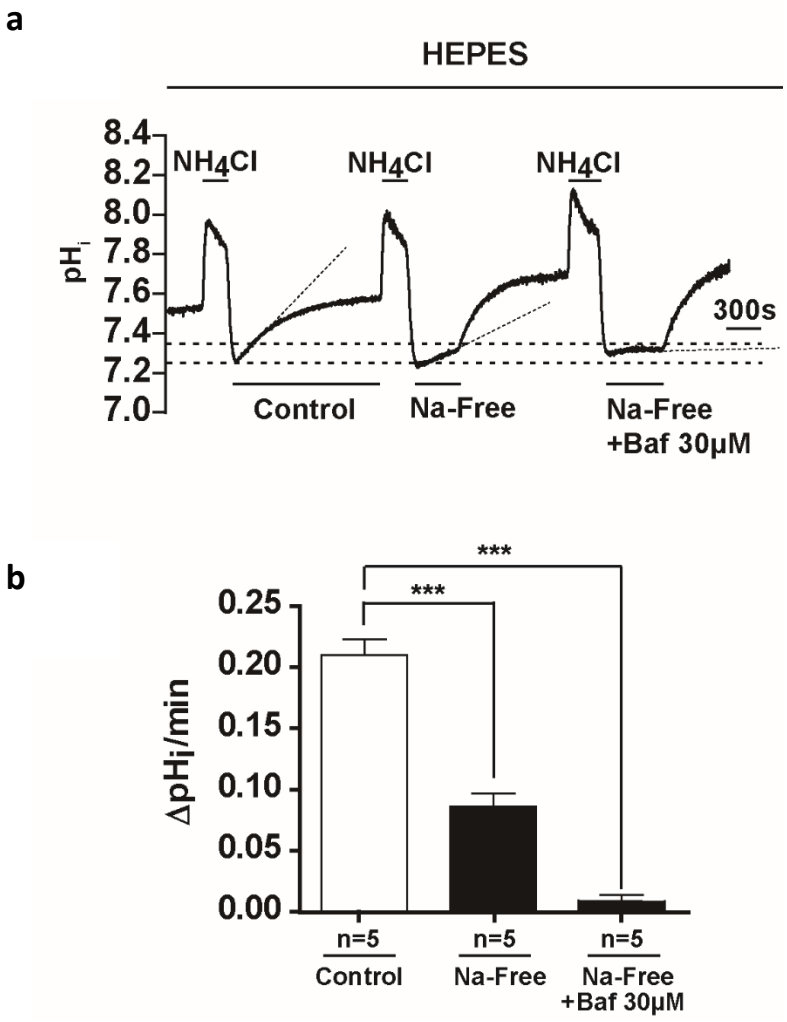

Figure 3.7 V-Type ATPase proton transport activity is present in A375 cells. Representative pH_i signal of A375 cells serially treated with 20mM NH_4Cl prepulses, Sodium-free conditions with and without Bafilomycin A1 treatment were applied during the pH_i recovery periods, as indicated. Quantification of pH_i recovery rates under control, sodium-free condition with, and sodium free condition without Bafilomyin A1 (n=5). Error bars: mean ± SEM. ***P<0.001. Statistical significance was calculated using unpaired *t*-test.

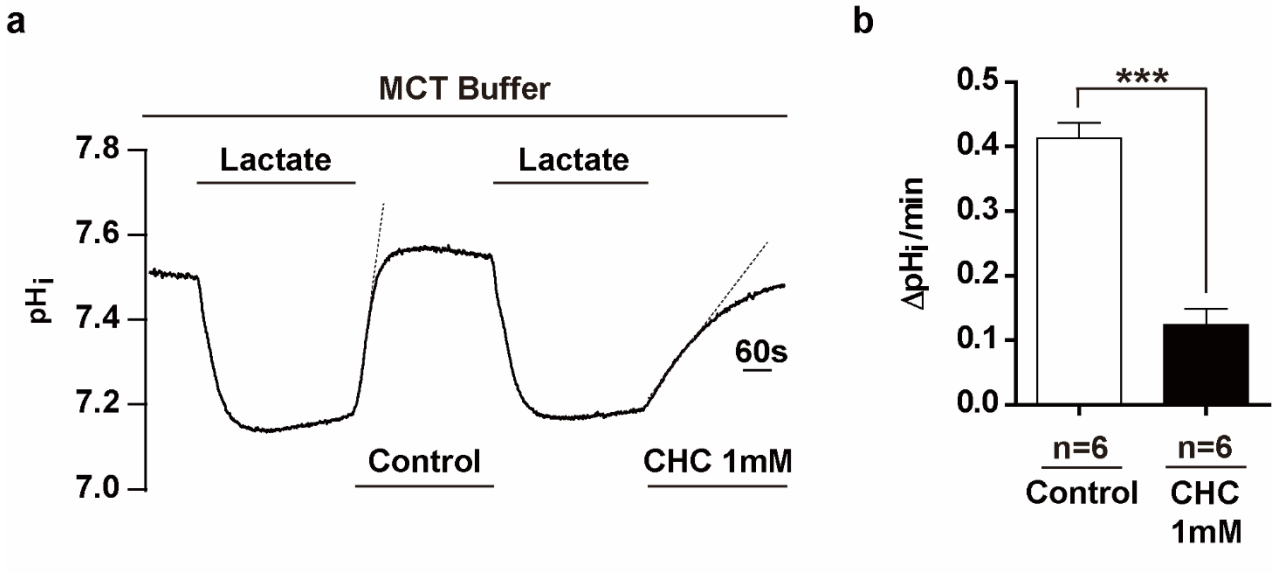

Figure 3.8 MCT Mediates Acid Extrusion in Melanoma Cell Line A375. Representative pH_i signal of A375 cells serially superfused with 10mM sodium lactate. CHC treatment was applied during the pHi recovery period, as indicated. Quantification of pH_i recovery rates under control and CHC treatments (n=6). Error bars: mean ± SEM. ***P<0.001. Statistical significance was calculated using unpaired *t*-test.

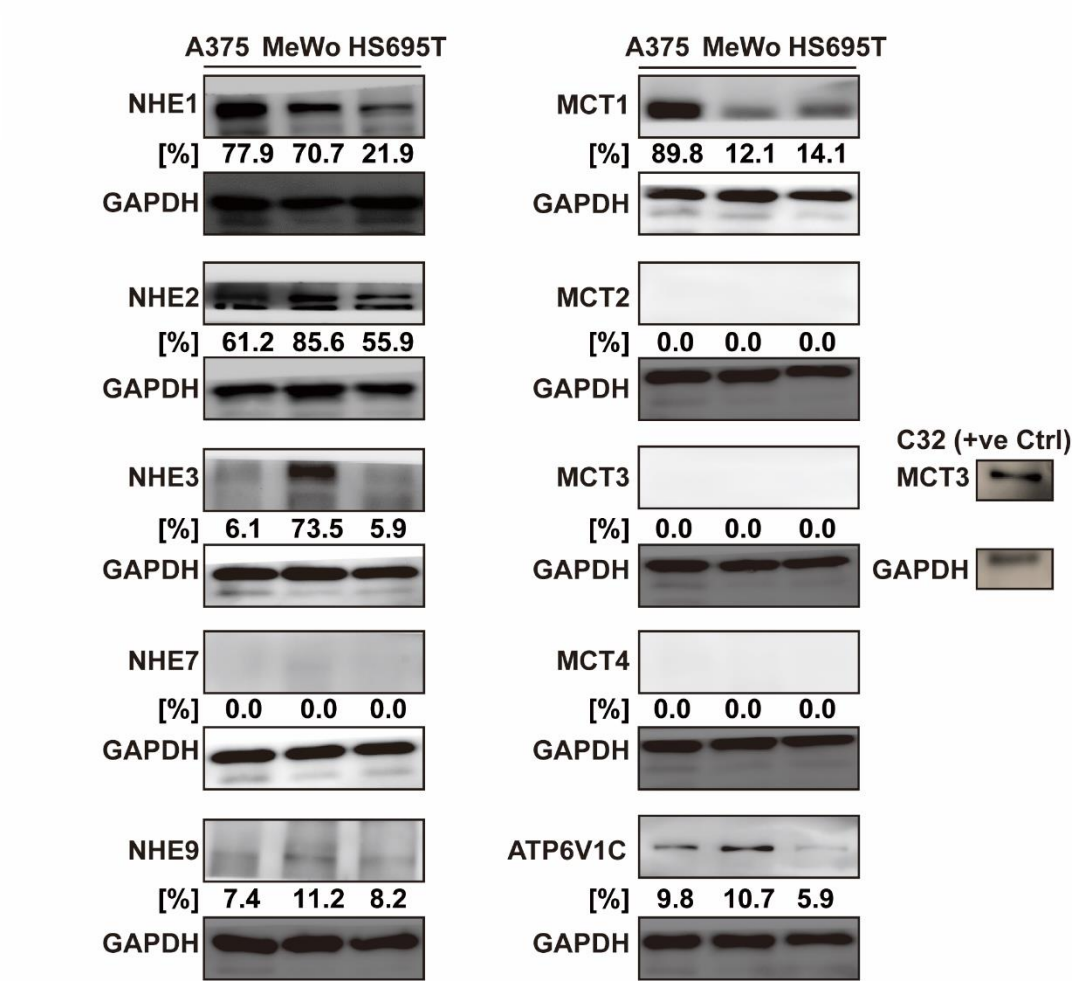

Figure 3.9 Expression of Proton Transporters in Melanoma Cells. Western blots of whole cell lysates from melanoma cell lines A375, MeWo, and HS695T. Primary antibodies: As indicated. Secondary antibodies: HRP conjugated. Loading control: GAPDH. Positive Control for the MCT3 antibody is the C32 melanoma cell line. Densitometric quantifications are shown below the western blots, representing signals normalised to the loading controls, expressed as percentages. Densitometric analysis was performed using the ImageJ software.

Given that the initial cell proliferation and viability experiments were performed in the presence of 5% CO_2 in the incubator (Figure 3.1-3.2), with the pH_e adjustments achieved by changing the concentration of bicarbonate in the cell culture medium (Figure 3.6-3.9), it was considered that the above functional and molecular characterization of the acid extruders in melanoma cells (Figure 3.6-3.9) – which until now was performed using BCECF microscpectrofluorometry in the absence of CO_2/Bicarbonate in the superfusing HEPES solution – likely did not account for the entirety of the acid extrusion repertoire present in melanoma cells. Sodium-Coupled Bicarbonate Transporters (NCBT) is an important class of base loaders also proven to counter intracellular acidification by coupling bicarbonate import with transmembrane sodium cotransport (Parker and Boron, 2013, Romero et al., 2013). A further search of the literature revealed that the presence of bicarbonate transporters in melanoma cells remained poorly determined (Koch and Schwab, 2019).

Therefore, for the BCECF microspectrofluorometry experiments to mimic the cell culture condition in the cell incubator, where the cells were cultured in 5% CO_2, the BCECF microspectrofluorometry and NH4Cl prepulse experiments were repeated, this time with 5% CO2 dissolved in the superfusing HEPES solution so make the BCECF microspectrofluorometry conditions similar to the cell incubator (Figure 3.10a). Compared to control pH_i recoveries, sodium restriction and the application of HOE694

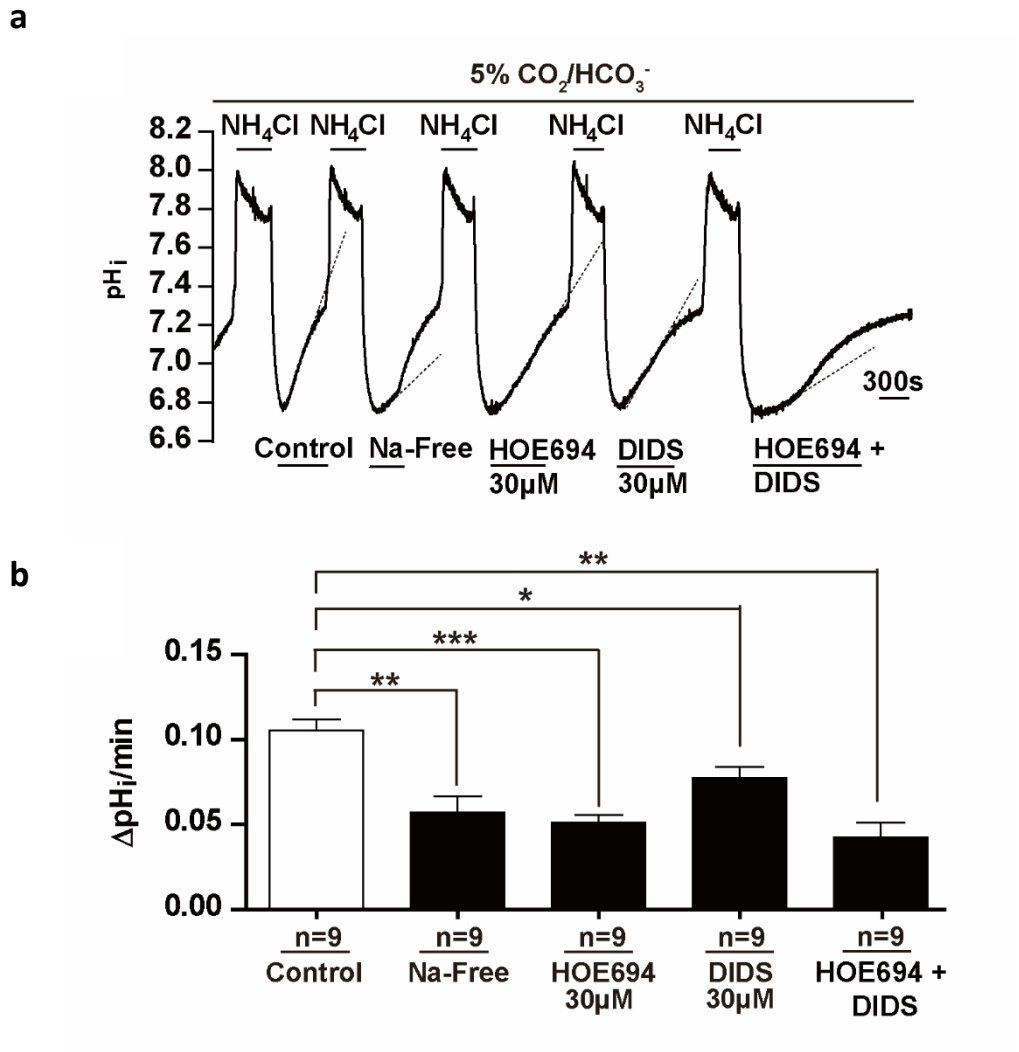

Figure 3.10 NCBT Mediates Acid Extrusion in Melanoma Cell Line A375. Representative pH_i signal of A375 cells serially treated with 20mM NH_4Cl prepulses. Sodium-free condition, HOE694 and DIDS treatments were applied during the pHi recovery periods, as indicated. (b) Quantification of pH_i recovery rates under control, sodium-free condition, HOE694 and DIDS treatments (n=9). Error bars: mean ± SEM. ***P<0.001. Statistical significance was calculated using unpaired *t*-test.

during the pH_i recovery phases still significantly reduced the ability of A375 cells to recover from intracellular acidification, (Figure 3.10a-b), suggesting that NHE transporters were active in the presence of 5% CO_2/bicarbonate.

In addition, the treatment of A375 with 4,4'-Diisothiocyano-2,2'-stilbenedisulfonic acid (DIDS), the specific inhibitor of NCBTs, also significantly reduced pH_i recovery in the presence of bicarbonate, much to a similar extent as HOE694 (Figure 3.10a-b). Furthermore, the combinational treatment of HOE694 and DIDS together restricted the rate of pHi recovery in A375 cells in an additive manner. (Figure 3.10a-b). This experiment showed that in the presence of 5% CO_2/bicarbonate, the NCBTs were at least as functionally active as the NHEs in mediating the net acid extrusion in response to acute intracellular acidification in A375 cells, and these proton transporters likely acted synergistically to maintain pH_i homeostasis in the presence of bicarbonate in the microenvironment.

Western blotting of whole-cell lysates from melanoma cell lines A375, MeWo, and HS695T showed that four members of the NCBT family of bicarbonate transporters were expressed to varying degrees in the human melanoma cell lines (Figure 3.11), including the electrogenic sodium-bicarbonate cotransporters 1 and 2 (NBCe1 and 2), the electroneutral sodium-bicarbonate cotransporter 1 (NBCn1), and the sodium-dependent chloride/bicarbonate exchanger (NDCBE). NDCBE and NBCn1 appeared

to be the most consistently expressed NCBTs across three different melanoma cell lines (Figure 3.11).

The Expression of Sodium-Coupled Bicarbonate Transporters Is Upregulated During Chronic Acidic Exposure in A375 Melanoma Cells.

A common feature demonstrated across multiple studies, and shared by individual NCBT members, is their expressional upregulation in response to metabolic acidosis exposure (Cooper et al., 2009, Kanaan et al., 2007, Lee et al., 2011, Nowik et al., 2008, Snead et al., 2011). Therefore, this study also tested whether chronic acidic exposure could upregulate the expression of the NCBTs in the A375 melanoma cells (Figure 3.12). Exposure to an acidic environment of pH_e 6.8 upregulated the expression of the four NCBT transporters in a time-dependent manner (Figure 3.12a), whereas exposure to the control environment of pH_e 7.4 had minimal effect (Figure 3.12b). the NCBTs were measurably upregulated beginning at 6 hours after the exposure to pH_e 6.8 (Figure 3.12c-f). Taken together, the results from this study suggest that upon exposure to mild acidic stress, the expression, regulation, and function of NCBTs in A375 cells were all potentiated to maintain pH_i balance.

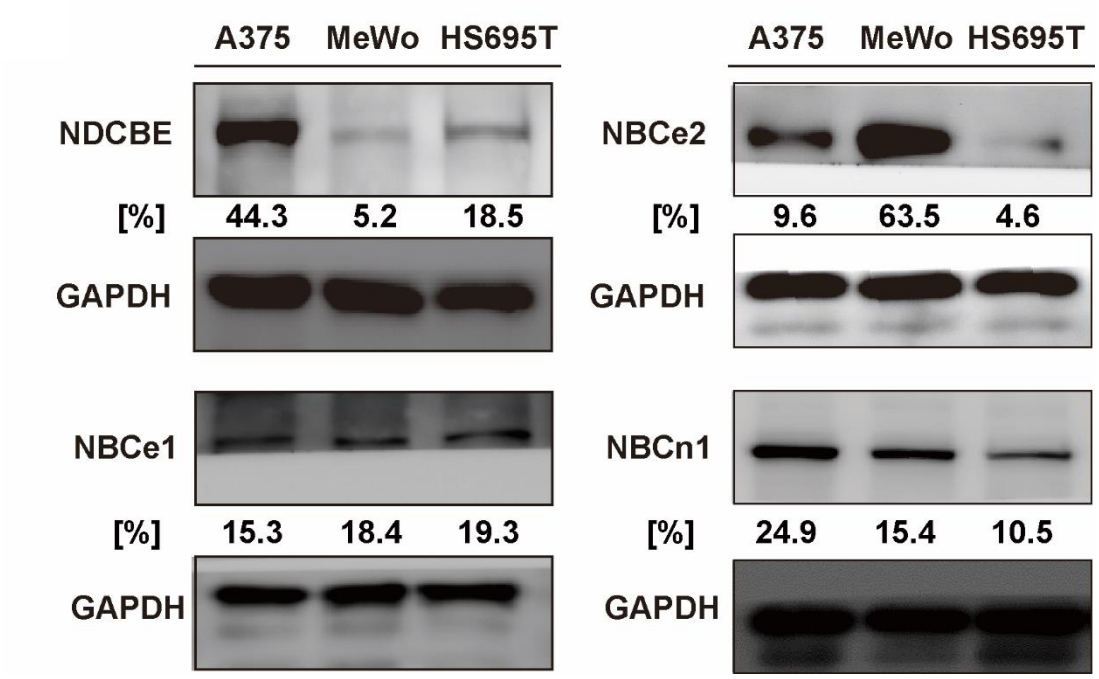

Figure 3.11 Expression of NCBT in Melanoma Cells. Western blots of whole cell lysates from melanoma cell lines A375, MeWo, and HS695T. Primary antibodies: As indicated. Secondary antibodies: HRP conjugated. Loading control: GAPDH. Densitometric quantification using ImageJ is shown below the western blots, representing signals normalised to the loading controls, expressed as percentages.

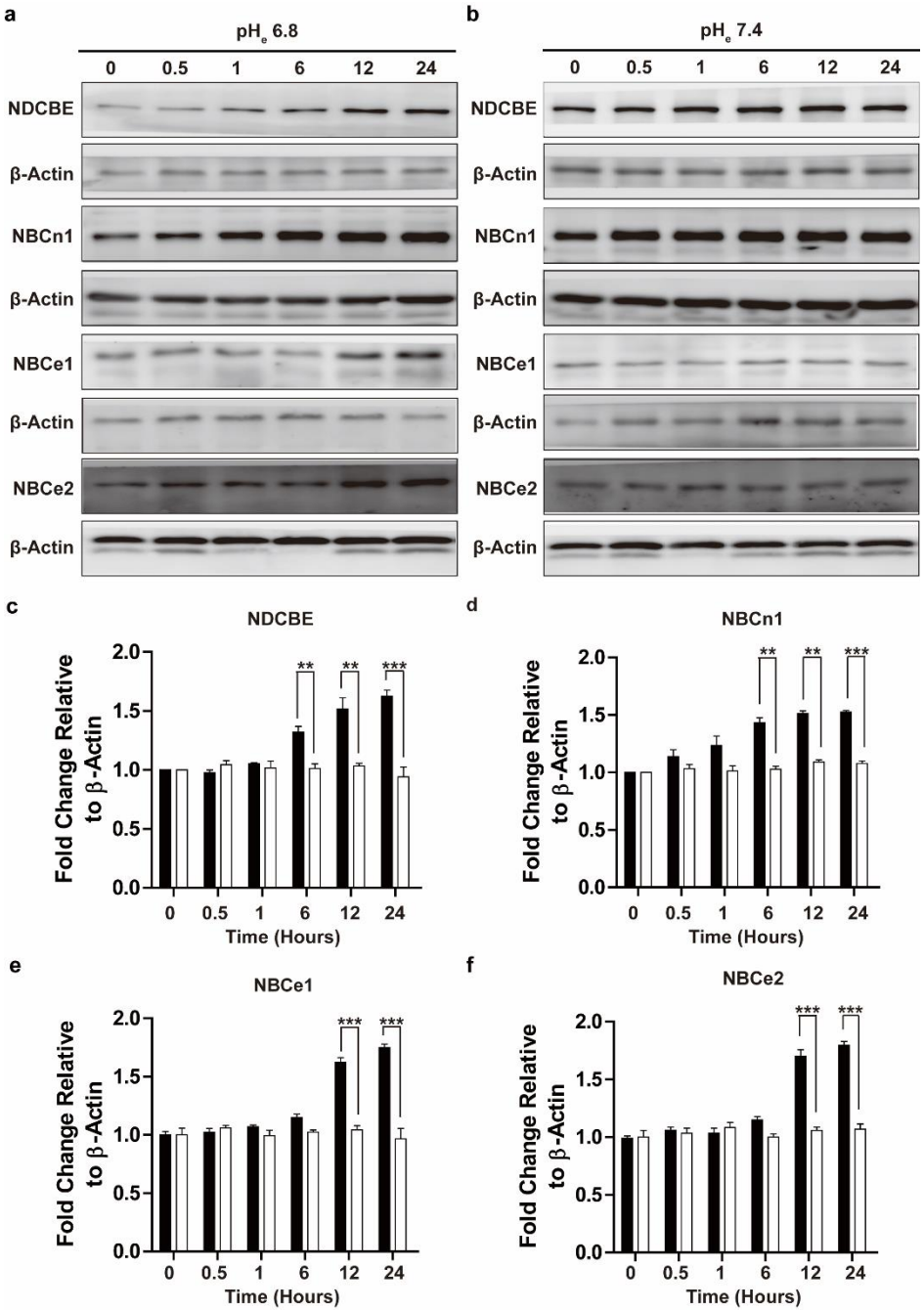

Figure 3.12 NCBT Protein Expression Levels are Upregulated in Response to Extracellular Acidification in Melanoma Cell Line A375. The protein expression levels of NCBTs in A375 cells exposed to (a) pH_e 6.8 and (b) pH_e 7.4 were evaluated over time (hours) by western blot. Primary antibodies: As indicated. Secondary antibodies: HRP conjugated. Loading control: β-Actin. (c-f) Densitometric quantifications of the fold changes in the NCBT: β-Actin expression ratios following exposure to pH_e 6.8 and 7.4 over time, relative untreated controls at time 0. Densitometric analysis was performed using the ImageJ software. Values were averaged over 4 experiments that were similar to those shown in (a) and (b). Error bars: mean ± SEM. **P<0.01; ***P<0.001. Statistical significance was calculated using unpaired *t*-test.

Proton extrusion is functionally active across multiple melanoma cell lines

Aside from A375, proton extrusion function was screened across multiple melanoma cell lines using BCECF microscospectrofluorometry coupled with the NH_4Cl pre-pulse technique (Figure 3.13-18). Since NHE function comprises a significant proportion of the cell's total acid extrusion capacity, proton extrusion in melanoma cells was screened by applying sodium-free condition and HOE694 treatment during the pHi recovery phases of NH4Cl prepulse, and comparing these pH_i recovery rates to pH_i recovery without treatment (control). As can be seen in figure 3.13, as compared to control pH_i recovery under superfusion with HEPES, pH_i recoveries exposed to sodium-free and HOE694 were significantly impaired in the MeWo melanoma cell line, suggesting that NHE-dependent proton extrusion function was present in MeWo cells. pH_i recovery occurred at the rate of 0.007±0.001/minute under normal HEPES condition (n=10; Figure 3.13b); -0.002±0.0005/minute upon exposure to sodium-free conditions (n=10; $p<0.0001$), and -0.001±0.0005/minute when treated with HOE694 (an NHE1-specific inhibitor, n=8; $p<0.0001$).

NHE-dependent proton extrusion function was tested in the IGR39 cell line. As can be seen in figure 3.14, compared to control pHi recovery superfused with HEPES, pHi recoveries under the exposure to sodium-free and HOE694 were also significantly impaired in the IGR39 melanoma cell line, suggesting that NHE was active in

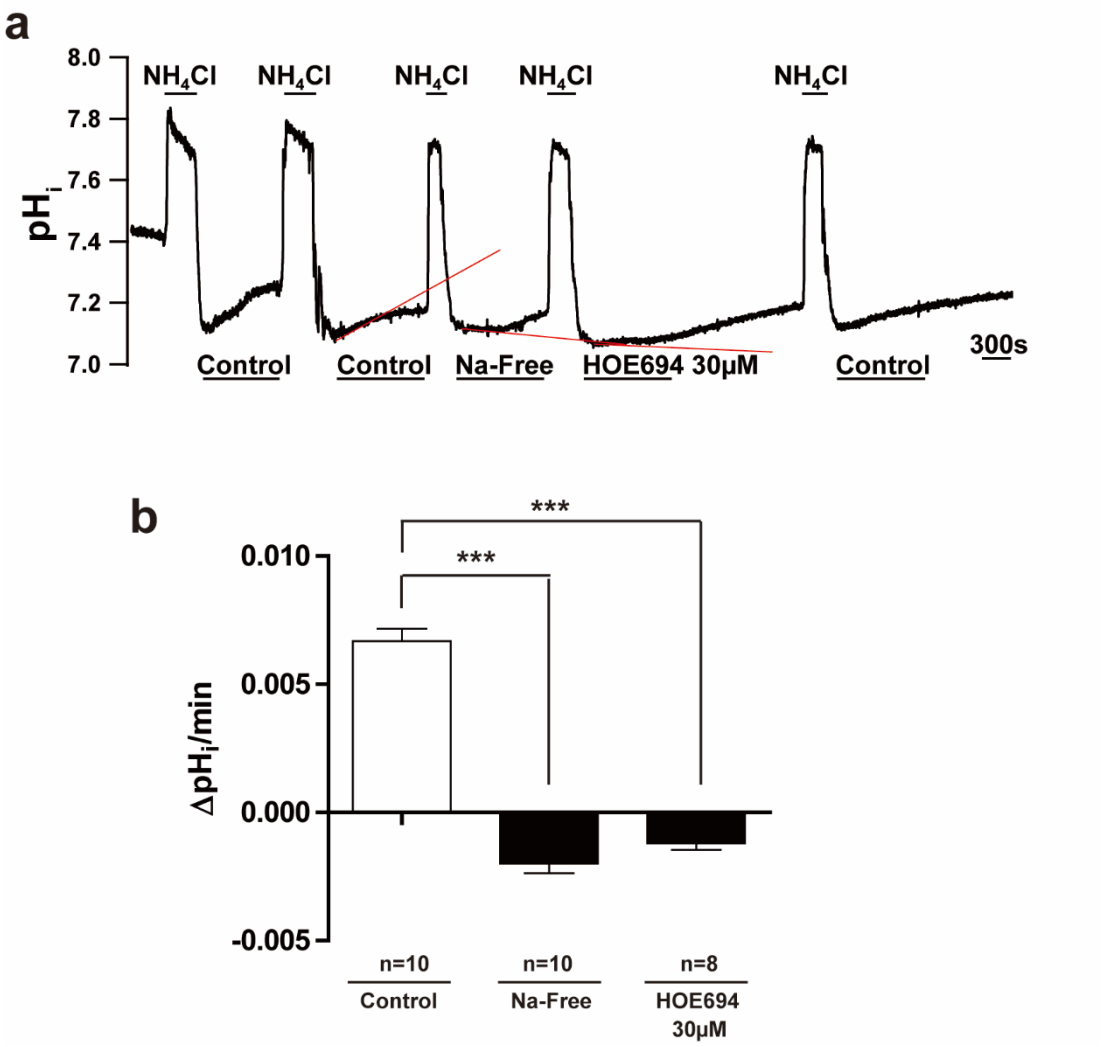

Figure 3.13: Characterisation of proton transporter function in MeWo cell line. (a) Representative pH_i signal of MeWo exposed to sequential prepulses of NH_4Cl 20mM. During the pH_i recovery periods, control (normal HEPES), sodium-free HEPES, and HEPES with HOE694 30µM (an NHE1 inhibitor) were sequentially superfused. The negative gradient during sodium free recovery suggested net proton influx was greater than the net proton efflux during the indicated time period, consistent with a lack of proton export function following physiological NHE1 inhibition via sodium removal. Time scale: as indicated bottom right. (B) Quantification of the minute-change in pH_i compared to control recovery within the same experiment (repeats as indicated in figure). Time Scales: As indicated. Error bars: mean ± SEM. ***P<0.0001. Statistical significance was calculated using unpaired *t*-tests.

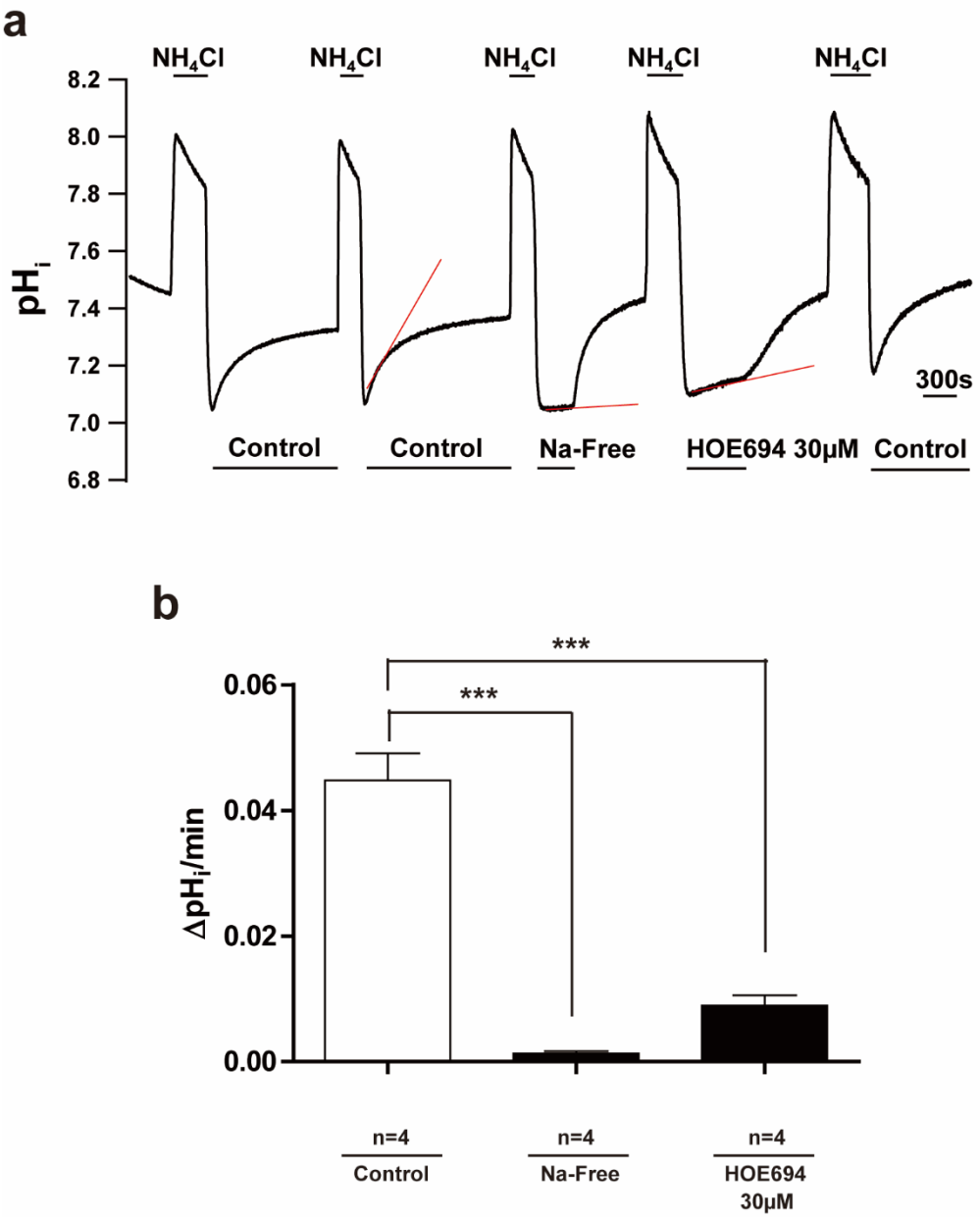

Figure 3.14: Characterisation of proton transporter function in IGR39 cell line. (a) Representative pH_i signal of IGR39 exposed to sequential prepulses of NH_4Cl 20mM. During the pH_i recovery periods, control (normal HEPES), sodium-free HEPES, and HEPES with HOE694 30µM (an NHE1 inhibitor) were sequentially superfused. Time scale: as indicated bottom right. (B) Quantification of the minute-change in pH_i compared to control recovery within the same experiment (repeats as indicated in figure). Time Scales: As indicated. Error bars: mean ± SEM. ***P<0.0001. Statistical significance was calculated using unpaired *t*-tests.

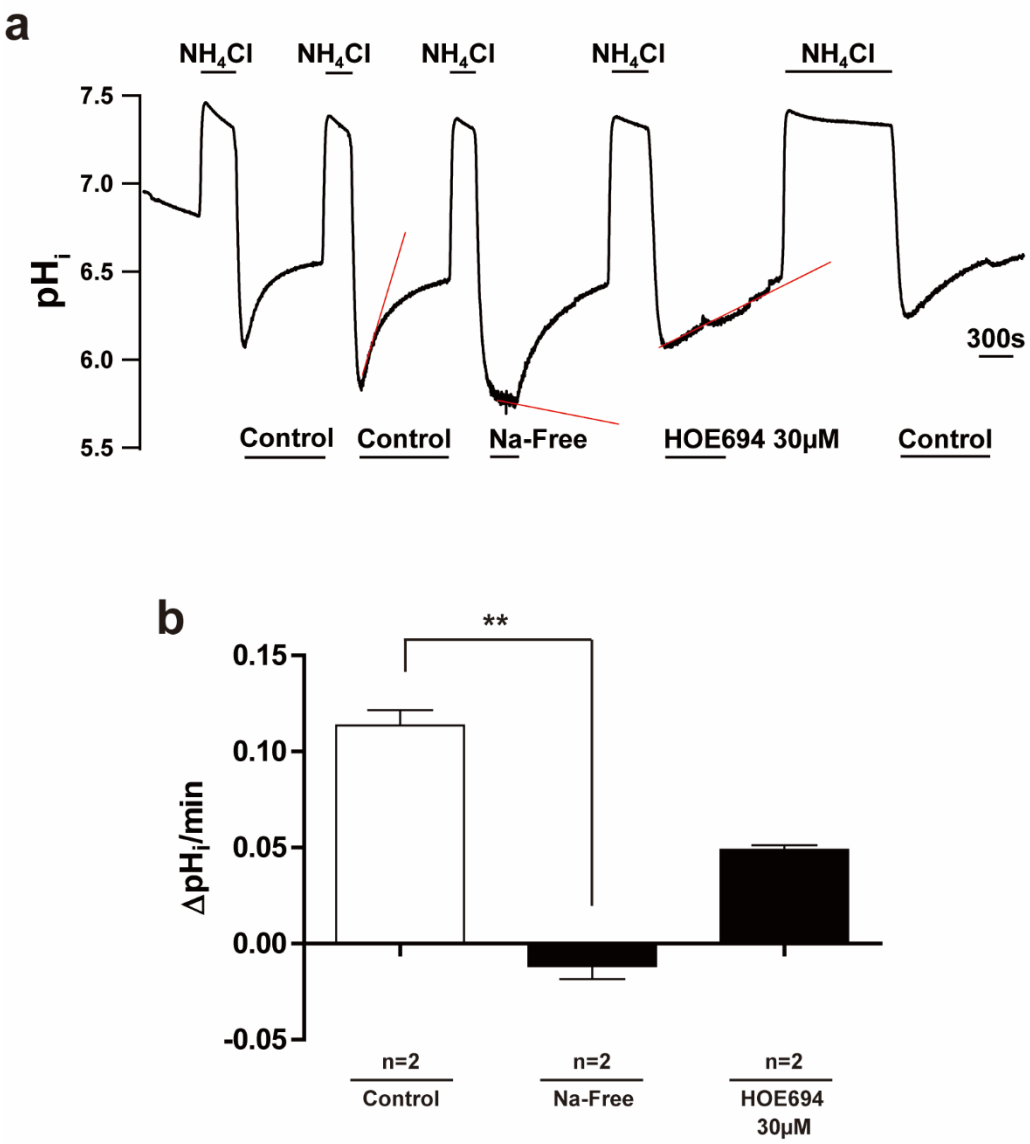

Figure 3.15: Characterisation of proton transporter function in IGR37 cell line. (a) Representative pH_i signal of IGR37 exposed to sequential prepulses of NH_4Cl 20mM. During the pH_i recovery periods, control (normal HEPES), sodium-free HEPES, and HEPES with HOE694 30µM (an NHE1 inhibitor) were sequentially superfused. Time scale: as indicated bottom right. (B) Quantification of the minute-change in pH_i compared to control recovery within the same experiment (repeats as indicated in figure). Time Scales: As indicated. Error bars: mean ± SEM. $^{**}P<0.001$. Statistical significance was calculated using unpaired *t*-tests.

mediating acid extrusion in IGR39 cells. pH_i recovery occurred at the rate of 0.042±0.005/minute under normal HEPES condition (n=4; Figure 3.14b); 0.002±0.001/minute upon exposure to sodium-free conditions (n=4; $p<0.0001$), and 0.011±0.002/minute when treated with HOE694 (n=5; $p<0.0001$).

In the IGR37 cell line, NHE-reliant acid extrusion function was also tested using NH_4Cl pre-pulse (Figure 3.15). pHi recoveries under the exposure to sodium-free and HOE694 treatements were significantly impaired in the IGR37 melanoma cell line, compared to control pHi recovery under the superfusion of normal HEPES (Figure 3.15a). For IGR37, pHi recovery occurred at the rate of 0.115±0.013/minute under normal HEPES condition (n=2; Figure 3.15b); -0.023±0.023/minute upon exposure to sodium-free conditions (n=2; $p<0.01$), and 0.042±0.005/minute when treated with HOE694 (n=2).

Proton extrusion was then tested in the C32 cell line. As can be seen in figure 3.16, as compared to control pHi recovery superfused with HEPES, pHi recovery under the exposure to sodium-free condition was also significantly impaired in the C32 melanoma cell line, suggesting that NHE was active in mediating acid extrusion in C32 cells (Figure 3.16a). pHi recovery occurred at the rate of 0.045±0.011/minute under normal HEPES condition (n=4; Figure 3.16b); and -0.002±0.001/minute upon exposure to sodium-free conditions (n=4; $p<0.01$).

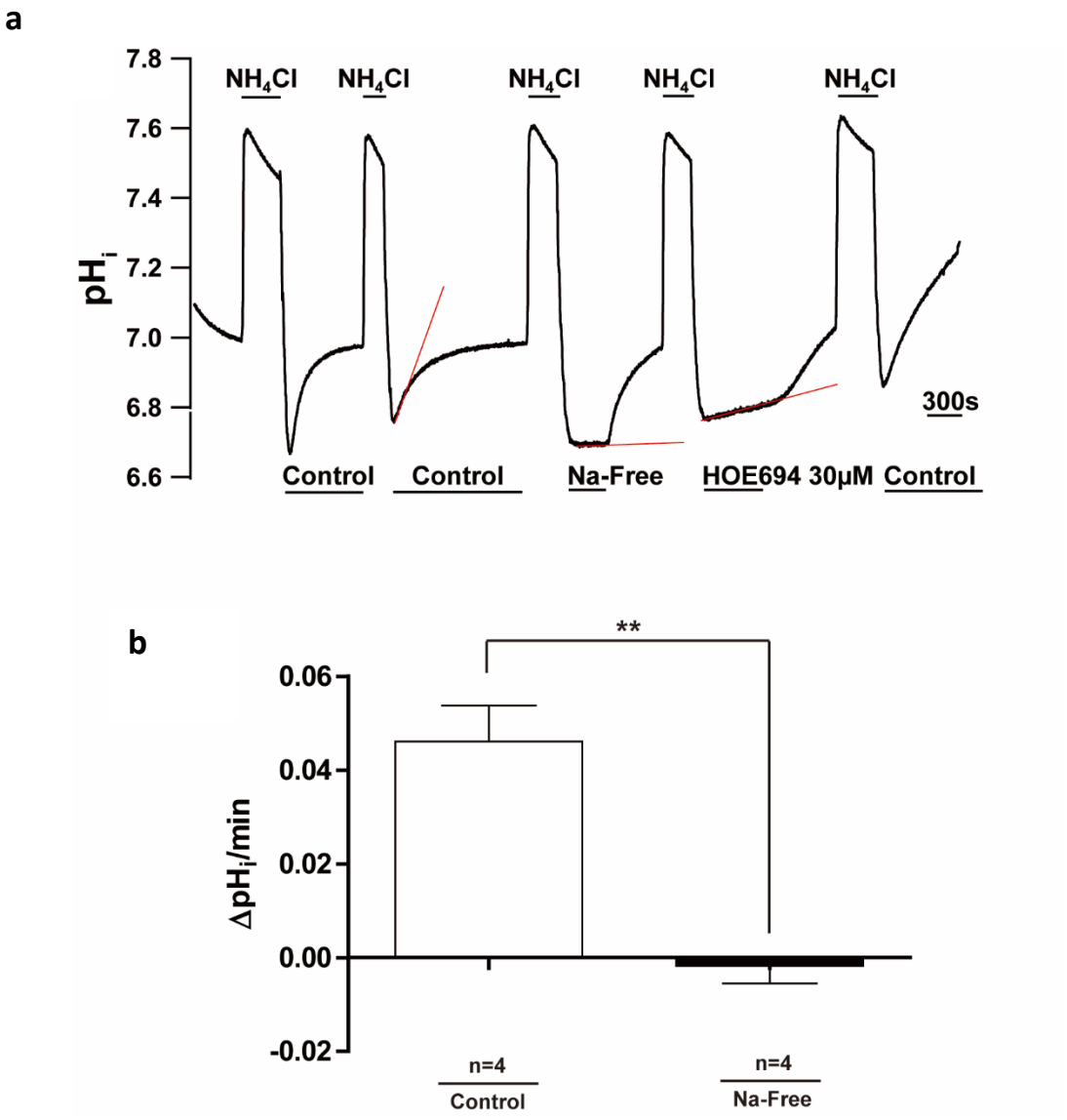

Figure 3.16: Characterisation of proton transporter function in C32 cell line. (a) Representative pH_i signal of C32 exposed to sequential prepulses of NH_4Cl 20mM. During the pH_i recovery periods, control (normal HEPES), sodium-free HEPES, and HEPES with HOE694 30µM (an NHE1 inhibitor) were sequentially superfused. Time scale: as indicated bottom right. (B) Quantification of the minute-change in pH_i compared to control recovery within the same experiment (repeats as indicated in figure). Time Scales: As indicated. Error bars: mean ± SEM. $^{**}P<0.001$. Statistical significance was calculated using unpaired *t*-tests.

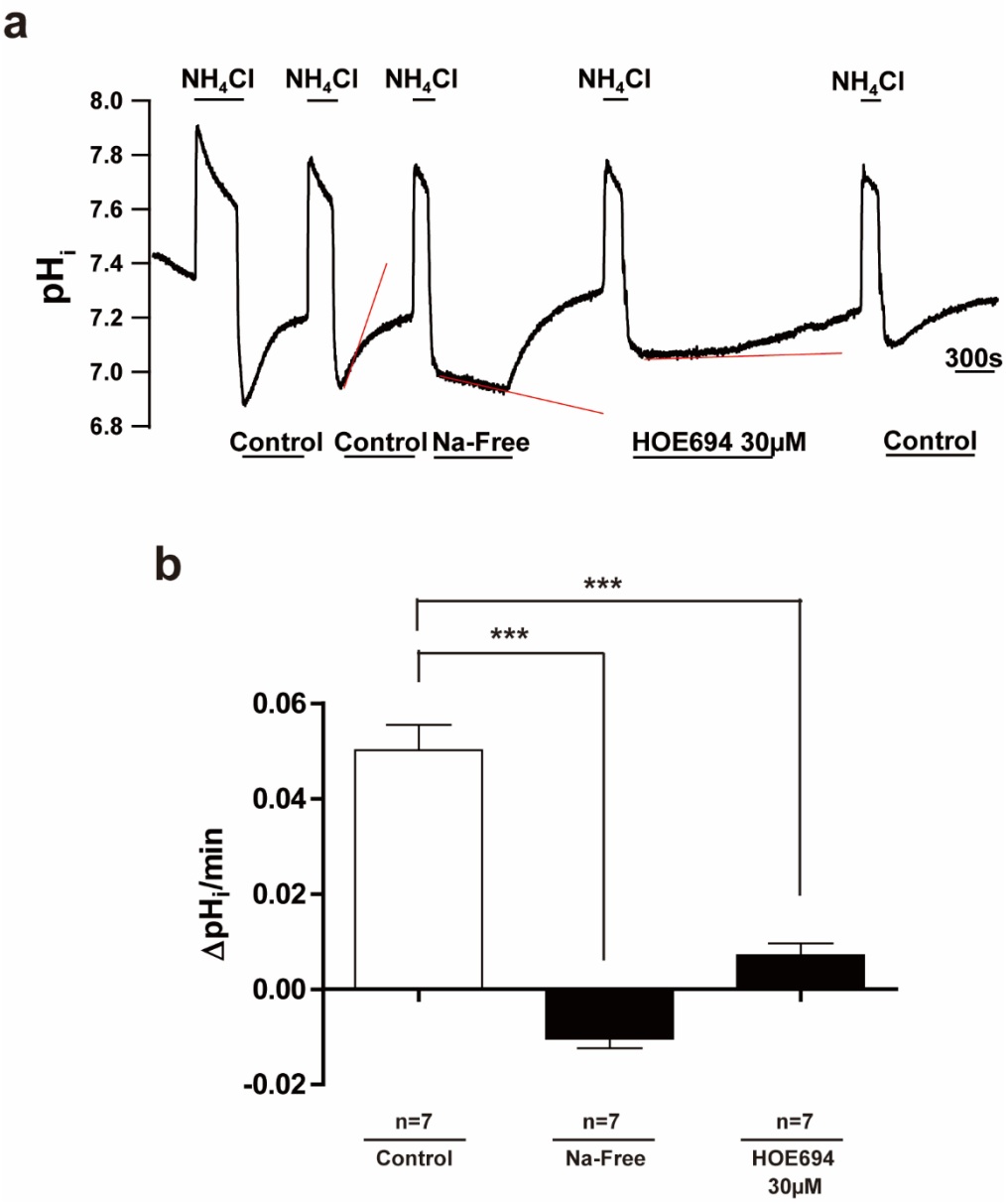

Figure 3.17: Characterisation of proton transporter function in HS695T cell line. (a) Representative pH_i signal of HS695T exposed to sequential prepulses of NH_4Cl 20mM. During the pH_i recovery periods, control (normal HEPES), sodium-free HEPES, and HEPES with HOE694 30µM (an NHE1 inhibitor) were sequentially superfused. Time scale: as indicated bottom right. (B) Quantification of the minute-change in pH_i compared to control recovery within the same experiment (repeats as indicated in figure). Time Scales: As indicated. Error bars: mean ± SEM. $^{**}P<0.001$. Statistical significance was calculated using unpaired *t*-tests.

with sodium-free, HOE694, DIDS, and HOE694 + DIDS treatments were all relatively impaired in HS695T, though only sodium-free treatment achieved statistical significance (Figure 3.18a). For HS695T, pHi recovery occurred at the rate of 0.023±0.003/minute under normal HEPES condition (n=7; Figure 3.18b); 0.009±0.003/minute upon exposure to sodium-free conditions (n=7; $p<0.001$); 0.019±0.002/minute upon exposure to HOE694 (n=7; n.s.); and 0.019±0.003/minute when treated with DIDS (n=7; n.s.). In the HS695T cell line, NHE-dependent acid extrusion function was again tested using NH_4Cl pre-pulse (Figure 3.17). pHi recoveries when superfused with sodium-free and HOE694 treatments were significantly impaired in HS695T, compared to control pHi recovery under the superfusion of normal HEPES (Figure 3.17). For HS695T, pHi recovery occurred at the rate of 0.052±0.008/minute under normal HEPES condition (n=7; Figure 3.17b); -0.023±0.023/minute upon exposure to sodium-free conditions (n=2; $p<0.01$), and 0.042±0.005/minute when treated with HOE694 (n=2).

For the HS695T cell line, NBC's alkali loading function was also tested using NH4Cl pre-pulse under 5% HCO_3^-/CO_2 conditions (Figure 3.18). Compared to control pHi recovery under the superfusion of normal HEPES, pHi recoveries when superfused with sodium-free, HOE694, DIDS, and HOE694 + DIDS treatments were all relatively impaired in HS695T, though only sodium-free treatment achieved statistical

significance (Figure 3.18a). For HS695T, pHi recovery occurred at the rate of 0.023±0.003/minute under normal HEPES condition (n=7; Figure 3.18b); 0.009±0.003/minute upon exposure to sodium-free conditions (n=7; $p<0.001$); 0.019±0.002/minute upon exposure to HOE694 (n=7; n.s.); and 0.019±0.003/minute when treated with DIDS (n=7; n.s.).

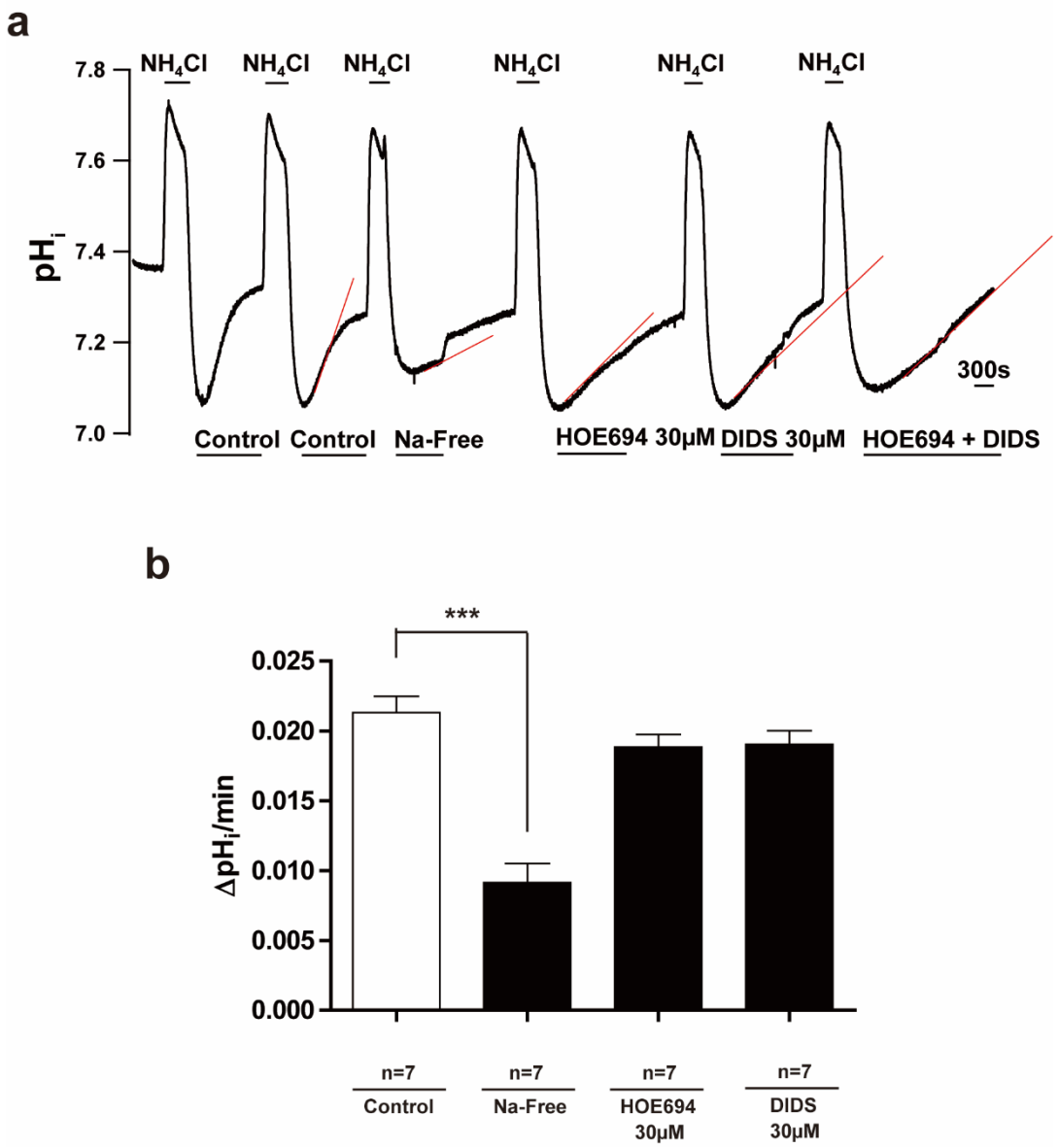

Figure 3.18: Characterisation of proton transporter function in the presence of bicarbonate in HS695T cell line. (A) Representative pH_i signal of HS695T superfused in bicarbonate solution and exposed to sequential prepulses of NH_4Cl 20mM. During the pH_i recovery periods, control (normal bicarbonate solution), sodium-free bicarbonate solution, bicarbonate solution with HOE694 30µM (an NHE1 inhibitor), bicarbonate solution with DIDS 30µM (an SLC4 inhibitor), and bicarbonate solution with HOE694 30µM plus DIDS 30µM were sequentially superfused. Time scale: as indicated bottom right. (B) Quantification of the minute-change in pH_i compared to control recovery within the same experiment (repeats as indicated in figure). Time Scales: As indicated. Error bars: mean ± SEM. ***P<0.0001. Statistical significance was calculated using unpaired *t*-tests.

DISCUSSION

This chapter characterized the A375 cell line as a model for studying proton transport in melanoma cells. A375 human melanoma cells exposed to acute acidic stress relied on different modalities of proton transporters to maintain their pH_i balance. This chapter also showed that under acidic stress, the sustenance of pH_i within the viable range contributes to cellular proliferation and viability in melanoma cells.

Interestingly, whilst severe acidification has been associated with the induction of acidic cell death in different cell types (Jeong et al., 2001, Goldman et al., 1989, Nedergaard et al., 1991), milder degrees of acidification above pH 6.5 have been shown to exert protective effects on cell survival (Khacho et al., 2014, Allen and Westerblad, 2004, Kaku et al., 1993). In the case of melanoma, survival under mild acidosis has been shown to contribute to melanomagenesis (Kato et al., 2013), via the induction of autophagic and beta-oxidative acidic adaptation (Marino et al., 2012, Corbet et al., 2016), with concurrent upregulation of proangiogenic factors VEGF and IL-8 (Rofstad et al., 2006b). This chapter showed that the threshold for viability and continued slow proliferation was pH_e 6.8 for A375 melanoma cells (Figures 3.1 and 3.2). The exact threshold pH_e for acidic cell death has been shown to vary depending on the cell type under acidic exposure (Lan et al., 2007), the duration of acidic exposure(Cooper et al., 2009), and the degree of intracellular acidification (Marino et al., 2012). In cortical

cultures of neurons for example, the threshold to induce 50% cell death is pH_e 6.4 for 6-hour acid exposure in the absence of CO_2/HCO_3^- in buffer (Nedergaard et al., 1991). In contrast, even mild acidosis at pH 7.0 induced growth arrest in glioma cells that retained wild type p53 function (Reichert et al., 2002). While it remains unclear how absolute thresholds for acidic cell survival are determined in different cell types (Marino et al., 2012), in melanoma cells different proton transport modalities have been shown to contribute to facilitating survival and the upkeep of pH_i under acidic stress (Kato et al., 2013). There is impetus therefore to individually define the functional presence of proton transporter modalities in melanoma (Wahl et al., 2002), as carried out in this study, in order to better understand how melanoma cells maintain the pH of its internal environment when exposed to acidification.

This chapter provided evidence to show that NCBTs were present and functional in melanoma cells, contributing to pH_i recovery in response to acute cellular acidification. Many cancer types including breast (Lee et al., 2015a), pancreatic (Kong et al., 2014), and renal cell carcinoma (Yamada et al., 2003) are known to rely on bicarbonate transporters for pH_i regulation, and the melanoma cells in this study were also dependent on the NCBT family. NCBTs import bicarbonate via the coupling to sodium symport, and as such requires the active generation of a sodium electrochemical gradient to facilitate bicarbonate transport activity (Parker and Boron, 2013). In our

hands, DIDS-dependent pH_i recovery was similar in rate compared to HOE694-dependent pH_i recovery, suggesting that NCBTs were at least as efficient as the canonical NHE transporters in facilitating pH_i regulation in melanoma cells (Figure 3.5a-b). However, CHC-dependent pH_i recovery from lactate withdrawal was still at least 2 orders of magnitude faster than either NHE or NCBT in the A375 cells (Figure 4b), suggesting that MCTs were still the most dominant form of acid extrusive mechanism in melanoma cells, consistent with previous experiments by Wahl and Colleagues (Wahl et al., 2002).

This study hypothesized that exposure of melanoma cells to chronic acidic stress would stimulate the expression of the NCBTs. This hypothesis was tested in A375 cells, a melanoma cell line that demonstrated functional NCBT activity and expression. The findings from this study suggested that acidic stress induced by exposure to pH_e 6.8 upregulated the expression of four NCBTs in melanoma cells, including NBCn1, NBCe1, NBCe2, and NDCBE. Statistically significant upregulation of NCBTs was measurable beginning at 6hrs, with 4 repeats performed per western blot (Figure 3.12c-f). In previous reports, NBCn1 from primary hippocampal neurons had been shown to increase in protein abundance following the lowering of cell culture pH_e to 6.8 (Cooper et al., 2009), and in response to chronic metabolic acidosis induced by orally feeding 0.4M NH_4Cl to rats (Park et al., 2010). Increased NBCn1 expression was also reported

in rodent kidneys following oral administration of NH_4Cl (Nowik et al., 2008), HCl (Cucoranu et al., 2004), and after induction of hyperkalaemic acidosis (Mrowiec et al., 2005). In addition, cardiac and renal NBCe1 expression levels had been shown to be upregulated in neonatal mice and rats, respectively, following chronic exposure to metabolic acidosis secondary to 12% CO_2 hypercapnia (de Seigneux et al., 2007, Kanaan et al., 2007). Furthermore, protein expression of NDCBE in the CA3 region of rat brain hippocampus also increased by 2.5 fold, secondary to the induction of chronic metabolic acidosis (Lee et al., 2011). The findings from this study are thus in support of results from other groups, suggesting that in the context of melanoma, NCBT expression may also be regulated by exposure to acidic stress. Previous reports had shown that MCT, NHE, and V-Type ATPase play functional rules in pHi regulation in melanoma cells (Smith et al., 2004, Wahl et al., 2002). This chapter also demonstrated the functional activities of these transporters in A375 cells. Concomitant activity of functionally overlapping acid extruders with NCBT in A375 suggests that targeted therapeutic strategies that caters for multiple proton transport systems may be more effective at lowering tumour pH_i than monotherapy approaches (Corbet and Feron, 2017).

The presence of NCBTs in melanoma provides further impetus to evaluate these acid extruders as molecular therapeutic targets (Lee et al., 2015a, Lee et al., 2018).

Figures 14-19 showed that acid extrusion was functionally present across all melanoma cell lines subjected to NH_4Cl prepulse, suggesting that proton transport was a ubiquitous and important component of melanoma pathophysiology. Indeed, the importance of tumour acidity regulation in melanoma has been aptly highlighted in a number of well-written review articles (Bohme and Bosserhoff, 2016) . The caveat here is that this chapter screened the sodium-free arm of pH recovery in different melanoma cell lines in order to identify A375 as having robust pHi recovery under sodium-free conditions. The presence of pHi recovery under sodium free conditions suggested that A375 possessed additional and detectable means of proton transportation outside of sodium-hydrogen exchanger function – the predominant mechanism of acid extrusion under HEPES conditions for most cell types (Stock and Pedersen, 2017). This opened up functional investigation of V-Type ATPase activity in A375 cells, as shown in figure 8 of this chapter.

Changes in pH_i and its regulation have been studied in melanoma (Bohme and Bosserhoff, 2016, Koch and Schwab, 2019). Proton transport exerts influence on acidic cell survival and proliferation (Kato et al., 2013). Especially in the case of melanoma, where malignant vertical growth into the acidic skin surface exposes melanoma cells to extremes of low pH_e (Ohman and Vahlquist, 1994, Schmid-Wendtner and Korting, 2006), melanoma cells adapt by developing mechanisms for removal of protons from

the interior of the cell (Spugnini et al., 2015). Demonstrating sodium-coupled bicarbonate transport in melanoma cells contributes to a greater understanding how melanoma cells survive under acidic stress, and identification of new pH_i regulatory mechanisms may provide viable therapeutic targets for developing melanoma treatments in the future (Alfarouk, 2016).

CHAPTER 4

Regulation of Proton Transporters Expression by MITF in Melanoma

Abstract

Developing a working experimental model of the various proton transporters in melanoma cell lines opened up further experiments that tested the regulatory effects of Microphthalmia-Associated Transcription Factor (MITF) on proton transport. MITF is a member of the basic helix-loop-helix leucine zipper family of transcription factors, known to play a prominent role in dysplastic melanomagenesis. This chapter addressed whether MITF-dependent phenotypic plasticity could reprogram the transcriptome of proton transporters in melanoma cells. High-Throughput RNA-Sequencing Analysis of the human melanoma samples in the TGCA dataset, as well as RNA-Seq analysis of the CCLE dataset of human melanoma cell lines, revealed that high and low levels of MITF in melanomas were significantly associated with the expression of two contrasting transcriptomic signatures of proton transporters that differed in terms of energy-coupling mechanisms. High MITF expression was associated with the expression of ATP hydrolysis-driven proton pumps, including F- and V-Type ATPases, at the expense of downregulating solute carrier proton transporters; whilst low MITF expression was significantly associated with the expression of secondary active solute carrier proton transporters, at the expense of downregulating proton pumps. This MITF-dependent regulation of proton transporters was verified *in vitro* using lentiviral MITF overexpression and knockdown in melanoma cells, coupled with analyses including

qRT-PCR, western blotting, and immunofluorescence. Taken together, this experimental chapter showed that functionally distinct proton transporter signatures were transcriptomically expressed in melanoma depending on MITF expression levels.

Attributions

This chapter is a slightly modified version of a manuscript in preparation.

All experiments and analyses were performed by Oscar Yang except as follows:

Experiments and analyses in **Figures 1** and **2** were performed by Jagat Chauhan.

INTRODUCTION

The functional presence of proton transporters in different melanoma cell lines demonstrated in the previous chapter showed that proton transport is ubiquitously carried out to regulate intracellular pH homeostasis in melanoma (Figures 3.6-3.18). In A375 cells, various proton coupled transport activities were detected, including that of proton transport coupled to sodium, monocarboxylates, bicarbonate, as well as primary active transport mediated by ATP hydrolysis (Figures 3.6-3.12). Functional proton extrusion in response to acid load was demonstrated across multiple melanoma cell lines, including MeWo, IGR39, IGR37, C32, and HS695T (Figures 3.13-3.18).

Given the wide variety of proton transporters with different mechanisms capable of handling intracellular pH homeostasis present in melanoma, an interesting question to address is whether the expression and function of these proton transporters could be transcriptionally regulated to resist acidotic stress, in a manner that reflects phenotypic plasticity in melanoma (Arozarena and Wellbrock, 2019). We tested a phenotypic switching model for proton transporters based on MITF expression level, since differential MITF expression is the key mechanism for facilitating lineage-restricted phenotypic switching in melanoma (Vivas-García et al., 2020, Bai et al., 2019).

MITF functions as the master melanocytic transcriptional regulator and a key

melanocytic lineage differentiation factor (Kawakami and Fisher, 2017). Oncogenic *MITF* amplification occurs in 30% of melanomas (Hartman and Czyz, 2015b), and as previously mentioned, germline $MITF^{E318K}$ mutations have also been detected in familial melanoma syndromes (Bertolotto et al., 2011). Melanomas with high MITF expression frequently display transcriptomic signatures associated with a proliferative phenotype, somewhat akin to clinical melanomas in radial growth phase (Konieczkowski et al., 2014). In contrast, reduced expression of MITF in melanoma cells is associated with transcriptomic profiles related to de-differentiation and epithelial-mesenchymal transition (Caramel et al., 2013), where the cells acquire an invasive phenotype concurrent with the upregulation of a variety of alternative transcription factors including TEADs, AP-1, as well RTKs including EGFR, AXL, and NGFR. (Kozar et al., 2019). Interestingly, both the MITF-High and the MITF-Low melanoma phenotypes have been shown to independently develop treatment resistance to small molecule BRAF and MEK targeted therapy, albeit via different mechanisms (Kozar et al., 2019). Therefore, if proton transporters were indeed transcriptionally regulated by MITF, it is possible that categorically different acidotic resistance phenotypes may also exist in melanoma, transcribed in manners reflective of the underlying MITF status.

This results chapter reports a phenotypic switching effect on the expression of

proton transporters modalities, dependent on the expression level of MITF in melanoma. Transcriptomic analysis, verified by lentiviral overexpression and knockdown cell modeling, quantitative reverse transcriptase polymerase chain reaction, western blotting, and immunofluorescence, demonstrated that the presence of MITF expression reprogrammed the global proton transporter expression profile, in favour of proton transport activity coupled to ATP-hydrolysis, exemplified by the upregulation of V- and F-Type ATPase transcripts following MITF overexpression. In contrast, MITF expression in melanoma cells repressed the expression of secondary active MCT and NHE transporters, reliant on ambient solutes for proton transport coupling. This proton transporter phenotype was reversed when MITF was knocked down using lentiviral shRNA vectors, a result supported by transcriptomic analysis of human melanoma samples and cell lines. This chapter thus demonstrated that as it pertains to the expression of proton transporters, MITF is in control of the lineage-restricted "transportomic" phenotypic plasticity in melanoma.

RESULTS

MITF Expression Reconfigures the Expression Profile of Proton Transporters in Melanoma

To demonstrate whether there was an association between MITF expression level and the transcriptomic profile of human proton transporters, Spearman correlations between the mRNA expression-levels of 102 known human proton transporter gene loci, and pertinent melanoma transcriptional cell-states dependent on MITF expression, were calculated *in silico* in the 471 human melanoma samples downloaded from the Skin Cutaneous Melanoma (SKCM) dataset from The Cancer Genome Atlas (TCGA) (Akbani et al., 2015) (Figure 4.1). Melanomas from the SKCM dataset was subtyped into four MITF-dependent transcriptional cell-states: Proliferative, MITF-High, Invasive, and Anexelekto Kinase (AXL)-High (Verfaillie et al., 2015, Boshuizen et al., 2018). AXL expression in melanoma correlates with invasive drug-resistant melanomas (Hugo et al., 2016) that show reciprocally low MITF expression (Konieczkowski et al., 2014, Müller et al., 2014, Tirosh et al., 2016), and high expression of the epithelial-mesenchymal transition-inducing transcription factors (EMT-TFs) (Caramel et al., 2013, Denecker et al., 2014). On the other hand, MITF-High and Proliferative transcriptional cell-states both express high levels of MITF (Hoek et al., 2008a).

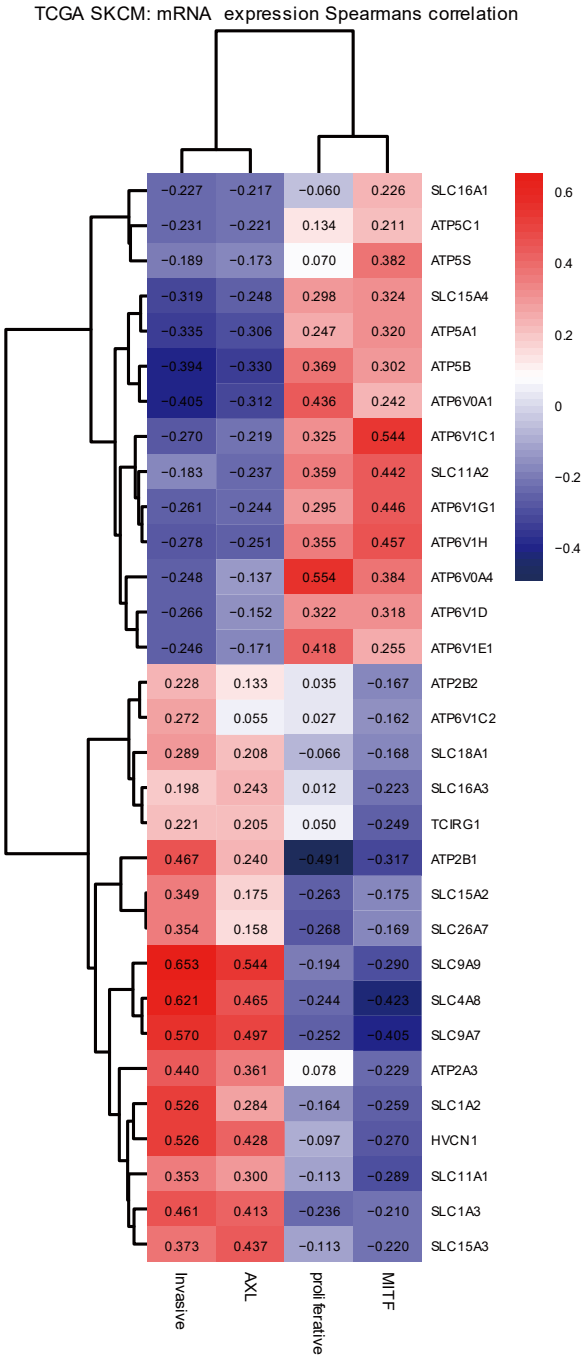

Figure 4.1: Spearman's correlation heat map of Proton Transporter Expression from the TCGA SKCM RNA-Seq dataset. The strength of correlation between the expression of the core subset of proton transporters and key MITF-dependent melanoma gene signatures is shown. Proton Transporters are listed in rows. Proliferative, MITF-High, Invasive, and AXL-High gene signatures are labelled at the bottom of the columns. Scale bar: Positive correlation coloured red; Negative correlation coloured blue, as shown in the side scale.

The Proliferative and Invasive transcriptomic clusters were identified based on the work by Verfaillie and colleagues, who showed that three robust stable transcriptomic clusters could be derived from the TCGA dataset, namely “Proliferative”, “Invasive”, and “Immune” transcriptomic clusters (Verfaillie et al., 2015). The immune cluster consisted of 116 samples, and was presumably present due to the presence of a high number of tumour-infiltrating lymphocytes (Verfaillie et al., 2015). The immune cluster was thus not included in the analysis. MITF and AXL transcriptomic clusters were another system of classifying the TCGA melanoma samples, based on the mRNA expression levels of the genes MITF and AXL (Konieczkowski et al., 2014). A portion of the tumours were excluded from analysis using the MITF and AXL classification, as MITF and AXL were either both expressed, or both not expressed in these samples – which was a known phenomenon described by Ennen and colleagues (Ennen et al., 2017).

Spearman’s correlations between the expression of individual proton transporters, and the expression of MITF were calculated, and the proton transporters with expression significantly correlated MITF expression were identified. A heat map of the expression levels of these proton transporters were then generated against the prominent transcriptomic states that were described in the literature, including the AXL, MITF, Proliferative, and Invasive states. As figure 4.1 showed, the expression of proton

transporters closely approximately for the MITF-High and proliferative melanoma cell-states (Carreira et al., 2006), whilst the expression of proton transporters also approximated for the invasive and AXL-High melanoma cell-states (Boshuizen et al., 2018). There was a clear distinction, with the mRNA expression of these of proton transporters either positively or negatively correlated with MITF-High and proliferative melanomas with statistical significance (Figure 1a). Interestingly, these same transporter genes showed a reverse correlation pattern when paired with AXL-High and invasive melanoma cell-states (Figure 4.1). Strikingly, 11/14 (78.6%) of the proton transporter genes showing statistically significant positive correlation with High-MITF expression were ATP-driven (Figure 1), whereas 12/17 (70.6%) of the proton transporter genes showing statistically significantly negative correlation with High-MITF expression were non-ATP-powered (Figure 1). In particular, the mRNA expression of multiple subunits of V-Type and F-Type ATPases, including *ATP6V0a1*, *ATP6V1C1*, *ATP6V1D*, and *ATP6V1H*; *ATP5A1*, *ATP5B*, and *ATP5C1*, were positively correlated with High-MITF expression. On the other hand, the expression of solute carrier proton transporters, including *SLC9A7*, *SLC9A9, SLC11A1, SLC15A2, and SLC16A3,* were negatively correlated with High-MITF expression (Figure 4.1). The relative expression of MITF and the proton transporters were also analysed in 62 melanoma cell lines from the Cancer Cell Line Encyclopaedia (CCLE) (Barretina et al.,

2012) database (Figure 4.2). Again, the CCLE dataset showed that melanoma cell lines with high MITF expression demonstrated high expression of V-type ATPase subunits such as *ATP6V1A*, *ATP6V1C*, and *ATP6V1H*, and low expression of MCT and NHE transporter isoforms including *SLC16A3*, *SLC9A7*, and *SLC9A9* (Figure 4.2).

This phenotypic class-switching effect on the expression of proton transporter modalities depending on MITF expression level in melanoma cells was verified experimentally *in vitro*. First, MITF-M was transiently overexpressed in the A375 and IGR39 melanoma cell lines (Martin et al., 1989, Vachtenheim et al., 2001) known to express low endogenous MITF (Kido et al., 2009, Konieczkowski et al., 2014), and exhibit functional presence of V-Type ATPase and other proton transporters (Pan et al., 2017, Yang and Loh, 2019) (Figure 4.3). MITF-M was overexpressed in A375 and IGR39 using an in-house lentiviral *MITF-M* expression construct, pLAS2w-MITFM-Ppuro (herein denoted "MITF"). Using qRT-PCR, the mRNA expression of proton transporters relative to β-actin were then compared with the negative control – the same melanoma cells transduced with the empty pLAS2w-Ppuro vector without the coding sequence of M-MITF subcloned into the construct (denoted "EV") (Figure 4.3a).

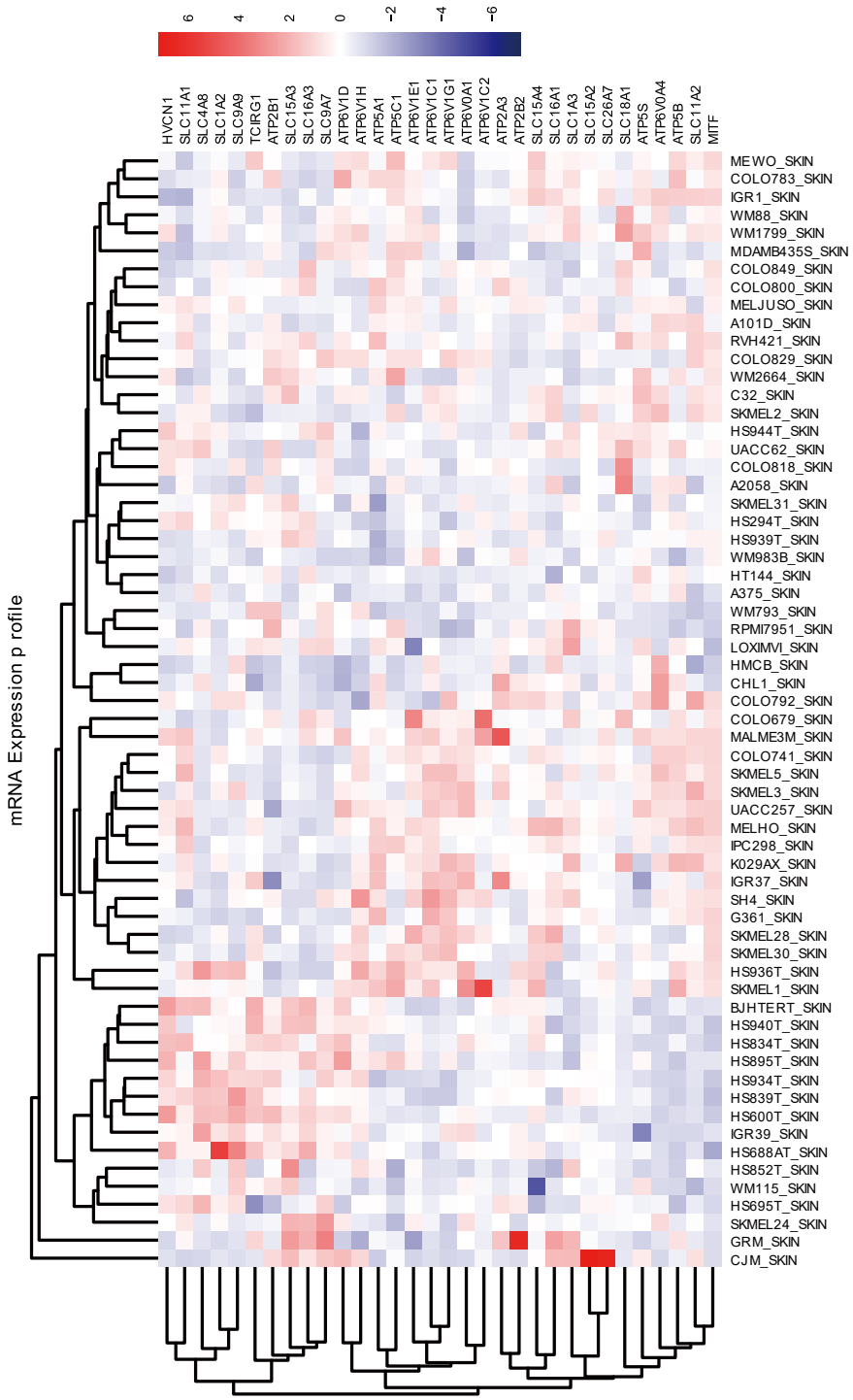

Figure 4.2: Proton transporters expression heat map of Proton Transporters Expression from the CCLE melanoma cell lines. The mRNA expression patterns of the core subset of proton transporters is shown for CCLE cell lines. Cell lines are listed in rows; Proton Transporters are listed in columns. MITF mRNA expression is shown in the first right column for comparison. Scale bar: Strong expression coloured red; weak expression coloured blue, as shown in the side scale.

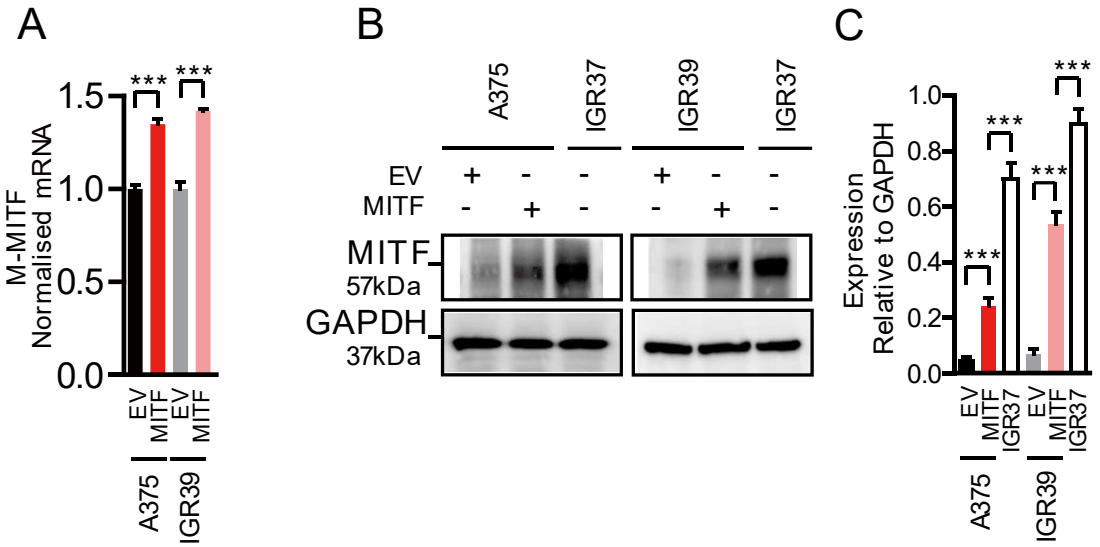

Figure 4.3: Experimental Validation of the *MITF-M* Overexpression Cell Line Models. (a) qRT-PCR analysis of *MITF-M* expression in A375 and IGR39 melanoma cells, transduced with either the lentiviral empty vector (EV) or the lentiviral *MITF-M* expression construct (*MITF*), as indicated. The relative expression levels of the *MITF-M* gene were determined by $2^{-\Delta\Delta Ct}$. Error bars represent standard deviation of at least 3 independent experimental replicates. (b) Western Blots, and (c) Densitometric analysis of MITF protein expression relative to GAPDH in A375 and IGR39 transduced with either the EV or MITF vector, as indicated. IGR37 was included as a positive control for endogenous MITF expression. Densitometry was calculated using the ImageJ software. For densitometric analysis in (c), n = 3 experiments, and data are presented as mean ± standard error of mean. *P < 0.05, **P < 0.01, ***P < 0.001. Statistical significance was calculated using unpaired *t*-test. *MITF-M: Microphthalmia-Associated Transcription Factor, M-Isoform.* GAPDH: Glyceraldehyde 3-phosphate dehydrogenase.

Accordingly, increased *M-MITF* transcript expression was demonstrated following lentiviral transfection of the MITF construct as opposed to the EV construct (Figure 4.3a). Next, increased MITF protein expression was also demonstrated via western blotting following the transduction of the MITF construct versus the EV construct in both A375 and IGR39 (Figure 4.3b). A positive control of endogenous MITF protein expression in the IGR37 cell line (Falletta et al., 2017) was included in the western blotting experiment to show that the experimental overexpression of the MITF end-product in either A375 or IGR39 did not exceed that of endogenous MITF expression in melanoma cells (Figure 4.3b-c).

Next, the mRNA transcript expressions of different proton transporters in EV and MITF-overexpressed A375 and IGR39 cells were verified using qRT-PCR (Figure 4.4). The proton transporters selected to be analysed via qRT-PCR were chosen based on the list of transporters that were identified to be genes identified to be differentially expressed in the TCGA data analysis in Figures 4.1 and 4.2, via high-throughput RNA-sequencing, as per figures 4.1 and 4.2. As can be shown in figure 4.4, overexpression of M-MITF in both A375 and IGR39 led to an increase in expression of proton pump subunits driven by ATP hydrolysis, particularly that of F- and V-Type ATPases. Namely, *ATP5A1*, *ATP5B, ATP5C1, ATP5S, ATP6Voa1, ATP6V1A, ATP6V1C*, and *ATP6V1D*

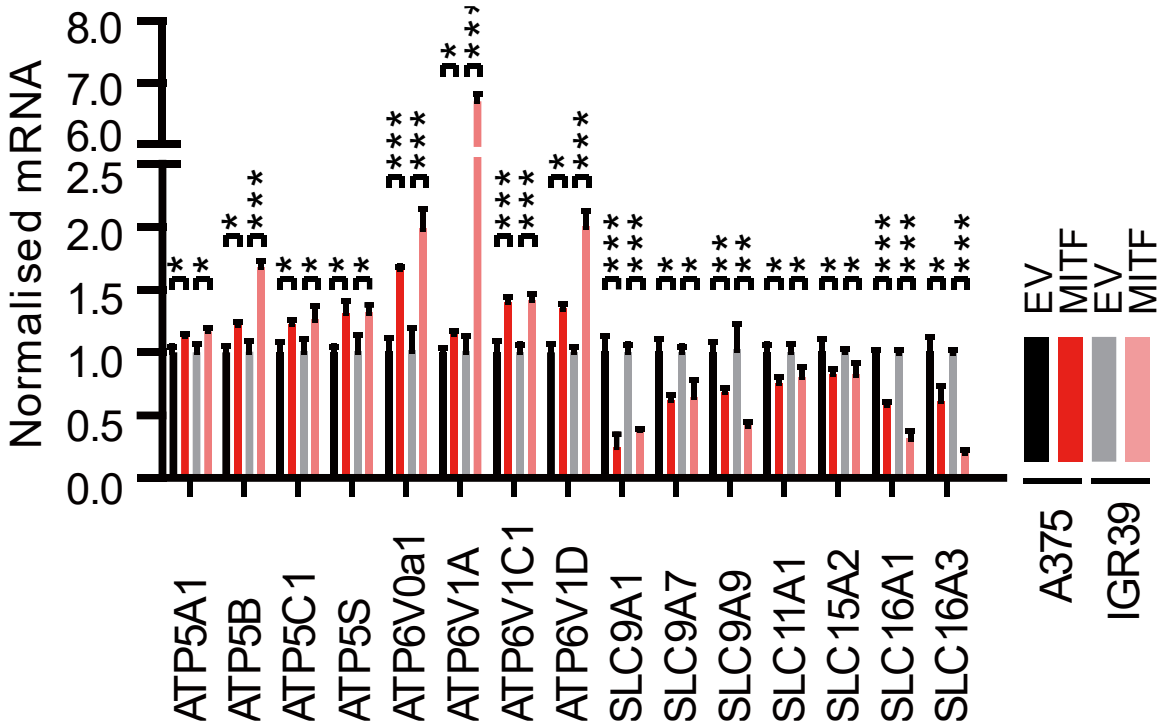

Figure 4.4: qRT-PCR Validation of the Effect of *MITF* Overexpression on Proton Transporters mRNA Abundance. qRT-PCR Expression of proton transporter genes in A375 and IGR39 melanoma cells, transduced with either the empty vector (EV) or the lentiviral *MITF-M* expression construct (*MITF*), as indicated. The relative expression levels of each selected gene were determined by $2^{-\Delta\Delta Ct}$. *P < 0.05, **P < 0.01, ***P < 0.001. *ATP: Adenosine Triphosphatase*; *SLC: Solute Carrier*; *MITF-M: Microphthalmia-Associated Transcription Factor, M-Isoform.* Error bars represent standard deviation of at least 3 independent experimental replicates.

were all upregulated relative to EV following ectopic MITF expression in A375 and IGR39 (Figure 4.4). In contrast, following MITF transduction, solute carrier proton transporters were mostly downregulated relative to EV, as was the case with *SLC9A1, SLC9A7, SLC9A9, SLC11A1, SLC15A2, SLC16A1, and SLC16A3* (Figure 4.4). Therefore, there appeared to be an expressive shift from solute carrier proton transporters to proton pumps as MITF expression was increased via ectopic lentiviral transduction in both A375 and IGR39.

As further proof of principle, the protein expression of selected proton transporters in EV and MITF-overexpressed A375 and IGR39 cells were immunoblotted (Figure 4.5). Western analysis showed that the expression of multiple solute carrier proton transporters was reduced following the overexpression of MITF-M in A375 and IGR39 (Figure 4.5a-c), including that of SLC9A1, SLC16A1, and SLC16A3, consistent with the RNA-seq data (Figure 4.1). In contrast, the expression of the primary active proton pump subunit ATP6V1D was significantly upregulated following MITF-M overexpression. The results from western blotting were consistent with both RNA-Seq and qRT-PCR.

In addition, to validate the target specificity of the antibodies used in the western blots, and to further visualise the effect of MITF overexpression on the expression of these proton transporters at the subcellular level, immunofluorescence was also

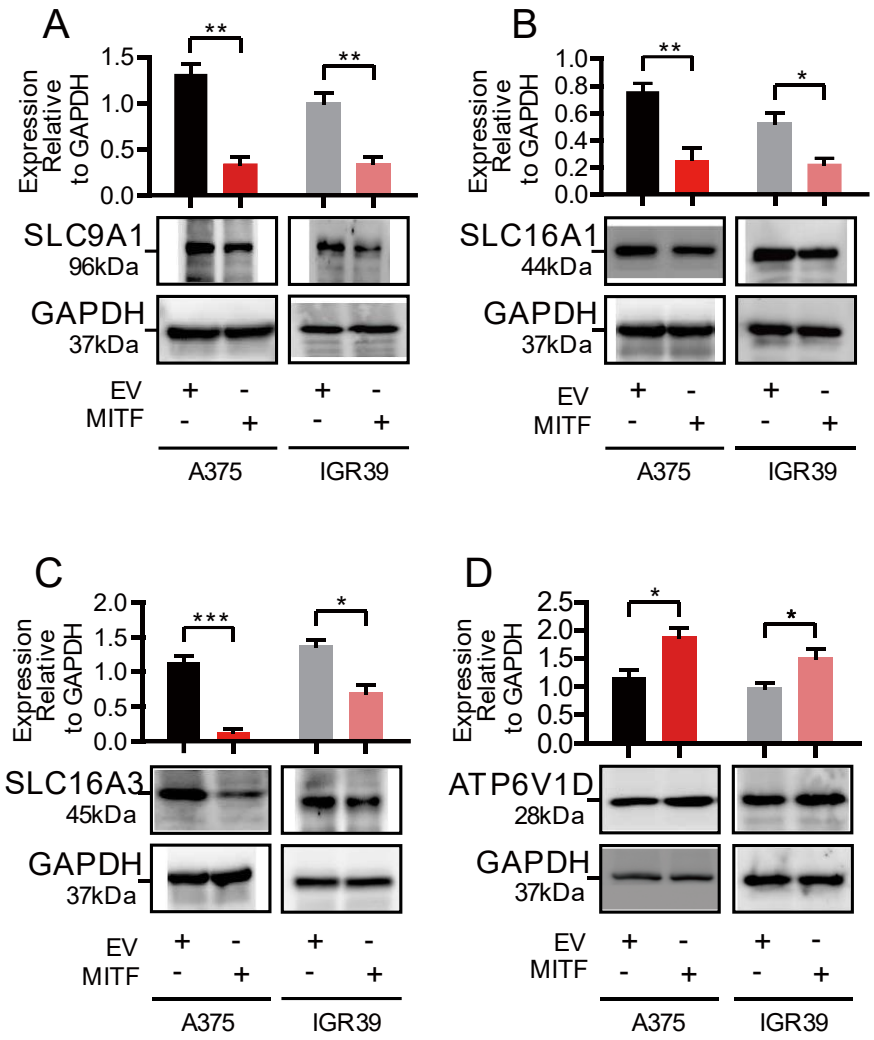

Figure 4.5: Ectopic *MITF-M* Expression in Melanoma Cells Alters Proton Transporter Protein Expression. (a-d) Western blots and densitometric analyses of whole cell lysates of A375 and IGR39, transduced with either empty vector (EV) or the *MITF-M* lentiviral expression vector (MITF), as indicated. Protein expression levels of (a) SLC9A1, (b) SLC16A1, (c) SLC16A3, and (d) ATP6V1D are shown. Secondary antibodies: HRP conjugated. Loading control: GAPDH. For densitometric analyses of protein expression levels of the proton transporters relative to GAPDH, n = 3 experiments, and data are presented as mean ± standard error of mean. Densitometry was calculated using the ImageJ software. *P < 0.05, **P < 0.01, ***P < 0.001. Statistical significance was calculated using unpaired *t*-test. SLC: Solute Carrier; ATP6V1D: Adenosine Triphosphatase 6, Subunit V1D. *MITF-M: Microphthalmia-Associated Transcription Factor, M-Isoform*. GAPDH: Glyceraldehyde 3-phosphate dehydrogenase.

performed for the A375 cell line transduced with the MITF lentiviral expression construct. As can be seen in figure 4.6, the subcellular distribution of these proton transporters (SLC9A1, 16A1, and 16A3), as indicated by alexa-488 fluorescence, was either cytoplasmic or plasmalemmal, with distinct nuclear sparing, consistent with the subcellular expression pattern typically expected of solute carriers. Furthermore, comparison between MITF-transduced and MITF-nontransduced A375 cells adjacent to each other, within the same field of view under fluorescent microscopy (as indicated by nuclear fluorescence of alexa-594) showed that the fluorescent intensity of SLC9A1, SLC16A1, and SLC16A3 was significantly less in the MITF-transduced cells than the MITF-nontransduced cells (Figure 4.6). Taken together, in the case of MITF overexpression models using A375 and IGR39, expression changes in the proton transporters both at transcript and end-product levels support the notion of MITF-dependent transcriptomic reprogramming, which was demonstrated via high-throughput RNA-Sequencing in the TCGA and CCLE datasets, and via qRT-PCR.

The effects of reducing MITF expression in melanoma cells was also verified experimentally by MITF knockdown in the IGR37 – the allogenic cell line counterpart to IGR39, which is known to express endogenous MITF (Figure 4.7). MITF-M was knocked down in IGR37 using a series of pLKO lentiviral anti-MITF shRNA

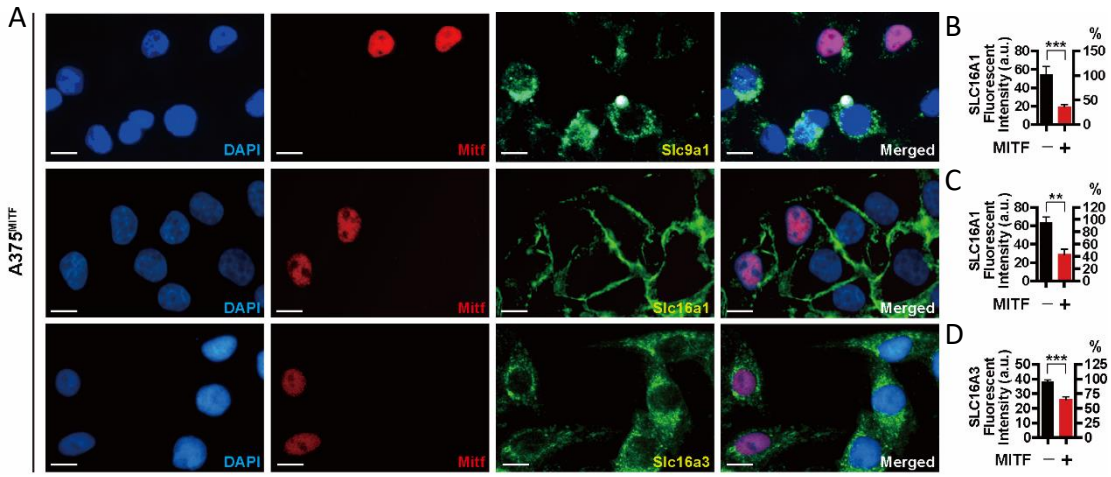

Figure 4.6: *MITF-M* Expression Alters Subcellular Abundance of Proton Transporters. (a) Immunofluorescence of proton transporters SLC9A1, SLC16A1, and SLC16A3 (green), MITF (red), and DAPI (blue) in A375 cells transduced and untransduced with the ectopic *MITF-M* vector, showing contrasting enrichment of the proton transport signals in the plasma membrane and cytoplasm, and enrichment of the MITF signal in the nuclei. On the right, graphical representations of fluorescent intensities and percentage changes in the expressions of (b) SLC9A1, (c) SLC16A1, and (d) SLC16A3 in A375 cells transduced and untransduced with *MITF-M* are shown (n = 3 experiments; 30-40 cells per condition per experiment). The SLC16A3 antibody has been validated using immunofluorescence, immunohistochemistry, flow cytometry, and western blotting (https://www.ptglab.com/products/SLC16A3-Antibody-22787-1-AP.htm#related-products). Fluorescent intensity was calculated using the ImageJ software. For graphical representations, data are presented as mean ± standard deviation. *P < 0.05, **P < 0.01, ***P < 0.001. Statistical significance was calculated using unpaired *t*-test. SLC: Solute Carrier; *MITF-M: Microphthalmia-Associated Transcription Factor, M-Isoform*; DAPI: 4',6-diamidino-2-phenylindole. Scale bar = 40µm

expression constructs described by Choi and Colleagues (Choi et al., 2017)– the constructs are herein denoted "shMITF" – and the most efficient lentiviral knockdown strains were used for downstream experiments. Using qRT-PCR, the mRNA expression of proton transporters relative to β-actin were then compared with the negative control – the same melanoma cells transduced with the pLKO vector containing shRNA targeted to the *LacZ* gene (the construct is herein denoted "shLacZ"), which is only present in prokaryotes. Accordingly, decreased *M-MITF* transcript expression was demonstrated following lentiviral knockdown of MITF using either of the two most knockdown-efficient lentiviral strains, shMITF#1 or shMITF#2, compared to shLacZ in IGR37 (Figure 4.7a). Decreased MITF protein expression was also demonstrated via western blotting by knocking down MITF with either shMITF#1 or shMITF#2, compared to shLacZ in IGR37 (Figure 4.7b-c).

Having established adequate MITF knockdown efficiency with the lentiviral vectors in IGR37, the expression of mRNA transcripts of different proton transporters was compared in MITF-knockdown and LacZ-knockdown IGR37 cells, via qRTPCR (Figure 4.8). The proton transporters analysed via qRT-PCR were chosen based on the list of transporters that were identified to be different depending on MITF expression as shown using high-throughput RNA-sequencing, as per figures 4.1 and 4.2. As can be seen in figure 4.8, knockdown of MITF in IGR37 using either shMITF#1 or shMITF#2

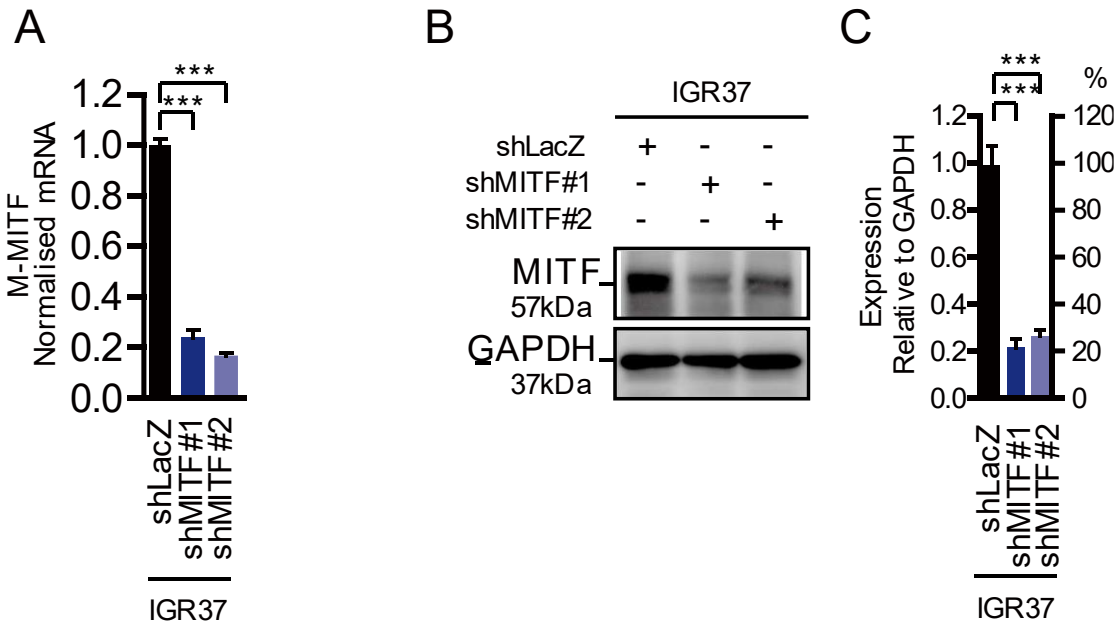

Figure 4.7: Experimental Validation of the *MITF-M* Knockdown Cell Line Models. (a) qRT-PCR analysis of *MITF-M* expression in IGR37 melanoma cells, transduced with either the lentiviral negative control, shLac, or the lentiviral *MITF-M* knockdown constructs, shMITF#1 and #2, as indicated. The relative expression levels of the *MITF-M* gene were determined by $2^{-\Delta\Delta Ct}$. Error bars represent standard deviation of at least 3 independent experimental replicates. (b) Western Blots, and (c) Densitometric analysis of MITF protein expression relative to GAPDH in A375 and IGR39 transduced with either the shLac or the shMITF vectors, as indicated. Densitometry was calculated using the ImageJ software. For densitometric analysis in (c), n = 3 experiments, and data are presented as mean ± standard error of mean. *P < 0.05, **P < 0.01, ***P < 0.001. Statistical significance was calculated using unpaired *t*-test. *MITF-M: Microphthalmia-Associated Transcription Factor, M-Isoform.* shLac: Short hairpin RNA targeted to *β-galactosidase*. shMITF: Short hairpin RNA targeted to *MITF-M*. GAPDH: Glyceraldehyde 3-phosphate dehydrogenase.

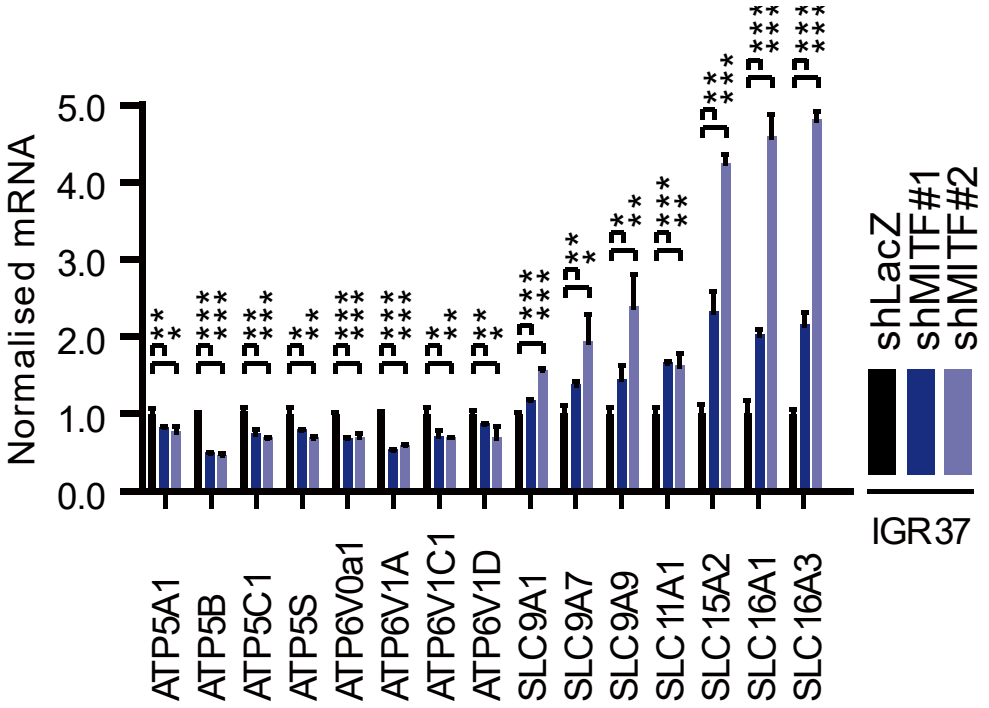

Figure 4.8: qRT-PCR Validation of the Effect of *MITF* Knockdown on Proton Transporter mRNA Abundance. qRT-PCR Expression of proton transporter genes in IGR37 melanoma cells, transduced with either the lentiviral negative control, shLac, or the lentiviral *MITF-M* knockdown constructs, shMITF#1 and #2, as indicated. The relative expression levels of each selected gene were determined by $2^{-\Delta\Delta Ct}$. *P < 0.05, **P < 0.01, ***P < 0.001. *ATP: Adenosine Triphosphatase*; *SLC: Solute Carrier*; *MITF-M: Microphthalmia-Associated Transcription Factor, M-Isoform.* shLac: Short hairpin RNA targeted to *β-galactosidase*. shMITF: Short hairpin RNA targeted to *MITF-M*. Error bars represent standard deviation of at least 3 independent experimental replicates.

led to a decrease in expression of proton pump subunits driven by ATP hydrolysis, particularly that of F- and V-Type ATPases – which was the opposite of what was observed upon MITF overexpression in A375 and IGR39 (Figure 4.4). Namely, *ATP5A1*, *ATP5B, ATP5C1, ATP5S, ATP6Voa1, ATP6V1A, ATP6V1C*, and *ATP6V1D* were all downregulated relative to shLacZ following MITF knockdown in IGR37 (Figure 4.8). In contrast, following MITF knockdown by either shMITF#1 or shMITF#2, solute carrier proton transporters were upregulated relative to shLacZ, which was the case for *SLC9A1, SLC9A7, SLC9A9, SLC11A1, SLC15A2, SLC16A1, and SLC16A3* (Figure 4.8). Therefore, there appeared to be a shift in expression from proton pumps to solute carrier proton transporters at the mRNA level, as MITF expression became downregulated via lentiviral knockdown in IGR37.

Next, the expressions of proton transporter proteins in IGR37 cells upon knockdown of either shMITF or shLacZ were compared using immunoblotting (Figure 4.9). Compared to the shLacZ negative control, multiple solute carrier proton transporters were significantly upregulated at the protein level following the knockdown of MITF-M with either shMITF#1 or shMITF#2 in IGR37 (Figure 4.9), including that of SLC9A1, SLC16A1, and SLC16A3, consistent with the RNA-seq data (Figure 4.1). In contrast, the expression of the primary active proton pump subunit ATP6V1D was significantly downregulated following MITF-M knockdown using

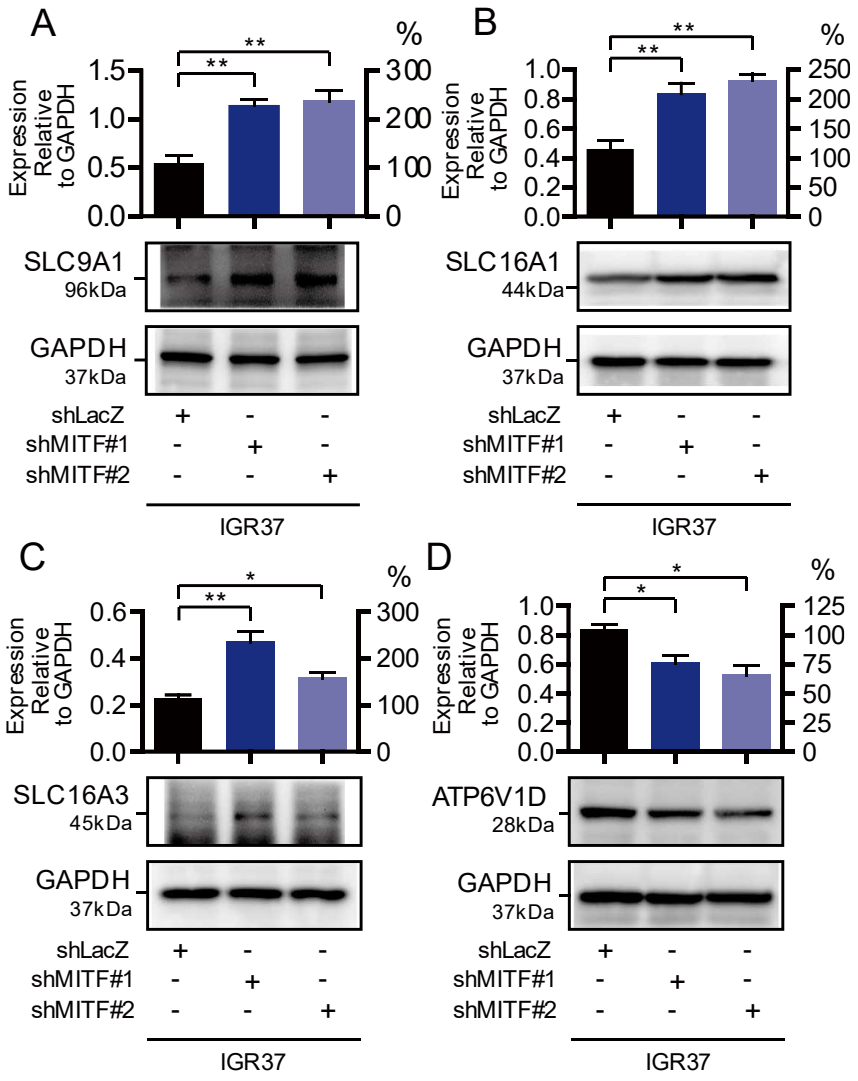

Figure 4.9: *MITF-M* Knockdown in Melanoma Cells Alters Proton Transporter Protein Expression. (a-d) Western blots and densitometric analyses of whole cell lysates of IGR37, transduced with either the lentiviral negative control, shLac, or the lentiviral *MITF-M* knockdown constructs, shMITF#1 and #2, as indicated. Protein expression levels of (a) SLC9A1, (b) SLC16A1, (c) SLC16A3, and (d) ATP6V1D are shown. Secondary antibodies: HRP conjugated. Loading control: GAPDH. For densitometric analyses of protein expression of the proton transporters relative to GAPDH, n = 3 experiments, and data are presented as mean ± standard error of mean. Densitometry was calculated using the ImageJ software. *P < 0.05, **P < 0.01, ***P < 0.001. Statistical significance was calculated using unpaired *t*-test. SLC: Solute Carrier; ATP6V1D: Adenosine Triphosphatase 6, Subunit V1D. *MITF-M: Microphthalmia-Associated Transcription Factor, M-Isoform*. shLac: Short hairpin RNA targeted to *β-galactosidase*. shMITF: Short hairpin RNA targeted to *MITF-M*. GAPDH: Glyceraldehyde 3-phosphate dehydrogenase.

either shMITF#1 or shMITF#2 (Figure 4.9). The results from western blotting were consistent with both RNA-Seq and qRT-PCR.

To validate the target specificity of the antibodies used in the western blots, and to further visualise the effect of MITF knockdown on the expression of proton pumps at the subcellular level, immunofluorescence was also performed for the IGR37 knocked down with either shMITF#1 or shMITF#2. As can be seen in figure 4.10, the subcellular distribution of the V-Type ATPase subunit ATP6V1D was cytoplasmic, as indicated by alexa-488 fluorescence, consistent with the subcellular expression pattern typically expected of proton pumps. Furthermore, comparison between IGR37 cells that achieved efficient MITF-knockdown and adjacent cells with minimal MITF-knockdown, within the same field of view under fluorescent microscopy (as indicated by nuclear fluorescence of alexa-594) showed that the fluorescent intensity of ATP6V1D was significantly less in the MITF-knockdown cells than the cells without MITF-knockdown (Figure 4.10). Taken together, in the case of MITF knockdown models using shMITF#1 and shMITF#2 in IGR37, expressional changes in the proton transporters at both the levels of transcript and protein support findings of MITF-dependent transcriptomic reprogramming, which was demonstrated via high-throughput RNA-Sequencing in the TGCA and CCLE datasets, and via qRT-PCR.

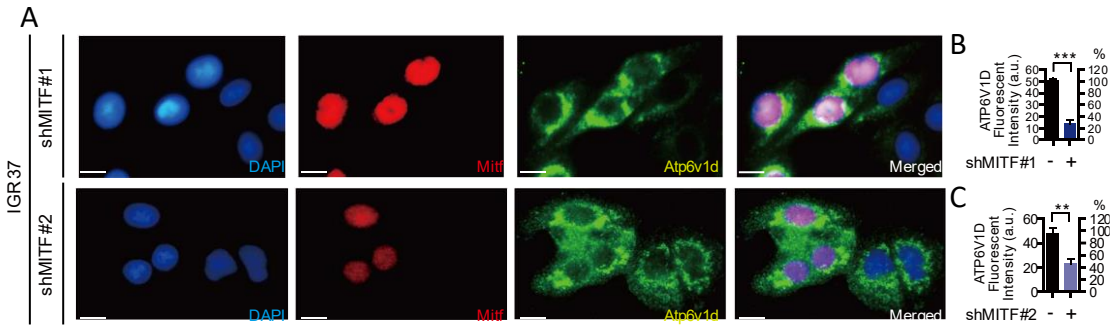

Figure 4.10: *MITF-M* Knockdown Alters Subcellular Abundance of Proton Transporters. (a) Immunofluorescence of the proton pump subunit, ATP6V1D (green), MITF (red), and DAPI (blue) in IGR37 cells transduced and untransduced with the lentiviral *MITF-M* knockdown vectors, shMITF#1 and #2, showing contrasting enrichment of the ATP6V1D signal in the cytoplasm, and enrichment of the MITF signal in the nuclei. On the right, graphical representation of fluorescent intensities and percentage changes in the expression of ATP6V1D in IGR37 cells transduced and untransduced with the shMITF vectors shMITF#1 (b) and shMITF#2 (c) are shown (n = 3 experiments; 30-40 cells per condition per experiment). Fluorescent intensity was calculated using the ImageJ software. For graphical representations, data are presented as mean ± standard deviation. *P < 0.05, **P < 0.01, ***P < 0.001. Statistical significance was calculated using unpaired *t*-test. ATP: Adenosine Triphosphatase; *MITF-M: Microphthalmia-Associated Transcription Factor, M-Isoform*; shLac: Short hairpin RNA targeted to *β-galactosidase*. shMITF: Short hairpin RNA targeted to *MITF-M*.DAPI: 4',6-diamidino-2-phenylindole. Scale bar = 40μm

DISCUSSION

This chapter showed that phenotypic plasticity as mediated by MITF in melanoma extended to the realm of proton transport. Contrasting proton transporter gene signatures were identified in MITF-High and MITF-Low melanomas, where MITF-High melanomas and cell lines were correlated predominantly with the expression of genes encoding ATP hydrolysis-dependent proton pumps, whilst MITF-Low melanomas and cell lines were associated with the expression of genes encoding solute carrier proton transporters (Figures 4.1-4.2). The direct correlation of MITF with the different proton pumps can also be investigated in TCGA. These findings were verified experimentally at the transcript and protein expression levels using qRT-PCR, western blotting, and immunofluorescence (Figure 4.3-4.10). Interesting questions that arise from this work are whether transcriptional regulation is the only/best way to regulate the expression of these genes, and whether the activities of proton transporters can also be regulated. The next chapter goes on to address the changes in proton transporter activities in these different MITF-dependent phenotypic states.

The phenotypic dichotomy in proton transporters gene signatures regulated by MITF expression likely reflects an underlying schism in the fundamental metabolic nature of the melanoma cell, since the deployment of proton pumps in MITF-High

melanomas would require endogenously synthesised ATP (Beyenbach and Wieczorek, 2006), whereas utilisation of secondary active proton transporters in MITF-Low melanomas relies on the presence of transmembrane electrochemical gradients of solutes, a regulatory feature that depends at least in part on the solute composition of the stromal microenvironment (Morotti et al., 2019). MITF has been shown to regulate mitochondrial biogenesis in melanoma via the transactivation of the transcriptional co-activator, PGC1α (Vazquez et al., 2013), and therefore high levels of oxidative phosphorylation and ATP availability characterise melanoma cells in which MITF is expressed (Parmenter et al., 2014). This chapter suggests that in these MITF-High cells, there is a corresponding increase in the recruitment of proton pumps that directly utilise ATP-hydrolysis as the means of energy expenditure to move protons against the electrochemical gradient (Figures 4.1-4.2). When MITF is knocked down or poorly expressed, recruitment of solute carrier proton transporters and downregulation of proton pumps shown in this chapter (Figures 4.7-4.10) likely reflects a diminishing supply of mitochondrial ATP via oxidative phosphorylation (Vazquez et al., 2013), precipitating a genomic shift towards secondary active transport, which is reliant on microenvironmental solute movement. This phenotypic plasticity in proton transport mechanisms may represent cellular contingencies to support the upkeep of intracellular pH homeostasis over a wide range of ATP availability, in concert with MITF's

regulatory adjustment of mitochondrial biogenesis and oxidative phosphorylation (Haq et al., 2013).

Recent comparative genomics studies in melanoma provided evidence to support proton transport as a transcriptomically regulated phenotype in melanoma (Mazzio and Soliman, 2018, Siena et al., 2019). A recent study on *ZEB1-Antisense RNA 1*-enriched melanomas used gene ontology and reactome enrichment analysis of the TCGA dataset to show that the biological processes most negatively correlated with ZEB1-AS1 expression in melanoma were ion transport, pH reduction, and ATP hydrolysis-coupled proton transport (Siena et al., 2019). Since ZEB1-AS1 is the transcriptional repressor of MITF in melanoma (Caramel et al., 2013), such findings support the analyses generated in this results chapter. Another basic array analysis of the lymph node metastasis SK-MEL-3 melanoma cells, also demonstrated that its gene signature showed an inherent dominance of altered gene expression in relation to intracellular pH reduction, regulation of intracellular pH, and ATP-coupled proton transport (Mazzio and Soliman, 2018). These studies agreed with the results from this chapter, pointing to the importance of controlling the proton transporters transcriptome as an important aspect of melanoma dysplasia.

It had been previously shown that MITF functions as the master regulator of the V-Type ATPase in *Drosophila* and human melanoma (Zhang et al., 2015), and the

results from this chapter showed that the influence of MITF on proton transport is far-reaching, extending to the regulation of solute carrier proton transporters as well. The incorporation of both solute carriers and proton pumps into contrasting gene signatures may enable the melanoma cell to dynamically adjust the amount of ATP production and energy required to maintain pH_i homeostasis, depending on the cellular environment. The deployment of proton-coupled solute transport likely also carries cellular nutritional value in addition to facilitating proton transport *per se*, since a large number of solutes, such as monocarboxylates and dipeptides, may also double as metabolic fuel as they enter the cellular metabolic system (Wu, 2009).

That the shift in energy coupling for proton transport exists at the transcriptomic level, regulated by the oncogenic transcription factor MITF in melanoma suggests that this genomic phenomenon likely has basic and clinical translational implications, which warrants further studies. Taken together, the results presented in this chapter uncovered novel MITF-dependent proton transport phenotypes in melanoma involving the mechanisms of energy coupling for proton transportation.

CHAPTER 5

Regulation of Proton Transporters Function by MITF in Melanoma

Abstract

The previous chapter showed that in melanoma, the expression of proton transporters is regulated by MITF. Whether such MITF-dependent transcriptomic organisation of proton transporters had any functional consequences on cell biology is unknown. This chapter showed that MITF knockdown increased the rate of MCT1-mediated proton-coupled monocarboxylate import in IGR37 cells, including that of pyruvate, lactate, and β-Hydroxybutyrate transportation. MCT1 transport activity was crucial for the acidotic survival of MITF-knockdown melanoma cells, as caspase 3/7 activation in MITF-knockdown cells could be selectively induced either by removal of ambient pyruvate, or by treatment with the small molecule MCT1 inhibitor, AR-C155858. Furthermore, AR-C155858 treatment combined with the $BRAF^{V600E}$ inhibitor, vemurafenib, to specifically potentiate cytotoxic killing in acidotic MITF-knockdown cells. Therefore, exploiting the phenotypic plasticity of proton transporters in melanoma, our study identified a novel approach to enhance cytotoxicity in the subset melanoma cells expressing low levels of MITF, via targeting their dependency

on monocarboxylate transport for acidotic survival.

Attributions

This chapter is a slightly modified version of a manuscript in preparation.

All experiments and analyses were performed by Oscar Yang.

INTRODUCTION

Melanoma cells dispose of metabolic acids generated from Warburg metabolism and pentose-phosphate-pathway shunting by exercising an elaborate system of transmembrane proton transporters (Bohme and Bosserhoff, 2016). In order to maintain intracellular pH (pH_i) homeostasis, these endergonic proton transporters extrude stoichiometric amounts of lactate and hydrogen ions from the cytosol into the extracellular space, or alternatively into the subcellular acidic compartments (Corbet and Feron, 2017). Three main types of proteins mediate proton transport in cells, and they are broadly categorised as proton channels, carriers, pumps (Maathuis, 2017). In total, more than one-hundred types of proton transporter genes and their gene products exist in melanoma cells (Alaxender et al., 2017). Well-known examples include the Vacuolar- and Factor-type adenosine triphosphatases (V- and F-Type ATPases, respectively) (Mulkidjanian et al., 2007); and isoforms of the sodium hydrogen exchanger (NHE) (Stock and Pedersen, 2017); the monocarboxylate transporter (MCT) (Pinheiro et al., 2016); the anion exchanger (AE) (Bohme and Bosserhoff, 2016); and the sodium bicarbonate co-transporter (NBC) (Hao et al., 2018).

Recent studies have increasingly demonstrated that deranged pH_i regulation comprises an important but underexplored aspect of melanocytic dysplasia (Siena et al.,

2019). Proton transport and intracellular pH regulation represent a sizable portion of genes whose expression is increased manifold in different melanoma cell lines (Mazzio and Soliman, 2018, Siena et al., 2019). However, characteristic proton transporter gene signatures in melanoma remain to be molecularly defined. In addition, it is currently unknown whether such proton transporter signatures may participate in MITF-dependent phenotypic switching (Arozarena and Wellbrock, 2019, Vivas-García et al., 2020).

In the previous chapter, high and low MITF expression levels in melanoma were shown to be significantly associated with the expression of two contrasting transcriptomic sets of proton transporters that differed in terms of energy-coupling mechanisms. High MITF expression was associated with the expression of ATP hydrolysis-driven proton pumps, including F- and V-Type ATPases, at the expense of downregulating solute carriers proton transporters; whilst low MITF expression was significantly associated with the expression of secondary active solute carrier proton transporters, at the expense of expressing proton pumps at a lower level (Figures 4.1 and 4.2). Overexpression and knockdown of MITF in cell lines via lentiviral transduction recapitulated MITF's transcriptomic effects on proton transport, and the changes in expression of individual proton transporters were characterised via qRT-PCR, western blotting, and immunofluorescence (Figures 4.3-4.10).

Such contrasting expression signatures of proton transporters would likely manifest functional consequences. This chapter characterised the functional effects that differential MITF expression had on pH_i regulation and proton-coupled solute transport in melanoma cells. To do so, IGR37 cells with stable MITF-knockdown were analysed using BCECF microspectrofluorometry, which enabled real-time measurement of intracellular pH in the individual cells. Proton-coupled solute influx and efflux capacities of melanoma cells with MITF knockdown were interrogated via superfusion with different experimental solutions containing monocarboxylates, including pyruvate, lactate, and β-hydroxybutyrate. Furthermore, survival of melanoma cells incubated at the acidotic extracellular pH of 6.8 was studied in MITF-knockdown and control cells.

This chapter showed the pyruvate was less potent at sustaining the acidotic viability of IGR37 cells following MITF knockdown, an effect likely attributed to the downregulation of MITF-dependent mitochondrial oxidative phosphorylation that metabolises pyruvate (Vazquez et al., 2013). The elevated concentration of pyruvate required to maintain acidotic viability in IGR37 after MITF-knockdown was associated with a comparative upregulation of MCT1-dependent proton-coupled pyruvate transport in the respective cells. To test whether the upregulation of MCT1 function in MITF-knockdown cells was a necessity for surviving acidosis, the small molecule MCT1 inhibitor, AR-C155858, was applied to IGR37 cells. AR-C155858 induced

significantly more acidotic caspase 3/7 activity, and potentiated more vemurafenib-induced acidotic cytotoxicity in the MITF-knockdown IGR37 cells than IGR37 with LacZ-knockdown. MITF-Low IGR37 was thus shown to be relatively more dependent on MCT1 function to resist acidotic stress – a finding that is consistent with the concept of proton transporter phenotypes participating in MITF-mediated phenotypic plasticity in melanoma. Importantly, this chapter showed that small molecule targeting of MCT1 in MITF-Low cells under acidotic stress was cytotoxic, which encompasses a novel approach to enhance treatment efficacy in the subset melanoma cells with low levels of MITF expression.

RESULTS

Since transient knockdown of *MITF-M* in IGR37 increased the expression of various solute carrier proton transporters in the previous chapter, *MITF-M* was stably knocked down in the IGR37 cells to investigate the functional consequences of such SLC induction. As seen in Figure 5.1a, the pigmentation of the melanoma cell pellets was significantly reduced following stable *MITF* knockdown with either the shMITF#1 or the shMITF#2 vector, compared to the negative control *LacZ* knockdown cells. As MITF is a well-described transcriptional driver of melanocytic pigmentation (Kawakami and Fisher, 2017), the depigmentation of the IGR37 cell pellets following stable MITF knockdown visually demonstrated the functional validity of the stable knockdown experiments. Such changes in cell pellet pigmentation had also been documented in previous studies (Haq et al., 2013, Ferretta et al., 2016).

Next, we grossly inspected the IGR37 cell lines following incubation with the live-cell fluorescent indicator of intracellular pH, BCECF-AM. Following 1-hour incubation, it was apparent under fluorescent microscopy that IGR37 cells with *MITF-M* stably knocked down (IGR37-shMITF#1 and IGR37-shMITF#2, respectively) were less fluorescent than IGR37 with *LacZ* stably knocked down (IGR37-shLacZ, Figure 5.1b). Less BCECF fluorescence in the MITF knock-down cells lines indicated a

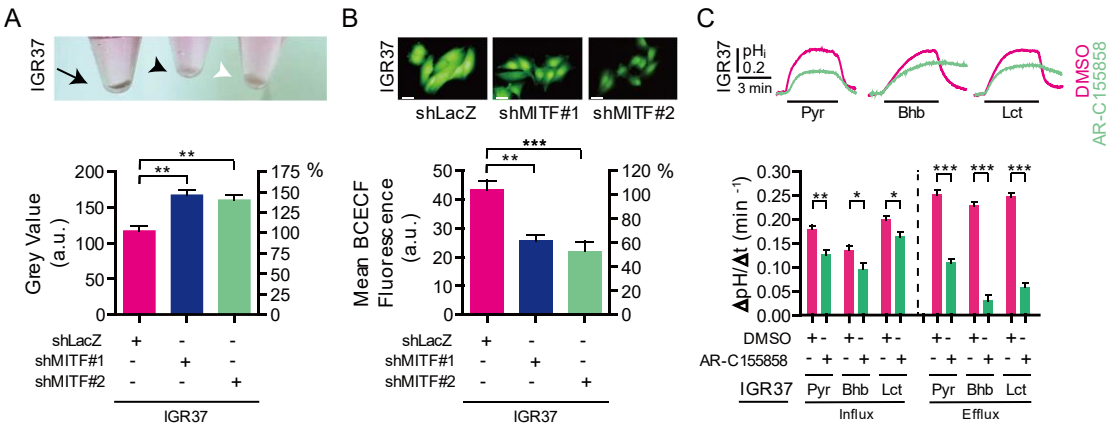

Figure 5.1: MITF-M Knockdown in Melanoma Cells Lowers Intracellular pH (a) Representative figure of the pigmentation in IGR37-shLacZ or IGR37-shMITF cell pellets. Quantification is shown in the lower panel (n = 3 individual experiments for each experimental condition, statistical analysis: unpaired t test). (b) Representative fluorescent images of IGR37-shLacZ or IGR37-shMITF cell lines incubated in BCECF-AM, showing differences in intracellular BCECF fluorescence. Quantification is shown in the lower panel (n = 3 individual experiments for each cell line, 30-40 cells included per experiment, statistical analysis: unpaired t test). (c) Representative traces of IGR37 cells superfused with 1µM AR-C155858 or 1:1000 DMSO, followed by treatment with10mM pyruvate (Pyr), 10mM β-Hydroxybutyrate (Bhb), or 10mM L-Lactate. Quantification is shown in the lower panel (n = 5 individual experiments for each experimental condition, statistical analysis: unpaired t test). *P < 0.05, **P < 0.01, ***P < 0.001. shLacZ: Short hairpin RNA targeting *β-galactosidase*. shMITF: Short hairpin RNA targeting *MITF-M*. BCECF: 2',7'-Bis(2-carboxyethyl)-5(6)-carboxyfluorescein. pH_i: Intracellular pH.

lower intracellular pH in these cells (Matamoros-Volante and Treviño, 2020). Interestingly, cellular import of lactic acid by MCT1 in invasive melanoma xenografts has been shown to promote intracellular acidification (Tasdogan et al., 2020). Given that MITF knockdown in the previous chapter resulted in a phenotypic switch from proton pumps to solute carriers proton transporters, it was possible that the observed intracellular acidification in MITF knockdown cells could also be, at least in part, the result of an increase in the net cellular importation of solutes and protons, secondary to the phenotypic upregulation of solute carrier proton transporters (Figures 4.1-4.2).

Amongst the implicated proton transporters, MCT1 was considered the key transporter that could be upregulated to mediate the observed intracellular acidification following MITF knockdown. First, MCT1 has been repeatedly shown to act as the major functional proton transporter in melanoma cells (Yang and Loh, 2019, Wahl et al., 2002); Second, the previous chapter had empirically shown MCT1 to be one of the most upregulated candidate solute carrier proton transporters following MITF knockdown (Figures 4.1-4.2). Logistically, MCT1's transport activity can be reliably assessed using in-house BCECF microspectrofluorometry (Yang and Loh, 2019). BCECF Microspectrofluorometry is an inverted epifluorescent microscopy technique, where cells loaded with BCECF are continuously recorded for their BCECF fluorescence, whilst being superfused with a customised isotonic solution (Chen et al.,

2018). By adjusting the composition of the superfusing solution, the effects of the superfusate on the cells' BCECF fluorescence can be recorded in real time, and converted to intracellular pH values following experimental calibration (Chen et al., 2018). Therefore, given the practical feasibility of experimentation, we examined whether the observed intracellular acidification in MITF-knockdown IGR37 could be explained, at least in part, by an upregulation of MCT1-mediated proton-coupled monocarboxylate transport associated with MITF-dependent phenotypic switching.

We first examined whether IGR37 cells could deploy MCT1 to import a range of monocarboxylates (Figure 5.1c). BCECF microspectrofluorometry showed that the addition of monocarboxylates pyruvate, L-lactate, and β-hydroxybutyrate, to IGR37 cells all resulted in significant reductions in intracellular pH. (Figure 5.1c). This suggested the functional presence of proton-coupled monocarboxylate import in IGR37. The concurrent superfusion of monocarboxylates with the addition of AR-C155858, a small molecular inhibitor of MCT1 , significantly decreased both the influx and efflux of all three types of monocarboxylates into and out of the IGR37 cells compared to superfusion with 1:1000 DMSO, suggesting that the transplasmalemmal proton-coupled movement of monocarboxylates in IGR37 was specifically mediated by MCT1 (Figure 5.1c).

Having shown that MCT1 was functional in IGR37 for carrying out proton-

coupled transport of a range of metabolically active monocarboxylates, we next sought to compare the rates of MCT1 transport activity in IGR37 cells with knockdown of either *MITF* or *LacZ*. As can be seen in Figure 5.2a, upon serial exposure to 10mM and 3mM pyruvate, the intracellular pH of IGR37-shMITF#1 and IGR37-shMITF#2 acidified more, and at a significantly faster rate than IGR37-shLacZ. This suggested that the proton-coupled transmembrane flux of pyruvate was significantly more active following MITF knockdown in IGR37 cells. Alternatively, MITF-M was also stably overexpressed in A375 cells (Figure 4.3), which are amelanotic melanoma cells without endogenous MITF expression (Kido et al., 2009). Following pyruvate superfusion, A375 with stably overexpressed MITF-M acidified less, and at a lower rate than A375 stably transduced with the empty vector (EV) (Figure 5.2b). This suggested that the ectopic expression of MITF-M in A375 reduced MCT1-mediated proton-coupled pyruvate transport, which further supported a role for MITF in the phenotypic regulation of MCT1 transport activity in melanoma cells.

MCT1's transport activities involving L-lactate and β-Hydroxybutyrate were also compared in IGR37 cells following knockdown of either *MITF* or *LacZ* (Figure 5.3a-b). Upon the addition of 10mM and 3mM of L-lactate or β-Hydroxybutyrate, the knockdown of *MITF-M* resulted in a comparatively faster rate of intracellular acidification than knockdown of LacZ, suggesting that proton-coupled lactate and β-

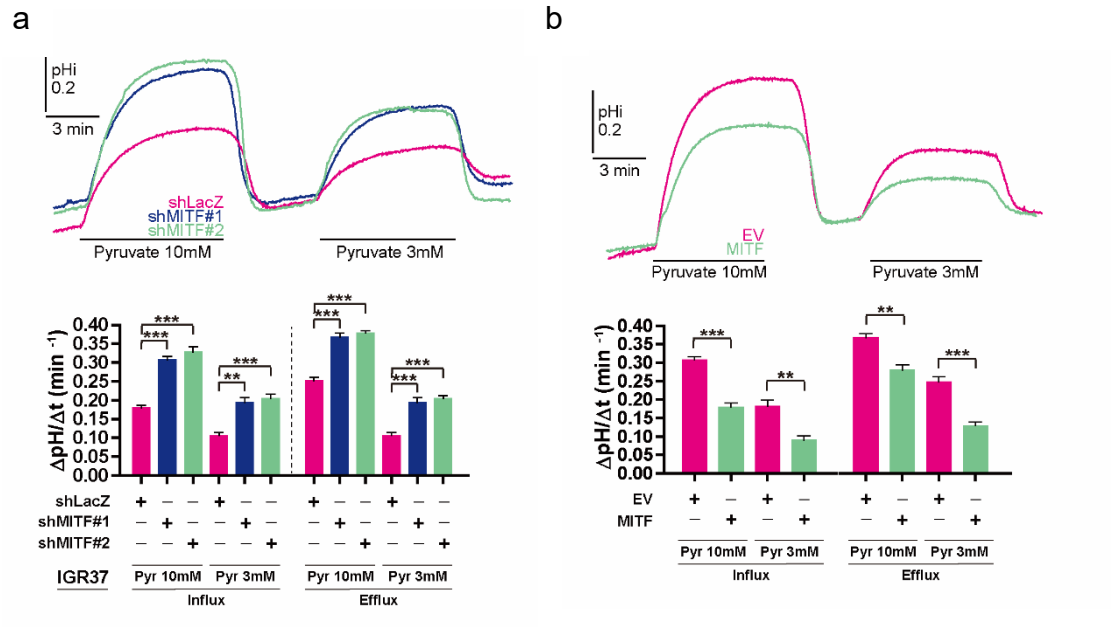

Figure 5.2: MITF-M Knockdown in Melanoma Cells Enhances Proton-Coupled Pyruvate Transport. (a) Representative traces of IGR37-shLacZ or IGR37-shMITF cell lines sequentially superfused with 10mM and 3mM pyruvate (Pyr). Quantification is shown in the lower panels (n = 5 individual experiments for each experimental condition, statistical analysis: unpaired t test). (b) Representative traces of A375-EV or A375-MITF cell lines sequentially superfused with 10mM and 3mM pyruvate (Pyr). Quantification is shown in the lower panels (n = 5 individual experiments for each experimental condition, statistical analysis: unpaired t test). *P < 0.05, **P < 0.01, ***P < 0.001. shLacZ: Short hairpin RNA targeting *β-galactosidase*. shMITF: Short hairpin RNA targeting *MITF-M*. pH_i: Intracellular pH.

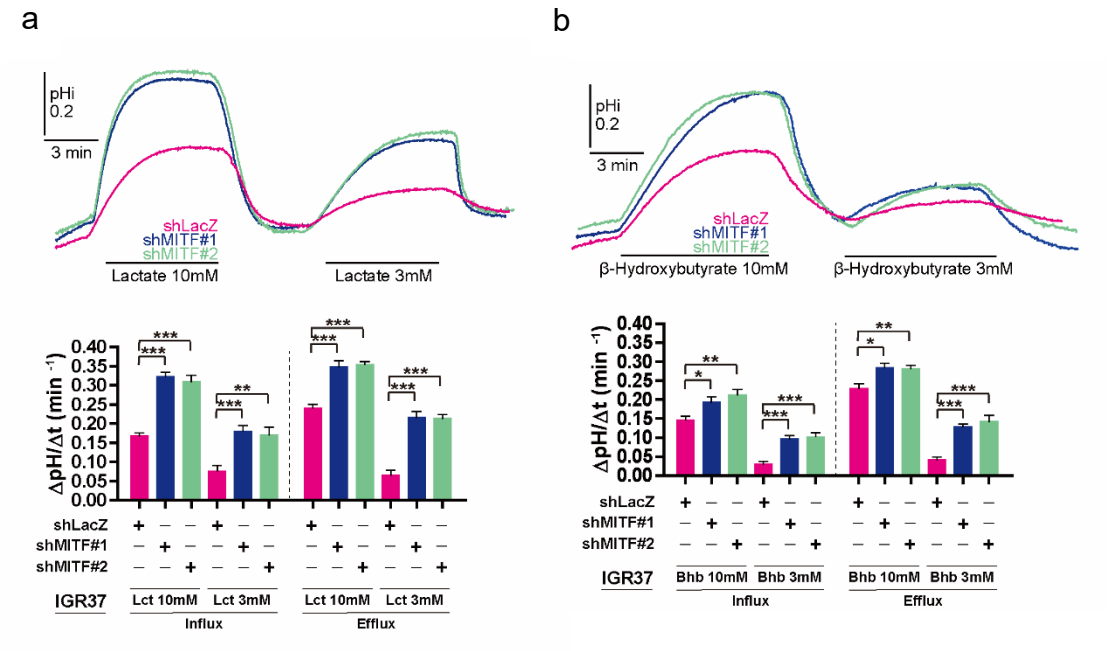

Figure 5.3: *MITF-M* Knockdown in Melanoma Cells Enhances Proton-Coupled L-Lactate and β-Hydroxybutyrate Transport. Representative traces of IGR37-shLacZ or IGR37-shMITF cell lines sequentially superfused with 10mM and 3mM of (a) L-Lactate (Lct), or (b) β-Hydroxybutyrate (Bhb)**.** Quantification is shown in the lower panels (n = 5 individual experiments for each experimental condition, statistical analysis: unpaired t test). *P < 0.05, **P < 0.01, ***P < 0.001. shLacZ: Short hairpin RNA targeting *β-galactosidase*. shMITF: Short hairpin RNA targeting *MITF-M*. pH_i: Intracellular pH.

Hydroxybutyrate transport mediated by MCT1 were more active following MITF knockdown in IGR37 (Figure 5.3a-b). The functional upregulation of MCT1 following MITF knockdown could also explain, at least in part, the relative intracellular acidification in these cells (Figure 5.1b).

It was previously shown in Chapter 3, that low pH_e (at pH_e 6.8) induced a slow-cycling phenotype in melanoma cells, associated with survival at a reduced rate of cellular proliferation (Figures 3.1-3.2) (Yang and Loh, 2019). This phenomenon has also been demonstrated in other studies (Bohme and Bosserhoff, 2020, Marino et al., 2012). Given MCT1 was the major determinant of intracellular pH in melanoma cells (Yang and Loh, 2019, Wahl et al., 2002), and here MCT1 was demonstrated to be functionally upregulated in IGR37 cells with MITF-knockdown (Figures 5.2-5.3), it raised the question of whether inhibition of MCT1 transport in the context of acidosis could be synthetically lethal for the subset of melanoma cells with low MITF expression.

To examine this possibility, we first tested melanoma cells' dependency on MCT1 substrates for acidotic survival (Figure 5.4a). Pyruvate was chosen as the experimental monocarboxylate supplement because its use in cell culture as an optional intermediate metabolite to support growth is established and standardised (Eagle et al., 1958). MITF- and LacZ-knockdown IGR37 cells were cultured at an extracellular pH (pH_e) of 6.8, supplemented with 1mM pyruvate for 72hrs. The experiments were controlled by

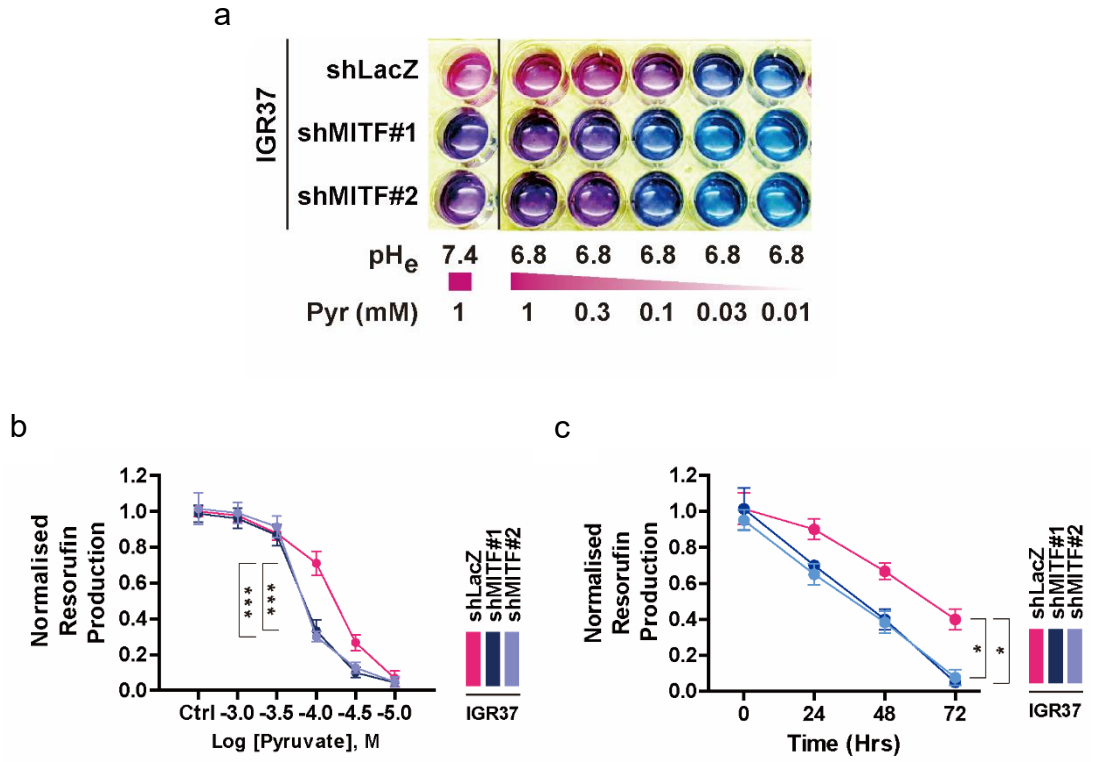

Figure 5.4: Pyruvate Starvation in Melanoma Cells with MITF-M Knockdown Reduces Acidotic Viability. (a) Representative figure of acidotic Resorufin production in IGR37-shLacZ or IGR37-shMITF cell lines subjected to a dose titration of pyruvate (Pyr) for 72hrs, at the pH_e of 6.8. Positive controls consisted of cells from respective cell lines incubated in 1mM pyruvate and at pH_e 7.4. Quantification is shown in (b), where the data are represented as mean ± SEM for technical replicates (n= 3) and are representative of 3 individual experiments. Statistical analysis: two-way ANOVA. (c) Time course of acidotic Resorufin production in IGR37-shLacZ or IGR37-shMITF cell lines cultured in 0.1mM pyruvate for 72hrs, at the pH_e of 6.8, normalised to cells from respective cell lines incubated in 1mM pyruvate at the pH_e 7.4. The data are represented as mean ± SEM for technical replicates (n= 3) and are representative of 3 individual experiments. Statistical analysis: two-way ANOVA. *P < 0.05, **P < 0.01, ***P < 0.001. shLacZ: Short hairpin RNA targeting *β-galactosidase*. shMITF: Short hairpin RNA targeting *MITF-M*. pH_i: Intracellular pH.

culturing the respective cells in parallel at the pH_e of 7.4, in the presence of 1mM pyruvate (Figure 5.4a). Different concentrations of pyruvate were withdrawn from the acidotic cell culture of pH_e 6.8 in a dose-titrated manner (Figure 5.4a).

Interestingly, in the presence of surplus amounts of pyruvate (1mM), the difference in cell viability as measured by resorufin production at 72hrs was not significantly different between culturing at pH_e 7.4 and pH_e 6.8 for all the cell lines involved. However, as pyruvate concentration in cell culture decreased, the rate of decline in normalised acidotic resorufin production was faster in the IGR37-shMITF cell lines compared with IGR37-shLacZ (Figure 5.4a). In pH 6.8 acidosis, all cell lines ceased to reduce resazurin below a pyruvate concentration of 30μM (Figure 5.4a-b), suggesting that pyruvate starvation was detrimental to acidotic melanoma viability. Pyruvate's EC50 value for maintaining normalised resarufin production at pH_e 6.8 was 57.86 ± 4.34μM for the IGR37-shLacZ cell line, whilst the EC50 value increased to 129.12 ± 6.28μM and 139.28 ± 4.68μM for IGR37-shMITF#1 and IGR37-shMITF#2, respectively ($p<0.001$, n=3, two-way ANOVA) (Figure 5.4b). The EC50 values suggested that pyruvate was significantly less potent at maintaining acidotic resorufin production in the IGR37-shMITF cell lines than in IGR37-shLacZ, which accounted for the greater decline in normalised resorufin production in the IGR37-shMITF cell lines upon acidotic pyruvate withdrawal. In addition, the reduced potency of pyruvate

for maintaining resorufin production in IGR37-shMITF cell lines was evident even in the positive control wells, where at neutral pH_e 7.4 the MITF knockdown cell lines carried out less resazurin conversion than IGR37-shLacZ (Figure 5.4a-b). This suggested that IGR37-shMITF cell lines were inherently less capable of reducing resazurin, and this deficit was exacerbated by the combination of exposures to acidosis and pyruvate starvation. The relative incapability of IGR37 to reduce resazurin at neutral pH following MITF knockdown is consistent with previous reports of MITF being a critical factor in driving the PGC1α transcriptional axis for mitochondrial biogenesis (Haq et al., 2013, Vazquez et al., 2013), since the biochemical reduction of resazurin requires aerobic respiration by cells actively participating in oxidative phosphorylation (Abu-Amero and Bosley, 2005, Zhang et al., 2004).

A further analysis of the time course of normalised resorufin production over a period of 72hrs also showed that normalised resorufin production in IGR37-shMITF#1 and IGR37-shMITF#2 was significantly curtailed compared with IGR37-shLacZ, when incubated at the fractional effective pyruvate concentration of 0.1mM at pH_e 6.8 (Figure 5.4c). This finding reinforced the results of the pyruvate dose-titration, as shown in Figures 5.4a and 5.4b.

To confirm that the comparative decline in acidotic cell viability in IGR37-shMITF cell lines upon pyruvate withdrawal was reflected in a reduction in cell number,

we additionally analysed normalised Hoechst 33342 cell counts in the same experimental set-up. At 72hrs of experimentation, all three of IGR37-LacZ, IGR37-shMITF#1, and -shMITF#2 cell lines showed a dose-dependent reduction in normalised Hoechst 33342 cell counts/mm^2 following pyruvate withdrawal from the acidic medium (Figure 5.5a). However, the rate of acidotic decline in normalised Hoechst 33342 cell counts was faster in the IGR37-shMITF cell lines compared with IGR37-shLacZ (Figure 5.5a-b). A time-course analysis of normalised Hoechst 33342 cell counts over 72hrs also showed that the rate of acidotic decline in normalised Hoechst 33342 cell counts was faster in the IGR37-shMITF cell lines than IGR37-shLacZ (Figure 5.5c). Therefore, the relative reduction in acidotic viability in IGR37-shMITF cell lines following pyruvate withdrawal was reflected in a comparative reduction in acidotic Hoechst 33342 cell counts.

We further characterised the nature of the pyruvate-starved decline in acidotic viability and cell number in the MITF-knockdown IGR37 cells to be apoptotic in nature. At 72hrs in acidotic culture, all three of IGR37-LacZ, IGR37-shMITF#1, and -shMITF#2 cell lines showed a dose-dependent increase in normalised caspase 3/7 activation following pyruvate withdrawal from the acidic medium (Figure 5.6a). The rate of acidotic increase in normalised green fluorescent cell counts/mm^2 – indicating live-cell caspase 3/7 activation) – was faster in the IGR37-shMITF cell lines compared

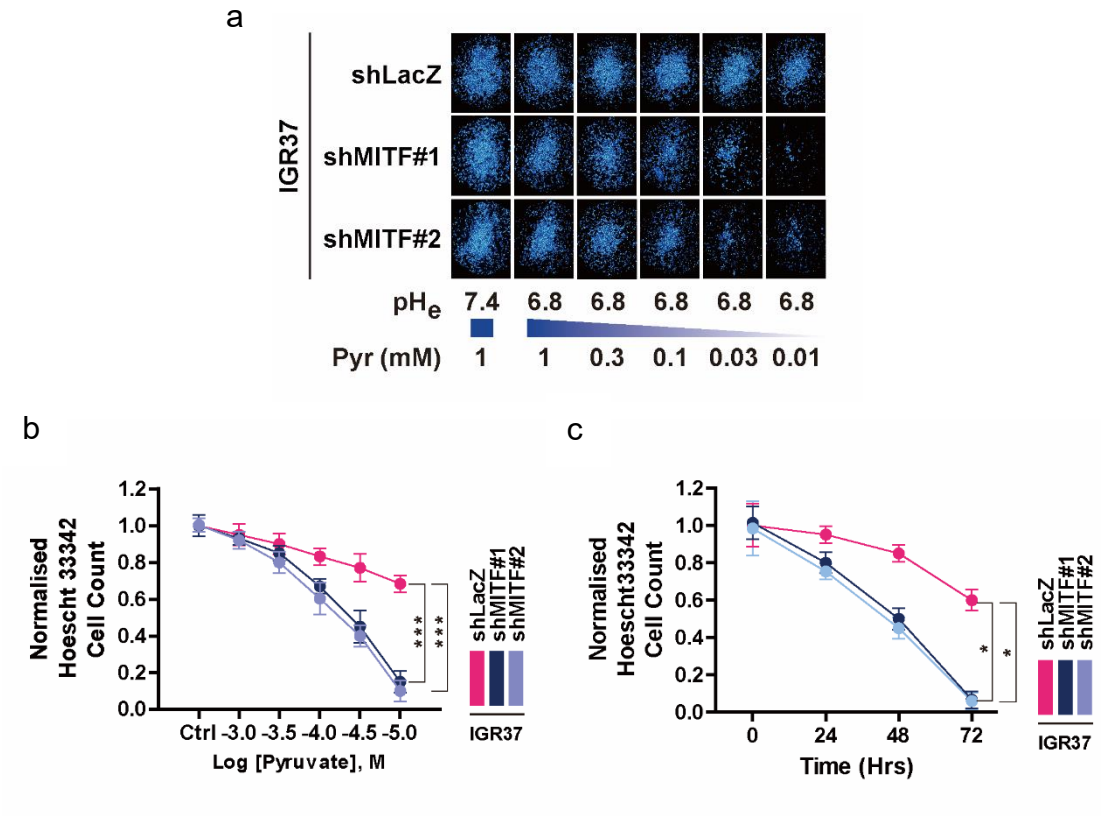

Figure 5.5: Pyruvate Starvation in Melanoma Cells with MITF-M Knockdown Reduces Acidotic Hoechst 33342 Cell Count. Representative figure of acidotic Hoechst 33342 cell counts in IGR37-shLacZ or IGR37-shMITF cell lines subjected to a dose titration of pyruvate (Pyr) for 72hrs, at the pH_e of 6.8. Positive controls consisted of cells from respective cell lines incubated in 1mM pyruvate and at pH_e 7.4. Quantification is shown in (b), where the data are represented as mean ± SEM for technical replicates (n= 3) and are representative of 3 individual experiments. Statistical analysis: two-way ANOVA. (c) Time course of acidotic Hoechst 33342 cell counts in IGR37-shLacZ or IGR37-shMITF cell lines cultured in 0.1mM pyruvate for 72hrs, at the pH_e of 6.8, normalised to cells from respective cell lines incubated in 1mM pyruvate at the pH_e 7.4. The data are represented as mean ± SEM for technical replicates (n= 3) and are representative of 3 individual experiments. Statistical analysis: two-way ANOVA. *P < 0.05, **P < 0.01, ***P < 0.001. shLacZ: Short hairpin RNA targeting *β-galactosidase*. shMITF: Short hairpin RNA targeting *MITF-M*. pH_i: Intracellular pH.

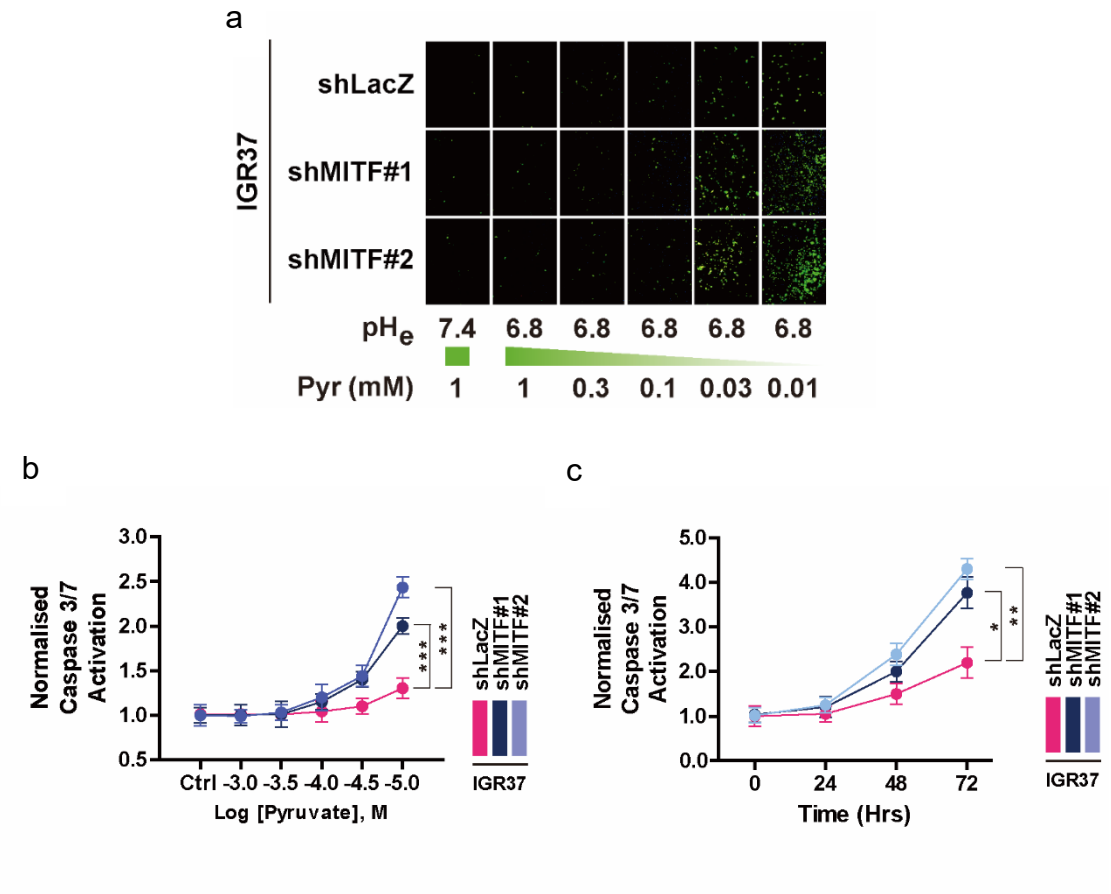

Figure 5.6: Pyruvate Starvation in Melanoma Cells with MITF-M Knockdown Increases Acidotic Caspase 3/7 Activation. Representative figure of acidotic caspase 3/7 activation in IGR37-shLacZ or IGR37-shMITF cell lines subjected to a dose titration of pyruvate (Pyr) for 72hrs, at the pH_e of 6.8. Negative controls consisted of cells from respective cell lines incubated in 1mM pyruvate and at pH_e 7.4. Quantification is shown in (b), where the data are represented as mean ± SEM for technical replicates (n= 3) and are representative of 3 individual experiments. Statistical analysis: two-way ANOVA. (c) Time course of acidotic caspase 3/7 activation in IGR37-shLacZ or IGR37-shMITF cell lines cultured in 0.1mM pyruvate for 72hrs, at the pH_e of 6.8, normalised to cells from respective cell lines incubated in 1mM pyruvate at the pH_e 7.4. The data are represented as mean ± SEM for technical replicates (n= 3) and are representative of 3 individual experiments. Statistical analysis: two-way ANOVA. *P < 0.05, **P < 0.01, ***P < 0.001. shLacZ: Short hairpin RNA targeting *β-galactosidase*. shMITF: Short hairpin RNA targeting *MITF-M*. pH_i: Intracellular pH.

with IGR37-shLacZ (Figures 5.6a-b). A time-course analysis of normalised caspase 3/7 activation over 72hrs also showed that the rate of acidotic rise in normalised caspase 3/7 activation was faster in the IGR37-shMITF cell lines than IGR37-shLacZ (Figure 5.6c). Therefore, the relative increase in acidotic apoptosis in IGR37-shMITF cell lines following pyruvate withdrawal accompanied a comparative reduction in acidotic viability and cell count (Figures 5.4-5.5).

The above result suggested that IGR37-shMITF cell lines were more dependent than IGR37-shLacZ on pyruvate for maintaining acidotic cell viability, Hoechst 33342 cell counts, and for preventing acidotic caspase 3/7 activation. If this is the case, then small molecule blockade of MCT1 via the inhibitor AR-C155858 should result in higher fractional cell killing in the MITF-knockdown IGR37 cells under acidotic stress. This hypothesis was tested by culturing MITF- and LacZ-knockdown IGR37 cells at an extracellular pH (pH_e) of 6.8, supplemented with 1mM pyruvate. The acidotic cells were then treated with a dose titration of AR-C155858 for 72hrs (Figure 5.7a). The experiments were controlled by treating the respective cells with 1:1000 DMSO, at the pH_e of 6.8, in the presence of 1mM pyruvate in parallel (Figure 5.7a). At 72hrs of experimentation, all three of IGR37-LacZ, IGR37-shMITF#1, and -shMITF#2 cell lines subjected to a dose titration of AR-C155858 in pH_e 6.8 showed a dose-dependent reduction in normalised Hoechst 33342 cell counts/mm^2 (Figure 5.7a). As expected, the

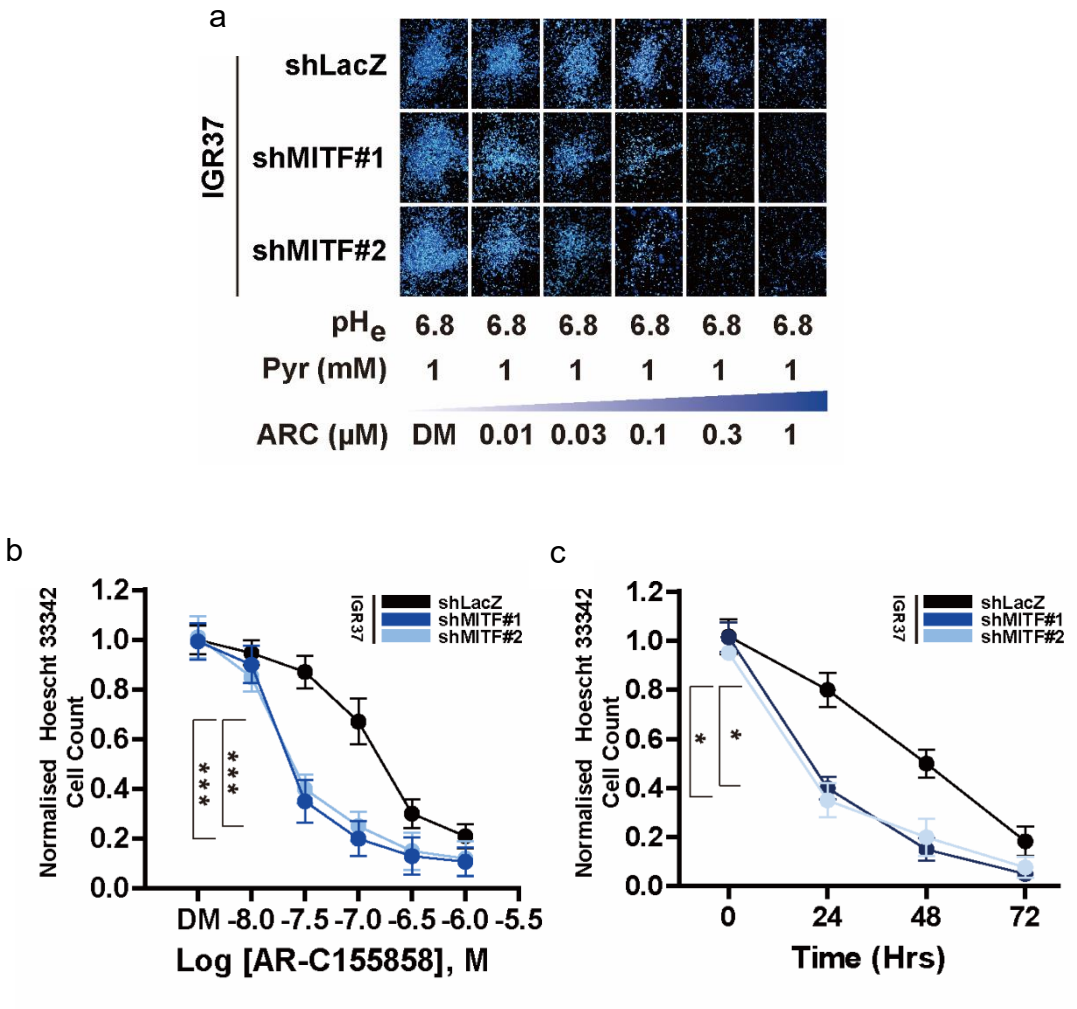

Figure 5.7: AR-C155858 Treatment in Melanoma Cells with MITF-M Knockdown Reduces Acidotic Hoechst 33342 Cell Count. Representative figure of acidotic Hoechst 33342 cell counts in IGR37-shLacZ or IGR37-shMITF cell lines subjected to a dose titration of AR-C155858 (ARC) for 72hrs, at the pH_e of 6.8 and in 1mM pyruvate. Negative controls consisted of cells from respective cell lines incubated in 1:1000 DMSO (DM), 1mM pyruvate, and at pH_e 6.8. Quantification is shown in (b), where the data are represented as mean ± SEM for technical replicates (n= 3) and are representative of 3 individual experiments. Statistical analysis: two-way ANOVA. (c) Time course of acidotic Hoechst 33342 cell counts in IGR37-shLacZ or IGR37-shMITF cell lines cultured in 1μM AR-C155858 for 72hrs, at the pH_e of 6.8, normalised to cells from respective cell lines incubated in 1:1000 DMSO at the pH_e 6.8. The data are represented as mean ± SEM for technical replicates (n= 3) and are representative of 3 individual experiments. Statistical analysis: two-way ANOVA. *P < 0.05, **P < 0.01, ***P < 0.001. shLacZ: Short hairpin RNA targeting *β-galactosidase*. shMITF: Short hairpin RNA targeting *MITF-M*. pH_i: Intracellular pH.

rate of decline in normalised Hoechst 33342 cell counts was faster in the IGR37-shMITF cell lines compared with IGR37-shLacZ (Figure 5.7a-b). A time-course analysis of normalised Hoechst 33342 cell counts in pH_e 6.8, at a fixed AR-C155858 concentration of 1μM over 72hrs also showed that the rate of decline in normalised Hoechst 33342 cell counts was faster in the IGR37-shMITF cell lines than IGR37-shLacZ (Figure 5.7c). Therefore, upon inhibition of MCT1 using AR-C155858, the reductions in acidotic Hoechst 33342 cell counts in the IGR37-shMITF cell lines were greater than in IGR37-shLacZ.

AR-C155858-induced decline in acidotic cell counts in the MITF-knockdown IGR37 cells was further shown to be due to an increase in apoptosis. At 72hrs, all three of IGR37-LacZ, IGR37-shMITF#1, and -shMITF#2 cell lines subjected to a dose titration of AR-C155858 in acidotic culture showed a dose-dependent increase in normalised caspase 3/7 activation (Figure 5.8a). The rate of acidotic increase in normalised green fluorescent cell counts/mm^2 – indicating live-cell caspase 3/7 activation) – was faster in the IGR37-shMITF cell lines compared with IGR37-shLacZ (Figure 5.8a-b). A time-course analysis of normalised caspase 3/7 activation over 72hrs also showed that the rate of acidotic rise in normalised caspase 3/7 activation was faster in the IGR37-shMITF cell lines than IGR37-shLacZ (Figure 5.8c). Therefore, the relative increase in acidotic apoptosis in IGR37-shMITF cell lines under AR-C155858

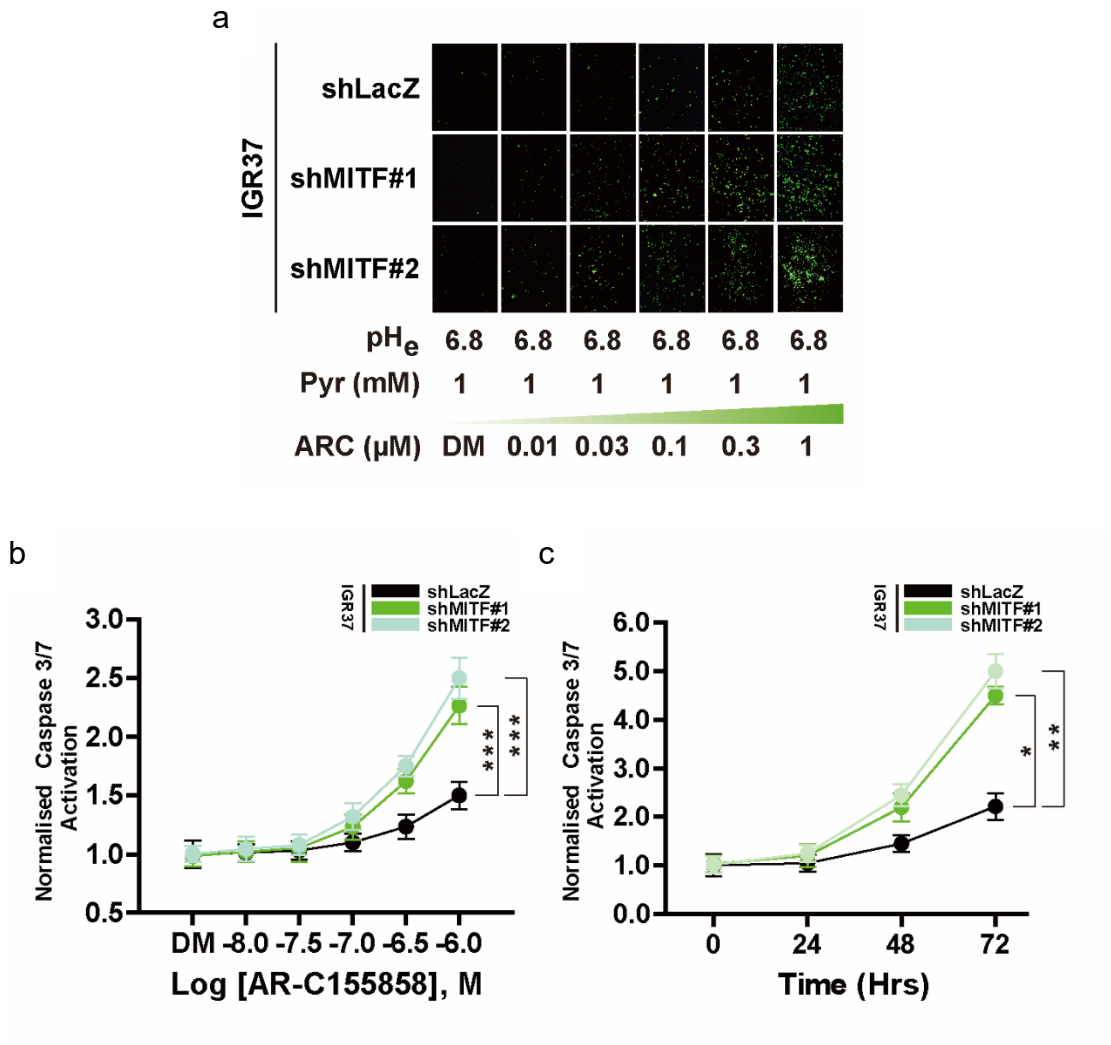

Figure 5.8: AR-C155858 Treatment in Melanoma Cells with MITF-M Knockdown Increases Acidotic Caspase 3/7 Activation. Representative figure of acidotic caspase 3/7 activation in IGR37-shLacZ or IGR37-shMITF cell lines subjected to a dose titration of AR-C155858 (ARC) for 72hrs, at the pH_e of 6.8 and in 1mM pyruvate. Negative controls consisted of cells from respective cell lines incubated in 1:1000 DMSO (DM), 1mM pyruvate, and at pH_e 6.8. Quantification is shown in (b), where the data are represented as mean ± SEM for technical replicates (n= 3) and are representative of 3 individual experiments. Statistical analysis: two-way ANOVA. (c) Time course of acidotic caspase 3/7 activation in IGR37-shLacZ or IGR37-shMITF cell lines cultured in 1μM AR-C155858 for 72hrs, at the pH_e of 6.8, normalised to cells from respective cell lines incubated in 1:1000 DMSO at the pH_e 6.8. The data are represented as mean ± SEM for technical replicates (n= 3) and are representative of 3 individual experiments. Statistical analysis: two-way ANOVA. *P < 0.05, **P < 0.01, ***P < 0.001. shLacZ: Short hairpin RNA targeting *β-galactosidase*. shMITF: Short hairpin RNA targeting *MITF-M*. pH_i: Intracellular pH.

treatment was consistent with a reduction in acidotic cell count (Figure 5.7). Taken together, MCT1 was critical for the survival of IGR37-shMITF cell lines under acidotic stress, and small molecule inhibition of MCT1 led to enhanced apoptosis and decreased cell counts following MITF knockdown.

The above finding prompted us to examine whether the cytotoxic effect of acidotic MCT1 inhibition on IGR37-shMITF cell lines could be additive in combination with vemurafenib (PLX4032), the current first line targeted therapy for advanced $BRAF^{V600E}$ mutant melanoma (Figure 5.9a). We cultured LacZ-knockdown IGR37 cells at an extracellular pH (pH_e) of 6.8, supplemented with 1mM pyruvate and 1:1000 DMSO (Figure 5.9a). Both of the IGR37-shMITF cell lines were exposed to two experimental conditions: one condition was culturing at an extracellular pH (pH_e) of 6.8, supplemented with 1mM pyruvate and 1:1000 DMSO – which was the same as the shLacZ-knockdown IGR37 – and the other condition was culturing at an extracellular pH (pH_e) of 6.8, supplemented with 1mM pyruvate and 1μM AR-C155858 (Figure 5.9a). The cells were then subjected to a dose titration of vemurafenib for 72hrs (Figure 5.9a). The experiments were controlled by treating the respective cells with 1:1000 DMSO, at the pH_e of 6.8, in the presence of 1mM pyruvate in parallel (Figure 5.9a). At 72hrs, IGR37 cells under all five experimental conditions demonstrated a dose-dependent reduction in normalised Hoechst 33342 cell counts with increasing

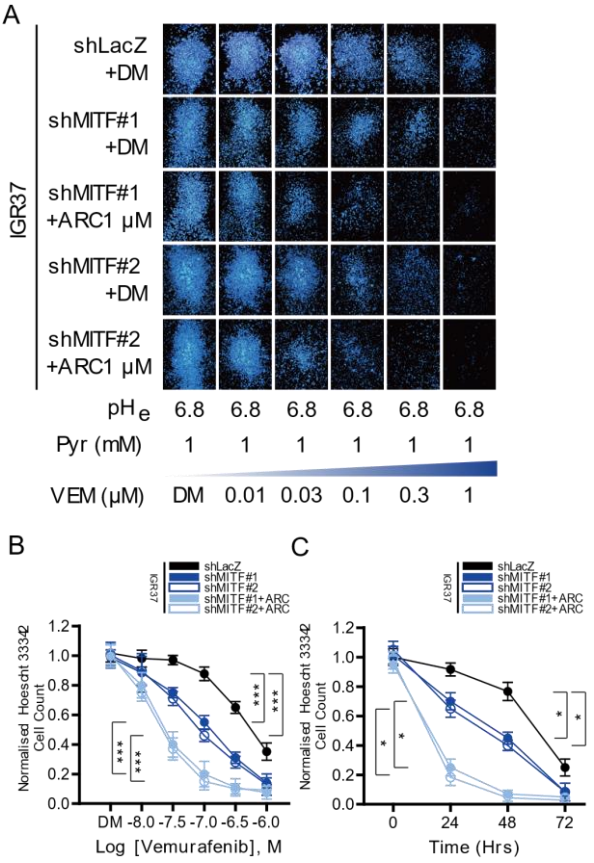

Figure 5.9: Combinational Treatment with AR-C155858 and Vemurafenib in Melanoma Cells with MITF-M Knockdown Further Reduces Acidotic Hoechst 33342 Cell Counts. Representative figure of acidotic Hoechst 33342 cell counts in cell lines IGR37-shLacZ or IGR37-shMITF subjected to a dose titration of vemurafenib (VEM) for 72hrs, at the pH_e of 6.8 and in 1mM pyruvate. IGR37-shMITF cell lines were either treated with 1:1000 DMSO (DM) or 1µM AR-C155858 (ARC) for further comparison. Negative controls consisted of cells from respective cell lines incubated in 1:1000 DMSO (DM), 1mM pyruvate, and at pH_e 6.8. Quantification is shown in (b), where the data are represented as mean ± SEM for technical replicates (n= 3) and are representative of 3 individual experiments. Statistical analysis: two-way ANOVA. (c) Time course of acidotic Hoechst 33342 cell counts in IGR37-shLacZ or IGR37-shMITF cell lines cultured in 1µM for 72hrs, at the pH_e of 6.8, normalised to cells from respective cell lines incubated in 1:1000 DMSO at the pH_e 6.8. IGR37-shMITF cell lines were either treated with 1:1000 DMSO (DM) or 1µM AR-C155858 (ARC) for further comparison. The data are represented as mean ± SEM for technical replicates (n= 3) and are representative of 3 individual experiments. Statistical analysis: two-way ANOVA. *P < 0.05, **P < 0.01, ***P < 0.001. shLacZ: Short hairpin RNA targeting *β-galactosidase*. shMITF: Short hairpin RNA targeting *MITF-M*. pH_i: Intracellular pH.

concentrations of vemurafenib (Figure 5.9a). The rate of decline in normalised Hoechst 33342 cell counts was faster in the IGR37-shMITF cell lines compared with IGR37-shLacZ (Figure 5.9a-b). This was expected because overexpressed MITF has been shown to confer vemurafenib resistance in melanoma (Smith et al., 2016, Johannessen et al., 2013). In addition, concurrent treatment of IGR37-shMITF cell lines with vemurafenib plus AR-C155858 further shifted the vemurafenib dose-response curve to the left, demonstrating a significant increase in acidotic cytotoxicity in the MITF-knockdown IGR37 cell lines when vemurafenib was combined with AR-C155858 (Figure 5.9a-b).

Over the course of 72hrs, normalised Hoechst 33342 cell counts in IGR37-shMITF cell lines treated with the combination of vemurafenib and AR-C155858 declined at a significantly faster rate than the IGR37-shMITF cell lines treated with vemurafenib alone (Figure 5.9c). These findings suggested that vemurafenib in combination with AR-C155858 was an effective approach to targeting IGR37-shMITF cell lines under acidotic stress.

The additive effect of vemurafenib with AR-C155858 on targeting MITF-knockdown IGR37 cells was confirmed by examining caspase 3/7 activation following combinational therapy (Figure 5.10a). At 72hrs, IGR37 cells under all five experimental

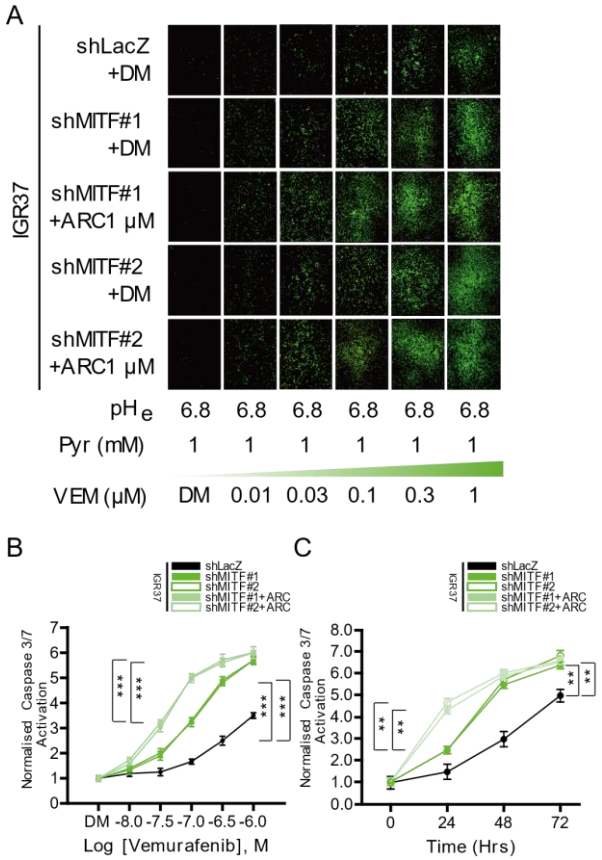

Figure 5.10: Combinational Treatment with AR-C155858 and Vemurafenib in Melanoma Cells with MITF-M Knockdown Further Increases Acidotic Caspase 3/7 Activation. Representative figure of acidotic caspase 3/7 activation in cell lines IGR37-shLacZ or IGR37-shMITF subjected to a dose titration of vemurafenib (VEM) for 72hrs, at the pH_e of 6.8 and in 1mM pyruvate. IGR37-shMITF cell lines were either treated with 1:1000 DMSO (DM) or 1µM AR-C155858 (ARC) for further comparison. Negative controls consisted of cells from respective cell lines incubated in 1:1000 DMSO (DM), 1mM pyruvate, and at pH_e 6.8. Quantification is shown in (b), where the data are represented as mean ± SEM for technical replicates (n= 3) and are representative of 3 individual experiments. Statistical analysis: two-way ANOVA. (c) Time course of acidotic caspase 3/7 activation in IGR37-shLacZ or IGR37-shMITF cell lines cultured in 1µM vemurafenib for 72hrs, at the pH_e of 6.8, normalised to cells from respective cell lines incubated in 1:1000 DMSO at the pH_e 6.8. IGR37-shMITF cell lines were either treated with 1:1000 DMSO (DM) or 1µM AR-C155858 (ARC) for further comparison. The data are represented as mean ± SEM for technical replicates (n= 3) and are representative of 3 individual experiments. Statistical analysis: two-way ANOVA. *P < 0.05, **P < 0.01, ***P < 0.001. shLacZ: Short hairpin RNA targeting *β-galactosidase*. shMITF: Short hairpin RNA targeting *MITF-M*. pH_i: Intracellular pH.

conditions demonstrated a dose-dependent increase in normalised caspase 3/7 activation with rising concentrations of vemurafenib (Figure 5.10a). The rate of increase in normalised caspase 3/7 activation was faster in the IGR37-shMITF cell lines compared with IGR37-shLacZ (Figures 5.10a-b), confirming that IGR37 cells with MITF knocked down were more vulnerable to vemurafenib (Johannessen et al., 2013). In addition, concurrent treatment of IGR37-shMITF cell lines with vemurafenib plus AR-C155858 further shifted the vemurafenib dose-response curve to the left, demonstrating a significant increase in acidotic apoptosis in the MITF-knockdown IGR37 cell lines when vemurafenib was combined with AR-C155858 (Figures 5.10a-b).

An analysis of normalised caspase 3/7 activation over time showed that over the course of 72hrs, normalised caspase 3/7 activation in IGR37-shMITF cell lines treated with the combination of vemurafenib and AR-C155858 increased at a significantly faster rate than the IGR37-shMITF cell lines treated with vemurafenib alone (Figure 5.10c). These findings confirmed that vemurafenib in combination with AR-C155858 was an effective approach to targeting IGR37-shMITF cell lines under acidotic stress. Taken together, MCT1 function was crucial for survival in acidotic melanoma cells with low levels of MITF expression. Inhibition of MCT1 via the use of the small molecule inhibitor AR-C155858, either alone or in combination with vemurafenib, provides a

means for targeting the subset of melanoma cells that express low levels of MITF under acidotic stress.

DISCUSSION

Clinically, there is an unmet need to develop novel therapies to treat advanced melanoma (Forschner et al., 2017). Current treatment options for metastatic melanoma include biological agents that target $BRAF^{V600E}$/MEK (Wong and Ribas, 2016), and immunotherapeutic agents that consist mainly of immune checkpoint inhibitors targeting CTLA-4 and PD-1 (Albertini, 2018). Though updated figures from the CheckMate 067 five-year follow-up study showed that the Nivolumab-plus-Ipilimumab treatment arm conferred a median overall survival of 60.0 months in advanced melanoma (Larkin et al., 2019), and outcomes from the COMBI-d/-v five-year follow-up study showed that the Dabrafenib-plus-Trametinib treatment arm conferred an overall survival of 34% at 5 years (Robert et al., 2019), in most cases metastatic melanoma tumors acquire resistance to these therapeutic agents, on route to disease progression (Kozar et al., 2019).

To this end, this thesis showed that proton transport phenotypes existed heterogeneously in different melanoma cells, with some cells favouring proton pumps, whilst others being solute carrier proton transporters-predominant, depending on the expression level of MITF (Figures 4.1-4.2). This chapter showed that MCT1 played an important role in the subset of melanoma cells with low levels of MITF expression

(Figures 5.2-5.3). We experimentally modelled low MITF expression in IGR37 melanoma cells by stably knocking down MITF, and pharmacological inhibition of MCT1 in MITF-knockdown IGR37 cells under acidotic stress induced significant amounts of cytotoxicity and apoptosis (Figures 5.7 and 5.8). Furthermore, combined treatment with AR-C155858 and Vemurafenib potentiated the cytotoxic effects of vemurafenib in MITF-knockdown IGR37 cells (Figures 5.9 and 5.10).

The resulted presented here are supported by a recent preclinical study that demonstrated the efficacy of MCT1 inhibition in reducing metastatic invasion in patient-derived melanoma xenografts and mouse melanomas (Tasdogan et al., 2020). The fact that invasive melanoma cells frequently display low expression levels of MITF (Tirosh et al., 2016) suggests that mechanistically, our finding of AR-C155858 being able to target acidotic MITF-knockdown cells with upregulated MCT1 expression and function, was consistent with the observed depletion of circulating invasive melanoma cells and reduced metastatic burden in patient-derived xenograft following MCT1 blockade (Tasdogan et al., 2020).

This chapter also showed that pyruvate was less potent at sustaining acidotic cell culture in the IGR37-shMITF cell lines (Figure 5.4). The EC50 for inducing normalised resorufin production was significantly elevated in the MITF-knockdown group (Figure 4b). The increase in MCT1 expression and transport function in the MITF-knockdown

cells may represent a compensatory mechanism to account for the intracellular deficit in pyruvate metabolism. As mentioned, MITF regulates the expression of PGC1α-mediated mitochondrial biogenesis in melanoma (Vazquez et al., 2013). The fact that the small molecule MCT1 inhibitor AR-C155858 was associated with the acidotic decompensation of IGR37-shMITF cell lines was consistent with a crucial role for MCT1 in the maintenance of survival in MITF-Low cells under acidotic stress.

Interestingly, in the presence of surplus concentration of supplementary pyruvate, acidotic culture alone did not adversely affect resorufin-indicated viability in IGR37-shMITF cell lines (Figure 5.4). However, when the MITF-knockdown cells were subjected to pyruvate deprivation in combination with acidotic exposure, apoptosis ensued in the MITF-knockdown cells at a significantly faster rate than IGR37 cells with LacZ-knockdown (Figure 5.6). There have been conflicting reports in the literature regarding the exact impact of acidosis on cell biology. Some studies, such as our own data in Chapter 3, showed that melanoma cells assumed a slow proliferative or senescence-like phenotype upon acidotic exposure (Figures 3.1-3.2) (Bohme and Bosserhoff, 2020, Yang and Loh, 2019, Marino et al., 2012), whilst others have documented frank apoptosis in cells following acidotic incubation (Huang et al., 2017, Thammasit et al., 2015, Park et al., 1999). Experiments presented here suggested that the cellular response to acidosis is in fact complex and multi-faceted, and can change

dynamically depending on additional factors including nutrient deprivation and transcriptional phenotypes. IGR37 cells tolerated acidosis in the surplus of ambient pyruvate, but underwent apoptosis when pyruvate restriction was imposed (Figure 5.4). Within this framework, cells with low expression of MITF induced by lentiviral knockdown were less resistant to acidotic pyruvate starvation than cells retaining endogenous MITF expression via LacZ knockdown (Figure 5.4). The dependence of MITF-knockdown IGR37 cells on MCT1 transport for acidotic survival was the most likely explanation to the above observation, since these cells apoptosed upon AR-C155858 treatment in acidosis (Figures 5.7-5.8).

In contrast, IGR37 cells with retained endogenous MITF expression were able to transactivate proton pumps including V- and F-Type ATPases (Figures 4.1-4.2) (Zhang et al., 2015). The expression of such proton pumps may enable MITF-High cells to bypass any solute constraints for acidotic survival via several mechanisms: First, V- and F-Type ATPase represent key effectors that facilitate autophagy and mitophagy, respectively (Pamarthy et al., 2018, Lefebvre et al., 2013). The recycling of cytosolic organelles during periods of acidotic stress may present MITF-High melanoma cells with an endogenous supply of intermediate metabolites and solutes, which would otherwise not be available to MITF-Low cells that shift to the solute carrier phenotype (He et al., 2018). Second, recent studies have demonstrated that the plasmalemmal

expression of V-Type ATPase enabled cells to carry out macropinocytosis, a non-selective nutrient acquisition strategy that is also significantly less stringent in terms of substrate specificity than that required for solute carrier-mediated transport (Ramirez et al., 2019). In either case, we showed that the upregulation of MCT1 in MITF-Knockdown IGR37 cells exposed these cells to unique vulnerabilities during periods of acidotic pyruvate starvation, vulnerabilities that were therapeutically exploited by treating the cells with small molecule MCT1 inhibition to induce apoptosis during acidosis. There remains the possibility that the acidotic MITF-Low cells may adapt to MCT1 inhibition by importing alternative metabolites from the microenvironment via the expression of different solute carriers. In this case, a combinational approach to solute carrier inhibition may be required, similar to approach of using BRAF, MEK, and potentially ERK inhibitors in combination, which has paved the way for targeted therapy in advanced melanoma (Robert et al., 2019).

A model based on the results presented here depicts the contrasting phenotypes for acidotic resistance in melanoma cells, taking into account MITF expression status and nutrient availability (Figure 5.11). MITF-High melanoma is shown to resist acidosis without requirement for specific solute conditions, whereas acidotic survival in MITF-Low melanoma is dependent on the presence of pyruvate, and may be curtailed upon the application of small molecule MCT1 inhibition. Taken together, MITF-dependent

phenotypic plasticity is a multi-faceted physiological phenomenon, an understanding of which may facilitate the innovation of novel treatment approaches for advanced melanoma.

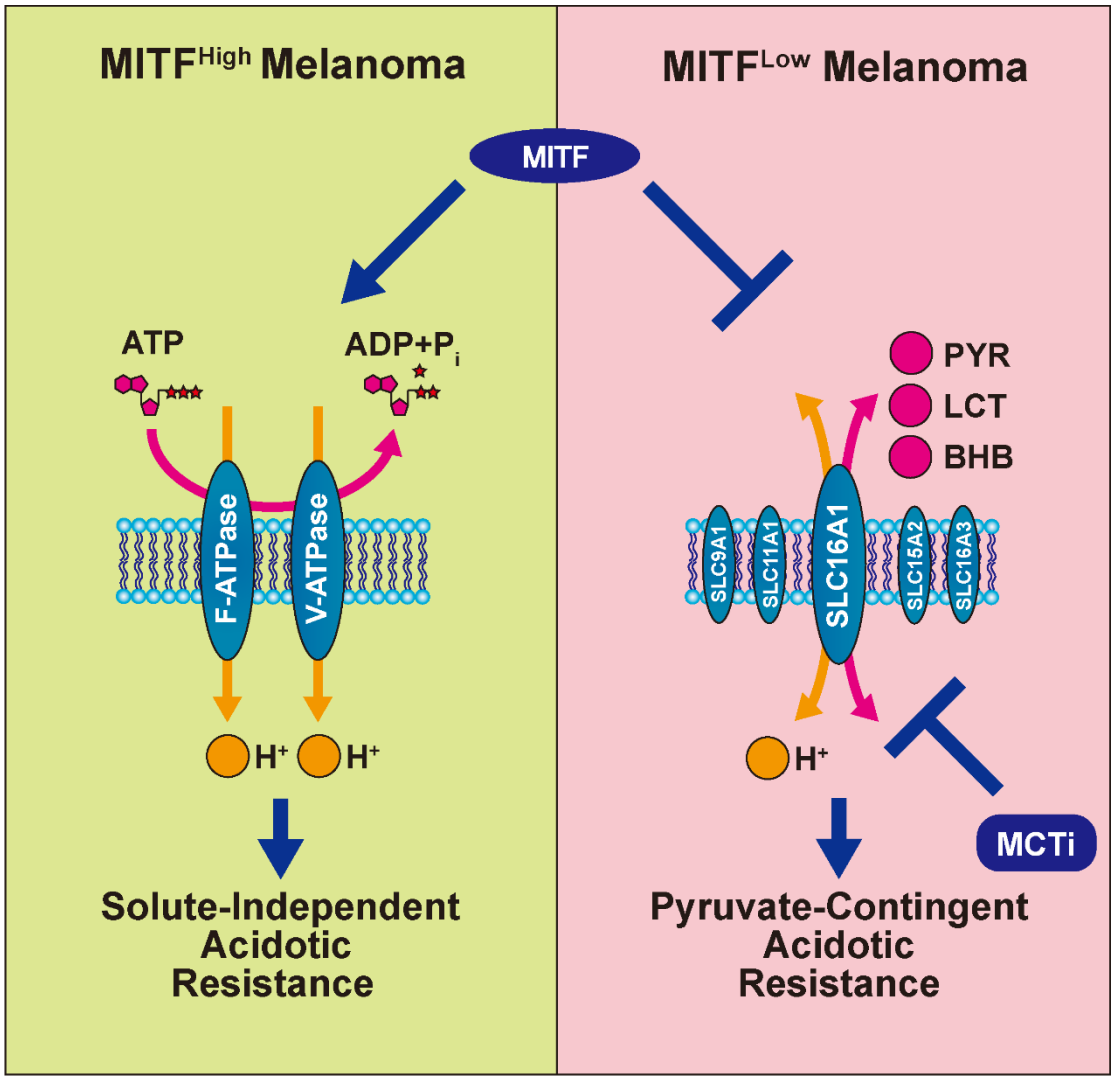

Figure 5.11 A Model for MITF-Dependent Phenotypic Plasticity in Acidotic Resistance. MITF-High melanoma is resists acidosis without requirement for specific solute conditions, whereas acidotic survival in MITF-Low melanoma relies on the presence of pyruvate, and may be curtailed upon the application of small molecule MCT1 inhibition.

\

CHAPTER 6

CONCLUSIONS

MITF-Dependent phenotypic plasticity models intratumoural heterogeneity in melanoma (Arozarena and Wellbrock, 2019). The data presented in this thesis demonstrated that the expression of proton transporters also participated in phenotypic plasticity in melanoma, determined by MITF expression (Figures 4.1-4.2). High levels of MITF were associated with the asymmetrical transcription of primary active proton pumps, whilst low levels of MITF correlated with a transcriptional shift to secondary active solute carrier proton transporters (Figures 4.1-4.2). This molecular dichotomy was shown to persist at the protein and functional levels.

Within this transcriptomic construct, MITF-Low cells modelled by stable MITF knockdown were shown to be highly dependent on the transport activity of MCT1 to survive acidotic stress (Figures 5.7-5.8). Melanoma cells with low MITF expression required high levels of pyruvate to maintain viability and avoid apoptosis under acidotic stress (Figures 5.4-5.6). Results from pyruvate deprivation or treatment with the MCT1 inhibitor, AR-C155858, both induced apoptosis and diminished cell counts in acidotic MITF-knockdown cells (Figures 5.7-5.8). Combined therapy using the $BRAF^{V600E}$

inhibitor, vemurafenib, and AR-C155858 enhanced apoptosis in the MITF-Low cells (Figures 5.9-5.10).

This thesis also identified the functional presence of sodium-bicarbonate co-transport in melanoma (Yang and Loh, 2019). The Sodium-Coupled Bicarbonate Transporters are an important class of intracellular pH regulators with oncogenic relevance in other solid cancers, including breast cancer, pancreatic adenocarcinoma, and renal cell carcinoma (Romero et al., 2013). This thesis characterised the molecular expression and demonstrated the transport function of NCBTs in melanoma cells (Yang and Loh, 2019). Identification of such novel classes of membrane transporter in melanoma may provide molecular targets for future therapeutic treatments (Alexander et al., 2019). Taken together, proton transporter biology represents an important aspect of melanoma biology that warrants further studies. The genomic expression of membrane transporters is regulated by transcription factors such as MITF, and such regulatory networks provide valuable insights into melanoma biology and therapy.

REFERENCES

ABBASI, N. R., SHAW, H. M., RIGEL, D. S., FRIEDMAN, R. J., MCCARTHY, W. H., OSMAN, I., KOPF, A. W. & POLSKY, D. 2004. Early diagnosis of cutaneous melanoma: revisiting the ABCD criteria. *JAMA,* 292**,** 2771-2776.

ABU-AMERO, K. K. & BOSLEY, T. M. 2005. Detection of mitochondrial respiratory dysfunction in circulating lymphocytes using resazurin. *Arch Pathol Lab Med,* 129**,** 1295-8.

ABU JAWDEH, B. G., KHAN, S., DESCH~NES, I., HOSHI, M., GOEL, M., LOCK, J. T., SHINLAPAWITTAYATORN, K., BABCOCK, G., LAKHE-REDDY, S., DECARO, G., YADAV, S. P., MOHAN, M. L., NAGA PRASAD, S. V., SCHILLING, W. P., FICKER, E. & SCHELLING, J. R. 2011. Phosphoinositide binding differentially regulates NHE1 Na+/H+ exchanger-dependent proximal tubule cell survival. *The Journal of biological chemistry,* 286**,** 42435-42445.

AHMED, S., THOMAS, G., GHOUSSAINI, M., HEALEY, C. S., HUMPHREYS, M. K., PLATTE, R., MORRISON, J., MARANIAN, M., POOLEY, K. A., LUBEN, R., ECCLES, D., EVANS, D. G., FLETCHER, O., JOHNSON, N., DOS SANTOS SILVA, I., PETO, J., STRATTON, M. R., RAHMAN, N., JACOBS, K., PRENTICE, R., ANDERSON, G. L., RAJKOVIC, A., CURB, J. D., ZIEGLER, R. G., BERG, C. D., BUYS, S. S., MCCARTY, C. A., FEIGELSON, H. S., CALLE, E. E., THUN, M. J., DIVER, W. R., BOJESEN, S., NORDESTGAARD, B. G., FLYGER, H., D*Nature genetics,* 41**,** 585-590.

AHN, A., CHATTERJEE, A. & ECCLES, M. R. 2017. The Slow Cycling Phenotype: A Growing Problem for Treatment Resistance in Melanoma. *Molecular cancer therapeutics,* 16**,** 1002-1009.

AKBANI, R., AKDEMIR, KADIR C., AKSOY, B. A., ALBERT, M., ALLY, A., AMIN, SAMIRKUMAR B., ARACHCHI, H., ARORA, A., AUMAN, J. T., AYALA, B., BABOUD, J., BALASUNDARAM, M., BALU, S., BARNABAS, N., BARTLETT, J., BARTLETT, P., BASTIAN, BORIS C., BAYLIN, STEPHEN B., BEHERA, M., BELYAEV, D., BENZ, C., BERNARD, B., BEROUKHIM, R., BIR, N., BLACK, AARON D., BODENHEIMER, T., BOICE, L., BOLAND, GENEVIEVE M., BONO, R., BOOTWALLA, MOIZ S., BOSENBERG, M., BOWEN, J., BOWLBY, R., BRISTOW, CHRISTOPHER A., BROCKWAY-LUNARDI, L., BROOKS, D., BRZEZINSKI, J., BSHARA, W., BUDA, E., BURNS, WILLIAM R., BUTTERFIELD, YARON S. N., BUTTON, M., CALDERONE, T., CAPPELLINI, GIANCARLO A., CARTER, C., CARTER, SCOTT L., CHERNEY, L., CHERNIACK, ANDREW D., CHEVALIER, A., CHIN, L., CHO, J., CHO, RAYMOND J., CHOI, Y.-L., CHU, A., CHUDAMANI, S., CIBULSKIS, K., CIRIELLO, G., CLARKE, A., COONS, S., COPE, L., CRAIN, D.,

CURLEY, E., DANILOVA, L., D'ATRI, S., DAVIDSEN, T., DAVIES, MICHAEL A., DELMAN, KEITH A., DEMCHOK, JOHN A., DENG, QIXIA A., DERIBE, YONATHAN L., DHALLA, N., DHIR, R., DICARA, D., DINIKIN, M., DUBINA, M., EBROM, J. S., EGEA, S., ELEY, G., ENGEL, J., ESCHBACHER, JENNIFER M., FEDOSENKO, KONSTANTIN V., FELAU, I., FENNELL, T., FERGUSON, MARTIN L., FISHER, S., FLAHERTY, KEITH T., FRAZER, S., FRICK, J., FULIDOU, V., GABRIEL, STACEY B., GAO, J., GARDNER, J., GARRAWAY, LEVI A., GASTIER-FOSTER, JULIE M., GAUDIOSO, C., GEHLENBORG, N., GENOVESE, G., GERKEN, M., GERSHENWALD, JEFFREY E., GETZ, G., et al. 2015. Genomic Classification of Cutaneous Melanoma. *Cell,* 161**,** 1681-1696.

ALAXENDER, S. P., KELLY, E., MARRION, N. V., PETERS, J. A., FACCENDA, E., HARDING, S. D., PAWSON, A. J., SHARMAN, J. L., SOUTHAN, C., DAVIES, J. A. & COLLABORATORS, C. 2017. The Concise Guide to Pharmacology 2017/18: Transporters. *British Journal of Pharmacology,* 174**,** S360-S446.

ALBERTINI, M. R. 2018. The age of enlightenment in melanoma immunotherapy. *Journal for ImmunoTherapy of Cancer,* 6**,** 80.

ALEXANDER, S. P. H., KELLY, E., MATHIE, A., PETERS, J. A., VEALE, E. L., ARMSTRONG, J. F., FACCENDA, E., HARDING, S. D., PAWSON, A. J., SHARMAN, J. L., SOUTHAN, C., DAVIES, J. A. & COLLABORATORS, C. 2019. THE CONCISE GUIDE TO PHARMACOLOGY 2019/20: Transporters. *Br J Pharmacol,* 176 Suppl 1**,** S397-S493.

ALEXANDROV, L. B., NIK-ZAINAL, S., WEDGE, D. C., APARICIO, S. A., BEHJATI, S., BIANKIN, A. V., BIGNELL, G. R., BOLLI, N., BORG, A., BORRESEN-DALE, A. L., BOYAULT, S., BURKHARDT, B., BUTLER, A. P., CALDAS, C., DAVIES, H. R., DESMEDT, C., EILS, R., EYFJORD, J. E., FOEKENS, J. A., GREAVES, M., HOSODA, F., HUTTER, B., ILICIC, T., IMBEAUD, S., IMIELINSKI, M., JAGER, N., JONES, D. T., JONES, D., KNAPPSKOG, S., KOOL, M., LAKHANI, S. R., LOPEZ-OTIN, C., MARTIN, S., MUNSHI, N. C., NAKAMURA, H., NORTHCOTT, P. A., PAJIC, M., PAPAEMMANUIL, E., PARADISO, A., PEARSON, J. V., PUENTE, X. S., RAINE, K., RAMAKRISHNA, M., RICHARDSON, A. L., RICHTER, J., ROSENSTIEL, P., SCHLESNER, M., SCHUMACHER, T. N., SPAN, P. N., TEAGUE, J. W., TOTOKI, Y., TUTT, A. N., VALDES-MAS, R., VAN BUUREN, M. M., VAN 'T VEER, L., VINCENT-SALOMON, A., WADDELL, N., YATES, L. R., ZUCMAN-ROSSI, J., FUTREAL, P. A., MCDERMOTT, U., LICHTER, P., MEYERSON, M., GRIMMOND, S. M., SIEBERT, R., CAMPO, E., SHIBATA, T., PFISTER, S. M., CAMPBELL, P. J. & STRATTON, M. R. 2013. Signatures of mutational processes in human cancer. *Nature,* 500**,** 415-21.

ALFAROUK, K. O. 2016. Tumor metabolism, cancer cell transporters, and

microenvironmental resistance. *Journal of Enzyme Inhibition and Medicinal Chemistry,* 31**,** 859-866.

ALI, Z., YOUSAF, N. & LARKIN, J. 2013. Melanoma epidemiology, biology and prognosis. *EJC supplements : EJC : official journal of EORTC, European Organization for Research and Treatment of Cancer ... [et al.],* 11**,** 81-91.

ALLEN, D. & WESTERBLAD, H. 2004. Physiology. Lactic acid--the latest performance-enhancing drug. *Science,* 305**,** 1112-3.

ALONSO-CURBELO, D., RIVEIRO-FALKENBACH, E., P¢REZ-GUIJARRO, E., CIFDALOZ, M., KARRAS, P., OSTERLOH, L., MEGýAS, D., CA*Cancer Cell,* 26**,** 61-76.

ALPER, S. L. 2009. Molecular physiology and genetics of Na+-independent SLC4 anion exchangers. *The Journal of experimental biology,* 212**,** 1672-1683.

ALPER, S. L. 2010. Familial renal tubular acidosis. *Journal of nephrology,* 23 Suppl 16**,** S57-S76.

ALPER, S. L., STUART-TILLEY, A., SIMMONS, C. F., BROWN, D. & DRENCKHAHN, D. 1994. The fodrin-ankyrin cytoskeleton of choroid plexus preferentially colocalizes with apical Na+K(+)-ATPase rather than with basolateral anion exchanger AE2. *The Journal of clinical investigation,* 93**,** 1430-1438.

ALTENBERG, B. & GREULICH, K. O. 2004. Genes of glycolysis are ubiquitously overexpressed in 24 cancer classes. *Genomics,* 84**,** 1014-20.

ALZAMORA, R., THALI, R. F., GONG, F., SMOLAK, C., LI, H., BATY, C. J., BERTRAND, C. A., AUCHLI, Y., BRUNISHOLZ, R. A., NEUMANN, D., HALLOWS, K. R. & PASTOR-SOLER, N. M. 2010. PKA regulates vacuolar H+-ATPase localization and activity via direct phosphorylation of the a subunit in kidney cells. *The Journal of biological chemistry,* 285**,** 24676-24685.

AMIEL, J., WATKIN, P. M., TASSABEHJI, M., READ, A. P. & WINTER, R. M. 1998. Mutation of the MITF gene in albinism-deafness syndrome (Tietz syndrome). *Clin Dysmorphol,* 7**,** 17-20.

AMITH, S. R. & FLIEGEL, L. 2013. Regulation of the Na⁺/H⁺ Exchanger (NHE1) in Breast Cancer Metastasis. *Cancer Research,* 73**,** 1259.

AMMAR, Y. B., TAKEDA, S., HISAMITSU, T., MORI, H. & WAKABAYASHI, S. 2006. Crystal structure of CHP2 complexed with NHE1-cytosolic region and an implication for pH regulation. *Embo j,* 25**,** 2315-25.

ANDREUCCI, E., PEPPICELLI, S., CARTA, F., BRISOTTO, G., BISCONTIN, E., RUZZOLINI, J., BIANCHINI, F., BIAGIONI, A., SUPURAN, C. T. & CALORINI, L. 2017. Carbonic anhydrase IX inhibition affects viability of cancer cells adapted to extracellular acidosis. *J Mol Med (Berl),* 95**,** 1341-1353.

ANELLO, M., DAVERIO, M. S., SILBESTRO, M. B., VIDAL-RIOJA, L. & DI ROCCO, F. 2019.

Characterization and expression analysis of KIT and MITF-M genes in llamas and their relation to white coat color. *Anim Genet,* 50**,** 143-149.

AOKI, H. & MORO, O. 2002. Involvement of microphthalmia-associated transcription factor (MITF) in expression of human melanocortin-1 receptor (MC1R). *Life Sciences,* 71**,** 2171-2179.

ARNHEITER, H. 2010. The discovery of the microphthalmia locus and its gene, Mitf. *Pigment cell & melanoma research,* 23**,** 729-735.

AROZARENA, I. & WELLBROCK, C. 2019. Phenotype plasticity as enabler of melanoma progression and therapy resistance. *Nature reviews. Cancer,* 19**,** 377-391.

ATEFI, M., VON EUW, E., ATTAR, N., NG, C., CHU, C., GUO, D., NAZARIAN, R., CHMIELOWSKI, B., GLASPY, J. A., COMIN-ANDUIX, B., MISCHEL, P. S., LO, R. S. & RIBAS, A. 2011. Reversing melanoma cross-resistance to BRAF and MEK inhibitors by co-targeting the AKT/mTOR pathway. *PloS one,* 6**,** e28973-e28973.

B¢JAR, J., HONG, Y. & SCHARTL, M. 2003. Mitf expression is sufficient to direct differentiation of medaka blastula derived stem cells to melanocytes. *Development,* 130**,** 6545.

BAHADORAN, P., ABERDAM, E., MANTOUX, F., BUSCð, R., BILLE, K., YALMAN, N., DE SAINT-BASILE, G., CASAROLI-MARANO, R., ORTONNE, J.-P. & BALLOTTI, R. 2001. Rab27a: A Key to Melanosome Transport in Human Melanocytes. *Journal of Cell Biology,* 152**,** 843-850.

BAI, X., FISHER, D. E. & FLAHERTY, K. T. 2019. Cell-state dynamics and therapeutic resistance in melanoma from the perspective of MITF and IFNγ pathways. *Nature reviews. Clinical oncology,* 16**,** 549-562.

BALAMURUGAN, K. 2016. HIF-1 at the crossroads of hypoxia, inflammation, and cancer. *Int J Cancer,* 138**,** 1058-66.

BAR-PELED, L., SCHWEITZER, L. D., ZONCU, R. & SABATINI, D. M. 2012. Ragulator is a GEF for the rag GTPases that signal amino acid levels to mTORC1. *Cell,* 150**,** 1196-1208.

BARKLEY, R. A., CHAKRAVARTI, A., COOPER, R. S., ELLISON, R. C., HUNT, S. C., PROVINCE, M. A., TURNER, S. T., WEDER, A. B., BOERWINKLE, E. & FAMILY BLOOD PRESSURE, P. 2004. Positional identification of hypertension susceptibility genes on chromosome 2. *Hypertension (Dallas, Tex. : 1979),* 43**,** 477-482.

BARRETINA, J., CAPONIGRO, G., STRANSKY, N., VENKATESAN, K., MARGOLIN, A. A., KIM, S., WILSON, C. J., LEHAR, J., KRYUKOV, G. V., SONKIN, D., REDDY, A., LIU, M., MURRAY, L., BERGER, M. F., MONAHAN, J. E., MORAIS, P., MELTZER, J., KOREJWA, A., JANE-VALBUENA, J., MAPA, F. A., THIBAULT, J., BRIC-FURLONG,

E., RAMAN, P., SHIPWAY, A., ENGELS, I. H., CHENG, J., YU, G. K., YU, J., ASPESI, P., JR., DE SILVA, M., JAGTAP, K., JONES, M. D., WANG, L., HATTON, C., PALESCANDOLO, E., GUPTA, S., MAHAN, S., SOUGNEZ, C., ONOFRIO, R. C., LIEFELD, T., MACCONAILL, L., WINCKLER, W., REICH, M., LI, N., MESIROV, J. P., GABRIEL, S. B., GETZ, G., ARDLIE, K., CHAN, V., MYER, V. E., WEBER, B. L., PORTER, J., WARMUTH, M., FINAN, P., HARRIS, J. L., MEYERSON, M., GOLUB, T. R., MORRISSEY, M. P., SELLERS, W. R., SCHLEGEL, R. & GARRAWAY, L. A. 2012. The Cancer Cell Line Encyclopedia enables predictive modelling of anticancer drug sensitivity. *Nature,* 483**,** 603-7.

BARZILAY, M., SHIP, S. & CABANTCHIK, Z. I. 1979. Anion transport in red blood cells. I. Chemical properties of anion recognition sites as revealed by structure-activity relationships of aromatic sulfonic acids. *Membrane biochemistry,* 2**,** 227-254.

BELL, R. E. & LEVY, C. 2011. The three M's: melanoma, microphthalmia-associated transcription factor and microRNA. *Pigment Cell Melanoma Res,* 24**,** 1088-106.

BENGA, G. 2001. Basic studies on gene therapy of human malignant melanoma by use of the human interferon β gene entrapped in cationic multilamellar liposomes.: 1. Morphology and growth rate of six melanoma cell lines used in transfection experiments with the human interferon β gene. *Journal of Cellular and Molecular Medicine,* 5**,** 402-408.

BENJAMIN, D., ROBAY, D., HINDUPUR, S. K., POHLMANN, J., COLOMBI, M., EL-SHEMERLY, M. Y., MAIRA, S.-M., MORONI, C., LANE, H. A. & HALL, M. N. 2018. Dual Inhibition of the Lactate Transporters MCT1 and MCT4 Is Synthetic Lethal with Metformin due to NAD+ Depletion in Cancer Cells. *Cell reports,* 25**,** 3047-3058.e4.

BENNETT, D. C. 2008. How to make a melanoma: what do we know of the primary clonal events? *Pigment Cell Melanoma Res,* 21**,** 27-38.

BENTLEY, N. J., EISEN, T. & GODING, C. R. 1994. Melanocyte-specific expression of the human tyrosinase promoter: activation by the microphthalmia gene product and role of the initiator. *Molecular and cellular biology,* 14**,** 7996-8006.

BERGERSEN, L., WöRHAUG, O., HELM, J., THOMAS, M., LAAKE, P., DAVIES, A. J., WILSON, M. C., HALESTRAP, A. P. & OTTERSEN, O. P. 2001. A novel postsynaptic density protein: the monocarboxylate transporter MCT2 is co-localized with δ-glutamate receptors in postsynaptic densities of parallel fiber–Purkinje cell synapses. *Experimental Brain Research,* 136**,** 523-534.

BERTOLOTTO, C., BUSCð, R., ABBE, P., BILLE, K., ABERDAM, E., ORTONNE, J. P. & BALLOTTI, R. 1998. Different cis-acting elements are involved in the regulation

of TRP1 and TRP2 promoter activities by cyclic AMP: pivotal role of M boxes (GTCATGTGCT) and of microphthalmia. *Molecular and cellular biology,* 18**,** 694-702.

BERTOLOTTO, C., LESUEUR, F., GIULIANO, S., STRUB, T., DE LICHY, M., BILLE, K., DESSEN, P., D'HAYER, B., MOHAMDI, H., REMENIERAS, A., MAUBEC, E., DE LA FOUCHARDIERE, A., MOLINIE, V., VABRES, P., DALLE, S., POULALHON, N., MARTIN-DENAVIT, T., THOMAS, L., ANDRY-BENZAQUEN, P., DUPIN, N., BOITIER, F., ROSSI, A., PERROT, J. L., LABEILLE, B., ROBERT, C., ESCUDIER, B., CARON, O., BRUGIERES, L., SAULE, S., GARDIE, B., GAD, S., RICHARD, S., COUTURIER, J., TEH, B. T., GHIORZO, P., PASTORINO, L., PUIG, S., BADENAS, C., OLSSON, H., INGVAR, C., ROULEAU, E., LIDEREAU, R., BAHADORAN, P., VIELH, P., CORDA, E., BLANCHE, H., ZELENIKA, D., GALAN, P., AUBIN, F., BACHOLLET, B., BECUWE, C., BERTHET, P., BIGNON, Y. J., BONADONA, V., BONAFE, J. L., BONNET-DUPEYRON, M. N., CAMBAZARD, F., CHEVRANT-BRETON, J., COUPIER, I., DALAC, S., DEMANGE, L., D'INCAN, M., DUGAST, C., FAIVRE, L., VINCENT-FETITA, L., GAUTHIER-VILLARS, M., GILBERT, B., GRANGE, F., GROB, J. J., HUMBERT, P., JANIN, N., JOLY, P., KEROB, D., LASSET, C., LEROUX, D., LEVANG, J., LIMACHER, J. M., LIVIDEANU, C., LONGY, M., LORTHOLARY, A., STOPPA-LYONNET, D., MANSARD, S., MANSUY, L., MARROU, K., MATEUS, C., MAUGARD, C., MEYER, N., NOGUES, C., SOUTEYRAND, P., VENAT-BOUVET, L., ZATTARA, H., CHAUDRU, V., LENOIR, G. M., LATHROP, M., DAVIDSON, I., AVRIL, M. F., DEMENAIS, F., BALLOTTI, R. & BRESSAC-DE PAILLERETS, B. 2011. A SUMOylation-defective MITF germline mutation predisposes to melanoma and renal carcinoma. *Nature,* 480**,** 94-8.

BEURET, L., FLORI, E., DENOYELLE, C., BILLE, K., BUSCA, R., PICARDO, M., BERTOLOTTO, C. & BALLOTTI, R. 2007. Up-regulation of MET expression by alpha-melanocyte-stimulating hormone and MITF allows hepatocyte growth factor to protect melanocytes and melanoma cells from apoptosis. *The Journal of biological chemistry,* 282**,** 14140-14147.

BEYENBACH, K. W. & WIECZOREK, H. 2006. The V-type H⁺ ATPase: molecular structure and function, physiological roles and regulation. *Journal of Experimental Biology,* 209**,** 577.

BIECHELE, T. L., KULIKAUSKAS, R. M., TORONI, R. A., LUCERO, O. M., SWIFT, R. D., JAMES, R. G., ROBIN, N. C., DAWSON, D. W., MOON, R. T. & CHIEN, A. J. 2012. Wnt/β-catenin signaling and AXIN1 regulate apoptosis triggered by inhibition of the mutant kinase BRAFV600E in human melanoma. *Science signaling,* 5**,** ra3-ra3.

BISMUTH, K., MARIC, D. & ARNHEITER, H. 2005. MITF and cell proliferation: the role

of alternative splice forms. *Pigment cell research,* 18**,** 349-359.

BITTNER, M., MELTZER, P., CHEN, Y., JIANG, Y., SEFTOR, E., HENDRIX, M., RADMACHER, M., SIMON, R., YAKHINI, Z., BEN-DOR, A., SAMPAS, N., DOUGHERTY, E., WANG, E., MARINCOLA, F., GOODEN, C., LUEDERS, J., GLATFELTER, A., POLLOCK, P., CARPTEN, J., GILLANDERS, E., LEJA, D., DIETRICH, K., BEAUDRY, C., BERENS, M., ALBERTS, D., SONDAK, V., HAYWARD, N. & TRENT, J. 2000. Molecular classification of cutaneous malignant melanoma by gene expression profiling. *Nature,* 406**,** 536-540.

BOHME, I. & BOSSERHOFF, A. 2020. Extracellular acidosis triggers a senescence-like phenotype in human melanoma cells. *Pigment Cell Melanoma Res,* 33**,** 41-51.

BOHME, I. & BOSSERHOFF, A. K. 2016. Acidic tumor microenvironment in human melanoma. *Pigment Cell Melanoma Res,* 29**,** 508-23.

BOK, D., GALBRAITH, G., LOPEZ, I., WOODRUFF, M., NUSINOWITZ, S., BELTRANDELRIO, H., HUANG, W., ZHAO, S., GESKE, R., MONTGOMERY, C., VAN SLIGTENHORST, I., FRIDDLE, C., PLATT, K., SPARKS, M. J., PUSHKIN, A., ABULADZE, N., ISHIYAMA, A., DUKKIPATI, R., LIU, W. & KURTZ, I. 2003. Blindness and auditory impairment caused by loss of the sodium bicarbonate cotransporter NBC3. *Nature genetics,* 34**,** 313-319.

BOK, D., SCHIBLER, M. J., PUSHKIN, A., SASSANI, P., ABULADZE, N., NASER, Z. & KURTZ, I. 2001. Immunolocalization of electrogenic sodium-bicarbonate cotransporters pNBC1 and kNBC1 in the rat eye. *American journal of physiology. Renal physiology,* 281**,** F920-F935.

BONDURAND, N., PINGAULT, V., GOERICH, D. E., LEMORT, N., SOCK, E., CAIGNEC, C. L., WEGNER, M. & GOOSSENS, M. 2000. Interaction among SOX10, PAX3 and MITF, three genes altered in Waardenburg syndrome. *Human Molecular Genetics,* 9**,** 1907-1917.

BORON, W. F., CHEN, L. & PARKER, M. D. 2009. Modular structure of sodium-coupled bicarbonate transporters. *The Journal of experimental biology,* 212**,** 1697-1706.

BORON, W. F. & DE WEER, P. 1976. Active proton transport stimulated by CO2/HCO3-, blocked by cyanide. *Nature,* 259**,** 240-241.

BORON, W. F., HOGAN, E. & RUSSELL, J. M. 1988. pH-sensitive activation of the intracellular-pH regulation system in squid axons by ATP-gamma-S. *Nature,* 332**,** 262-265.

BOSHUIZEN, J., KOOPMAN, L. A., KRIJGSMAN, O., SHAHRABI, A., VAN DEN HEUVEL, E. G., LIGTENBERG, M. A., VREDEVOOGD, D. W., KEMPER, K., KUILMAN, T., SONG, J.-Y., PENCHEVA, N., MORTENSEN, J. T., FOPPEN, M. G., ROZEMAN, E. A., BLANK, C. U., JANMAAT, M. L., SATIJN, D., BREIJ, E. C. W., PEEPER, D. S. &

PARREN, P. W. H. I. 2018. Cooperative targeting of melanoma heterogeneity with an AXL antibody-drug conjugate and BRAF/MEK inhibitors. *Nature Medicine,* 24**,** 203.

BOUCH¢, V., ESPINOSA, A. P., LEONE, L., SARDIELLO, M., BALLABIO, A. & BOTAS, J. 2016. Drosophila Mitf regulates the V-ATPase and the lysosomal-autophagic pathway. *Autophagy,* 12**,** 484-498.

BOUMAHDI, S. & DE SAUVAGE, F. J. 2020. The great escape: tumour cell plasticity in resistance to targeted therapy. *Nature Reviews Drug Discovery,* 19**,** 39-56.

BOUTROS, C., TARHINI, A., ROUTIER, E., LAMBOTTE, O., LADURIE, F. L., CARBONNEL, F., IZZEDDINE, H., MARABELLE, A., CHAMPIAT, S., BERDELOU, A., LANOY, E., TEXIER, M., LIBENCIUC, C., EGGERMONT, A. M. M., SORIA, J.-C., MATEUS, C. & ROBERT, C. 2016. Safety profiles of anti-CTLA-4 and anti-PD-1 antibodies alone and in combination. *Nature Reviews Clinical Oncology,* 13**,** 473-486.

BOYLE, G. M., WOODS, S. L., BONAZZI, V. F., STARK, M. S., HACKER, E., AOUDE, L. G., DUTTON-REGESTER, K., COOK, A. L., STURM, R. A. & HAYWARD, N. K. 2011. Melanoma cell invasiveness is regulated by miR-211 suppression of the BRN2 transcription factor. *Pigment Cell Melanoma Res,* 24**,** 525-37.

BR*The Biochemical journal,* 341 (Pt 3)**,** 529-535.

BRESLOW, A. 1970. Thickness, cross-sectional areas and depth of invasion in the prognosis of cutaneous melanoma. *Annals of surgery,* 172**,** 902-908.

BRETON, S. & BROWN, D. 2013. Regulation of luminal acidification by the V-ATPase. *Physiology (Bethesda),* 28**,** 318-29.

BROWN, V. L., HARWOOD, C. A., CROOK, T., CRONIN, J. G., KELSELL, D. P. & PROBY, C. M. 2004. p16INK4a and p14ARF tumor suppressor genes are commonly inactivated in cutaneous squamous cell carcinoma. *The Journal of investigative dermatology,* 122**,** 1284-1292.

BUKA, R., FRIEDMAN, K. A., PHELPS, R. G., SILVER, L., CALERO, F. & RUDIKOFF, D. 2001. Childhood longitudinal melanonychia: case reports and review of the literature. *The Mount Sinai journal of medicine, New York,* 68**,** 331-335.

CAPECCI, J. & FORGAC, M. 2013. The function of vacuolar ATPase (V-ATPase) a subunit isoforms in invasiveness of MCF10a and MCF10CA1a human breast cancer cells. *The Journal of biological chemistry,* 288**,** 32731-32741.

CARAMEL, J., PAPADOGEORGAKIS, E., HILL, L., BROWNE, GARETH J., RICHARD, G., WIERINCKX, A., SALDANHA, G., OSBORNE, J., HUTCHINSON, P., TSE, G., LACHUER, J., PUISIEUX, A., PRINGLE, J. H., ANSIEAU, S. & TULCHINSKY, E. 2013. A Switch in the Expression of Embryonic EMT-Inducers Drives the Development of Malignant Melanoma. *Cancer Cell,* 24**,** 466-480.

CARREIRA, S., GOODALL, J., AKSAN, I., LA ROCCA, S. A., GALIBERT, M.-D., DENAT, L.,

LARUE, L. & GODING, C. R. 2005. Mitf cooperates with Rb1 and activates p21Cip1 expression to regulate cell cycle progression. *Nature,* 433**,** 764-769.

CARREIRA, S., GOODALL, J., DENAT, L., RODRIGUEZ, M., NUCIFORO, P., HOEK, K. S., TESTORI, A., LARUE, L. & GODING, C. R. 2006. Mitf regulation of Dia1 controls melanoma proliferation and invasiveness. *Genes & Development,* 20**,** 3426-3439.

CH'EN, F. F., VILLAFUERTE, F. C., SWIETACH, P., COBDEN, P. M. & VAUGHAN-JONES, R. D. 2008. S0859, an N-cyanosulphonamide inhibitor of sodium-bicarbonate cotransport in the heart. *Br J Pharmacol,* 153**,** 972-82.

CHAPMAN, P. B., HAUSCHILD, A., ROBERT, C., HAANEN, J. B., ASCIERTO, P., LARKIN, J., DUMMER, R., GARBE, C., TESTORI, A., MAIO, M., HOGG, D., LORIGAN, P., LEBBE, C., JOUARY, T., SCHADENDORF, D., RIBAS, A., O'DAY, S. J., SOSMAN, J. A., KIRKWOOD, J. M., EGGERMONT, A. M. M., DRENO, B., NOLOP, K., LI, J., NELSON, B., HOU, J., LEE, R. J., FLAHERTY, K. T. & MCARTHUR, G. A. 2011. Improved Survival with Vemurafenib in Melanoma with BRAF V600E Mutation. *New England Journal of Medicine,* 364**,** 2507-2516.

CHELI, Y., OHANNA, M., BALLOTTI, R. & BERTOLOTTO, C. 2010. Fifteen-year quest for microphthalmia-associated transcription factor target genes. *Pigment Cell Melanoma Res,* 23**,** 27-40.

CHEN, G.-S., LEE, S.-P., HUANG, S.-F., CHAO, S.-C., CHANG, C.-Y., WU, G.-J., LI, C.-H. & LOH, S.-H. 2018. Functional and molecular characterization of transmembrane intracellular pH regulators in human dental pulp stem cells. *Archives of oral biology,* 90**,** 19-26.

CHEN, T., WANG, H., LIU, Y., ZHAO, B., ZHAO, Y., FAN, R., WANG, P. & DONG, C. 2016. Ocular Albinism Type 1 Regulates Melanogenesis in Mouse Melanocytes. *International journal of molecular sciences,* 17**,** 1596.

CHEN, Y., HU, S., MU, L., ZHAO, B., WANG, M., YANG, N., BAO, G., ZHU, C. & WU, X. 2019. Slc7a11 Modulated by POU2F1 is Involved in Pigmentation in Rabbit. *International journal of molecular sciences,* 20**,** 2493.

CHEUNG, J. C., LI, J. & REITHMEIER, R. A. F. 2005. Topology of transmembrane segments 1-4 in the human chloride/bicarbonate anion exchanger 1 (AE1) by scanning N-glycosylation mutagenesis. *The Biochemical journal,* 390**,** 137-144.

CHIAVERINI, C., BEURET, L., FLORI, E., BUSCA, R., ABBE, P., BILLE, K., BAHADORAN, P., ORTONNE, J. P., BERTOLOTTO, C. & BALLOTTI, R. 2008. Microphthalmia-associated transcription factor regulates RAB27A gene expression and controls melanosome transport. *J Biol Chem,* 283**,** 12635-42.

CHICHE, J., BRAHIMI-HORN, M. C. & POUYSS¢GUR, J. 2010. Tumour hypoxia induces a metabolic shift causing acidosis: a common feature in cancer. *Journal of*

cellular and molecular medicine, 14**,** 771-794.

CHOI, I., AALKJAER, C., BOULPAEP, E. L. & BORON, W. F. 2000. An electroneutral sodium/bicarbonate cotransporter NBCn1 and associated sodium channel. *Nature,* 405**,** 571-575.

CHOI, J., XU, M., MAKOWSKI, M. M., ZHANG, T., LAW, M. H., KOVACS, M. A., GRANZHAN, A., KIM, W. J., PARIKH, H., GARTSIDE, M., TRENT, J. M., TEULADE-FICHOU, M.-P., ILES, M. M., NEWTON-BISHOP, J. A., BISHOP, D. T., MACGREGOR, S., HAYWARD, N. K., VERMEULEN, M. & BROWN, K. M. 2017. A common intronic variant of PARP1 confers melanoma risk and mediates melanocyte growth via regulation of MITF. *Nature Genetics,* 49**,** 1326.

CHUNG, C., MADER, C. C., SCHMITZ, J. C., ATLADOTTIR, J., FITCHEV, P., CORNWELL, M. L., KOLESKE, A. J., CRAWFORD, S. E. & GORELICK, F. 2011. The vacuolar-ATPase modulates matrix metalloproteinase isoforms in human pancreatic cancer. *Laboratory investigation; a journal of technical methods and pathology,* 91**,** 732-743.

CICHOREK, M., WACHULSKA, M., STASIEWICZ, A. & TYMIŃSKA, A. 2013. Skin melanocytes: biology and development. *Postepy dermatologii i alergologii,* 30**,** 30-41.

CLARK, W. H., JR., ELDER, D. E. & VAN HORN, M. 1986. The biologic forms of malignant melanoma. *Human pathology,* 17**,** 443-450.

CLARK, W. H., JR., FROM, L., BERNARDINO, E. A. & MIHM, M. C. 1969. The histogenesis and biologic behavior of primary human malignant melanomas of the skin. *Cancer research,* 29**,** 705-727.

CLARK, W. H., JR. & MIHM, M. C., JR. 1969. Lentigo maligna and lentigo-maligna melanoma. *The American journal of pathology,* 55**,** 39-67.

CLEMENT, D. L., MALLY, S., STOCK, C., LETHAN, M., SATIR, P., SCHWAB, A., PEDERSEN, S. F. & CHRISTENSEN, S. T. 2013. PDGFRα signaling in the primary cilium regulates NHE1-dependent fibroblast migration via coordinated differential activity of MEK1/2-ERK1/2-p90RSK and AKT signaling pathways. *Journal of cell science,* 126**,** 953-965.

COLEMAN, W. P., 3RD, LORIA, P. R., REED, R. J. & KREMENTZ, E. T. 1980. Acral lentiginous melanoma. *Archives of dermatology,* 116**,** 773-776.

COLES, L., LITT, J., HATTA, H. & BONEN, A. 2004. Exercise rapidly increases expression of the monocarboxylate transporters MCT1 and MCT4 in rat muscle. *The Journal of physiology,* 561**,** 253-261.

COOPER, D. S., YANG, H. S., HE, P., KIM, E., RAJBHANDARI, I., YUN, C. C. & CHOI, I. 2009. Sodium/bicarbonate cotransporter NBCn1/slc4a7 increases cytotoxicity in magnesium depletion in primary cultures of hippocampal neurons.

European Journal of Neuroscience, 29**,** 437-446.

CORBET, C. & FERON, O. 2017. Tumour acidosis: from the passenger to the driver's seat. *Nat Rev Cancer,* 17**,** 577-593.

CORBET, C., PINTO, A., MARTHERUS, R., SANTIAGO DE JESUS, J. P., POLET, F. & FERON, O. 2016. Acidosis Drives the Reprogramming of Fatty Acid Metabolism in Cancer Cells through Changes in Mitochondrial and Histone Acetylation. *Cell Metab,* 24**,** 311-23.

CORCORAN, R. B., DIAS-SANTAGATA, D., BERGETHON, K., IAFRATE, A. J., SETTLEMAN, J. & ENGELMAN, J. A. 2010. BRAF gene amplification can promote acquired resistance to MEK inhibitors in cancer cells harboring the BRAF V600E mutation. *Science signaling,* 3**,** ra84-ra84.

COTTER, K., CAPECCI, J., SENNOUNE, S., HUSS, M., MAIER, M., MARTINEZ-ZAGUILAN, R. & FORGAC, M. 2015a. Activity of plasma membrane V-ATPases is critical for the invasion of MDA-MB231 breast cancer cells. *The Journal of biological chemistry,* 290**,** 3680-3692.

COTTER, K., STRANSKY, L., MCGUIRE, C. & FORGAC, M. 2015b. Recent Insights into the Structure, Regulation, and Function of the V-ATPases. *Trends in biochemical sciences,* 40**,** 611-622.

CRAIG, E. A. & SPIEGELMAN, V. S. 2012. Inhibition of coding region determinant binding protein sensitizes melanoma cells to chemotherapeutic agents. *Pigment Cell Melanoma Res,* 25**,** 83-7.

CRONIN, J. C., WUNDERLICH, J., LOFTUS, S. K., PRICKETT, T. D., WEI, X., RIDD, K., VEMULA, S., BURRELL, A. S., AGRAWAL, N. S., LIN, J. C., BANISTER, C. E., BUCKHAULTS, P., ROSENBERG, S. A., BASTIAN, B. C., PAVAN, W. J. & SAMUELS, Y. 2009. Frequent mutations in the MITF pathway in melanoma. *Pigment Cell Melanoma Res,* 22**,** 435-44.

CRUCIAT, C.-M., OHKAWARA, B., ACEBRON, S. P., KARAULANOV, E., REINHARD, C., INGELFINGER, D., BOUTROS, M. & NIEHRS, C. 2010. Requirement of prorenin receptor and vacuolar H+-ATPase-mediated acidification for Wnt signaling. *Science (New York, N.Y.),* 327**,** 459-463.

CUCORANU, D., COOPER, D., SHYNTUM, D., CHEN, G., KLEIN, J., SANDS, J. & CHOI, I. Quantitative measurements of the electroneutral Na/bicarbonate cotransporter (NBCn1) expression in chronic metabolic acidosis. FASEB JOURNAL, 2004. FEDERATION AMER SOC EXP BIOL 9650 ROCKVILLE PIKE, BETHESDA, MD 20814-3998 USA, A1018-A1018.

CURTIS, N. J., MOONEY, L., HOPCROFT, L., MICHOPOULOS, F., WHALLEY, N., ZHONG, H., MURRAY, C., LOGIE, A., REVILL, M., BYTH, K. F., BENJAMIN, A. D., FIRTH, M. A., GREEN, S., SMITH, P. D. & CRITCHLOW, S. E. 2017. Pre-clinical

pharmacology of AZD3965, a selective inhibitor of MCT1: DLBCL, NHL and Burkitt's lymphoma anti-tumor activity. *Oncotarget,* 8**,** 69219-69236.

D'MELLO, S. A. N., FINLAY, G. J., BAGULEY, B. C. & ASKARIAN-AMIRI, M. E. 2016. Signaling Pathways in Melanogenesis. *International journal of molecular sciences,* 17**,** 1144.

DAVIES, H., BIGNELL, G. R., COX, C., STEPHENS, P., EDKINS, S., CLEGG, S., TEAGUE, J., WOFFENDIN, H., GARNETT, M. J., BOTTOMLEY, W., DAVIS, N., DICKS, E., EWING, R., FLOYD, Y., GRAY, K., HALL, S., HAWES, R., HUGHES, J., KOSMIDOU, V., MENZIES, A., MOULD, C., PARKER, A., STEVENS, C., WATT, S., HOOPER, S., WILSON, R., JAYATILAKE, H., GUSTERSON, B. A., COOPER, C., SHIPLEY, J., HARGRAVE, D., PRITCHARD-JONES, K., MAITLAND, N., CHENEVIX-TRENCH, G., RIGGINS, G. J., BIGNER, D. D., PALMIERI, G., COSSU, A., FLANAGAN, A., NICHOLSON, A., HO, J. W., LEUNG, S. Y., YUEN, S. T., WEBER, B. L., SEIGLER, H. F., DARROW, T. L., PATERSON, H., MARAIS, R., MARSHALL, C. J., WOOSTER, R., STRATTON, M. R. & FUTREAL, P. A. 2002. Mutations of the BRAF gene in human cancer. *Nature,* 417**,** 949-54.

DAVIES, M. A. 2012. The role of the PI3K-AKT pathway in melanoma. *Cancer journal (Sudbury, Mass.),* 18**,** 142-147.

DAVIS, L. E., SHALIN, S. C. & TACKETT, A. J. 2019. Current state of melanoma diagnosis and treatment. *Cancer Biology & Therapy,* 20**,** 1366-1379.

DE LA SERNA, I. L., OHKAWA, Y., HIGASHI, C., DUTTA, C., OSIAS, J., KOMMAJOSYULA, N., TACHIBANA, T. & IMBALZANO, A. N. 2006. The microphthalmia-associated transcription factor requires SWI/SNF enzymes to activate melanocyte-specific genes. *The Journal of biological chemistry,* 281**,** 20233-20241.

DE SEIGNEUX, S., MALTE, H., DIMKE, H., FR*American Journal of Physiology-Renal Physiology,* 292**,** F1256-F1266.

DECHANT, R., SAAD, S., IBñ*Molecular cell,* 55**,** 409-421.

DELGADO-GONI, T., MINIOTIS, M. F., WANTUCH, S., PARKES, H. G., MARAIS, R., WORKMAN, P., LEACH, M. O. & BELOUECHE-BABARI, M. 2016. The BRAF Inhibitor Vemurafenib Activates Mitochondrial Metabolism and Inhibits Hyperpolarized Pyruvate-Lactate Exchange in BRAF-Mutant Human Melanoma Cells. *Molecular cancer therapeutics,* 15**,** 2987-2999.

DEMIERRE, M.-F., CHUNG, C., MILLER, D. R. & GELLER, A. C. 2005. Early detection of thick melanomas in the United States: beware of the nodular subtype. *Archives of dermatology,* 141**,** 745-750.

DEMUTH, D. R., SHOWE, L. C., BALLANTINE, M., PALUMBO, A., FRASER, P. J., CIOE, L., ROVERA, G. & CURTIS, P. J. 1986. Cloning and structural characterization of a human non-erythroid band 3-like protein. *The EMBO journal,* 5**,** 1205-1214.

DENECKER, G., VANDAMME, N., AKAY, Ö., KOLUDROVIC, D., TAMINAU, J., LEMEIRE, K., GHELDOF, A., DE CRAENE, B., VAN GELE, M., BROCHEZ, L., UDUPI, G. M., RAFFERTY, M., BALINT, B., GALLAGHER, W. M., GHANEM, G., HUYLEBROECK, D., HAIGH, J., VAN DEN OORD, J., LARUE, L., DAVIDSON, I., MARINE, J. C. & BERX, G. 2014. Identification of a ZEB2-MITF-ZEB1 transcriptional network that controls melanogenesis and melanoma progression. *Cell Death And Differentiation,* 21**,** 1250.

DENKER, S. P., HUANG, D. C., ORLOWSKI, J., FURTHMAYR, H. & BARBER, D. L. 2000. Direct binding of the Na--H exchanger NHE1 to ERM proteins regulates the cortical cytoskeleton and cell shape independently of H(+) translocation. *Molecular cell,* 6**,** 1425-1436.

DEUTICKE, B. 1982. Monocarboxylate transport in erythrocytes. *The Journal of Membrane Biology,* 70**,** 89-103.

DING, J., NG, R. W. P. & FLIEGEL, L. 2007. Functional characterization of the transmembrane segment VII of the NHE1 isoform of the Na+/H+ exchanger. *Canadian journal of physiology and pharmacology,* 85**,** 319-325.

DIX, J. A., VERKMAN, A. S., SOLOMON, A. K. & CANTLEY, L. C. 1979. Human erythrocyte anion exchange site characterised using a fluorescent probe. *Nature,* 282**,** 520-522.

DOHERTY, J. R., YANG, C., SCOTT, K. E. N., CAMERON, M. D., FALLAHI, M., LI, W., HALL, M. A., AMELIO, A. L., MISHRA, J. K., LI, F., TORTOSA, M., GENAU, H. M., ROUNBEHLER, R. J., LU, Y., DANG, C. V., KUMAR, K. G., BUTLER, A. A., BANNISTER, T. D., HOOPER, A. T., UNSAL-KACMAZ, K., ROUSH, W. R. & CLEVELAND, J. L. 2014. Blocking lactate export by inhibiting the Myc target MCT1 Disables glycolysis and glutathione synthesis. *Cancer research,* 74**,** 908-920.

DOOLEY, C. M., SCHWARZ, H., MUELLER, K. P., MONGERA, A., KONANTZ, M., NEUHAUSS, S. C. F., N*Pigment cell & melanoma research,* 26**,** 205-217.

DORAN, D. M., KULKARNI-DATAR, K., COOL, D. R. & BROWN, T. L. 2011. Hypoxia activates constitutive luciferase reporter constructs. *Biochimie,* 93**,** 361-368.

DU, J. & FISHER, D. E. 2002. Identification of Aim-1 as the underwhite mouse mutant and its transcriptional regulation by MITF. *J Biol Chem,* 277**,** 402-6.

DU, J., MILLER, A. J., WIDLUND, H. R., HORSTMANN, M. A., RAMASWAMY, S. & FISHER, D. E. 2003. MLANA/MART1 and SILV/PMEL17/GP100 are transcriptionally regulated by MITF in melanocytes and melanoma. *The American journal of pathology,* 163**,** 333-343.

DU, J., WIDLUND, H. R., HORSTMANN, M. A., RAMASWAMY, S., ROSS, K., HUBER, W. E., NISHIMURA, E. K., GOLUB, T. R. & FISHER, D. E. 2004. Critical role of CDK2

for melanoma growth linked to its melanocyte-specific transcriptional regulation by MITF. *Cancer Cell,* 6**,** 565-576.

DUFFY, D. L., ZHAO, Z. Z., STURM, R. A., HAYWARD, N. K., MARTIN, N. G. & MONTGOMERY, G. W. 2010. Multiple pigmentation gene polymorphisms account for a substantial proportion of risk of cutaneous malignant melanoma. *The Journal of investigative dermatology,* 130**,** 520-528.

DýAZ, R. G., ESCUDERO, D. S., BREA, M. S., MORGAN, P. E. & P¢REZ, N. G. 2019. p38 mitogen activated protein kinase mediates cardiac Na(+)/H(+) exchanger inhibition induced by Sildenafil. *European journal of pharmacology,* 849**,** 96-105.

EAGLE, H., BARBAN, S., LEVY, M. & SCHULZE, H. O. 1958. The utilization of carbohydrates by human cell cultures. *The Journal of biological chemistry,* 233**,** 551-558.

ECCLES, M. R., HE, S., AHN, A., SLOBBE, L. J., JEFFS, A. R., YOON, H.-S. & BAGULEY, B. C. 2013. MITF and PAX3 Play Distinct Roles in Melanoma Cell Migration; Outline of a "Genetic Switch" Theory Involving MITF and PAX3 in Proliferative and Invasive Phenotypes of Melanoma. *Frontiers in oncology,* 3**,** 229-229.

EDLUND, G. L. & HALESTRAP, A. P. 1988. The kinetics of transport of lactate and pyruvate into rat hepatocytes. Evidence for the presence of a specific carrier similar to that in erythrocytes. *The Biochemical journal,* 249**,** 117-126.

EFEYAN, A., ZONCU, R., CHANG, S., GUMPER, I., SNITKIN, H., WOLFSON, R. L., KIRAK, O., SABATINI, D. D. & SABATINI, D. M. 2013. Regulation of mTORC1 by the Rag GTPases is necessary for neonatal autophagy and survival. *Nature,* 493**,** 679-683.

EGGERMONT, A. M., CHIARION-SILENI, V., GROB, J. J., DUMMER, R., WOLCHOK, J. D., SCHMIDT, H., HAMID, O., ROBERT, C., ASCIERTO, P. A., RICHARDS, J. M., LEBBE, C., FERRARESI, V., SMYLIE, M., WEBER, J. S., MAIO, M., BASTHOLT, L., MORTIER, L., THOMAS, L., TAHIR, S., HAUSCHILD, A., HASSEL, J. C., HODI, F. S., TAITT, C., DE PRIL, V., DE SCHAETZEN, G., SUCIU, S. & TESTORI, A. 2016. Prolonged Survival in Stage III Melanoma with Ipilimumab Adjuvant Therapy. *N Engl J Med,* 375**,** 1845-1855.

EINHORN, Z., TRAPANI, J. G., LIU, Q. & NICOLSON, T. 2012. Rabconnectin3α promotes stable activity of the H+ pump on synaptic vesicles in hair cells. *The Journal of neuroscience : the official journal of the Society for Neuroscience,* 32**,** 11144-11156.

EKBERG, H., QI, Z., PAHLMAN, C., VERESS, B., BUNDICK, R. V., CRAGGS, R. I., HOLNESS, E., EDWARDS, S., MURRAY, C. M., FERGUSON, D., KERRY, P. J., WILSON, E. & DONALD, D. K. 2007. The specific monocarboxylate transporter-1 (MCT-1)

inhibitor, AR-C117977, induces donor-specific suppression, reducing acute and chronic allograft rejection in the rat. *Transplantation,* 84**,** 1191-9.

ELMORE, J. G., BARNHILL, R. L., ELDER, D. E., LONGTON, G. M., PEPE, M. S., REISCH, L. M., CARNEY, P. A., TITUS, L. J., NELSON, H. D., ONEGA, T., TOSTESON, A. N. A., WEINSTOCK, M. A., KNEZEVICH, S. R. & PIEPKORN, M. W. 2017. Pathologists' diagnosis of invasive melanoma and melanocytic proliferations: observer accuracy and reproducibility study. *BMJ (Clinical research ed.),* 357**,** j2813-j2813.

ENNEN, M., KEIME, C., GAMBI, G., KIENY, A., COASSOLO, S., THIBAULT-CARPENTIER, C., MARGERIN-SCHALLER, F., DAVIDSON, G., VAGNE, C., LIPSKER, D. & DAVIDSON, I. 2017. MITF-High and MITF-Low Cells and a Novel Subpopulation Expressing Genes of Both Cell States Contribute to Intra- and Intertumoral Heterogeneity of Primary Melanoma. *Clinical Cancer Research,* 23**,** 7097-7107.

ERKURT, M. A., AYDOGDU, I., KUKU, I., KAYA, E. & BASARAN, Y. 2009. Nodular melanoma presenting with rapid progression and widespread metastases: a case report. *Journal of medical case reports,* 3**,** 50-50.

EROGLU, Z. & RIBAS, A. 2016. Combination therapy with BRAF and MEK inhibitors for melanoma: latest evidence and place in therapy. *Therapeutic advances in medical oncology,* 8**,** 48-56.

ESENSTEN, JONATHAN H., HELOU, YNES A., CHOPRA, G., WEISS, A. & BLUESTONE, JEFFREY A. 2016. CD28 Costimulation: From Mechanism to Therapy. *Immunity,* 44**,** 973-988.

FADAKA, A., AJIBOYE, B., OJO, O., ADEWALE, O., OLAYIDE, I. & EMUOWHOCHERE, R. 2017. Biology of glucose metabolization in cancer cells. *Journal of Oncological Sciences,* 3**,** 45-51.

FALLETTA, P., SANCHEZ-DEL-CAMPO, L., CHAUHAN, J., EFFERN, M., KENYON, A., KERSHAW, C. J., SIDDAWAY, R., LISLE, R., FRETER, R., DANIELS, M. J., LU, X., TUTING, T., MIDDLETON, M., BUFFA, F. M., WILLIS, A. E., PAVITT, G., RONAI, Z. A., SAUKA-SPENGLER, T., HOLZEL, M. & GODING, C. R. 2017. Translation reprogramming is an evolutionarily conserved driver of phenotypic plasticity and therapeutic resistance in melanoma. *Genes Dev,* 31**,** 18-33.

FAN, S.-H., WANG, Y.-Y., WU, Z.-Y., ZHANG, Z.-F., LU, J., LI, M.-Q., SHAN, Q., WU, D.-M., SUN, C.-H., HU, B. & ZHENG, Y.-L. 2015. AGPAT9 suppresses cell growth, invasion and metastasis by counteracting acidic tumor microenvironment through KLF4/LASS2/V-ATPase signaling pathway in breast cancer. *Oncotarget,* 6**,** 18406-18417.

FANE, M. E., CHHABRA, Y., SMITH, A. G. & STURM, R. A. 2019. BRN2, a POUerful

driver of melanoma phenotype switching and metastasis. *Pigment Cell Melanoma Res,* 32**,** 9-24.

FEDERICI, C., LUGINI, L., MARINO, M. L., CARTA, F., IESSI, E., AZZARITO, T., SUPURAN, C. T. & FAIS, S. 2016. Lansoprazole and carbonic anhydrase IX inhibitors sinergize against human melanoma cells. *J Enzyme Inhib Med Chem,* 31**,** 119-125.

FEICHTINGER, R. G., LANG, R., GEILBERGER, R., RATHJE, F., MAYR, J. A., SPERL, W., BAUER, J. W., HAUSER-KRONBERGER, C., KOFLER, B. & EMBERGER, M. 2018. Melanoma tumors exhibit a variable but distinct metabolic signature. *Exp Dermatol,* 27**,** 204-207.

FEIGE, E., YOKOYAMA, S., LEVY, C., KHALED, M., IGRAS, V., LIN, R. J., LEE, S., WIDLUND, H. R., GRANTER, S. R., KUNG, A. L. & FISHER, D. E. 2011. Hypoxia-induced transcriptional repression of the melanoma-associated oncogene MITF. *Proc Natl Acad Sci U S A,* 108**,** E924-33.

FERON, O. 2009. Pyruvate into lactate and back: From the Warburg effect to symbiotic energy fuel exchange in cancer cells. *Radiotherapy and Oncology,* 92**,** 329-333.

FERRETTA, A., MAIDA, I., GUIDA, S., AZZARITI, A., PORCELLI, L., TOMMASI, S., ZANNA, P., COCCO, T., GUIDA, M. & GUIDA, G. 2016. New insight into the role of metabolic reprogramming in melanoma cells harboring BRAF mutations. *Biochimica et Biophysica Acta (BBA) - Molecular Cell Research,* 1863**,** 2710-2718.

FISHER, R. & LARKIN, J. 2012. Vemurafenib: a new treatment for BRAF-V600 mutated advanced melanoma. *Cancer management and research,* 4**,** 243-252.

FLAHERTY, K. T., PUZANOV, I., KIM, K. B., RIBAS, A., MCARTHUR, G. A., SOSMAN, J. A., O'DWYER, P. J., LEE, R. J., GRIPPO, J. F., NOLOP, K. & CHAPMAN, P. B. 2010. Inhibition of mutated, activated BRAF in metastatic melanoma. *N Engl J Med,* 363**,** 809-19.

FORGAC, M. 2007. Vacuolar ATPases: rotary proton pumps in physiology and pathophysiology. *Nature reviews. Molecular cell biology,* 8**,** 917-929.

FORSCHNER, A., EICHNER, F., AMARAL, T., KEIM, U., GARBE, C. & EIGENTLER, T. K. 2017. Improvement of overall survival in stage IV melanoma patients during 2011–2014: analysis of real-world data in 441 patients of the German Central Malignant Melanoma Registry (CMMR). *Journal of Cancer Research and Clinical Oncology,* 143**,** 533-540.

FORSEA, A. M., DEL MARMOL, V., STRATIGOS, A. & GELLER, A. C. 2014. Melanoma prognosis in Europe: far from equal. *Br J Dermatol,* 171**,** 179-82.

FOX, J. E. M., MEREDITH, D. & HALESTRAP, A. P. 2000. Characterisation of human

monocarboxylate transporter 4 substantiates its role in lactic acid efflux from skeletal muscle. *The Journal of Physiology,* 529**,** 285-293.

FRIEDMAN, R. J., RIGEL, D. S. & KOPF, A. W. 1985. Early detection of malignant melanoma: the role of physician examination and self-examination of the skin. *CA: a cancer journal for clinicians,* 35**,** 130-151.

FRIESEMA, E. C. H., GANGULY, S., ABDALLA, A., FOX, J. E. M., HALESTRAP, A. P. & VISSER, T. J. 2003. Identification of Monocarboxylate Transporter 8 as a Specific Thyroid Hormone Transporter. *Journal of Biological Chemistry,* 278**,** 40128-40135.

GACHON, J., BEAULIEU, P., SEI, J. F., GOUVERNET, J., CLAUDEL, J. P., LEMAITRE, M., RICHARD, M. A. & GROB, J. J. 2005. First prospective study of the recognition process of melanoma in dermatological practice. *Archives of dermatology,* 141**,** 434-438.

GAJOS-MICHNIEWICZ, A., DUECHLER, M. & CZYZ, M. 2014. MiRNA in melanoma-derived exosomes. *Cancer Lett,* 347**,** 29-37.

GARCýA-GARCýA, A., P¢REZ-SAYñNS, M., RODRýGUEZ, M. J., ANT*Biotechnic & histochemistry : official publication of the Biological Stain Commission,* 87**,** 133-139.

GARRAWAY, L. A., WIDLUND, H. R., RUBIN, M. A., GETZ, G., BERGER, A. J., RAMASWAMY, S., BEROUKHIM, R., MILNER, D. A., GRANTER, S. R., DU, J., LEE, C., WAGNER, S. N., LI, C., GOLUB, T. R., RIMM, D. L., MEYERSON, M. L., FISHER, D. E. & SELLERS, W. R. 2005. Integrative genomic analyses identify MITF as a lineage survival oncogene amplified in malignant melanoma. *Nature,* 436**,** 117.

GATENBY, R. A. & GILLIES, R. J. 2004. Why do cancers have high aerobic glycolysis? *Nat Rev Cancer,* 4**,** 891-9.

GEISOW, M. J. 1984. Fluorescein conjugates as indicators of subcellular pH. A critical evaluation. *Exp Cell Res,* 150**,** 29-35.

GELINEAU-VAN WAES, J., SMITH, L., VAN WAES, M., WILBERDING, J., EUDY, J. D., BAUER, L. K. & MADDOX, J. 2008. Altered expression of the iron transporter Nramp1 (Slc11a1) during fetal development of the retinal pigment epithelium in microphthalmia-associated transcription factor Mitf(mi) and Mitf(vitiligo) mouse mutants. *Experimental eye research,* 86**,** 419-433.

GELLER, A. C., ELWOOD, M., SWETTER, S. M., BROOKS, D. R., AITKEN, J., YOUL, P. H., DEMIERRE, M.-F. & BAADE, P. D. 2009. Factors related to the presentation of thin and thick nodular melanoma from a population-based cancer registry in Queensland Australia. *Cancer,* 115**,** 1318-1327.

GENOVESE, G., GHOSH, P., LI, H., RETTINO, A., SIOLETIC, S., CITTADINI, A. &

SGAMBATO, A. 2012. The tumor suppressor HINT1 regulates MITF and beta-catenin transcriptional activity in melanoma cells. *Cell Cycle,* 11**,** 2206-15.

GEORGE, A., ZAND, DINA J., HUFNAGEL, ROBERT B., SHARMA, R., SERGEEV, YURI V., LEGARE, JANET M., RICE, GREGORY M., SCOTT SCHWOERER, J. A., RIUS, M., TETRI, L., GAMM, DAVID M., BHARTI, K. & BROOKS, BRIAN P. 2016. Biallelic Mutations in MITF Cause Coloboma, Osteopetrosis, Microphthalmia, Macrocephaly, Albinism, and Deafness. *The American Journal of Human Genetics,* 99**,** 1388-1394.

GERSTENBLITH, M. R., SHI, J. & LANDI, M. T. 2010. Genome-wide association studies of pigmentation and skin cancer: a review and meta-analysis. *Pigment cell & melanoma research,* 23**,** 587-606.

GLAZER, A. M., WINKELMANN, R. R., FARBERG, A. S. & RIGEL, D. S. 2017. Analysis of trends in us melanoma incidence and mortality. *JAMA Dermatology,* 153**,** 225-226.

GODING, C. R. 2000. Mitf from neural crest to melanoma: signal transduction and transcription in the melanocyte lineage. *Genes & development,* 14**,** 1712-1728.

GODING, C. R. 2011. A picture of Mitf in melanoma immortality. *Oncogene,* 30**,** 2304-2306.

GODING, C. R. & ARNHEITER, H. 2019. MITF—the first 25 years. *Genes & Development*.

GOLDMAN, S. A., PULSINELLI, W. A., CLARKE, W. Y., KRAIG, R. P. & PLUM, F. 1989. The effects of extracellular acidosis on neurons and glia in vitro. *J Cereb Blood Flow Metab,* 9**,** 471-7.

GOLDSTEIN, A. M., CHAN, M., HARLAND, M., GILLANDERS, E. M., HAYWARD, N. K., AVRIL, M.-F., AZIZI, E., BIANCHI-SCARRA, G., BISHOP, D. T., BRESSAC-DE PAILLERETS, B., BRUNO, W., CALISTA, D., CANNON ALBRIGHT, L. A., DEMENAIS, F., ELDER, D. E., GHIORZO, P., GRUIS, N. A., HANSSON, J., HOGG, D., HOLLAND, E. A., KANETSKY, P. A., KEFFORD, R. F., LANDI, M. T., LANG, J., LEACHMAN, S. A., MACKIE, R. M., MAGNUSSON, V., MANN, G. J., NIENDORF, K., NEWTON BISHOP, J., PALMER, J. M., PUIG, S., PUIG-BUTILLE, J. A., DE SNOO, F. A., STARK, M., TSAO, H., TUCKER, M. A., WHITAKER, L. & YAKOBSON, E. 2006. High-risk Melanoma Susceptibility Genes and Pancreatic Cancer, Neural System Tumors, and Uveal Melanoma across GenoMEL. *Cancer Research,* 66**,** 9818.

GOODALL, J., CARREIRA, S., DENAT, L., KOBI, D., DAVIDSON, I., NUCIFORO, P., STURM, R. A., LARUE, L. & GODING, C. R. 2008. Brn-2 represses microphthalmia-associated transcription factor expression and marks a distinct subpopulation

of microphthalmia-associated transcription factor-negative melanoma cells. *Cancer Res,* 68**,** 7788-94.

GOODALL, J., WELLBROCK, C., DEXTER, T. J., ROBERTS, K., MARAIS, R. & GODING, C. R. 2004. The Brn-2 transcription factor links activated BRAF to melanoma proliferation. *Molecular and cellular biology,* 24**,** 2923-2931.

GOPAL, Y. N. V., RIZOS, H., CHEN, G., DENG, W., FREDERICK, D. T., COOPER, Z. A., SCOLYER, R. A., PUPO, G., KOMUROV, K., SEHGAL, V., ZHANG, J., PATEL, L., PEREIRA, C. G., BROOM, B. M., MILLS, G. B., RAM, P., SMITH, P. D., WARGO, J. A., LONG, G. V. & DAVIES, M. A. 2014. Inhibition of mTORC1/2 overcomes resistance to MAPK pathway inhibitors mediated by PGC1α and oxidative phosphorylation in melanoma. *Cancer research,* 74**,** 7037-7047.

GORBATENKO, A., OLESEN, C. W., BOEDTKJER, E. & PEDERSEN, S. F. 2014. Regulation and roles of bicarbonate transporters in cancer. *Frontiers in physiology,* 5**,** 130-130.

GR*Human molecular genetics,* 21**,** 1025-1036.

GRAY-SCHOPFER, V., WELLBROCK, C. & MARAIS, R. 2007. Melanoma biology and new targeted therapy. *Nature,* 445**,** 851-7.

GREEN, A. C., WILLIAMS, G. M., LOGAN, V. & STRUTTON, G. M. 2011. Reduced melanoma after regular sunscreen use: randomized trial follow-up. *J Clin Oncol,* 29**,** 257-63.

GRICHTCHENKO, I. I., CHOI, I., ZHONG, X., BRAY-WARD, P., RUSSELL, J. M. & BORON, W. F. 2001. Cloning, characterization, and chromosomal mapping of a human electroneutral Na(+)-driven Cl-HCO3 exchanger. *The Journal of biological chemistry,* 276**,** 8358-8363.

GRILL, C., BERGSTEINSD*Human molecular genetics,* 22**,** 4357-4367.

GROLLMAN, E. F., PHILP, N. J., MCPHIE, P., WARD, R. D. & SAUER, B. 2000. Determination of Transport Kinetics of Chick MCT3 Monocarboxylate Transporter from Retinal Pigment Epithelium by Expression in Genetically Modified Yeast. *Biochemistry,* 39**,** 9351-9357.

GUAN, X., RODRIGUEZ-CRUZ, V. & MORRIS, M. E. 2019. Cellular Uptake of MCT1 Inhibitors AR-C155858 and AZD3965 and Their Effects on MCT-Mediated Transport of L-Lactate in Murine 4T1 Breast Tumor Cancer Cells. *AAPS J,* 21**,** 13.

HAASS, N. K. & HERLYN, M. 2005. Normal Human Melanocyte Homeostasis as a Paradigm for Understanding Melanoma. *Journal of Investigative Dermatology Symposium Proceedings,* 10**,** 153-163.

HAFLIDADOTTIR, B. S., BERGSTEINSDOTTIR, K., PRAETORIUS, C. & STEINGRIMSSON, E. 2010. miR-148 regulates Mitf in melanoma cells. *PLoS One,* 5**,** e11574.

HALABAN, R., ZHANG, W., BACCHIOCCHI, A., CHENG, E., PARISI, F., ARIYAN, S., KRAUTHAMMER, M., MCCUSKER, J. P., KLUGER, Y. & SZNOL, M. 2010. PLX4032, a selective BRAF(V600E) kinase inhibitor, activates the ERK pathway and enhances cell migration and proliferation of BRAF melanoma cells. *Pigment Cell Melanoma Res,* 23**,** 190-200.

HALESTRAP, A. P. 1975. The mitochondrial pyruvate carrier. Kinetics and specificity for substrates and inhibitors. *The Biochemical journal,* 148**,** 85-96.

HALESTRAP, A. P. 1976. The mechanism of the inhibition of the mitochondrial pyruvate transportater by alpha-cyanocinnamate derivatives. *The Biochemical journal,* 156**,** 181-183.

HALESTRAP, A. P. 2012. The monocarboxylate transporter family--Structure and functional characterization. *IUBMB life,* 64**,** 1-9.

HALESTRAP, A. P. & MEREDITH, D. 2004. The SLC16 gene family—from monocarboxylate transporters (MCTs) to aromatic amino acid transporters and beyond. *Pflügers Archiv,* 447**,** 619-628.

HALESTRAP, A. P. & PRICE, N. T. 1999. The proton-linked monocarboxylate transporter (MCT) family: structure, function and regulation. *The Biochemical journal,* 343 Pt 2**,** 281-299.

HALFORD, S. E. R., JONES, P., WEDGE, S., HIRSCHBERG, S., KATUGAMPOLA, S., VEAL, G., PAYNE, G., BACON, C., POTTER, S., GRIFFIN, M., CHENARD-POIRIER, M., PETRIDES, G., HOLDER, G., KEUN, H. C., BANERJI, U. & PLUMMER, E. R. 2017. A first-in-human first-in-class (FIC) trial of the monocarboxylate transporter 1 (MCT1) inhibitor AZD3965 in patients with advanced solid tumours. *Journal of Clinical Oncology,* 35**,** 2516-2516.

HALLSSON, J. H., HAFLIDADOTTIR, B. S., SCHEPSKY, A., ARNHEITER, H. & STEINGRIMSSON, E. 2007. Evolutionary sequence comparison of the Mitf gene reveals novel conserved domains. *Pigment Cell Res,* 20**,** 185-200.

HALUSKA, F., PEMBERTON, T., IBRAHIM, N. & KALINSKY, K. 2007. The RTK/RAS/BRAF/PI3K pathways in melanoma: biology, small molecule inhibitors, and potential applications. *Seminars in oncology,* 34**,** 546-554.

HAO, G., XU, Z. P. & LI, L. 2018. Manipulating extracellular tumour pH: an effective target for cancer therapy. *RSC Advances,* 8**,** 22182-22192.

HAQ, R., SHOAG, J., ANDREU-PEREZ, P., YOKOYAMA, S., EDELMAN, H., ROWE, GLENN C., FREDERICK, DENNIE T., HURLEY, AERON D., NELLORE, A., KUNG, ANDREW L., WARGO, JENNIFER A., SONG, JUN S., FISHER, DAVID E., ARANY, Z. & WIDLUND, HANS R. 2013. Oncogenic BRAF Regulates Oxidative Metabolism via PGC1α and MITF. *Cancer Cell,* 23**,** 302-315.

HARRIS, A. L. 2002. Hypoxia — a key regulatory factor in tumour growth. *Nature*

Reviews Cancer, 2**,** 38-47.

HARTMAN, M. L. & CZYZ, M. 2015a. MITF in melanoma: mechanisms behind its expression and activity. *Cell Mol Life Sci,* 72**,** 1249-60.

HARTMAN, M. L. & CZYZ, M. 2015b. Pro-Survival Role of MITF in Melanoma. *Journal of Investigative Dermatology,* 135**,** 352-358.

HAWRYLUK, E. B. & TSAO, H. 2014. Melanoma: Clinical Features and Genomic Insights. *Cold Spring Harbor Perspectives in Medicine,* 4.

HE, L., ZHANG, J., ZHAO, J., MA, N., KIM, S. W., QIAO, S. & MA, X. 2018. Autophagy: The Last Defense against Cellular Nutritional Stress. *Adv Nutr,* 9**,** 493-504.

HEMESATH, T. J., PRICE, E. R., TAKEMOTO, C., BADALIAN, T. & FISHER, D. E. 1998. MAP kinase links the transcription factor Microphthalmia to c-Kit signalling in melanocytes. *Nature,* 391**,** 298-301.

HEMESATH, T. J., STEINGRIMSSON, E., MCGILL, G., HANSEN, M. J., VAUGHT, J., HODGKINSON, C. A., ARNHEITER, H., COPELAND, N. G., JENKINS, N. A. & FISHER, D. E. 1994. microphthalmia, a critical factor in melanocyte development, defines a discrete transcription factor family. *Genes Dev,* 8**,** 2770-80.

HERTWIG, P. 1942. Neue Mutationen und Koppelungsgruppen bei der Hausmaus. *Zeitschrift für Induktive Abstammungs- und Vererbungslehre,* 80**,** 220-246.

HERTZMAN JOHANSSON, C., AZIMI, A., FROSTVIK STOLT, M., SHOJAEE, S., WIBERG, H., GRAFSTR*Melanoma research,* 23**,** 360-365.

HINTON, A., SENNOUNE, S. R., BOND, S., FANG, M., REUVENI, M., SAHAGIAN, G. G., JAY, D., MARTINEZ-ZAGUILAN, R. & FORGAC, M. 2009. Function of a subunit isoforms of the V-ATPase in pH homeostasis and in vitro invasion of MDA-MB231 human breast cancer cells. *The Journal of biological chemistry,* 284**,** 16400-16408.

HIRATA, R., GRAHAM, L. A., TAKATSUKI, A., STEVENS, T. H. & ANRAKU, Y. 1997. VMA11 and VMA16 encode second and third proteolipid subunits of the Saccharomyces cerevisiae vacuolar membrane H+-ATPase. *The Journal of biological chemistry,* 272**,** 4795-4803.

HIRATA, T., IWAMOTO-KIHARA, A., SUN-WADA, G.-H., OKAJIMA, T., WADA, Y. & FUTAI, M. 2003. Subunit rotation of vacuolar-type proton pumping ATPase: relative rotation of the G and C subunits. *The Journal of biological chemistry,* 278**,** 23714-23719.

HIREMATH, S. A., SURULESCU, C., JAMALI, S., AMES, S., DEITMER, J. W. & BECKER, H. M. 2018. Modeling of pH regulation in tumor cells: Direct interaction between proton-coupled lactate transporters and cancer-associated carbonic anhydrase. *Mathematical biosciences and engineering : MBE,* 16**,** 320-337.

HODGKINSON, C. A., MOORE, K. J., NAKAYAMA, A., STEINGRIMSSON, E., COPELAND, N. G., JENKINS, N. A. & ARNHEITER, H. 1993. Mutations at the mouse microphthalmia locus are associated with defects in a gene encoding a novel basic-helix-loop-helix-zipper protein. *Cell,* 74**,** 395-404.

HOEK, K. S., EICHHOFF, O. M., SCHLEGEL, N. C., DOBBELING, U., KOBERT, N., SCHAERER, L., HEMMI, S. & DUMMER, R. 2008a. In vivo switching of human melanoma cells between proliferative and invasive states. *Cancer Res,* 68**,** 650-6.

HOEK, K. S., SCHLEGEL, N. C., EICHHOFF, O. M., WIDMER, D. S., PRAETORIUS, C., EINARSSON, S. O., VALGEIRSDOTTIR, S., BERGSTEINSDOTTIR, K., SCHEPSKY, A., DUMMER, R. & STEINGRIMSSON, E. 2008b. Novel MITF targets identified using a two-step DNA microarray strategy. *Pigment Cell Melanoma Res,* 21**,** 665-76.

HOLLESTEIN, L. M., VAN DEN AKKER, S. A., NIJSTEN, T., KARIM-KOS, H. E., COEBERGH, J. W. & DE VRIES, E. 2012. Trends of cutaneous melanoma in The Netherlands: increasing incidence rates among all Breslow thickness categories and rising mortality rates since 1989. *Ann Oncol,* 23**,** 524-30.

HORECKER, B. L. 2002. The pentose phosphate pathway. *J Biol Chem,* 277**,** 47965-71.

HORNYAK, T. J., HAYES, D. J., CHIU, L.-Y. & ZIFF, E. B. 2001. Transcription factors in melanocyte development: distinct roles for Pax-3 and Mitf. *Mechanisms of Development,* 101**,** 47-59.

HUANG, S., HE, P., XU, D., LI, J., PENG, X. & TANG, Y. 2017. Acidic stress induces apoptosis and inhibits angiogenesis in human bone marrow-derived endothelial progenitor cells. *Oncology letters,* 14**,** 5695-5702.

HUBER, V., CAMISASCHI, C., BERZI, A., FERRO, S., LUGINI, L., TRIULZI, T., TUCCITTO, A., TAGLIABUE, E., CASTELLI, C. & RIVOLTINI, L. 2017. Cancer acidity: An ultimate frontier of tumor immune escape and a novel target of immunomodulation. *Seminars in Cancer Biology,* 43**,** 74-89.

HUBER, W. E., PRICE, E. R., WIDLUND, H. R., DU, J., DAVIS, I. J., WEGNER, M. & FISHER, D. E. 2003. A tissue-restricted cAMP transcriptional response: SOX10 modulates alpha-melanocyte-stimulating hormone-triggered expression of microphthalmia-associated transcription factor in melanocytes. *J Biol Chem,* 278**,** 45224-30.

HUGHES, M. J., LINGREL, J. B., KRAKOWSKY, J. M. & ANDERSON, K. P. 1993. A helix-loop-helix transcription factor-like gene is located at the mi locus. *J Biol Chem,* 268**,** 20687-90.

HUGO, W., ZARETSKY, J. M., SUN, L., SONG, C., MORENO, B. H., HU-LIESKOVAN, S., BERENT-MAOZ, B., PANG, J., CHMIELOWSKI, B., CHERRY, G., SEJA, E., LOMELI,

S., KONG, X., KELLEY, M. C., SOSMAN, J. A., JOHNSON, D. B., RIBAS, A. & LO, R. S. 2016. Genomic and Transcriptomic Features of Response to Anti-PD-1 Therapy in Metastatic Melanoma. *Cell,* 165**,** 35-44.

IACONO, K. T., BROWN, A. L., GREENE, M. I. & SAOUAF, S. J. 2007. CD147 immunoglobulin superfamily receptor function and role in pathology. *Experimental and Molecular Pathology,* 83**,** 283-295.

IDENO, M., KOBAYASHI, M., SASAKI, S., FUTAGI, Y., NARUMI, K., FURUGEN, A. & ISEKI, K. 2018. Involvement of monocarboxylate transporter 1 (SLC16A1) in the uptake of l-lactate in human astrocytes. *Life sciences,* 192**,** 110-114.

IGAL, R. A. 2016. Stearoyl CoA desaturase-1: New insights into a central regulator of cancer metabolism. *Biochimica et Biophysica Acta (BBA) - Molecular and Cell Biology of Lipids,* 1861**,** 1865-1880.

ISHIGURO, H., STEWARD, M. C., LINDSAY, A. R. & CASE, R. M. 1996. Accumulation of intracellular HCO3- by Na(+)-HCO3- cotransport in interlobular ducts from guinea-pig pancreas. *The Journal of physiology,* 495 (Pt 1)**,** 169-178.

IVES, H. E. & RECTOR, F. C., JR. 1984. Proton transport and cell function. *The Journal of clinical investigation,* 73**,** 285-290.

IWAI, Y., ISHIDA, M., TANAKA, Y., OKAZAKI, T., HONJO, T. & MINATO, N. 2002. Involvement of PD-L1 on tumor cells in the escape from host immune system and tumor immunotherapy by PD-L1 blockade. *Proc Natl Acad Sci U S A,* 99**,** 12293-7.

IWANAGA, T. & KISHIMOTO, A. 2015. Cellular distributions of monocarboxylate transporters: a review. *Biomed Res,* 36**,** 279-301.

JABŁOŃSKA-TRYPUĆ, A., MATEJCZYK, M. & ROSOCHACKI, S. 2016. Matrix metalloproteinases (MMPs), the main extracellular matrix (ECM) enzymes in collagen degradation, as a target for anticancer drugs. *Journal of enzyme inhibition and medicinal chemistry,* 31**,** 177-183.

JACKSON, V. N. & HALESTRAP, A. P. 1996. The kinetics, substrate, and inhibitor specificity of the monocarboxylate (lactate) transporter of rat liver cells determined using the fluorescent intracellular pH indicator, 2',7'-bis(carboxyethyl)-5(6)-carboxyfluorescein. *The Journal of biological chemistry,* 271**,** 861-868.

JAVELAUD, D., ALEXAKI, V. I., PIERRAT, M. J., HOEK, K. S., DENNLER, S., VAN KEMPEN, L., BERTOLOTTO, C., BALLOTTI, R., SAULE, S., DELMAS, V. & MAUVIEL, A. 2011. GLI2 and M-MITF transcription factors control exclusive gene expression programs and inversely regulate invasion in human melanoma cells. *Pigment Cell Melanoma Res,* 24**,** 932-43.

JENNINGS, M. L. 1976. Proton fluxes associated with erythrocyte membrane anion

exchange. *The Journal of membrane biology,* 28**,** 187-205.

JENNINGS, M. L. 2013. Transport of H2S and HS(-) across the human red blood cell membrane: rapid H2S diffusion and AE1-mediated Cl(-)/HS(-) exchange. *American journal of physiology. Cell physiology,* 305**,** C941-C950.

JENSEN, L. J., SCHMITT, B. M., BERGER, U. V., NSUMU, N. N., BORON, W. F., HEDIGER, M. A., BROWN, D. & BRETON, S. 1999. Localization of sodium bicarbonate cotransporter (NBC) protein and messenger ribonucleic acid in rat epididymis. *Biology of reproduction,* 60**,** 573-579.

JEONG, D.-W., KIM, T. S., LEE, J. W., KIM, K. T., KIM, H. J., KIM, I.-H. & KIM, I. Y. 2001. Blocking of Acidosis-Mediated Apoptosis by a Reduction of Lactate Dehydrogenase Activity through Antisense mRNA Expression. *Biochemical and Biophysical Research Communications,* 289**,** 1141-1149.

JI, A. L., BICHAKJIAN, C. K. & SWETTER, S. M. 2016. Molecular Profiling in Cutaneous Melanoma. *Journal of the National Comprehensive Cancer Network : JNCCN,* 14**,** 475-480.

JI, Z., ERIN CHEN, Y., KUMAR, R., TAYLOR, M., JENNY NJAUW, C.-N., MIAO, B., FREDERICK, D. T., WARGO, J. A., FLAHERTY, K. T., J*The Journal of investigative dermatology,* 135**,** 1863-1872.

JIANG, B. 2017. Aerobic glycolysis and high level of lactate in cancer metabolism and microenvironment. *Genes & diseases,* 4**,** 25-27.

JIN, L. & ZHOU, Y. 2019. Crucial role of the pentose phosphate pathway in malignant tumors. *Oncology letters,* 17**,** 4213-4221.

JIPPO, T., MORII, E., TSUJINO, K., TSUJIMURA, T., LEE, Y. M., KIM, D. K., MATSUDA, H., KIM, H. M. & KITAMURA, Y. 1997. Involvement of transcription factor encoded by the mouse mi locus (MITF) in expression of p75 receptor of nerve growth factor in cultured mast cells of mice. *Blood,* 90**,** 2601-2608.

JOHANNESSEN, C. M., JOHNSON, L. A., PICCIONI, F., TOWNES, A., FREDERICK, D. T., DONAHUE, M. K., NARAYAN, R., FLAHERTY, K. T., WARGO, J. A., ROOT, D. E. & GARRAWAY, L. A. 2013. A melanocyte lineage program confers resistance to MAP kinase pathway inhibition. *Nature,* 504**,** 138-42.

JONES, O. T., JURASCHECK, L. C., VAN MELLE, M. A., HICKMAN, S., BURROWS, N. P., HALL, P. N., EMERY, J. & WALTER, F. M. 2019. Dermoscopy for melanoma detection and triage in primary care: a systematic review. *BMJ Open,* 9**,** e027529.

JONES, R. S. & MORRIS, M. E. 2016. Monocarboxylate Transporters: Therapeutic Targets and Prognostic Factors in Disease. *Clinical pharmacology and therapeutics,* 100**,** 454-463.

JUNE, C. H., WARSHAUER, J. T. & BLUESTONE, J. A. 2017. Is autoimmunity the Achilles'

heel of cancer immunotherapy? *Nat Med,* 23**,** 540-547.

K*Cell Stem Cell,* 21**,** 679-693.e6.

KAKU, D. A., GIFFARD, R. G. & CHOI, D. W. 1993. Neuroprotective effects of glutamate antagonists and extracellular acidity. *Science,* 260**,** 1516-8.

KALLIFATIDIS, G., HOEPFNER, D., JAEG, T., GUZMñN, E. A. & WRIGHT, A. E. 2013. The marine natural product manzamine A targets vacuolar ATPases and inhibits autophagy in pancreatic cancer cells. *Marine drugs,* 11**,** 3500-3516.

KALLINOWSKI, F., RUNKEL, S., FORTMEYER, H. P., F*Journal of Cancer Research and Clinical Oncology,* 113**,** 209-215.

KANAAN, A., DOUGLAS, R. M., ALPER, S. L., BORON, W. F. & HADDAD, G. G. 2007. Effect of chronic elevated carbon dioxide on the expression of acid-base transporters in the neonatal and adult mouse. *American Journal of Physiology-Regulatory, Integrative and Comparative Physiology,* 293**,** R1294-R1302.

KANE, P. M. 2012. Targeting reversible disassembly as a mechanism of controlling V-ATPase activity. *Current protein & peptide science,* 13**,** 117-123.

KASPRZAK, J. M. & XU, Y. G. 2015. Diagnosis and management of lentigo maligna: a review. *Drugs in context,* 4**,** 212281-212281.

KATO, T., SUETAKE, T., TABATA, N., TAKAHASHI, K. & TAGAMI, H. 1999. Epidemiology and prognosis of plantar melanoma in 62 Japanese patients over a 28-year period. *International journal of dermatology,* 38**,** 515-519.

KATO, Y., OZAWA, S., MIYAMOTO, C., MAEHATA, Y., SUZUKI, A., MAEDA, T. & BABA, Y. 2013. Acidic extracellular microenvironment and cancer. *Cancer cell international,* 13**,** 89-89.

KAWAKAMI, A. & FISHER, D. E. 2017. The master role of microphthalmia-associated transcription factor in melanocyte and melanoma biology. *Laboratory Investigation,* 97**,** 649.

KAWASAKI-NISHI, S., NISHI, T. & FORGAC, M. 2001. Arg-735 of the 100-kDa subunit a of the yeast V-ATPase is essential for proton translocation. *Proceedings of the National Academy of Sciences of the United States of America,* 98**,** 12397-12402.

KEENEN, B., QI, H., SALADI, S. V., YEUNG, M. & DE LA SERNA, I. L. 2010. Heterogeneous SWI/SNF chromatin remodeling complexes promote expression of microphthalmia-associated transcription factor target genes in melanoma. *Oncogene,* 29**,** 81-92.

KHACHO, M., TARABAY, M., PATTEN, D., KHACHO, P., MACLAURIN, J. G., GUADAGNO, J., BERGERON, R., CREGAN, S. P., HARPER, M.-E., PARK, D. S. & SLACK, R. S. 2014. Acidosis overrides oxygen deprivation to maintain mitochondrial

function and cell survival. *Nature communications,* 5**,** 3550-3550.

KIDO, K., SUMIMOTO, H., ASADA, S., OKADA, S. M., YAGUCHI, T., KAWAMURA, N., MIYAGISHI, M., SAIDA, T. & KAWAKAMI, Y. 2009. Simultaneous suppression of MITF and BRAF V600E enhanced inhibition of melanoma cell proliferation. *Cancer Sci,* 100**,** 1863-9.

KILIC, M., KASPERCZYK, H., FULDA, S. & DEBATIN, K. M. 2007. Role of hypoxia inducible factor-1 alpha in modulation of apoptosis resistance. *Oncogene,* 26**,** 2027-2038.

KIM, D. K., KANAI, Y., CHAIROUNGDUA, A., MATSUO, H., CHA, S. H. & ENDOU, H. 2001. Expression Cloning of a Na+-independent Aromatic Amino Acid Transporter with Structural Similarity to H+/Monocarboxylate Transporters. *Journal of Biological Chemistry,* 276**,** 17221-17228.

KIM, E., GORAKSHA-HICKS, P., LI, L., NEUFELD, T. P. & GUAN, K.-L. 2008. Regulation of TORC1 by Rag GTPases in nutrient response. *Nature cell biology,* 10**,** 935-945.

KIM, E., ZUCCONI, B. E., WU, M., NOCCO, S. E., MEYERS, D. J., MCGEE, J. S., VENKATESH, S., COHEN, D. L., GONZALEZ, E. C., RYU, B., COLE, P. A. & ALANI, R. M. 2019. MITF Expression Predicts Therapeutic Vulnerability to p300 Inhibition in Human Melanoma. *Cancer Res,* 79**,** 2649-2661.

KIM, H. K., LEE, I., BANG, H., KIM, H. C., LEE, W. Y., YUN, S. H., LEE, J., LEE, S. J., PARK, Y. S., KIM, K.-M. & KANG, W. K. 2018. MCT4 Expression Is a Potential Therapeutic Target in Colorectal Cancer with Peritoneal Carcinomatosis. *Molecular Cancer Therapeutics,* 17**,** 838.

KIM, J.-W., TCHERNYSHYOV, I., SEMENZA, G. L. & DANG, C. V. 2006. HIF-1-mediated expression of pyruvate dehydrogenase kinase: A metabolic switch required for cellular adaptation to hypoxia. *Cell Metabolism,* 3**,** 177-185.

KIRK, P., WILSON, M. C., HEDDLE, C., BROWN, M. H., BARCLAY, A. N. & HALESTRAP, A. P. 2000. CD147 is tightly associated with lactate transporters MCT1 and MCT4 and facilitates their cell surface expression. *The EMBO Journal,* 19**,** 3896-3904.

KITAOKA, Y., TAKAHASHI, Y., MACHIDA, M., TAKEDA, K., TAKEMASA, T. & HATTA, H. 2014. Effect of AMPK activation on monocarboxylate transporter (MCT)1 and MCT4 in denervated muscle. *The journal of physiological sciences : JPS,* 64**,** 59-64.

KLIER, M., SCH*The Journal of biological chemistry,* 286**,** 27781-27791.

KLING, B., B*Journal of Natural Products,* 77**,** 446-454.

KNACKSTEDT, T., KNACKSTEDT, R. W., COUTO, R. & GASTMAN, B. 2018. Malignant Melanoma: Diagnostic and Management Update. *Plastic and reconstructive surgery,* 142**,** 202e-216e.

KO, S. B. H., LUO, X., HAGER, H., ROJEK, A., CHOI, J. Y., LICHT, C., SUZUKI, M., MUALLEM, S., NIELSEN, S. & ISHIBASHI, K. 2002. AE4 is a DIDS-sensitive Cl(-)/HCO(-)(3) exchanger in the basolateral membrane of the renal CCD and the SMG duct. *American journal of physiology. Cell physiology,* 283**,** C1206-C1218.

KOBAYASHI, M., FUJITA, I., ITAGAKI, S., HIRANO, T. & ISEKI, K. 2005. Transport mechanism for L-lactic acid in human myocytes using human prototypic embryonal rhabdomyosarcoma cell line (RD cells). *Biological & pharmaceutical bulletin,* 28**,** 1197-1201.

KOBAYASHI, S., MORGANS, C. W., CASEY, J. R. & KOPITO, R. R. 1994. AE3 anion exchanger isoforms in the vertebrate retina: developmental regulation and differential expression in neurons and glia. *The Journal of neuroscience : the official journal of the Society for Neuroscience,* 14**,** 6266-6279.

KOCH, A. & SCHWAB, A. 2019. Cutaneous pH landscape as a facilitator of melanoma initiation and progression. *Acta Physiol (Oxf),* 225**,** e13105.

KONG, S. C., GIANUZZO, A., NOVAK, I. & PEDERSEN, S. F. 2014. Acid-base transport in pancreatic cancer: Molecular mechanisms and clinical potential. *Biochemistry and Cell Biology,* 92**,** 449-459.

KONIECZKOWSKI, D. J., JOHANNESSEN, C. M., ABUDAYYEH, O., KIM, J. W., COOPER, Z. A., PIRIS, A., FREDERICK, D. T., BARZILY-ROKNI, M., STRAUSSMAN, R., HAQ, R., FISHER, D. E., MESIROV, J. P., HAHN, W. C., FLAHERTY, K. T., WARGO, J. A., TAMAYO, P. & GARRAWAY, L. A. 2014. A Melanoma Cell State Distinction Influences Sensitivity to MAPK Pathway Inhibitors. *Cancer Discovery,* 4**,** 816-827.

KOPITO, R. R., LEE, B. S., SIMMONS, D. M., LINDSEY, A. E., MORGANS, C. W. & SCHNEIDER, K. 1989. Regulation of intracellular pH by a neuronal homolog of the erythrocyte anion exchanger. *Cell,* 59**,** 927-937.

KOPITO, R. R. & LODISH, H. F. 1985. Primary structure and transmembrane orientation of the murine anion exchange protein. *Nature,* 316**,** 234-238.

KOWALIK, M. A., COLUMBANO, A. & PERRA, A. 2017. Emerging Role of the Pentose Phosphate Pathway in Hepatocellular Carcinoma. *Front Oncol,* 7**,** 87.

KOZAR, I., MARGUE, C., ROTHENGATTER, S., HAAN, C. & KREIS, S. 2019. Many ways to resistance: How melanoma cells evade targeted therapies. *Biochimica et Biophysica Acta (BBA) - Reviews on Cancer,* 1871**,** 313-322.

KUMAR, R., ANGELINI, S., CZENE, K., SAUROJA, I., HAHKA-KEMPPINEN, M., PYRHONEN, S. & HEMMINKI, K. 2003. BRAF mutations in metastatic melanoma: a possible association with clinical outcome. *Clin Cancer Res,* 9**,** 3362-8.

KUMAR, S. M., YU, H., EDWARDS, R., CHEN, L., KAZIANIS, S., BRAFFORD, P., ACS, G., HERLYN, M. & XU, X. 2007. Mutant V600E BRAF increases hypoxia inducible factor-1alpha expression in melanoma. *Cancer research,* 67**,** 3177-3184.

KUO, R.-L., LI, L.-H., LIN, S.-J., LI, Z.-H., CHEN, G.-W., CHANG, C.-K., WANG, Y.-R., TAM, E.-H., GONG, Y.-N., KRUG, R. M. & SHIH, S.-R. 2016. Role of N Terminus-Truncated NS1 Proteins of Influenza A Virus in Inhibiting IRF3 Activation. *Journal of Virology,* 90**,** 4696-4705.

KURTZ, I., PETRASEK, D. & TATISHCHEV, S. 2004. Molecular Mechanisms of Electrogenic Sodium Bicarbonate Cotransport: Structural and Equilibrium Thermodynamic Considerations. *The Journal of Membrane Biology,* 197**,** 77-90.

KWON, T.-H., FULTON, C., WANG, W., KURTZ, I., FR*American journal of physiology. Renal physiology,* 282**,** F341-F351.

LAGORY, E. L., WU, C., TANIGUCHI, C. M., DING, C.-K. C., CHI, J.-T., VON EYBEN, R., SCOTT, D. A., RICHARDSON, A. D. & GIACCIA, A. J. 2015. Suppression of PGC-1α Is Critical for Reprogramming Oxidative Metabolism in Renal Cell Carcinoma. *Cell reports,* 12**,** 116-127.

LAN, A., LAGADIC-GOSSMANN, D., LEMAIRE, C., BRENNER, C. & JAN, G. 2007. Acidic extracellular pH shifts colorectal cancer cell death from apoptosis to necrosis upon exposure to propionate and acetate, major end-products of the human probiotic propionibacteria. *Apoptosis,* 12**,** 573-91.

LAPLANTE, M. & SABATINI, D. M. 2012. mTOR signaling in growth control and disease. *Cell,* 149**,** 274-293.

LARKIN, J., CHIARION-SILENI, V., GONZALEZ, R., GROB, J.-J., RUTKOWSKI, P., LAO, C. D., COWEY, C. L., SCHADENDORF, D., WAGSTAFF, J., DUMMER, R., FERRUCCI, P. F., SMYLIE, M., HOGG, D., HILL, A., MñRQUEZ-RODAS, I., HAANEN, J., GUIDOBONI, M., MAIO, M., SCH*New England Journal of Medicine,* 381**,** 1535-1546.

LARRIBERE, L., HILMI, C., KHALED, M., GAGGIOLI, C., BILLE, K., AUBERGER, P., ORTONNE, J. P., BALLOTTI, R. & BERTOLOTTO, C. 2005. The cleavage of microphthalmia-associated transcription factor, MITF, by caspases plays an essential role in melanocyte and melanoma cell apoptosis. *Genes Dev,* 19**,** 1980-5.

LASITHIOTAKIS, K. G., LEITER, U., GORKIEVICZ, R., EIGENTLER, T., BREUNINGER, H., METZLER, G., STROBEL, W. & GARBE, C. 2006. The incidence and mortality of cutaneous melanoma in Southern Germany: trends by anatomic site and pathologic characteristics, 1976 to 2003. *Cancer,* 107**,** 1331-1339.

LEE, H. J., PARK, H. J., LEE, S., KIM, Y. H. & CHOI, I. 2011. The sodium-driven

chloride/bicarbonate exchanger NDCBE in rat brain is upregulated by chronic metabolic acidosis. *Brain Research,* 1377**,** 13-20.

LEE, S., AXELSEN, T. V., ANDERSEN, A. P., VAHL, P., PEDERSEN, S. F. & BOEDTKJER, E. 2015a. Disrupting Na+,HCO3–-cotransporter NBCn1 (Slc4a7) delays murine breast cancer development. *Oncogene,* 35**,** 2112.

LEE, S., AXELSEN, T. V., JESSEN, N., PEDERSEN, S. F., VAHL, P. & BOEDTKJER, E. 2018. Na(+),HCO3(-)-cotransporter NBCn1 (Slc4a7) accelerates ErbB2-induced breast cancer development and tumor growth in mice. *Oncogene,* 37**,** 5569-5584.

LEE, S., LEE, H. J., YANG, H. S., THORNELL, I. M., BEVENSEE, M. O. & CHOI, I. 2010. Sodium-bicarbonate cotransporter NBCn1 in the kidney medullary thick ascending limb cell line is upregulated under acidic conditions and enhances ammonium transport. *Experimental physiology,* 95**,** 926-937.

LEE, W. J., LEE, J. H., WON, C. H., CHANG, S. E., CHOI, J. H., MOON, K. C. & LEE, M. W. 2015b. Nail apparatus melanoma: A comparative, clinicoprognostic study of the initial clinical and morphological characteristics of 49 patients. *Journal of the American Academy of Dermatology,* 73**,** 213-220.

LEFEBVRE, V., DU, Q., BAIRD, S., NG, A. C., NASCIMENTO, M., CAMPANELLA, M., MCBRIDE, H. M. & SCREATON, R. A. 2013. Genome-wide RNAi screen identifies ATPase inhibitory factor 1 (ATPIF1) as essential for PARK2 recruitment and mitophagy. *Autophagy,* 9**,** 1770-9.

LEHOUX, S., ABE, J., FLORIAN, J. A. & BERK, B. C. 2001. 14-3-3 Binding to Na+/H+ exchanger isoform-1 is associated with serum-dependent activation of Na+/H+ exchange. *The Journal of biological chemistry,* 276**,** 15794-15800.

LEMMON, M. A. & SCHLESSINGER, J. 2010. Cell signaling by receptor tyrosine kinases. *Cell,* 141**,** 1117-1134.

LEVENE, A. 1980. On the histological diagnosis and prognosis of malignant melanoma. *Journal of clinical pathology,* 33**,** 101-124.

LEVY, C. & FISHER, D. E. 2011. Dual roles of lineage restricted transcription factors: the case of MITF in melanocytes. *Transcription,* 2**,** 19-22.

LEVY, C., KHALED, M. & FISHER, D. E. 2006. MITF: master regulator of melanocyte development and melanoma oncogene. *Trends in Molecular Medicine,* 12**,** 406-414.

LEVY, C., SONNENBLICK, A. & RAZIN, E. 2003. Role played by microphthalmia transcription factor phosphorylation and its Zip domain in its transcriptional inhibition by PIAS3. *Mol Cell Biol,* 23**,** 9073-80.

LI, X., ALVAREZ, B., CASEY, J. R., REITHMEIER, R. A. & FLIEGEL, L. 2002. Carbonic anhydrase II binds to and enhances activity of the Na+/H+ exchanger. *J Biol*

Chem, 277**,** 36085-91.

LI, X., YU, W., QIAN, X., XIA, Y., ZHENG, Y., LEE, J. H., LI, W., LYU, J., RAO, G., ZHANG, X., QIAN, C. N., ROZEN, S. G., JIANG, T. & LU, Z. 2017. Nucleus-Translocated ACSS2 Promotes Gene Transcription for Lysosomal Biogenesis and Autophagy. *Mol Cell,* 66**,** 684-697.e9.

LIBERMAN, R., BOND, S., SHAINHEIT, M. G., STADECKER, M. J. & FORGAC, M. 2014. Regulated assembly of vacuolar ATPase is increased during cluster disruption-induced maturation of dendritic cells through a phosphatidylinositol 3-kinase/mTOR-dependent pathway. *The Journal of biological chemistry,* 289**,** 1355-1363.

LIBERTI, M. V. & LOCASALE, J. W. 2016. The Warburg Effect: How Does it Benefit Cancer Cells? *Trends in biochemical sciences,* 41**,** 211-218.

LICCIULLI, S., LUISE, C., SCAFETTA, G., CAPRA, M., GIARDINA, G., NUCIFORO, P., BOSARI, S., VIALE, G., MAZZAROL, G., TONELLI, C., LANFRANCONE, L. & ALCALAY, M. 2011. Pirin inhibits cellular senescence in melanocytic cells. *The American journal of pathology,* 178**,** 2397-2406.

LINN, S. C., KUDRYCKI, K. E. & SHULL, G. E. 1992. The predicted translation product of a cardiac AE3 mRNA contains an N terminus distinct from that of the brain AE3 Cl-/HCO3- exchanger. Cloning of a cardiac AE3 cDNA, organization of the AE3 gene, and identification of an alternative transcription initiation site. *The Journal of biological chemistry,* 267**,** 7927-7935.

LIU, F., FU, Y. & MEYSKENS, F. L., JR. 2009a. MiTF Regulates Cellular Response to Reactive Oxygen Species through Transcriptional Regulation of APE-1/Ref-1. *Journal of Investigative Dermatology,* 129**,** 422-431.

LIU, F. & MEYSKENS, F. 2007. Microphthalmic transcription factor(MITF) regulates cellular response to reactive oxygen species through transcriptional regulation of Ape1/Ref1. 67**,** 873-873.

LIU, P., CHEN, H., HAN, L., ZOU, X. & SHEN, W. 2015. Expression and role of V1A subunit of V-ATPases in gastric cancer cells. *International journal of clinical oncology,* 20**,** 725-735.

LIU, X., WILLIAMS, J. B., SUMPTER, B. R. & BEVENSEE, M. O. 2007. Inhibition of the Na/bicarbonate cotransporter NBCe1-A by diBAC oxonol dyes relative to niflumic acid and a stilbene. *The Journal of membrane biology,* 215**,** 195-204.

LIU, Y., YE, F., LI, Q., TAMIYA, S., DARLING, D. S., KAPLAN, H. J. & DEAN, D. C. 2009b. Zeb1 represses Mitf and regulates pigment synthesis, cell proliferation, and epithelial morphology. *Invest Ophthalmol Vis Sci,* 50**,** 5080-8.

LLOYD, R. V., ERICKSON, L. A., JIN, L., KULIG, E., QIAN, X., CHEVILLE, J. C. & SCHEITHAUER, B. W. 1999. p27kip1: a multifunctional cyclin-dependent

kinase inhibitor with prognostic significance in human cancers. *The American journal of pathology,* 154**,** 313-323.

LO, J. A. & FISHER, D. E. 2014. The melanoma revolution: from UV carcinogenesis to a new era in therapeutics. *Science,* 346**,** 945-9.

LOERCHER, A. E., TANK, E. M. H., DELSTON, R. B. & HARBOUR, J. W. 2005. MITF links differentiation with cell cycle arrest in melanocytes by transcriptional activation of INK4A. *The Journal of cell biology,* 168**,** 35-40.

LOH, S. H., SUN, B. & VAUGHAN-JONES, R. D. 1996. Effect of Hoe 694, a novel Na(+)-H+ exchange inhibitor, on intracellular pH regulation in the guinea-pig ventricular myocyte. *British Journal of Pharmacology,* 118**,** 1905-1912.

LONG, G. V., STROYAKOVSKIY, D., GOGAS, H., LEVCHENKO, E., DE BRAUD, F., LARKIN, J., GARBE, C., JOUARY, T., HAUSCHILD, A., GROB, J. J., CHIARION-SILENI, V., LEBBE, C., MANDALA, M., MILLWARD, M., ARANCE, A., BONDARENKO, I., HAANEN, J. B., HANSSON, J., UTIKAL, J., FERRARESI, V., KOVALENKO, N., MOHR, P., PROBACHAI, V., SCHADENDORF, D., NATHAN, P., ROBERT, C., RIBAS, A., DEMARINI, D. J., IRANI, J. G., SWANN, S., LEGOS, J. J., JIN, F., MOOKERJEE, B. & FLAHERTY, K. 2015. Dabrafenib and trametinib versus dabrafenib and placebo for Val600 BRAF-mutant melanoma: a multicentre, double-blind, phase 3 randomised controlled trial. *Lancet,* 386**,** 444-51.

LOO, S. Y., CHANG, M. K. X., CHUA, C. S. H., KUMAR, A. P., PERVAIZ, S. & CLEMENT, M. V. 2012. NHE-1: a promising target for novel anti-cancer therapeutics. *Current pharmaceutical design,* 18**,** 1372-1382.

LU, X., QIN, W., LI, J., TAN, N., PAN, D., ZHANG, H., XIE, L., YAO, G., SHU, H., YAO, M., WAN, D., GU, J. & YANG, S. 2005. The growth and metastasis of human hepatocellular carcinoma xenografts are inhibited by small interfering RNA targeting to the subunit ATP6L of proton pump. *Cancer research,* 65**,** 6843-6849.

LUO, C., MERZ, P. R., CHEN, Y., DICKES, E., PSCHERER, A., SCHADENDORF, D. & EICHMULLER, S. B. 2013. MiR-101 inhibits melanoma cell invasion and proliferation by targeting MITF and EZH2. *Cancer Lett,* 341**,** 240-7.

LUO, J., KINTNER, D. B., SHULL, G. E. & SUN, D. 2007. ERK1/2-p90RSK-mediated phosphorylation of Na+/H+ exchanger isoform 1. A role in ischemic neuronal death. *The Journal of biological chemistry,* 282**,** 28274-28284.

LURIA, S. E. & DELBRUCK, M. 1943. Mutations of Bacteria from Virus Sensitivity to Virus Resistance. *Genetics,* 28**,** 491-511.

M*Nature Communications,* 5**,** 5712.

MAATHUIS, F. J. 2017. Solute Transport: Basic Concepts. *In:* CLEMENS, S. (ed.) *Plant Physiology and Function.* New York, NY: Springer New York.

MACKIE, R. M. 2000. Malignant melanoma: clinical variants and prognostic indicators. 25**,** 471-475.

MACLEOD, K. J., VASILYEVA, E., BALEJA, J. D. & FORGAC, M. 1998. Mutational analysis of the nucleotide binding sites of the yeast vacuolar proton-translocating ATPase. *The Journal of biological chemistry,* 273**,** 150-156.

MAHONEY, K. M., FREEMAN, G. J. & MCDERMOTT, D. F. 2015. The Next Immune-Checkpoint Inhibitors: PD-1/PD-L1 Blockade in Melanoma. *Clinical Therapeutics,* 37**,** 764-782.

MANN, M. B., BLACK, M. A., JONES, D. J., WARD, J. M., YEW, C. C., NEWBERG, J. Y., DUPUY, A. J., RUST, A. G., BOSENBERG, M. W., MCMAHON, M., PRINT, C. G., COPELAND, N. G. & JENKINS, N. A. 2015. Transposon mutagenesis identifies genetic drivers of Braf(V600E) melanoma. *Nat Genet,* 47**,** 486-95.

MANOHARAN, C., MANOHARAN, C., WILSON, M. C., MANOHARAN, C., WILSON, M. C., SESSIONS, R. B. & HALESTRAP, A. P. 2006. The role of charged residues in the transmembrane helices of monocarboxylate transporter 1 and its ancillary protein basigin in determining plasma membrane expression and catalytic activity. *Molecular Membrane Biology,* 23**,** 486-498.

MANSKY, K. C., SANKAR, U., HAN, J. & OSTROWSKI, M. C. 2002. Microphthalmia transcription factor is a target of the p38 MAPK pathway in response to receptor activator of NF-kappa B ligand signaling. *J Biol Chem,* 277**,** 11077-83.

MANU, K. A., CAO, P. H. A., CHAI, T. F., CASEY, P. J. & WANG, M. 2019. p21cip1/waf1 Coordinate Autophagy, Proliferation and Apoptosis in Response to Metabolic Stress. *Cancers,* 11**,** 1112.

MARINO, M. L., FAIS, S., DJAVAHERI-MERGNY, M., VILLA, A., MESCHINI, S., LOZUPONE, F., VENTURI, G., DELLA MINA, P., PATTINGRE, S., RIVOLTINI, L., CODOGNO, P. & DE MILITO, A. 2010. Proton pump inhibition induces autophagy as a survival mechanism following oxidative stress in human melanoma cells. *Cell death & disease,* 1**,** e87-e87.

MARINO, M. L., PELLEGRINI, P., DI LERNIA, G., DJAVAHERI-MERGNY, M., BRNJIC, S., ZHANG, X., HAGG, M., LINDER, S., FAIS, S., CODOGNO, P. & DE MILITO, A. 2012. Autophagy is a protective mechanism for human melanoma cells under acidic stress. *J Biol Chem,* 287**,** 30664-76.

MARJUKI, H., GORNITZKY, A., MARATHE, B. M., ILYUSHINA, N. A., ALDRIDGE, J. R., DESAI, G., WEBBY, R. J. & WEBSTER, R. G. 2011. Influenza A virus-induced early activation of ERK and PI3K mediates V-ATPase-dependent intracellular pH change required for fusion. *Cellular microbiology,* 13**,** 587-601.

MARSDEN, J. R., NEWTON-BISHOP, J. A., BURROWS, L., COOK, M., CORRIE, P. G., COX, N. H., GORE, M. E., LORIGAN, P., MACKIE, R., NATHAN, P., PEACH, H., POWELL,

B., WALKER, C. & BRITISH ASSOCIATION OF DERMATOLOGISTS CLINICAL STANDARDS, U. 2010. Revised U.K. guidelines for the management of cutaneous melanoma 2010. *The British journal of dermatology,* 163**,** 238-256.

MARSH DURBAN, V., DEUKER, M. M., BOSENBERG, M. W., PHILLIPS, W. & MCMAHON, M. 2013. Differential AKT dependency displayed by mouse models of BRAFV600E-initiated melanoma. *The Journal of Clinical Investigation,* 123**,** 5104-5118.

MARSHANSKY, V., RUBINSTEIN, J. L. & GR*Biochimica et biophysica acta,* 1837**,** 857-879.

MARTIN, J. M., LUIS, J., MARVALDI, J., PICHON, J. & PIC, P. 1989. A human melanoma-derived cell line (IGR39) with a very high number of vasoactive-intestinal-peptide (VIP) receptors. 2. Effect of VIP on cAMP production and on cell-surface VIP-binding sites. *Eur J Biochem,* 180**,** 435-9.

MARTINEZ-ZAGUILAN, R., LYNCH, R. M., MARTINEZ, G. M. & GILLIES, R. J. 1993. Vacuolar-type H(+)-ATPases are functionally expressed in plasma membranes of human tumor cells. *The American journal of physiology,* 265**,** C1015-C1029.

MARTINEZ-ZAGUILAN, R., SEFTOR, E. A., SEFTOR, R. E., CHU, Y. W., GILLIES, R. J. & HENDRIX, M. J. 1996. Acidic pH enhances the invasive behavior of human melanoma cells. *Clin Exp Metastasis,* 14**,** 176-86.

MATALLANAS, D., BIRTWISTLE, M., ROMANO, D., ZEBISCH, A., RAUCH, J., VON KRIEGSHEIM, A. & KOLCH, W. 2011. Raf family kinases: old dogs have learned new tricks. *Genes & cancer,* 2**,** 232-260.

MATAMOROS-VOLANTE, A. & TREVI*Journal of Cell Science,* 133**,** jcs238816.

MATHEW, R., KARP, C. M., BEAUDOIN, B., VUONG, N., CHEN, G., CHEN, H.-Y., BRAY, K., REDDY, A., BHANOT, G., GELINAS, C., DIPAOLA, R. S., KARANTZA-WADSWORTH, V. & WHITE, E. 2009. Autophagy suppresses tumorigenesis through elimination of p62. *Cell,* 137**,** 1062-1075.

MATHUPALA, S. P., PARAJULI, P. & SLOAN, A. E. 2004. Silencing of monocarboxylate transporters via small interfering ribonucleic acid inhibits glycolysis and induces cell death in malignant glioma: an in vitro study. *Neurosurgery,* 55**,** 1410-9; discussion 1419.

MATSUI, T. & AMAGAI, M. 2015. Dissecting the formation, structure and barrier function of the stratum corneum. *International immunology,* 27**,** 269-280.

MAUVEZIN, C., NAGY, P., JUHñSZ, G. & NEUFELD, T. P. 2015. Autophagosome-lysosome fusion is independent of V-ATPase-mediated acidification. *Nature communications,* 6**,** 7007-7007.

MAZZIO, E. A. & SOLIMAN, K. F. A. 2018. Whole-transcriptomic Profile of SK-MEL-3 Melanoma Cells Treated with the Histone Deacetylase Inhibitor: Trichostatin

A. *Cancer Genomics Proteomics,* 15**,** 349-364.

MCARTHUR, G. A., CHAPMAN, P. B., ROBERT, C., LARKIN, J., HAANEN, J. B., DUMMER, R., RIBAS, A., HOGG, D., HAMID, O., ASCIERTO, P. A., GARBE, C., TESTORI, A., MAIO, M., LORIGAN, P., LEBBE, C., JOUARY, T., SCHADENDORF, D., O'DAY, S. J., KIRKWOOD, J. M., EGGERMONT, A. M., DRENO, B., SOSMAN, J. A., FLAHERTY, K. T., YIN, M., CARO, I., CHENG, S., TRUNZER, K. & HAUSCHILD, A. 2014. Safety and efficacy of vemurafenib in BRAF(V600E) and BRAF(V600K) mutation-positive melanoma (BRIM-3): extended follow-up of a phase 3, randomised, open-label study. *Lancet Oncol,* 15**,** 323-32.

MCBRIAN, M. A., BEHBAHAN, I. S., FERRARI, R., SU, T., HUANG, T. W., LI, K., HONG, C. S., CHRISTOFK, H. R., VOGELAUER, M., SELIGSON, D. B. & KURDISTANI, S. K. 2013. Histone acetylation regulates intracellular pH. *Mol Cell,* 49**,** 310-21.

MCCLOY, R. A., ROGERS, S., CALDON, C. E., LORCA, T., CASTRO, A. & BURGESS, A. 2014. Partial inhibition of Cdk1 in G 2 phase overrides the SAC and decouples mitotic events. *Cell Cycle,* 13**,** 1400-12.

MCCUBREY, J. A., STEELMAN, L. S., ABRAMS, S. L., LEE, J. T., CHANG, F., BERTRAND, F. E., NAVOLANIC, P. M., TERRIAN, D. M., FRANKLIN, R. A., D'ASSORO, A. B., SALISBURY, J. L., MAZZARINO, M. C., STIVALA, F. & LIBRA, M. 2006. Roles of the RAF/MEK/ERK and PI3K/PTEN/AKT pathways in malignant transformation and drug resistance. *Adv Enzyme Regul,* 46**,** 249-79.

MCDERMOTT, N. C., HAYES, D. P., AL-SADER, M. H., HOGAN, J. M., WALSH, C. B., KAY, E. W. & LEADER, M. B. 1998. Identification of vertical growth phase in malignant melanoma. A study of interobserver agreement. *American journal of clinical pathology,* 110**,** 753-757.

MCGILL, G. G., HAQ, R., NISHIMURA, E. K. & FISHER, D. E. 2006. c-Met expression is regulated by Mitf in the melanocyte lineage. *J Biol Chem,* 281**,** 10365-73.

MCGILL, G. G., HORSTMANN, M., WIDLUND, H. R., DU, J., MOTYCKOVA, G., NISHIMURA, E. K., LIN, Y.-L., RAMASWAMY, S., AVERY, W., DING, H.-F., JORDAN, S. A., JACKSON, I. J., KORSMEYER, S. J., GOLUB, T. R. & FISHER, D. E. 2002. Bcl2 Regulation by the Melanocyte Master Regulator Mitf Modulates Lineage Survival and Melanoma Cell Viability. *Cell,* 109**,** 707-718.

MEHTA, G., KUMARASAMY, S., WU, J., WALSH, A., LIU, L., WILLIAMS, K., JOE, B. & DE LA SERNA, I. L. 2015. MITF interacts with the SWI/SNF subunit, BRG1, to promote GATA4 expression in cardiac hypertrophy. *Journal of molecular and cellular cardiology,* 88**,** 101-110.

MEIMA, M. E., WEBB, B. A., WITKOWSKA, H. E. & BARBER, D. L. 2009. The sodium-hydrogen exchanger NHE1 is an Akt substrate necessary for actin filament reorganization by growth factors. *The Journal of biological chemistry,* 284**,**

26666-26675.

MEREDITH, D. & CHRISTIAN, H. C. 2008. The SLC16 monocaboxylate transporter family. *Xenobiotica,* 38**,** 1072-1106.

MICHIELIN, O., VAN AKKOOI, A. C. J., ASCIERTO, P. A., DUMMER, R., KEILHOLZ, U. & COMMITTEE, T. E. G. 2019. Cutaneous melanoma: ESMO Clinical Practice Guidelines for diagnosis, treatment and follow-up†. *Annals of Oncology,* 30**,** 1884-1901.

MICHNE, W. F., SCHROEDER, J. D., GUILES, J. W., TREASURYWALA, A. M., WEIGELT, C. A., STANSBERRY, M. F., MCAVOY, E., SHAH, C. R., BAINE, Y., SAWUTZ, D. G. & ET AL. 1995. Novel inhibitors of the nuclear factor of activated T cells (NFAT)-mediated transcription of beta-galactosidase: potential immunosuppressive and antiinflammatory agents. *J Med Chem,* 38**,** 2557-69.

MILLER, A. J., LEVY, C., DAVIS, I. J., RAZIN, E. & FISHER, D. E. 2005. Sumoylation of MITF and its related family members TFE3 and TFEB. *J Biol Chem,* 280**,** 146-55.

MONGERA, A. & DOOLEY, C. M. 2013. Of white tigers and solute carriers. *Pigment cell & melanoma research,* 26**,** 787-789.

MONZON, J., LIU, L., BRILL, H., GOLDSTEIN, A. M., TUCKER, M. A., FROM, L., MCLAUGHLIN, J., HOGG, D. & LASSAM, N. J. 1998. CDKN2A Mutations in Multiple Primary Melanomas. *New England Journal of Medicine,* 338**,** 879-887.

MOON, H., DONAHUE, L. R., CHOI, E., SCUMPIA, P. O., LOWRY, W. E., GRENIER, J. K., ZHU, J. & WHITE, A. C. 2017. Melanocyte Stem Cell Activation and Translocation Initiate Cutaneous Melanoma in Response to UV Exposure. *Cell Stem Cell,* 21**,** 665-678.e6.

MOROTTI, M., BRIDGES, E., VALLI, A., CHOUDHRY, H., SHELDON, H., WIGFIELD, S., GRAY, N., ZOIS, C. E., GRIMM, F., JONES, D., TEOH, E. J., CHENG, W.-C., LORD, S., ANASTASIOU, D., HAIDER, S., MCINTYRE, A., GOBERDHAN, D. C. I., BUFFA, F. & HARRIS, A. L. 2019. Hypoxia-induced switch in SNAT2/SLC38A2 regulation generates endocrine resistance in breast cancer. *Proceedings of the National Academy of Sciences,* 116**,** 12452.

MOTZIK, A., AMIR, E., ERLICH, T., WANG, J., KIM, B. G., HAN, J. M., KIM, J. H., NECHUSHTAN, H., GUO, M., RAZIN, E. & TSHORI, S. 2017. Post-translational modification of HINT1 mediates activation of MITF transcriptional activity in human melanoma cells. *Oncogene,* 36**,** 4732-4738.

MROWIEC, A., JENSEN, B., PRAETORIUS, J., BUUS, C. & AALKJAER, C. The NBCn1 protein expression is increased through different mechanisms in two models of enhanced renal distal tubular NH4+ delivery. FASEB JOURNAL, 2005.

FEDERATION AMER SOC EXP BIOL 9650 ROCKVILLE PIKE, BETHESDA, MD 20814-3998 USA, A141-A141.

MULKIDJANIAN, A. Y., MAKAROVA, K. S., GALPERIN, M. Y. & KOONIN, E. V. 2007. Inventing the dynamo machine: the evolution of the F-type and V-type ATPases. *Nature Reviews Microbiology,* 5**,** 892.

MURAKAMI, H. & ARNHEITER, H. 2005. Sumoylation modulates transcriptional activity of MITF in a promoter-specific manner. *Pigment Cell Res,* 18**,** 265-77.

MURRAY, C. M., HUTCHINSON, R., BANTICK, J. R., BELFIELD, G. P., BENJAMIN, A. D., BRAZMA, D., BUNDICK, R. V., COOK, I. D., CRAGGS, R. I., EDWARDS, S., EVANS, L. R., HARRISON, R., HOLNESS, E., JACKSON, A. P., JACKSON, C. G., KINGSTON, L. P., PERRY, M. W., ROSS, A. R., RUGMAN, P. A., SIDHU, S. S., SULLIVAN, M., TAYLOR-FISHWICK, D. A., WALKER, P. C., WHITEHEAD, Y. M., WILKINSON, D. J., WRIGHT, A. & DONALD, D. K. 2005. Monocarboxylate transporter MCT1 is a target for immunosuppression. *Nat Chem Biol,* 1**,** 371-6.

NAKAYAMA, A., NGUYEN, M.-T. T., CHEN, C. C., OPDECAMP, K., HODGKINSON, C. A. & ARNHEITER, H. 1998. Mutations in microphthalmia, the mouse homolog of the human deafness gene MITF, affect neuroepithelial and neural crest-derived melanocytes differently. *Mechanisms of Development,* 70**,** 155-166.

NAMKOONG, S., LEE, K. I., LEE, J. I., PARK, R., LEE, E.-J., JANG, I.-S. & PARK, J. 2015. The integral membrane protein ITM2A, a transcriptional target of PKA-CREB, regulates autophagic flux via interaction with the vacuolar ATPase. *Autophagy,* 11**,** 756-768.

NAZARIAN, R., SHI, H., WANG, Q., KONG, X., KOYA, R. C., LEE, H., CHEN, Z., LEE, M. K., ATTAR, N., SAZEGAR, H., CHODON, T., NELSON, S. F., MCARTHUR, G., SOSMAN, J. A., RIBAS, A. & LO, R. S. 2010. Melanomas acquire resistance to B-RAF(V600E) inhibition by RTK or N-RAS upregulation. *Nature,* 468**,** 973-7.

NEDERGAARD, M., GOLDMAN, S. A., DESAI, S. & PULSINELLI, W. A. 1991. Acid-induced death in neurons and glia. *J Neurosci,* 11**,** 2489-97.

NISHIMURA, H., NOSE, M., HIAI, H., MINATO, N. & HONJO, T. 1999. Development of Lupus-like Autoimmune Diseases by Disruption of the PD-1 Gene Encoding an ITIM Motif-Carrying Immunoreceptor. *Immunity,* 11**,** 141-151.

NISHISHO, T., HATA, K., NAKANISHI, M., MORITA, Y., SUN-WADA, G.-H., WADA, Y., YASUI, N. & YONEDA, T. 2011. The a3 isoform vacuolar type H^+-ATPase promotes distant metastasis in the mouse B16 melanoma cells. *Molecular cancer research : MCR,* 9**,** 845-855.

NOGUCHI, K., DALTON, A. C., HOWLEY, B. V., MCCALL, B. J., YOSHIDA, A., DIEHL, J. A. & HOWE, P. H. 2017. Interleukin-like EMT inducer regulates partial phenotype switching in MITF-low melanoma cell lines. *PLoS ONE,* 12**,** e0177830.

NOOR, S. I., JAMALI, S., AMES, S., LANGER, S., DEITMER, J. W. & BECKER, H. M. 2018. A surface proton antenna in carbonic anhydrase II supports lactate transport in cancer cells. *eLife,* 7**,** e35176.

NOWIK, M., LECCA, M. R., VELIC, A., REHRAUER, H., BRôNDLI, A. W. & WAGNER, C. A. 2008. Genome-wide gene expression profiling reveals renal genes regulated during metabolic acidosis. *Physiological Genomics,* 32**,** 322-334.

OHGAKI, R., VAN IJZENDOORN, S. C. D., MATSUSHITA, M., HOEKSTRA, D. & KANAZAWA, H. 2011. Organellar Na+/H+ Exchangers: Novel Players in Organelle pH Regulation and Their Emerging Functions. *Biochemistry,* 50**,** 443-450.

OHMAN, H. & VAHLQUIST, A. 1994. In vivo studies concerning a pH gradient in human stratum corneum and upper epidermis. *Acta dermato-venereologica,* 74**,** 375-379.

OHSIE, S. J., SARANTOPOULOS, G. P., COCHRAN, A. J. & BINDER, S. W. 2008. Immunohistochemical characteristics of melanoma. *Journal of cutaneous pathology,* 35**,** 433-444.

OHTA, T., ARAKAWA, H., FUTAGAMI, F., FUSHIDA, S., KITAGAWA, H., KAYAHARA, M., NAGAKAWA, T., MIWA, K., KURASHIMA, K., NUMATA, M., KITAMURA, Y., TERADA, T. & OHKUMA, S. 1998. Bafilomycin A1 induces apoptosis in the human pancreatic cancer cell line Capan-1. *The Journal of pathology,* 185**,** 324-330.

OHTANI, N., YAMAKOSHI, K., TAKAHASHI, A. & HARA, E. 2004. The p16INK4a-RB pathway: molecular link between cellular senescence and tumor suppression. *The journal of medical investigation : JMI,* 51**,** 146-153.

OLSON, O. C. & JOYCE, J. A. 2015. Cysteine cathepsin proteases: regulators of cancer progression and therapeutic response. *Nature Reviews Cancer,* 15**,** 712-729.

ORLOWSKI, J. & GRINSTEIN, S. 2004. Diversity of the mammalian sodium/proton exchanger SLC9 gene family. *Pflugers Archiv : European journal of physiology,* 447**,** 549-565.

OTERO-REY, E. M., SOMOZA-MARTýN, M., BARROS-ANGUEIRA, F. & GARCýA-GARCýA, A. 2008. Intracellular pH regulation in oral squamous cell carcinoma is mediated by increased V-ATPase activity via over-expression of the ATP6V1C1 gene. *Oral oncology,* 44**,** 193-199.

OVENS, M. J., DAVIES, A. J., WILSON, M. C., MURRAY, C. M. & HALESTRAP, A. P. 2010a. AR-C155858 is a potent inhibitor of monocarboxylate transporters MCT1 and MCT2 that binds to an intracellular site involving transmembrane helices 7-10. *The Biochemical journal,* 425**,** 523-530.

OVENS, MATTHEW J., MANOHARAN, C., WILSON, MARIEANGELA C., MURRAY,

CLAREY M. & HALESTRAP, ANDREW P. 2010b. The inhibition of monocarboxylate transporter 2 (MCT2) by AR-C155858 is modulated by the associated ancillary protein. *Biochemical Journal,* 431**,** 217-225.

P¢REZ-ESCUREDO, J., VAN H¢E, V. F., SBOARINA, M., FALCES, J., PAYEN, V. L., PELLERIN, L. & SONVEAUX, P. 2016. Monocarboxylate transporters in the brain and in cancer. *Biochimica et Biophysica Acta (BBA) - Molecular Cell Research,* 1863**,** 2481-2497.

P¢REZ DE HEREDIA, F., WOOD, I. S. & TRAYHURN, P. 2010. Hypoxia stimulates lactate release and modulates monocarboxylate transporter (MCT1, MCT2, and MCT4) expression in human adipocytes. *Pflugers Archiv : European journal of physiology,* 459**,** 509-518.

PAHLMAN, C., QI, Z., MURRAY, C. M., FERGUSON, D., BUNDICK, R. V., DONALD, D. K. & EKBERG, H. 2013. Immunosuppressive properties of a series of novel inhibitors of the monocarboxylate transporter MCT-1. *Transpl Int,* 26**,** 22-9.

PALMIERI, G., COLOMBINO, M., CASULA, M., BUDRONI, M., MANCA, A., SINI, M. C., LISSIA, A., STANGANELLI, I., ASCIERTO, P. A. & COSSU, A. 2015. Epidemiological and genetic factors underlying melanoma development in Italy. *Melanoma Management,* 2**,** 149-163.

PAMARTHY, S., KULSHRESTHA, A., KATARA, G. K. & BEAMAN, K. D. 2018. The curious case of vacuolar ATPase: regulation of signaling pathways. *Molecular Cancer,* 17**,** 41.

PAMPENA, R., KYRGIDIS, A., LALLAS, A., MOSCARELLA, E., ARGENZIANO, G. & LONGO, C. 2017. A meta-analysis of nevus-associated melanoma: Prevalence and practical implications. *Journal of the American Academy of Dermatology,* 77**,** 938-945.e4.

PAN, L., MA, X., WEN, B., SU, Z., ZHENG, X., LIU, Y., LI, H., CHEN, Y., WANG, J., LU, F., QU, J. & HOU, L. 2015. Microphthalmia-associated transcription factor/T-box factor-2 axis acts through Cyclin D1 to regulate melanocyte proliferation. *Cell proliferation,* 48**,** 631-642.

PAN, S., CAI, H., GU, L. & CAO, S. 2017. Cleistanthin A inhibits the invasion and metastasis of human melanoma cells by inhibiting the expression of matrix metallopeptidase-2 and -9. *Oncol Lett,* 14**,** 6217-6223.

PAPALE, M., FERRETTI, E., BATTAGLIA, G., BELLAVIA, D., MAI, A. & TAFANI, M. 2018. EZH2, HIF-1, and Their Inhibitors: An Overview on Pediatric Cancers. *Front Pediatr,* 6**,** 328.

PARK, H.-Y., WU, C., YONEMOTO, L., MURPHY-SMITH, M., WU, H., STACHUR, CHRISTINA M. & GILCHREST, BARBARA A. 2006. MITF mediates cAMP-induced protein kinase C-β expression in human melanocytes. *Biochemical Journal,*

395**,** 571-578.

PARK, H. J., LYONS, J. C., OHTSUBO, T. & SONG, C. W. 1999. Acidic environment causes apoptosis by increasing caspase activity. *British Journal of Cancer,* 80**,** 1892-1897.

PARK, H. J., RAJBHANDARI, I., YANG, H. S., LEE, S., CUCORANU, D., COOPER, D. S., KLEIN, J. D., SANDS, J. M. & CHOI, I. 2010. Neuronal expression of sodium/bicarbonate cotransporter NBCn1 (SLC4A7) and its response to chronic metabolic acidosis. *American Journal of Physiology-Cell Physiology,* 298**,** C1018-C1028.

PARK, M., KO, S. B. H., CHOI, J. Y., MUALLEM, G., THOMAS, P. J., PUSHKIN, A., LEE, M.-S., KIM, J. Y., LEE, M. G., MUALLEM, S. & KURTZ, I. 2002. The cystic fibrosis transmembrane conductance regulator interacts with and regulates the activity of the HCO3- salvage transporter human Na+-HCO3- cotransport isoform 3. *The Journal of biological chemistry,* 277**,** 50503-50509.

PARKER, M. D. & BORON, W. F. 2013. The divergence, actions, roles, and relatives of sodium-coupled bicarbonate transporters. *Physiological reviews,* 93**,** 803-959.

PARKER, M. D., MUSA-AZIZ, R., ROJAS, J. D., CHOI, I., DALY, C. M. & BORON, W. F. 2008. Characterization of human SLC4A10 as an electroneutral Na/HCO3 cotransporter (NBCn2) with Cl- self-exchange activity. *The Journal of biological chemistry,* 283**,** 12777-12788.

PARMENTER, T. J., KLEINSCHMIDT, M., KINROSS, K. M., BOND, S. T., LI, J., KAADIGE, M. R., RAO, A., SHEPPARD, K. E., HUGO, W., PUPO, G. M., PEARSON, R. B., MCGEE, S. L., LONG, G. V., SCOLYER, R. A., RIZOS, H., LO, R. S., CULLINANE, C., AYER, D. E., RIBAS, A., JOHNSTONE, R. W., HICKS, R. J. & MCARTHUR, G. A. 2014. Response of BRAF mutant melanoma to BRAF inhibition is mediated by a network of transcriptional regulators of glycolysis. *Cancer Discovery*.

PASTOR-SOLER, N., BEAULIEU, V., LITVIN, T. N., DA SILVA, N., CHEN, Y., BROWN, D., BUCK, J., LEVIN, L. R. & BRETON, S. 2003. Bicarbonate-regulated adenylyl cyclase (sAC) is a sensor that regulates pH-dependent V-ATPase recycling. *The Journal of biological chemistry,* 278**,** 49523-49529.

PAVLOVA, N. N. & THOMPSON, C. B. 2016. The Emerging Hallmarks of Cancer Metabolism. *Cell metabolism,* 23**,** 27-47.

PAYEN, V. L., MINA, E., VAN H¢E, V. F., PORPORATO, P. E. & SONVEAUX, P. 2019. Monocarboxylate transporters in cancer. *Molecular Metabolism*.

PEERS, C., BRAHIMI-HORN, M. C. & POUYSS¢GUR, J. J. E. I. B. 2007. Hypoxia in cancer cell metabolism and pH regulation. 43**,** 165-178.

PEREZ, I. R., FENSKE, N. A. & BROZENA, S. J. 1993. Malignant melanoma: differential diagnosis of the pigmented lesion. *Seminars in surgical oncology,* 9**,** 168-173.

PETZOLDT, A. G., GLEIXNER, E. M., FUMAGALLI, A., VACCARI, T. & SIMONS, M. 2013. Elevated expression of the V-ATPase C subunit triggers JNK-dependent cell invasion and overgrowth in a Drosophila epithelium. *Disease models & mechanisms,* 6**,** 689-700.

PEYTON, K. J., LIU, X.-M., YU, Y., YATES, B., BEHNAMMANESH, G. & DURANTE, W. 2018. Glutaminase-1 stimulates the proliferation, migration, and survival of human endothelial cells. *Biochemical pharmacology,* 156**,** 204-214.

PHILP, N., CHU, P., PAN, T.-C., ZHANG, R. Z., CHU, M.-L., STARK, K., BOETTIGER, D., YOON, H. & KIEBER-EMMONS, T. 1995. Developmental Expression and Molecular Cloning of REMP, a Novel Retinal Epithelial Membrane Protein. *Experimental Cell Research,* 219**,** 64-73.

PHUNG, B., SUN, J., SCHEPSKY, A., STEINGRIMSSON, E. & R*PloS one,* 6**,** e24064-e24064.

PIERRAT, M. J., MARSAUD, V., MAUVIEL, A. & JAVELAUD, D. 2012. Expression of microphthalmia-associated transcription factor (MITF), which is critical for melanoma progression, is inhibited by both transcription factor GLI2 and transforming growth factor-beta. *J Biol Chem,* 287**,** 17996-8004.

PIERRE, K. & PELLERIN, L. 2005. Monocarboxylate transporters in the central nervous system: distribution, regulation and function. *Journal of neurochemistry,* 94**,** 1-14.

PINHEIRO, C., MIRANDA-GON÷ALVES, V., LONGATTO-FILHO, A., VICENTE, A. L. S. A., BERARDINELLI, G. N., SCAPULATEMPO-NETO, C., COSTA, R. F. A., VIANA, C. R., REIS, R. M., BALTAZAR, F. & VAZQUEZ, V. L. 2016. The metabolic microenvironment of melanomas: Prognostic value of MCT1 and MCT4. *Cell Cycle,* 15**,** 1462-1470.

PLAITAKIS, A., KALEF-EZRA, E., KOTZAMANI, D., ZAGANAS, I. & SPANAKI, C. 2017. The Glutamate Dehydrogenase Pathway and Its Roles in Cell and Tissue Biology in Health and Disease. *Biology,* 6**,** 11.

POGENBERG, V., OGMUNDSD*Genes & development,* 26**,** 2647-2658.

POLANSKI, R., HODGKINSON, C. L., FUSI, A., NONAKA, D., PRIEST, L., KELLY, P., TRAPANI, F., BISHOP, P. W., WHITE, A., CRITCHLOW, S. E., SMITH, P. D., BLACKHALL, F., DIVE, C. & MORROW, C. J. 2014. Activity of the monocarboxylate transporter 1 inhibitor AZD3965 in small cell lung cancer. *Clin Cancer Res,* 20**,** 926-937.

POOLE, R. C. & HALESTRAP, A. P. 1993. Transport of lactate and other monocarboxylates across mammalian plasma membranes. *The American journal of physiology,* 264**,** C761-C782.

POOLE, R. C. & HALESTRAP, A. P. 1997. Interaction of the Erythrocyte Lactate

Transporter (Monocarboxylate Transporter 1) with an Integral 70-kDa Membrane Glycoprotein of the Immunoglobulin Superfamily. *Journal of Biological Chemistry,* 272**,** 14624-14628.

POOLE, R. C., HALESTRAP, A. P., PRICE, S. J. & LEVI, A. J. 1989. The kinetics of transport of lactate and pyruvate into isolated cardiac myocytes from guinea pig. Kinetic evidence for the presence of a carrier distinct from that in erythrocytes and hepatocytes. *The Biochemical journal,* 264**,** 409-418.

POOLE, R. C., SANSOM, C. E. & HALESTRAP, A. P. 1996. Studies of the membrane topology of the rat erythrocyte H+/lactate cotransporter (MCT1). *Biochemical Journal,* 320**,** 817-824.

POTTER, C. & HARRIS, A. L. 2004. Hypoxia inducible carbonic anhydrase IX, marker of tumour hypoxia, survival pathway and therapy target. *Cell cycle (Georgetown, Tex.),* 3**,** 164-167.

POULIKAKOS, P. I., PERSAUD, Y., JANAKIRAMAN, M., KONG, X., NG, C., MORICEAU, G., SHI, H., ATEFI, M., TITZ, B., GABAY, M. T., SALTON, M., DAHLMAN, K. B., TADI, M., WARGO, J. A., FLAHERTY, K. T., KELLEY, M. C., MISTELI, T., CHAPMAN, P. B., SOSMAN, J. A., GRAEBER, T. G., RIBAS, A., LO, R. S., ROSEN, N. & SOLIT, D. B. 2011. RAF inhibitor resistance is mediated by dimerization of aberrantly spliced BRAF(V600E). *Nature,* 480**,** 387-90.

POWELL, B., GRAHAM, L. A. & STEVENS, T. H. 2000. Molecular characterization of the yeast vacuolar H+-ATPase proton pore. *The Journal of biological chemistry,* 275**,** 23654-23660.

PRAETORIUS, J., KIM, Y.-H., BOUZINOVA, E. V., FRISCHE, S., ROJEK, A., AALKJAER, C. & NIELSEN, S. 2004. NBCn1 is a basolateral Na+-HCO3- cotransporter in rat kidney inner medullary collecting ducts. *American journal of physiology. Renal physiology,* 286**,** F903-F912.

PRICE, N. M., RYWLIN, A. M. & ACKERMAN, A. B. 1976. Histologic criteria for the diagnosis of superficial spreading malignant melanoma: formulated on the basis of proven metastatic lesions. *Cancer,* 38**,** 2434-2441.

PRICE, N. T., JACKSON, V. N. & HALESTRAP, A. P. 1998. Cloning and sequencing of four new mammalian monocarboxylate transporter (MCT) homologues confirms the existence of a transporter family with an ancient past. *The Biochemical journal,* 329 (Pt 2)**,** 321-328.

PUSHKIN, A., ABULADZE, N., NEWMAN, D., LEE, I., XU, G. & KURTZ, I. 2000. Cloning, characterization and chromosomal assignment of NBC4, a new member of the sodium bicarbonate cotransporter family. *Biochimica et biophysica acta,* 1493**,** 215-218.

PUTNEY, L. K., DENKER, S. P. & BARBER, D. L. 2002. The changing face of the Na+/H+

exchanger, NHE1: structure, regulation, and cellular actions. *Annu Rev Pharmacol Toxicol,* 42**,** 527-52.

QUANZ, M., BENDER, E., KOPITZ, C., GRUNEWALD, S., SCHLICKER, A., SCHWEDE, W., EHEIM, A., TOSCHI, L., NEUHAUS, R., RICHTER, C., TOEDLING, J., MERZ, C., LESCHE, R., KAMBUROV, A., SIEBENEICHER, H., BAUSER, M. & HAGEBARTH, A. 2018. Preclinical Efficacy of the Novel Monocarboxylate Transporter 1 Inhibitor BAY-8002 and Associated Markers of Resistance. *Mol Cancer Ther,* 17**,** 2285-2296.

RABBIE, R., FERGUSON, P., MOLINA-AGUILAR, C., ADAMS, D. J. & ROBLES-ESPINOZA, C. D. 2019. Melanoma subtypes: genomic profiles, prognostic molecular markers and therapeutic possibilities. *The Journal of pathology,* 247**,** 539-551.

RACKER, E. 1974. History of the Pasteur effect and its pathobiology. *Molecular and cellular biochemistry,* 5**,** 17-23.

RAJA, D. A., GOTHERWAL, V., BURSE, S. A., SUBRAMANIAM, Y. J., SULTAN, F., VATS, A., GAUTAM, H., SHARMA, B., SHARMA, S., SINGH, A., SIVASUBBU, S., GOKHALE, R. S. & NATARAJAN, V. T. 2020. pH-controlled histone acetylation amplifies melanocyte differentiation downstream of MITF. *EMBO reports,* 21**,** e48333.

RAMBOW, F., ROGIERS, A., MARIN-BEJAR, O., AIBAR, S., FEMEL, J., DEWAELE, M., KARRAS, P., BROWN, D., CHANG, Y. H., DEBIEC-RYCHTER, M., ADRIAENS, C., RADAELLI, E., WOLTER, P., BECHTER, O., DUMMER, R., LEVESQUE, M., PIRIS, A., FREDERICK, D. T., BOLAND, G., FLAHERTY, K. T., VAN DEN OORD, J., VOET, T., AERTS, S., LUND, A. W. & MARINE, J. C. 2018. Toward Minimal Residual Disease-Directed Therapy in Melanoma. *Cell,* 174**,** 843-855.e19.

RAMIREZ, C., HAUSER, A. D., VUCIC, E. A. & BAR-SAGI, D. 2019. Plasma membrane V-ATPase controls oncogenic RAS-induced macropinocytosis. *Nature,* 576**,** 477-481.

RAPOSO, G. & MARKS, M. S. 2007. Melanosomes--dark organelles enlighten endosomal membrane transport. *Nature reviews. Molecular cell biology,* 8**,** 786-797.

RASTRELLI, M., TROPEA, S., ROSSI, C. R. & ALAIBAC, M. 2014. Melanoma: epidemiology, risk factors, pathogenesis, diagnosis and classification. *In Vivo,* 28**,** 1005-11.

RATNIKOV, B. I., SCOTT, D. A., OSTERMAN, A. L., SMITH, J. W. & RONAI, Z. A. 2016. Metabolic rewiring in melanoma. *Oncogene,* 36**,** 147.

REICHERT, M., STEINBACH, J. P., SUPRA, P. & WELLER, M. 2002. Modulation of growth and radiochemosensitivity of human malignant glioma cells by acidosis. *Cancer,* 95**,** 1113-9.

RICHARDS, W. L., SONG, M. K., KRUTZSCH, H., EVARTS, R. P., MARSDEN, E. &

THORGEIRSSON, S. S. 1985. Measurement of cell proliferation in microculture using hoechst 33342 for the rapid semiautomated microfluorimetric determination of chromatin DNA. *Experimental Cell Research,* 159**,** 235-246.

RIOS, M., HABECKER, B., SASAOKA, T., EISENHOFER, G., TIAN, H., LANDIS, S., CHIKARAISHI, D. & ROFFLER-TARLOV, S. 1999. Catecholamine synthesis is mediated by tyrosinase in the absence of tyrosine hydroxylase. *J Neurosci,* 19**,** 3519-26.

ROBERT, C., GROB, J. J., STROYAKOVSKIY, D., KARASZEWSKA, B., HAUSCHILD, A., LEVCHENKO, E., CHIARION SILENI, V., SCHACHTER, J., GARBE, C., BONDARENKO, I., GOGAS, H., MANDALñ, M., HAANEN, J. B. A. G., LEBB¢, C., MACKIEWICZ, A., RUTKOWSKI, P., NATHAN, P. D., RIBAS, A., DAVIES, M. A., FLAHERTY, K. T., BURGESS, P., TAN, M., GASAL, E., VOI, M., SCHADENDORF, D. & LONG, G. V. 2019. Five-Year Outcomes with Dabrafenib plus Trametinib in Metastatic Melanoma. *New England Journal of Medicine,* 381**,** 626-636.

ROBERT, C., KARASZEWSKA, B., SCHACHTER, J., RUTKOWSKI, P., MACKIEWICZ, A., STROIAKOVSKI, D., LICHINITSER, M., DUMMER, R., GRANGE, F., MORTIER, L., CHIARION-SILENI, V., DRUCIS, K., KRAJSOVA, I., HAUSCHILD, A., LORIGAN, P., WOLTER, P., LONG, G. V., FLAHERTY, K., NATHAN, P., RIBAS, A., MARTIN, A.-M., SUN, P., CRIST, W., LEGOS, J., RUBIN, S. D., LITTLE, S. M. & SCHADENDORF, D. 2014. Improved Overall Survival in Melanoma with Combined Dabrafenib and Trametinib. *New England Journal of Medicine,* 372**,** 30-39.

ROBERT, C., LONG, G. V., BRADY, B., DUTRIAUX, C., MAIO, M., MORTIER, L., HASSEL, J. C., RUTKOWSKI, P., MCNEIL, C., KALINKA-WARZOCHA, E., SAVAGE, K. J., HERNBERG, M. M., LEBBE, C., CHARLES, J., MIHALCIOIU, C., CHIARION-SILENI, V., MAUCH, C., COGNETTI, F., ARANCE, A., SCHMIDT, H., SCHADENDORF, D., GOGAS, H., LUNDGREN-ERIKSSON, L., HORAK, C., SHARKEY, B., WAXMAN, I. M., ATKINSON, V. & ASCIERTO, P. A. 2015a. Nivolumab in previously untreated melanoma without BRAF mutation. *N Engl J Med,* 372**,** 320-30.

ROBERT, C., SCHACHTER, J., LONG, G. V., ARANCE, A., GROB, J. J., MORTIER, L., DAUD, A., CARLINO, M. S., MCNEIL, C., LOTEM, M., LARKIN, J., LORIGAN, P., NEYNS, B., BLANK, C. U., HAMID, O., MATEUS, C., SHAPIRA-FROMMER, R., KOSH, M., ZHOU, H., IBRAHIM, N., EBBINGHAUS, S. & RIBAS, A. 2015b. Pembrolizumab versus Ipilimumab in Advanced Melanoma. *N Engl J Med,* 372**,** 2521-32.

ROBERTS, C. W. M. & ORKIN, S. H. 2004. The SWI/SNF complex — chromatin and cancer. *Nature Reviews Cancer,* 4**,** 133-142.

ROBILLIARD, L. D., KHO, D. T., JOHNSON, R. H., ANCHAN, A., O'CARROLL, S. J. & GRAHAM, E. S. 2018. The Importance of Multifrequency Impedance Sensing of Endothelial Barrier Formation Using ECIS Technology for the Generation of

a Strong and Durable Paracellular Barrier. *Biosensors,* 8**,** 64.

ROFSTAD, E. K., MATHIESEN, B., KINDEM, K. & GALAPPATHI, K. 2006a. Acidic Extracellular pH Promotes Experimental Metastasis of Human Melanoma Cells in Athymic Nude Mice. *Cancer Research,* 66**,** 6699.

ROFSTAD, E. K., MATHIESEN, B., KINDEM, K. & GALAPPATHI, K. 2006b. Acidic extracellular pH promotes experimental metastasis of human melanoma cells in athymic nude mice. *Cancer Res,* 66**,** 6699-707.

ROMERO, M. F. 2001. The electrogenic Na+/HCO3- cotransporter, NBC. *JOP : Journal of the pancreas,* 2**,** 182-191.

ROMERO, M. F. & BORON, W. F. 1999. ELECTROGENIC Na+/HCO−3 COTRANSPORTERS: Cloning and Physiology. *Annual Review of Physiology,* 61**,** 699-723.

ROMERO, M. F., CHEN, A.-P., PARKER, M. D. & BORON, W. F. 2013. The SLC4 family of bicarbonate (HCO_3^-) transporters. *Molecular aspects of medicine,* 34**,** 159-182.

ROMERO, M. F., HEDIGER, M. A., BOULPAEP, E. L. & BORON, W. F. 1997. Expression cloning and characterization of a renal electrogenic Na+/HCO3- cotransporter. *Nature,* 387**,** 409-413.

ROSSI, M., PELLEGRINI, C., CARDELLI, L., CICIARELLI, V., DI NARDO, L. & FARGNOLI, M. C. 2019. Familial Melanoma: Diagnostic and Management Implications. *Dermatology practical & conceptual,* 9**,** 10-16.

ROTHBERG, J. M., BAILEY, K. M., WOJTKOWIAK, J. W., BEN-NUN, Y., BOGYO, M., WEBER, E., MOIN, K., BLUM, G., MATTINGLY, R. R., GILLIES, R. J. & SLOANE, B. F. 2013. Acid-mediated tumor proteolysis: contribution of cysteine cathepsins. *Neoplasia (New York, N.Y.),* 15**,** 1125-1137.

SAHA, B., SINGH, S. K., SARKAR, C., BERA, R., RATHA, J., TOBIN, D. J. & BHADRA, R. 2006. Activation of the Mitf promoter by lipid-stimulated activation of p38-stress signalling to CREB. *Pigment Cell Res,* 19**,** 595-605.

SAITO, H., YASUMOTO, K., TAKEDA, K., TAKAHASHI, K., FUKUZAKI, A., ORIKASA, S. & SHIBAHARA, S. 2002. Melanocyte-specific microphthalmia-associated transcription factor isoform activates its own gene promoter through physical interaction with lymphoid-enhancing factor 1. *J Biol Chem,* 277**,** 28787-94.

SALAMEH, A. I., H*The Journal of physiology,* 595**,** 93-124.

SALMANINEJAD, A., VALILOU, S. F., SHABGAH, A. G., ASLANI, S., ALIMARDANI, M., PASDAR, A. & SAHEBKAR, A. 2019. PD-1/PD-L1 pathway: Basic biology and role in cancer immunotherapy. *J Cell Physiol,* 234**,** 16824-16837.

SARANGARAJAN, R., SHUMAKER, H., SOLEIMANI, M., LE POOLE, C. & BOISSY, R. E. 2001. Molecular and functional characterization of sodium–hydrogen

exchanger in skin as well as cultured keratinocytes and melanocytes1Part of this study was presented as a poster at the 8th Meeting of the PanAmerican Society for Pigment Cell Research, Snowmass, Colorado, August 15–18, 1998.1. *Biochimica et Biophysica Acta (BBA) - Biomembranes,* 1511**,** 181-192.

SARDIELLO, M., PALMIERI, M., DI RONZA, A., MEDINA, D. L., VALENZA, M., GENNARINO, V. A., DI MALTA, C., DONAUDY, F., EMBRIONE, V., POLISHCHUK, R. S., BANFI, S., PARENTI, G., CATTANEO, E. & BALLABIO, A. 2009. A Gene Network Regulating Lysosomal Biogenesis and Function. *Science,* 325**,** 473.

SAUTIN, Y. Y., LU, M., GAUGLER, A., ZHANG, L. & GLUCK, S. L. 2005. Phosphatidylinositol 3-kinase-mediated effects of glucose on vacuolar H+-ATPase assembly, translocation, and acidification of intracellular compartments in renal epithelial cells. *Molecular and cellular biology,* 25**,** 575-589.

SCHMID-WENDTNER, M. H. & KORTING, H. C. 2006. The pH of the skin surface and its impact on the barrier function. *Skin pharmacology and physiology,* 19**,** 296-302.

SCHMITT, B. M., BIEMESDERFER, D., ROMERO, M. F., BOULPAEP, E. L. & BORON, W. F. 1999. Immunolocalization of the electrogenic Na+-HCO-3 cotransporter in mammalian and amphibian kidney. *The American journal of physiology,* 276**,** F27-F38.

SCHMITTGEN, T. D. & LIVAK, K. J. 2008. Analyzing real-time PCR data by the comparative CT method. *Nature Protocols,* 3**,** 1101-1108.

SCHWAB, A., FABIAN, A., HANLEY, P. J. & STOCK, C. 2012. Role of ion channels and transporters in cell migration. *Physiological reviews,* 92**,** 1865-1913.

SCHWEDE, M., GARBETT, K., MIRNICS, K., GESCHWIND, D. H. & MORROW, E. M. 2014. Genes for endosomal NHE6 and NHE9 are misregulated in autism brains. *Molecular psychiatry,* 19**,** 277-279.

SCIORTINO, C. M. & ROMERO, M. F. 1999. Cation and voltage dependence of rat kidney electrogenic Na(+)-HCO(-)(3) cotransporter, rkNBC, expressed in oocytes. *The American journal of physiology,* 277**,** F611-F623.

SEAGROVES, T. N., RYAN, H. E., LU, H., WOUTERS, B. G., KNAPP, M., THIBAULT, P., LADEROUTE, K. & JOHNSON, R. S. 2001. Transcription factor HIF-1 is a necessary mediator of the pasteur effect in mammalian cells. *Molecular and cellular biology,* 21**,** 3436-3444.

SEGURA, M. F., HANNIFORD, D., MENENDEZ, S., REAVIE, L., ZOU, X., ALVAREZ-DIAZ, S., ZAKRZEWSKI, J., BLOCHIN, E., ROSE, A., BOGUNOVIC, D., POLSKY, D., WEI, J., LEE, P., BELITSKAYA-LEVY, I., BHARDWAJ, N., OSMAN, I. & HERNANDO, E. 2009. Aberrant miR-182 expression promotes melanoma metastasis by repressing

FOXO3 and microphthalmia-associated transcription factor. *Proc Natl Acad Sci U S A,* 106**,** 1814-9.

SEKLER, I., LO, R. S. & KOPITO, R. R. 1995. A Conserved Glutamate Is Responsible for Ion Selectivity and pH Dependence of the Mammalian Anion Exchangers AE1 and AE2. *Journal of Biological Chemistry,* 270**,** 28751-28758.

SELZER, E., WACHECK, V., LUCAS, T., HEERE-RESS, E., WU, M., WEILBAECHER, K. N., SCHLEGEL, W., VALENT, P., WRBA, F., PEHAMBERGER, H., FISHER, D. & JANSEN, B. 2002. The melanocyte-specific isoform of the microphthalmia transcription factor affects the phenotype of human melanoma. *Cancer Res,* 62**,** 2098-103.

SEMENZA, G. L. 2003. Targeting HIF-1 for cancer therapy. *Nature Reviews Cancer,* 3**,** 721-732.

SESTAKOVA, B., ONDRUSOVA, L. & VACHTENHEIM, J. 2010. Cell cycle inhibitor p21/ WAF1/ CIP1 as a cofactor of MITF expression in melanoma cells. *Pigment Cell Melanoma Res,* 23**,** 238-51.

SETTEMBRE, C., ZONCU, R., MEDINA, D. L., VETRINI, F., ERDIN, S., ERDIN, S., HUYNH, T., FERRON, M., KARSENTY, G., VELLARD, M. C., FACCHINETTI, V., SABATINI, D. M. & BALLABIO, A. 2012. A lysosome-to-nucleus signalling mechanism senses and regulates the lysosome via mTOR and TFEB. *The EMBO Journal,* 31**,** 1095-1108.

SHAFFER, S. M., DUNAGIN, M. C., TORBORG, S. R., TORRE, E. A., EMERT, B., KREPLER, C., BEQIRI, M., SPROESSER, K., BRAFFORD, P. A., XIAO, M., EGGAN, E., ANASTOPOULOS, I. N., VARGAS-GARCIA, C. A., SINGH, A., NATHANSON, K. L., HERLYN, M. & RAJ, A. 2017. Rare cell variability and drug-induced reprogramming as a mode of cancer drug resistance. *Nature,* 546**,** 431.

SHAIN, A. H. & BASTIAN, B. C. 2016. From melanocytes to melanomas. *Nature Reviews Cancer,* 16**,** 345-358.

SHARPE, A. H. & PAUKEN, K. E. 2018. The diverse functions of the PD1 inhibitory pathway. *Nature Reviews Immunology,* 18**,** 153-167.

SHIMODA, L. A., FALLON, M., PISARCIK, S., WANG, J. & SEMENZA, G. L. 2006. HIF-1 regulates hypoxic induction of NHE1 expression and alkalinization of intracellular pH in pulmonary arterial myocytes. *American journal of physiology. Lung cellular and molecular physiology,* 291**,** L941-L949.

SHIN, S.-S., JEONG, B.-S., WALL, B. A., LI, J., SHAN, N. L., WEN, Y., GOYDOS, J. S. & CHEN, S. 2018. Participation of xCT in melanoma cell proliferation in vitro and tumorigenesis in vivo. *Oncogenesis,* 7**,** 86-86.

SIENA, Á. D. D., PLA÷A, J. R., ARA*Scientific Reports,* 9**,** 11350.

SIMMONS, J. L., PIERCE, C. J., AL-EJEH, F. & BOYLE, G. M. 2017. MITF and BRN2 contribute to metastatic growth after dissemination of melanoma. *Scientific*

Reports, 7**,** 10909.

SLEPKOV, E. R., RAINEY, J. K., SYKES, B. D. & FLIEGEL, L. 2007. Structural and functional analysis of the Na+/H+ exchanger. *The Biochemical journal,* 401**,** 623-633.

SMITH, D. R., SPAULDING, D. T., GLENN, H. M. & FULLER, B. B. 2004. The relationship between Na(+)/H(+) exchanger expression and tyrosinase activity in human melanocytes. *Exp Cell Res,* 298**,** 521-34.

SMITH, J. P., UHERNIK, A. L., LI, L., LIU, Z. & DREWES, L. R. 2012. Regulation of Mct1 by cAMP-dependent internalization in rat brain endothelial cells. *Brain Res,* 1480**,** 1-11.

SMITH, M. P., BRUNTON, H., ROWLING, E. J., FERGUSON, J., AROZARENA, I., MISKOLCZI, Z., LEE, J. L., GIROTTI, M. R., MARAIS, R., LEVESQUE, M. P., DUMMER, R., FREDERICK, D. T., FLAHERTY, K. T., COOPER, Z. A., WARGO, J. A. & WELLBROCK, C. 2016. Inhibiting Drivers of Non-mutational Drug Tolerance Is a Salvage Strategy for Targeted Melanoma Therapy. *Cancer Cell,* 29**,** 270-284.

SNEAD, C. M., SMITH, S. M., SADEGHEIN, N., LACRUZ, R. S., HU, P., KURTZ, I. & PAINE, M. L. 2011. Identification of a pH-responsive DNA region upstream of the transcription start site of human NBCe1-B. *European Journal of Oral Sciences,* 119**,** 136-141.

SOENGAS, M. S. & PATTON, E. E. 2017. Location, Location, Location: Spatio-Temporal Cues That Define the Cell of Origin in Melanoma. *Cell Stem Cell,* 21**,** 559-561.

SOLEIMANI, M. & BURNHAM, C. E. 2001. Na+:HCO(3-) cotransporters (NBC): cloning and characterization. *The Journal of membrane biology,* 183**,** 71-84.

SOLIT, D. & SAWYERS, C. L. 2010. Drug discovery: How melanomas bypass new therapy. *Nature,* 468**,** 902-3.

SONNENBLICK, A., LEVY, C. & RAZIN, E. 2004. Interplay between MITF, PIAS3, and STAT3 in mast cells and melanocytes. *Molecular and cellular biology,* 24**,** 10584-10592.

SPUGNINI, E. P., SONVEAUX, P., STOCK, C., PEREZ-SAYANS, M., DE MILITO, A., AVNET, S., GARCüA, A. G., HARGUINDEY, S. & FAIS, S. 2015. Proton channels and exchangers in cancer. *Biochimica et Biophysica Acta (BBA) - Biomembranes,* 1848**,** 2715-2726.

STEINGRýMSSON, E., MOORE, K. J., LAMOREUX, M. L., FERR¢-D'AMAR¢, A. R., BURLEY, S. K., SANDERS ZIMRING, D. C., SKOW, L. C., HODGKINSON, C. A., ARNHEITER, H., COPELAND, N. G. & JENKINS, N. A. 1994. Molecular basis of mouse microphthalmia (mi) mutations helps explain their developmental and phenotypic consequences. *Nature Genetics,* 8**,** 256-263.

STEWART, A. K., CHERNOVA, M. N., SHMUKLER, B. E., WILHELM, S. & ALPER, S. L.

2002. Regulation of AE2-mediated Cl- transport by intracellular or by extracellular pH requires highly conserved amino acid residues of the AE2 NH2-terminal cytoplasmic domain. *The Journal of general physiology,* 120**,** 707-722.

STOCK, C., GASSNER, B., HAUCK, C. R., ARNOLD, H., MALLY, S., EBLE, J. A., DIETERICH, P. & SCHWAB, A. 2005. Migration of human melanoma cells depends on extracellular pH and Na+/H+ exchange. *The Journal of physiology,* 567**,** 225-238.

STOCK, C. & PEDERSEN, S. F. 2017. Roles of pH and the Na+/H+ exchanger NHE1 in cancer: From cell biology and animal models to an emerging translational perspective? *Seminars in Cancer Biology,* 43**,** 5-16.

STRANSKY, L., COTTER, K. & FORGAC, M. 2016. The Function of V-ATPases in Cancer. *Physiological Reviews,* 96**,** 1071-1091.

STRANSKY, L. A. & FORGAC, M. 2015. Amino Acid Availability Modulates Vacuolar H+-ATPase Assembly. *The Journal of biological chemistry,* 290**,** 27360-27369.

STUART-TILLEY, A., SARDET, C., POUYSSEGUR, J., SCHWARTZ, M. A., BROWN, D. & ALPER, S. L. 1994. Immunolocalization of anion exchanger AE2 and cation exchanger NHE-1 in distinct adjacent cells of gastric mucosa. *The American journal of physiology,* 266**,** C559-C568.

STUTTFELD, E., AYLETT, C. H., IMSENG, S., BOEHRINGER, D., SCAIOLA, A., SAUER, E., HALL, M. N., MAIER, T. & BAN, N. 2018. Architecture of the human mTORC2 core complex. *eLife,* 7**,** e33101.

SU, Y., WEI, W., ROBERT, L., XUE, M., TSOI, J., GARCIA-DIAZ, A., HOMET MORENO, B., KIM, J., NG, R. H., LEE, J. W., KOYA, R. C., COMIN-ANDUIX, B., GRAEBER, T. G., RIBAS, A. & HEATH, J. R. 2017. Single-cell analysis resolves the cell state transition and signaling dynamics associated with melanoma drug-induced resistance. *Proceedings of the National Academy of Sciences of the United States of America,* 114**,** 13679-13684.

SUN-WADA, G.-H. & WADA, Y. 2013. Vacuolar-type proton pump ATPases: acidification and pathological relationships. *Histology and histopathology,* 28**,** 805-815.

SUN, J., HAO, Z., LUO, H., HE, C., MEI, L., LIU, Y., WANG, X., NIU, Z., CHEN, H., LI, J.-D. & FENG, Y. 2017. Functional analysis of a nonstop mutation in MITF gene identified in a patient with Waardenburg syndrome type 2. *Journal of Human Genetics,* 62**,** 703-709.

SUPEK, F., SUPEKOVA, L., MANDIYAN, S., PAN, Y. C., NELSON, H. & NELSON, N. 1994. A novel accessory subunit for vacuolar H(+)-ATPase from chromaffin granules. *The Journal of biological chemistry,* 269**,** 24102-24106.

SUPURAN, C. T. 2018. Carbonic Anhydrases and Metabolism. *Metabolites,* 8**,** 25.

SWETTER, S. M., BOLDRICK, J. C., JUNG, S. Y., EGBERT, B. M. & HARVELL, J. D. 2005. Increasing incidence of lentigo maligna melanoma subtypes: northern California and national trends 1990-2000. *The Journal of investigative dermatology,* 125**,** 685-691.

SYRJANEN, L., LUUKKAALA, T., LEPPILAMPI, M., KALLIOINEN, M., PASTOREKOVA, S., PASTOREK, J., WAHEED, A., SLY, W. S., PARKKILA, S. & KARTTUNEN, T. 2014. Expression of cancer-related carbonic anhydrases IX and XII in normal skin and skin neoplasms. *Apmis,* 122**,** 880-9.

TABBAKH, T., VOLKOV, A., WAKEFIELD, M. & DOBBINSON, S. 2019. Implementation of the SunSmart program and population sun protection behaviour in Melbourne, Australia: Results from cross-sectional summer surveys from 1987 to 2017. *PLoS Med,* 16**,** e1002932.

TACHIBANA, M., TAKEDA, K., NOBUKUNI, Y., URABE, K., LONG, J. E., MEYERS, K. A., AARONSON, S. A. & MIKI, T. 1996. Ectopic expression of MITF, a gene for Waardenburg syndrome type 2, converts fibroblasts to cells with melanocyte characteristics. *Nature Genetics,* 14**,** 50-54.

TADESSE, S., CALDON, E. C., TILLEY, W. & WANG, S. 2019. Cyclin-Dependent Kinase 2 Inhibitors in Cancer Therapy: An Update. *Journal of medicinal chemistry,* 62**,** 4233-4251.

TAKEDA, K., TAKEMOTO, C., KOBAYASHI, I., WATANABE, A., NOBUKUNI, Y., FISHER, D. E. & TACHIBANA, M. 2000a. Ser298 of MITF, a mutation site in Waardenburg syndrome type 2, is a phosphorylation site with functional significance. *Hum Mol Genet,* 9**,** 125-32.

TAKEDA, K., YASUMOTO, K., TAKADA, R., TAKADA, S., WATANABE, K., UDONO, T., SAITO, H., TAKAHASHI, K. & SHIBAHARA, S. 2000b. Induction of melanocyte-specific microphthalmia-associated transcription factor by Wnt-3a. *J Biol Chem,* 275**,** 14013-6.

TAKIMOTO, M., TAKEYAMA, M. & HAMADA, T. 2013. Possible involvement of AMPK in acute exercise-induced expression of monocarboxylate transporters MCT1 and MCT4 mRNA in fast-twitch skeletal muscle. *Metabolism: clinical and experimental,* 62**,** 1633-1640.

TAN, Z., LUO, X., XIAO, L., TANG, M., BODE, A. M., DONG, Z. & CAO, Y. 2016. The Role of PGC1α in Cancer Metabolism and its Therapeutic Implications. *Molecular cancer therapeutics,* 15**,** 774-782.

TANNOCK, I. F. & ROTIN, D. 1989. Acid pH in tumors and its potential for therapeutic exploitation. *Cancer Res,* 49**,** 4373-84.

TANNOUS, Z. S., LERNER, L. H., DUNCAN, L. M., MIHM, M. C., JR. & FLOTTE, T. J. 2000.

Progression to invasive melanoma from malignant melanoma in situ, lentigo maligna type. *Human pathology,* 31**,** 705-708.

TASDOGAN, A., FAUBERT, B., RAMESH, V., UBELLACKER, J. M., SHEN, B., SOLMONSON, A., MURPHY, M. M., GU, Z., GU, W., MARTIN, M., KASITINON, S. Y., VANDERGRIFF, T., MATHEWS, T. P., ZHAO, Z., SCHADENDORF, D., DEBERARDINIS, R. J. & MORRISON, S. J. 2020. Metabolic heterogeneity confers differences in melanoma metastatic potential. *Nature,* 577**,** 115-120.

TASSABEHJI, M., NEWTON, V. E. & READ, A. P. 1994. Waardenburg syndrome type 2 caused by mutations in the human microphthalmia (MITF) gene. *Nature Genetics,* 8**,** 251-255.

TERRAGNI, J., NAYAK, G., BANERJEE, S., MEDRANO, J. L., GRAHAM, J. R., BRENNAN, J. F., SEPULVEDA, S. & COOPER, G. M. 2011. The E-box binding factors Max/Mnt, MITF, and USF1 act coordinately with FoxO to regulate expression of proapoptotic and cell cycle control genes by phosphatidylinositol 3-kinase/Akt/glycogen synthase kinase 3 signaling. *J Biol Chem,* 286**,** 36215-27.

THAMMASIT, P., SANGBOONRUANG, S., SUWANPAIROJ, S., KHAMAIKAWIN, W., INTASAI, N., KASINRERK, W., TAYAPIWATANA, C. & TRAGOOLPUA, K. 2015. Intracellular Acidosis Promotes Mitochondrial Apoptosis Pathway: Role of EMMPRIN Down-regulation via Specific Single-chain Fv Intrabody. *Journal of Cancer,* 6**,** 276-286.

THE CANCER GENOME ATLAS RESEARCH, N. 2008. Comprehensive genomic characterization defines human glioblastoma genes and core pathways. *Nature,* 455**,** 1061.

TIROSH, I., IZAR, B., PRAKADAN, S. M., WADSWORTH, M. H., TREACY, D., TROMBETTA, J. J., ROTEM, A., RODMAN, C., LIAN, C., MURPHY, G., FALLAHI-SICHANI, M., DUTTON-REGESTER, K., LIN, J.-R., COHEN, O., SHAH, P., LU, D., GENSHAFT, A. S., HUGHES, T. K., ZIEGLER, C. G. K., KAZER, S. W., GAILLARD, A., KOLB, K. E., VILLANI, A.-C., JOHANNESSEN, C. M., ANDREEV, A. Y., VAN ALLEN, E. M., BERTAGNOLLI, M., SORGER, P. K., SULLIVAN, R. J., FLAHERTY, K. T., FREDERICK, D. T., JAN¢-VALBUENA, J., YOON, C. H., ROZENBLATT-ROSEN, O., SHALEK, A. K., REGEV, A. & GARRAWAY, L. A. 2016. Dissecting the multicellular ecosystem of metastatic melanoma by single-cell RNA-seq. *Science,* 352**,** 189-196.

TOEI, M., TOEI, S. & FORGAC, M. 2011. Definition of membrane topology and identification of residues important for transport in subunit a of the vacuolar ATPase. *The Journal of biological chemistry,* 286**,** 35176-35186.

TSAO, H., OLAZAGASTI, J. M., CORDORO, K. M., BREWER, J. D., TAYLOR, S. C., BORDEAUX, J. S., CHREN, M.-M., SOBER, A. J., TEGELER, C., BHUSHAN, R. & BEGOLKA, W. S. 2015. Early detection of melanoma: Reviewing the ABCDEs.

Journal of the American Academy of Dermatology, 72**,** 717-723.

TSCHAN, M. P. & SIMON, H. U. 2010. The role of autophagy in anticancer therapy: promises and uncertainties. *Journal of internal medicine,* 268**,** 410-418.

UGUREL, S., HOUBEN, R., SCHRAMA, D., VOIGT, H., ZAPATKA, M., SCHADENDORF, D., BR*Clinical Cancer Research,* 13**,** 6344.

ULLAH, M. S., DAVIES, A. J. & HALESTRAP, A. P. 2006. The plasma membrane lactate transporter MCT4, but not MCT1, is up-regulated by hypoxia through a HIF-1alpha-dependent mechanism. *The Journal of biological chemistry,* 281**,** 9030-9037.

URSO, C., RONGIOLETTI, F., INNOCENZI, D., BATOLO, D., CHIMENTI, S., FANTI, P. L., FILOTICO, R., GIANOTTI, R., LENTINI, M., TOMASINI, C. & PIPPIONE, M. 2005. Histological features used in the diagnosis of melanoma are frequently found in benign melanocytic naevi. *Journal of Clinical Pathology,* 58**,** 409.

VACHTENHEIM, J., NOVOTNA, H. & GHANEM, G. 2001. Transcriptional Repression of the Microphthalmia Gene in Melanoma Cells Correlates with the Unresponsiveness of Target Genes to Ectopic Microphthalmia-Associated Transcription Factor. *Journal of Investigative Dermatology,* 117**,** 1505-1511.

VALLES, P. G., BOCANEGRA, V., GIL LORENZO, A. & COSTANTINO, V. V. 2015. Physiological Functions and Regulation of the Na+/H+ Exchanger [NHE1] in Renal Tubule Epithelial Cells. *Kidney Blood Press Res,* 40**,** 452-66.

VANDER HEIDEN, M. G., CANTLEY, L. C. & THOMPSON, C. B. 2009. Understanding the Warburg effect: the metabolic requirements of cell proliferation. *Science (New York, N.Y.),* 324**,** 1029-1033.

VAZQUEZ, F., LIM, J.-H., CHIM, H., BHALLA, K., GIRNUN, G., PIERCE, K., CLISH, C. B., GRANTER, S. R., WIDLUND, H. R., SPIEGELMAN, B. M. & PUIGSERVER, P. 2013. PGC1α expression defines a subset of human melanoma tumors with increased mitochondrial capacity and resistance to oxidative stress. *Cancer cell,* 23**,** 287-301.

VEIS, D. J., SORENSON, C. M., SHUTTER, J. R. & KORSMEYER, S. J. 1993. Bcl-2-deficient mice demonstrate fulminant lymphoid apoptosis, polycystic kidneys, and hypopigmented hair. *Cell,* 75**,** 229-240.

VENZA, M., VISALLI, M., BENINATI, C., DE GAETANO, G. V., TETI, D. & VENZA, I. 2015. Cellular Mechanisms of Oxidative Stress and Action in Melanoma. *Oxidative medicine and cellular longevity,* 2015**,** 481782-481782.

VERFAILLIE, A., IMRICHOVA, H., ATAK, Z. K., DEWAELE, M., RAMBOW, F., HULSELMANS, G., CHRISTIAENS, V., SVETLICHNYY, D., LUCIANI, F., VAN DEN MOOTER, L., CLAERHOUT, S., FIERS, M., JOURNE, F., GHANEM, G.-E., HERRMANN, C., HALDER, G., MARINE, J.-C. & AERTS, S. 2015. Decoding the

regulatory landscape of melanoma reveals TEADS as regulators of the invasive cell state. *Nature Communications,* 6**,** 6683.

VETRINI, F., AURICCHIO, A., DU, J., ANGELETTI, B., FISHER, D. E., BALLABIO, A. & MARIGO, V. 2004. The microphthalmia transcription factor (Mitf) controls expression of the ocular albinism type 1 gene: link between melanin synthesis and melanosome biogenesis. *Molecular and cellular biology,* 24**,** 6550-6559.

VIDO, M. J., LE, K., HARTSOUGH, E. J. & APLIN, A. E. 2018. BRAF Splice Variant Resistance to RAF Inhibitor Requires Enhanced MEK Association. *Cell reports,* 25**,** 1501-1510.e3.

VIJAY, N. & MORRIS, M. E. 2014. Role of monocarboxylate transporters in drug delivery to the brain. *Current pharmaceutical design,* 20**,** 1487-1498.

VINCE, J. W. & REITHMEIER, R. A. 1998. Carbonic anhydrase II binds to the carboxyl terminus of human band 3, the erythrocyte C1-/HCO3- exchanger. *The Journal of biological chemistry,* 273**,** 28430-28437.

VIRAY, H., BRADLEY, W. R., SCHALPER, K. A., RIMM, D. L. & GOULD ROTHBERG, B. E. 2013. Marginal and joint distributions of S100, HMB-45, and Melan-A across a large series of cutaneous melanomas. *Archives of pathology & laboratory medicine,* 137**,** 1063-1073.

VIRKKI, L. V., CHOI, I., DAVIS, B. A. & BORON, W. F. 2003. Cloning of a Na+-driven Cl/HCO3 exchanger from squid giant fiber lobe. *American journal of physiology. Cell physiology,* 285**,** C771-C780.

VIVAS-GARCýA, Y., FALLETTA, P., LIEBING, J., LOUPHRASITTHIPHOL, P., FENG, Y., CHAUHAN, J., SCOTT, D. A., GLODDE, N., CHOCARRO-CALVO, A., BONHAM, S., OSTERMAN, A. L., FISCHER, R., RONAI, Z. E., GARCýA-JIM¢NEZ, C., H*Molecular Cell,* 77**,** 120-137.e9.

VON SCHWARZENBERG, K., WIEDMANN, R. M., OAK, P., SCHULZ, S., ZISCHKA, H., WANNER, G., EFFERTH, T., TRAUNER, D. & VOLLMAR, A. M. 2013. Mode of cell death induction by pharmacological vacuolar H+-ATPase (V-ATPase) inhibition. *The Journal of biological chemistry,* 288**,** 1385-1396.

VON THALER, A. K., KAMENISCH, Y. & BERNEBURG, M. 2010. The role of ultraviolet radiation in melanomagenesis. *Exp Dermatol,* 19**,** 81-8.

WAHL, M. L., OWEN, J. A., BURD, R., HERLANDS, R. A., NOGAMI, S. S., RODECK, U., BERD, D., LEEPER, D. B. & OWEN, C. S. 2002. Regulation of Intracellular pH in Human Melanoma: Potential Therapeutic Implications 1 Supported by NIH Grant P01 CA56690 (to M. L. W., R. B., C. S. O., D. B. L.); Grant R25CA48010 from National Cancer Institute, NIH, and Department of Health and Human Services, National Science Foundation MCB RUI Grant 9057010 (to J. A. O., S. S. N., R. A. H.); and NIH Grant CA39248 (to D. B.).<a id="xref-fn-1-

1" class="xref-" href="#fn-1">1</a&gt. *Molecular Cancer Therapeutics,* 1**,** 617.

WAKABAYASHI, S., BERTRAND, B., IKEDA, T., POUYSS¢GUR, J. & SHIGEKAWA, M. 1994. Mutation of calmodulin-binding site renders the Na+/H+ exchanger (NHE1) highly H(+)-sensitive and Ca2+ regulation-defective. *The Journal of biological chemistry,* 269**,** 13710-13715.

WAKABAYASHI, S., IKEDA, T., IWAMOTO, T., POUYSSEGUR, J. & SHIGEKAWA, M. 1997. Calmodulin-binding autoinhibitory domain controls "pH-sensing" in the Na+/H+ exchanger NHE1 through sequence-specific interaction. *Biochemistry,* 36**,** 12854-61.

WANG, H., YANG, C., DOHERTY, J. R., ROUSH, W. R., CLEVELAND, J. L. & BANNISTER, T. D. 2014a. Synthesis and structure-activity relationships of pteridine dione and trione monocarboxylate transporter 1 inhibitors. *J Med Chem,* 57**,** 7317-24.

WANG, R. & GREEN, D. R. 2012. Metabolic reprogramming and metabolic dependency in T cells. *Immunological reviews,* 249**,** 14-26.

WANG, T., LIU, G. & WANG, R. 2014b. The Intercellular Metabolic Interplay between Tumor and Immune Cells. *Front Immunol,* 5**,** 358.

WANG, Y., RADFAR, S., LIU, S., RIKER, A. I. & KHONG, H. T. 2010. Mitf-Mdel, a novel melanocyte/melanoma-specific isoform of microphthalmia-associated transcription factor-M, as a candidate biomarker for melanoma. *BMC Med,* 8**,** 14.

WANG, Y., TOEI, M. & FORGAC, M. 2008. Analysis of the membrane topology of transmembrane segments in the C-terminal hydrophobic domain of the yeast vacuolar ATPase subunit a (Vph1p) by chemical modification. *The Journal of biological chemistry,* 283**,** 20696-20702.

WANG, Z., LIU, S., KAKIZAKI, M., HIROSE, Y., ISHIKAWA, Y., FUNATO, H., YANAGISAWA, M., YU, Y. & LIU, Q. 2014c. Orexin/hypocretin activates mTOR complex 1 (mTORC1) via an Erk/Akt-independent and calcium-stimulated lysosome v-ATPase pathway. *The Journal of biological chemistry,* 289**,** 31950-31959.

WARBURG, O. 1956a. On respiratory impairment in cancer cells. *Science,* 124**,** 269-70.

WARBURG, O. 1956b. On the origin of cancer cells. *Science,* 123**,** 309-14.

WARYCHA, M. A., CHRISTOS, P. J., MAZUMDAR, M., DARVISHIAN, F., SHAPIRO, R. L., BERMAN, R. S., PAVLICK, A. C., KOPF, A. W., POLSKY, D. & OSMAN, I. 2008. Changes in the presentation of nodular and superficial spreading melanomas over 35 years. *Cancer,* 113**,** 3341-3348.

WASMEIER, C., HUME, A. N., BOLASCO, G. & SEABRA, M. C. 2008. Melanosomes at a glance. *Journal of Cell Science,* 121**,** 3995.

WEBB, B. A., CHIMENTI, M., JACOBSON, M. P. & BARBER, D. L. 2011. Dysregulated pH: a perfect storm for cancer progression. *Nature reviews. Cancer,* 11**,** 671-677.

WEI, S. C., DUFFY, C. R. & ALLISON, J. P. 2018. Fundamental Mechanisms of Immune Checkpoint Blockade Therapy. *Cancer Discov,* 8**,** 1069-1086.

WELLBROCK, C. & AROZARENA, I. 2015. Microphthalmia-associated transcription factor in melanoma development and MAP-kinase pathway targeted therapy. *Pigment cell & melanoma research,* 28**,** 390-406.

WHITAKER, A. M., SCHAICH, M. A., SMITH, M. R., FLYNN, T. S. & FREUDENTHAL, B. D. 2017. Base excision repair of oxidative DNA damage: from mechanism to disease. *Frontiers in bioscience (Landmark edition),* 22**,** 1493-1522.

WIDLUND, H. R., HORSTMANN, M. A., PRICE, E. R., CUI, J., LESSNICK, S. L., WU, M., HE, X. & FISHER, D. E. 2002. Beta-catenin-induced melanoma growth requires the downstream target Microphthalmia-associated transcription factor. *The Journal of cell biology,* 158**,** 1079-1087.

WIDMER, D. S., HOEK, K. S., CHENG, P. F., EICHHOFF, O. M., BIEDERMANN, T., RAAIJMAKERS, M. I. G., HEMMI, S., DUMMER, R. & LEVESQUE, M. P. 2013. Hypoxia contributes to melanoma heterogeneity by triggering HIF1alpha-dependent phenotype switching. *J Invest Dermatol,* 133**,** 2436-2443.

WIEDMANN, R. M., VON SCHWARZENBERG, K., PALAMIDESSI, A., SCHREINER, L., KUBISCH, R., LIEBL, J., SCHEMPP, C., TRAUNER, D., VEREB, G., ZAHLER, S., WAGNER, E., M*Cancer research,* 72**,** 5976-5987.

WILSON, M. C., MEREDITH, D., FOX, J. E. M., MANOHARAN, C., DAVIES, A. J. & HALESTRAP, A. P. 2005. Basigin (CD147) Is the Target for Organomercurial Inhibition of Monocarboxylate Transporter Isoforms 1 and 4: THE ANCILLARY PROTEIN FOR THE INSENSITIVE MCT2 IS EMBIGIN (gp70). *Journal of Biological Chemistry,* 280**,** 27213-27221.

WILSON, M. C., MEREDITH, D. & HALESTRAP, A. P. 2002. Fluorescence Resonance Energy Transfer Studies on the Interaction between the Lactate Transporter MCT1 and CD147 Provide Information on the Topology and Stoichiometry of the Complex in Situ. *Journal of Biological Chemistry,* 277**,** 3666-3672.

WINDER, M. & VIR*Handbook of experimental pharmacology,* 249**,** 91-108.

WOLCHOK, J. D., CHIARION-SILENI, V., GONZALEZ, R., RUTKOWSKI, P., GROB, J. J., COWEY, C. L., LAO, C. D., WAGSTAFF, J., SCHADENDORF, D., FERRUCCI, P. F., SMYLIE, M., DUMMER, R., HILL, A., HOGG, D., HAANEN, J., CARLINO, M. S., BECHTER, O., MAIO, M., MARQUEZ-RODAS, I., GUIDOBONI, M., MCARTHUR, G., LEBBE, C., ASCIERTO, P. A., LONG, G. V., CEBON, J., SOSMAN, J., POSTOW, M. A., CALLAHAN, M. K., WALKER, D., ROLLIN, L., BHORE, R., HODI, F. S. & LARKIN, J. 2017. Overall Survival with Combined Nivolumab and Ipilimumab in

Advanced Melanoma. *N Engl J Med,* 377**,** 1345-1356.

WONG, D. J. L. & RIBAS, A. 2016. Targeted Therapy for Melanoma. *Cancer treatment and research,* 167**,** 251-262.

WU, C.-C., KLAESSON, A., BUSKAS, J., RANEFALL, P., MIRZAZADEH, R., S*The Journal of experimental biology,* 222**,** jeb194431.

WU, G. 2009. Amino acids: metabolism, functions, and nutrition. *Amino Acids,* 37**,** 1-17.

WU, M., HEMESATH, T. J., TAKEMOTO, C. M., HORSTMANN, M. A., WELLS, A. G., PRICE, E. R., FISHER, D. Z. & FISHER, D. E. 2000. c-Kit triggers dual phosphorylations, which couple activation and degradation of the essential melanocyte factor Mi. *Genes Dev,* 14**,** 301-12.

WYKOFF, C. C., BEASLEY, N. J., WATSON, P. H., TURNER, K. J., PASTOREK, J., SIBTAIN, A., WILSON, G. D., TURLEY, H., TALKS, K. L., MAXWELL, P. H., PUGH, C. W., RATCLIFFE, P. J. & HARRIS, A. L. 2000. Hypoxia-inducible expression of tumor-associated carbonic anhydrases. *Cancer Res,* 60**,** 7075-83.

XU, J., XIE, R., LIU, X., WEN, G., JIN, H., YU, Z., JIANG, Y., ZHAO, Z., YANG, Y., JI, B., DONG, H. & TUO, B. 2012. Expression and functional role of vacuolar H(+)-ATPase in human hepatocellular carcinoma. *Carcinogenesis,* 33**,** 2432-2440.

XU, M., MCCANNA, D. J. & SIVAK, J. G. 2015. Use of the viability reagent PrestoBlue in comparison with alamarBlue and MTT to assess the viability of human corneal epithelial cells. *Journal of Pharmacological and Toxicological Methods,* 71**,** 1-7.

XU, W., GONG, L., HADDAD, M. M., BISCHOF, O., CAMPISI, J., YEH, E. T. & MEDRANO, E. E. 2000. Regulation of microphthalmia-associated transcription factor MITF protein levels by association with the ubiquitin-conjugating enzyme hUBC9. *Exp Cell Res,* 255**,** 135-43.

YAAR, M. & GILCHREST, B. A. 1991. Human Melanocyte Growth and Differentiation: A Decade of New Data. *Journal of Investigative Dermatology,* 97**,** 611-617.

YAJIMA, I., KUMASAKA, M. Y., THANG, N. D., GOTO, Y., TAKEDA, K., IIDA, M., OHGAMI, N., TAMURA, H., YAMANOSHITA, O., KAWAMOTO, Y., FURUKAWA, K. & KATO, M. 2011. Molecular Network Associated with MITF in Skin Melanoma Development and Progression. *Journal of skin cancer,* 2011**,** 730170-730170.

YAJIMA, I., KUMASAKA, M. Y., THANG, N. D., GOTO, Y., TAKEDA, K., YAMANOSHITA, O., IIDA, M., OHGAMI, N., TAMURA, H., KAWAMOTO, Y. & KATO, M. 2012. RAS/RAF/MEK/ERK and PI3K/PTEN/AKT Signaling in Malignant Melanoma Progression and Therapy. *Dermatology research and practice,* 2012**,** 354191-354191.

YAMADA, H., YAMAZAKI, S., MORIYAMA, N., HARA, C., HORITA, S., ENOMOTO, Y.,

KUDO, A., KAWAKAMI, H., TANAKA, Y., FUJITA, T. & SEKI, G. 2003. Localization of NBC-1 variants in human kidney and renal cell carcinoma. *Biochemical and Biophysical Research Communications,* 310**,** 1213-1218.

YAMAMOTO, T., SWIETACH, P., ROSSINI, A., LOH, S.-H., VAUGHAN-JONES, R. D. & SPITZER, K. W. 2005. Functional diversity of electrogenic Na+-HCO3- cotransport in ventricular myocytes from rat, rabbit and guinea pig. *The Journal of physiology,* 562**,** 455-475.

YAMAZAKI, H., CHIJIWA, T., INOUE, Y., ABE, Y., SUEMIZU, H., KAWAI, K., WAKUI, M., FURUKAWA, D., MUKAI, M., KUWAO, S., SAEGUSA, M. & NAKAMURA, M. 2012. Overexpression of the miR-34 family suppresses invasive growth of malignant melanoma with the wild-type p53 gene. *Experimental and therapeutic medicine,* 3**,** 793-796.

YAN, D., DONG, X. D., CHEN, X., YAO, S., WANG, L., WANG, J., WANG, C., HU, D. N., QU, J. & TU, L. 2012. Role of microRNA-182 in posterior uveal melanoma: regulation of tumor development through MITF, BCL2 and cyclin D2. *PLoS One,* 7**,** e40967.

YANG, G., LI, Y., NISHIMURA, E. K., XIN, H., ZHOU, A., GUO, Y., DONG, L., DENNING, M. F., NICKOLOFF, B. J. & CUI, R. 2008. Inhibition of PAX3 by TGF-beta modulates melanocyte viability. *Mol Cell,* 32**,** 554-63.

YANG, L., VENNETI, S. & NAGRATH, D. 2017. Glutaminolysis: A Hallmark of Cancer Metabolism. *Annual review of biomedical engineering,* 19**,** 163-194.

YANG, O. C. Y. & LOH, S.-H. 2019. Acidic Stress Triggers Sodium-Coupled Bicarbonate Transport and Promotes Survival in A375 Human Melanoma Cells. *Scientific Reports,* 9**,** 6858.

YANG, Z. J., CHEE, C. E., HUANG, S. & SINICROPE, F. A. 2011. The role of autophagy in cancer: therapeutic implications. *Molecular cancer therapeutics,* 10**,** 1533-1541.

YASUMOTO, K.-I., TAKEDA, K., SAITO, H., WATANABE, K.-I., TAKAHASHI, K. & SHIBAHARA, S. 2002. Microphthalmia-associated transcription factor interacts with LEF-1, a mediator of Wnt signaling. *The EMBO journal,* 21**,** 2703-2714.

YASUMOTO, K., YOKOYAMA, K., SHIBATA, K., TOMITA, Y. & SHIBAHARA, S. 1994. Microphthalmia-associated transcription factor as a regulator for melanocyte-specific transcription of the human tyrosinase gene. *Molecular and Cellular Biology,* 14**,** 8058.

YETKIN-ARIK, B., VOGELS, I. M. C., NOWAK-SLIWINSKA, P., WEISS, A., HOUTKOOPER, R. H., VAN NOORDEN, C. J. F., KLAASSEN, I. & SCHLINGEMANN, R. O. 2019. The role of glycolysis and mitochondrial respiration in the formation and functioning of endothelial tip cells during angiogenesis. *Scientific Reports,* 9**,**

12608.

YOKOYAMA, S., WOODS, S. L., BOYLE, G. M., AOUDE, L. G., MACGREGOR, S., ZISMANN, V., GARTSIDE, M., CUST, A. E., HAQ, R., HARLAND, M., TAYLOR, J. C., DUFFY, D. L., HOLOHAN, K., DUTTON-REGESTER, K., PALMER, J. M., BONAZZI, V., STARK, M. S., SYMMONS, J., LAW, M. H., SCHMIDT, C., LANAGAN, C., O'CONNOR, L., HOLLAND, E. A., SCHMID, H., MASKIELL, J. A., JETANN, J., FERGUSON, M., JENKINS, M. A., KEFFORD, R. F., GILES, G. G., ARMSTRONG, B. K., AITKEN, J. F., HOPPER, J. L., WHITEMAN, D. C., PHAROAH, P. D., EASTON, D. F., DUNNING, A. M., NEWTON-BISHOP, J. A., MONTGOMERY, G. W., MARTIN, N. G., MANN, G. J., BISHOP, D. T., TSAO, H., TRENT, J. M., FISHER, D. E., HAYWARD, N. K. & BROWN, K. M. 2011. A novel recurrent mutation in MITF predisposes to familial and sporadic melanoma. *Nature,* 480**,** 99-103.

YU, L., CHEN, Y. & TOOZE, S. A. 2018. Autophagy pathway: Cellular and molecular mechanisms. *Autophagy,* 14**,** 207-215.

YUAN, J., NARAYANAN, L., ROCKWELL, S. & GLAZER, P. M. 2000. Diminished DNA repair and elevated mutagenesis in mammalian cells exposed to hypoxia and low pH. *Cancer Res,* 60**,** 4372-6.

ZENG, H., JUDSON-TORRES, R. L. & SHAIN, A. H. 2020. The Evolution of Melanoma – Moving beyond Binary Models of Genetic Progression. *Journal of Investigative Dermatology,* 140**,** 291-297.

ZHANG, D., KIYATKIN, A., BOLIN, J. T. & LOW, P. S. 2000. Crystallographic structure and functional interpretation of the cytoplasmic domain of erythrocyte membrane band 3. *Blood,* 96**,** 2925-2933.

ZHANG, H. X., DU, G. H. & ZHANG, J. T. 2004. Assay of mitochondrial functions by resazurin in vitro. *Acta Pharmacol Sin,* 25**,** 385-9.

ZHANG, T., ZHOU, Q., OGMUNDSDOTTIR, M. H., MOLLER, K., SIDDAWAY, R., LARUE, L., HSING, M., KONG, S. W., GODING, C. R., PALSSON, A., STEINGRIMSSON, E. & PIGNONI, F. 2015. Mitf is a master regulator of the v-ATPase, forming a control module for cellular homeostasis with v-ATPase and TORC1. *J Cell Sci,* 128**,** 2938-50.

ZHANG, Z., ZHENG, Y., MAZON, H., MILGROM, E., KITAGAWA, N., KISH-TRIER, E., HECK, A. J. R., KANE, P. M. & WILKENS, S. 2008. Structure of the yeast vacuolar ATPase. *The Journal of biological chemistry,* 283**,** 35983-35995.

ZHAO, J., BENLEKBIR, S. & RUBINSTEIN, J. L. 2015. Electron cryomicroscopy observation of rotational states in a eukaryotic V-ATPase. *Nature,* 521**,** 241-245.

ZHAO, X., FISKE, B., KAWAKAMI, A., LI, J. & FISHER, D. E. 2011. Regulation of MITF stability by the USP13 deubiquitinase. *Nat Commun,* 2**,** 414.

ZHU, L., HUANG, X., CHOI, K. Y., MA, Y., ZHANG, F., LIU, G., LEE, S. & CHEN, X. 2012. Real-time monitoring of caspase cascade activation in living cells. *Journal of Controlled Release,* 163**,** 55-62.

ZHU, Q., LEE, D. W. K. & CASEY, J. R. 2003. Novel topology in C-terminal region of the human plasma membrane anion exchanger, AE1. *The Journal of biological chemistry,* 278**,** 3112-3120.

ZONCU, R., BAR-PELED, L., EFEYAN, A., WANG, S., SANCAK, Y. & SABATINI, D. M. 2011. mTORC1 senses lysosomal amino acids through an inside-out mechanism that requires the vacuolar H(+)-ATPase. *Science (New York, N.Y.),* 334**,** 678-683.

ZUNDEL, W., SCHINDLER, C., HAAS-KOGAN, D., KOONG, A., KAPER, F., CHEN, E., GOTTSCHALK, A. R., RYAN, H. E., JOHNSON, R. S., JEFFERSON, A. B., STOKOE, D. & GIACCIA, A. J. 2000. Loss of PTEN facilitates HIF-1-mediated gene expression. *Genes & development,* 14**,** 391-396.